EFE2026
ENERGY FUELS ENVIRONMENT
INTERNATIONAL CONFERENCE

17 – 20 November 2026
AGH University of Krakow
Kraków (Poland)

Book of Abstracts



Copyright by AGH University of Krakow
Faculty of Energy and Fuels
al. A. Mickiewicza 30
30-059 Kraków
Poland

Editor:
Bogdan Samojeden
AGH University of Krakow

Edition: 1
Kraków (Poland) November, 2026

ISBN **978-83-969343-8-3**

Cover photograph by Bogdan Samojeden

The Conference's Honorary Patrons

His Magnificence
Professor Jerzy Lis
Rector of AGH University of Krakow

His Magnificence
Professor Andrzej Szarata
Rector of the Krakow University of Technology

Ministry of Energy
Republic of Poland

Platinum Sponsor

ORLEN

POLSKA SPÓŁKA GAZOWNICTWA

gotowinabiometan.pl

Gold Sponsor





Energy Transition Campus Amsterdam
Together with Shell



ArcelorMittal

Sponsors

KEYENCE

GREENCELL

Partners

mpec



WODOCIĄGI Miasta Krakowa
125 lat! Jesteśmy z Wami. Każdego dnia.

W KRAKOWIE DOBRA WODA
prosto z kranu

Scientific Patronage

przemysł chemiczny

POLSKIE TOWARZYSTWO NUKLEONICZNE

POLSKIE TOWARZYSTWO CHEMICZNE

SITP Chem

POLSKIE STOWARZYSZENIE WODORU I OGNIW PALIWOWYCH * PSWiOP *

RENMINE

Research Fund for Coal & Steel

Co-funded by the European Union

Ministry of Science and Higher Education
Republic of Poland

Media Patronages

Energetyka 24

GRAMWZIELONE.PL

wysokieNapiecie.pl

nowa Energia

technologia wody

Table of Contents

The Conference's Honorary Patrons 3

Platinum Sponsor 4

Gold Sponsor 5

Sponsors 6

Partners 7

Scientific Patronage 8

Media Patronages 9

Table of Contents 10

Scientific Committee 23

Organizing Committee 25

Preface 26

Hybrid type biosorbents - formulation and preparation

Grzegorz S. Jodłowski, Marta Wójcik 27

Enhanced Sustainable Production of Drop-in Fuel Precursors and High-Calorific Gas from Coal-Plastic Hybrids via Iron-dolomite Catalysed Microwave Thermochemical Conversion.

Kanak Kumar, B. Rajasekhar Reddy 29

Flow Properties of Hydrophobized Fine Particulate Sorbents

Elżbieta Vogt, Eliza Wolak, Agnieszka Orzechowska-Zięba 30

Natural Aluminosilicate-Supported Ni and NiCe Catalysts for CO_2 Methanation

Agnieszka Szymaszek-Wawryca, Tomasz Piechówka, Michał Szymaszek, Monika Motak 32

Development of a One-Dimensional Transient Coking Model for Top-Charged and Stamp-Charged Systems

Mieszko Tokarski, Rafał Buczyński, Michał Ponikowski, Dariusz Zych, Paweł Cieślar 33

Declining Energy Intensity Without Energy Savings? Hotspots And Rebound Effects Across The EU Agribusiness Production Chain

Kacper Mankowski, Bartłomiej Bajan, Aldona Mrowczyńska-Kamińska 35

The Promotional Effect Of Ceria On Ni/Sba-15 Catalysts Prepared By The Solid-State Grinding For Co_2 Methanation

Dominika Książek, Jakub Mokrzycki, Agnieszka Szymaszek-Wawryca 37

Nanomaterials as Additives Supporting Biogas Production: Effects on Microorganisms Involved in Anaerobic Digestion

Katarzyna Kapusta, Katarzyna Moskalewicz, Krzysztof Kogut 39

Advanced Solid Oxide Electrochemical Technologies for Future Energy Systems: From Green Hydrogen Production to Carbon-Neutral Fuels

Zhihong Du, Tong Wang, Konrad Świerczek, Hailei Zhao 41

Assessment of The Third-Party Access Potential in The Decarbonisation of The Polish District Heating Market: Lessons from Lithuania

Aleksandra Bałys, Aleksandra Komorowska..... 43

A Microporous Channel Anode Support Structure for the Efficient and Safe Conversion of Low-Concentration Coal Mine Methane in High-Temperature Fuel Cells

Yihan Ling..... 45

Analysis Of The Transient Temperature And Stress Fields In The Wall Of A Component During A Thermal Shock, Considering The Finite Heat Capacity Of The Coolant

Jan Taler, Dawid Taler..... 46

Designing Atmosphere-Adaptive Perovskite Nanofiber Electrodes for Symmetrical SOFCs

Jakub Lach, Kun Zheng, Michał Gogacz, Cristian Radu, Damian Kaufmann, Yihan Ling, Adam Rokosz..... 47

Modeling of Syngas Production from Biomass Gasification Using Aspen Plus

Natalia Dulęba, Marcin Moździerz, Alicja Klimkowicz..... 49

Critical Mineral Security and Macroeconomic Resilience after the EU Critical Raw Materials Act: A Multiple-Outcome Synthetic-Control Assessment

Atif Khan, Artur Wyrwa 51

Morphological Enhancement of A-Site Deficient and B-Site Substituted NdBa-Based Cobalites for High Performance IT-SOC Electrodes

Rameez Zafar, Amir Sultan, Laiba Amir, Kun Zheng 53

Redox-Induced Exsolution in Multicomponent Perovskite Electrodes for Solid Oxide Cells

Zihao Chen, Kun Zheng 55

Commercial Fluid Catalytic Cracking Catalysts for Polymer Chemical Recycling

Oliwia Rogala, Karolina A. Tarach, Agata Kordek, Yuying Shu, Jean-Pierre Gilson, Louwanda Lakiss, Kinga Góra-Marek..... 57

Inclusion of Nuclear Energy in a Renewable Energy-Based Mix

Duarte M. Sousa, Maria Margarida Faustino Pinheiro, Bernardo Miguel Grilo Marçal 59

Surface Reconstruction Enables High-Performance and Fluctuation-Resistant Cathodes for Proton Ceramic Fuel Cells

Youmin Guo, Mengen Shao..... 62

Mechanistic Insights into CO_x Methanation of CO_2/CO Mixtures over Nanostructured NiO–CeO_2

Ivan Martinez-Lopez, Juan Bueno-Ferrer, Iris Martin-Garcia, Esteban Guillen-Bas, Arantxa Davo-Quinonero, Virginia Perez-Dieste, Dolores Lozano-Castello, Agustin Bueno-Lopez 64

Natural Materials Powering Tomorrow's Buildings

Verónica de Zea Bermudez 66

Influence of Alkali Species on the Work Function of Cobalt Materials: Combined Experimental and Theoretical Insights

Mariia Bordulenko, Andrzej Wójtowicz, Filip Zasada, Witold Piskorz, Andrzej Kotarba, Gabriela Grzybek 68

From Microscale Pyrolysis Characterisation to Aspen Plus Process Modelling: Preliminary Pilot-Scale Assessment of Fuel-Range Hydrocarbon Separation and Recovery from Polypropylene Waste

Łukasz Korzeniowski, Mariusz Wądrzyk, Abul Hassan Quddusi, Chunfei Wu, Aneta Magdziarz .. 70

Reduction-Induced Changes in the Chemical State and Surface Dispersion of Potassium on Fe_2O_3

Andrzej Wójtowicz, Ivan Martinez Lopez, Andrzej Kotarba, Gabriela Grzybek 72

Creating and Adjusting Iron-Based Perovskites for Potential Use in Waste Biomass Combustion Through Chemical Looping Processes

Ewelina Ksepko, Aleksandra Bobowska 74

The Influence of Coal Ash on the Durability of Titanium-Containing Perovskite Oxygen Carriers

Aleksandra Bobowska, Ewelina Ksepko 75

Zn Sites in Zeolites During CH_4 and CO_2 Transformation – How the Zeolite Matrix Shapes the Catalytic Activity

Julia Sobalska, Agnieszka Kornas, Mathieu Vidal, Kinga Mlekodaj, Olena Tynkevych, Dalibor Kaucky, Dariusz Wardecki, Milan Bernauer, Miloslav Lhotka, Przemysław Rzepka, Kinga Góra-Marek, Edyta Tabor 76

Application of CO_2 and Manganite Mineral as Oxidants in Municipal Solid Waste Gasification

Ewelina Ksepko, Uzeru Haruna, Rui Zhang 78

Study on the Steam Gasification of Chars from the Pyrolysis of Polyester, Cotton and Their Mixtures

Piotr Soprych, Grzegorz Czerski, Katarzyna Śpiewak, Jarema Stańczyk 79

Formation of Potassium Ferrites during Reduction of K/Fe_2O_3 Systems: A Study of Fischer-Tropsch Synthesis Catalysts

Andrzej Wójtowicz, Mariia Bordulenko, Iván Martínez López, Marcin Oszajca, Joanna Gryboś, Józef Korecki, Kinga Freindl, Nika Spiridis, Andrzej Kotarba, Gabriela Grzybek 80

Efficient Nitrous Oxide Electrochemical Hydrogenation via Defect-Engineered Protonic Ceramic Electrolysis Cells

Zilin Ma, Yan Chen 82

Dynamic Iron Sites in Ferrierite During CO_2 and CH_4 Conversion

Kinga Mlekodaj, Agnieszka Kornas, Julia Sobalska, Oliwia Rogala, Karolina Tarach, Lukáš Grajciar, Carlos Bornes, Dariusz Wardecki, Przemysław Rzepka, Dalibor Kaucký, Olena Tynkevych, Kinga Góra-Marek, Edyta Tabor 83

Identification of Gas Phase Parameters in Water-Air Flow in A Horizontal Pipeline

Patryk Marczak, Marcin Zych, Andrzej Mrowiec, Artur Andruszkiewicz, Piotr Piechota, Ariel Dzwonkowski, Olena Ulitska, Anna Golijanek-Jędrzejczyk, Katarzyna Zbroja, Marek Jaszczur 85

Biopolymer-based Hydrogel Electrolytes for Energy-efficient Smart Windows

Ana Queijo, Yasmine Fernine, Tomé Júnior, Verónica de Zea Bermudez, Rosa Rego 86

High-Entropy B-Site Engineering Coupled with In Situ Exsolution for High-Performance Sr-Free $LaCrO_3$-Based Fuel Electrodes in Reversible Solid Oxide Cells

Ziheng Yi, Hao Wang, Xu Xu, Linghong Luo, Liang Cheng, Leying Wang, Kun Zheng 88

Design and Construction of Safe High-Energy-Density Zinc-Halogen Batteries

Panpan Zhu, Haibo Hu 90

Do Municipal Advantages Persist? From Photovoltaics to Energy Storage in Poland's "Mój Prąd" Programme

Przemysław Grzelczyk, Aldona Mrówczyńska-Kamińska 91

Insights into the MTH Reaction over SSZ-13 by Operando Spectroscopy and MCR-ALS Analysis

Agata Kordek, Anna Walczyk, Karolina Tarach, Kinga Góra-Marek 92

Zn-Modified Zeolites with Different Topologies for Catalytic Cracking of Polypropylene

Kamil Zawadziński, Shinya Kokuryo, Kinga Góra-Marek, Karolina A. Tarach, Edyta Tabor, Norikazu Nishiyama, Oliwia Rogala, Agata Kordek 94

A General Metal Acetate-Assisted Alcohol Thermal Strategy to Fabricate Flexible Carbon Nanofiber Films for Supercapacitors

Helin Niu, Wei Song 96

Cation-Driven Charge Modulation and In-Situ Exsolved Nanoparticles Enable a Self-Assembled Cathode for Proton Ceramic Solid Oxide Cells

Mengen Shao, Youmin Guo 97

Estimation of Diffuse Solar Radiation Using a Machine Learning Approach

Olushola Olapade, Szymon Wieteska, Marek Jaszczur 98

Dynamic Interface and Lattice Defect Engineering of Perovskite Electrodes for Intermediate-Temperature Solid Oxide Cells

Kun Zheng 99

Aminal- and Imine-Linked Covalent Organic Framework Thin Films for Solar Energy Conversion

Tomasz Polczyk, Jakub Ostapko, Jan Nawrocki, Sylwester Gawnikowki, Joanna Gryboś, Andrzej Adamski 101

Utilisation of Cenospheres as Support for CuO- and ZnO-Based Catalysts for Redox Processes of Environmental Importance

Tomasz Polczyk, Paweł Rybowicz, Allison Proszowska, Yana Vitushynska, Bogdan Samojeden, Monika Motak, Agata Łamacz, Andrzej Adamski.....103

Tuning Hydrogen Sorption in $La_{1-x}Tb_xNi_{5-y}Sn_y$ Intermetallics: Effects of Tb and Sn Substitution on Structure and Storage Properties

Andrzej Budziak, Julia Karweta, Maksymilian Skrzypiec 104

Tailoring the Structural and Electrochemical Properties of Fe-based $La_{1-x}Sr_xFe_{0.7}Co_{0.2}Ni_{0.1}O_{3-\delta}$ Perovskite Oxides as Cathode Materials for IT-SOFCs

Laiba Amir, Amir Sultan, Rameez Zafar, Kun Zheng 106

Pyrolysis of Oxidized Bitumen Residue: Preliminary Investigation of Gas and Solid Products

Małgorzata Cierpińska 108

Mn-Co-Cu-Doped Potassium Silicate Glass as a Catalyst for Simultaneous Combustion of Soot and Ethylene

Piotr Legutko, Patrycja Przedwojska, Gabriela Grzybek, Michał Dziadek, Mateusz Marzec, Katarzyna Cholewa-Kowalska, Andrzej Adamski 110

An Energy Management Framework for Peer-to-Peer Energy Trading under Preference Uncertainty

Pablo Benalcazar, Maciej Kalka, Despoina Antoniadou 112

Ammonia Content as One of the Important Parameters Determining Pathways for the Efficient Valorization of Fly Ashes from the Energy Sector

Andrzej Adamski, Paweł Rybowicz, Michał Mochnaczewski, Stefania Wasiela, Michal Marko, František Šoukal 113

Research on the Effect of Solvent Processing on Changing the Low-Temperature Properties of Jojoba Oil

Stefan Ptak.....115

Real-World Emissions from Polish Waste-to-Energy Plants in the Context of Evolving EU Regulatory Requirements

Anna Korzeniewska, Katarzyna Szramowiat-Sala 116

Waste-to-Energy Plants under Evolving Environmental and Climate Requirements: From Emission Control to Climate Neutrality

Anna Korzeniewska, Weronika Stępak, Katarzyna Szramowiat-Sala, Jerzy Górecki.....118

Advanced Materials and System Integration for Thermal and Electrochemical Energy Conversion

Ming Chen, Mehrdad Faraji, Emil Riis Hansen, Emil Frederik Tauris, Akhil Panicker, Rafael Nogueira Nakashima, Soheil Khosravi 119

Effect of the Si/Al Ratio of Zeolite ZSM-5 on the Performance of Cu-Based NH_3-SCR of NO Catalysts Derived from HKUST-1

Jakub Mokrzycki, Katarzyna Rączka, Monika Motak..... 121

Spatio-Temporal Complementarity of Photovoltaic Systems Across Poland

Erkin Jafarov, Marek Borowski, Marek Jaszczur 123

Pyrolysis of Wastewater Sludges: Yield and Composition Differences Between Municipal and Industrial Feedstocks

Dorota Makowska, Karolina Kolarz, Roksana Muzyka, Przemysław Grzywacz, Katarzyna Kapusta 124

Development and Demonstration of an Intelligent Cooling System for Blast Furnace Cooling Circuit Integration and Increased Operational Reliability

Marek Berliński 125

Fibre-Dependent Thermal Decomposition Behaviour of Textile Materials

Marcelina Bury 126

Electrochemical and Thermochemical Pathways to E-Chemicals and Solar-Chemicals

Massimo Santarelli 127

Development of Numerical Models for Sodium-Cooled Fast Reactors for Thermal-Hydraulics, Neutronics, and Nuclear Data Library Preparation

Anna Bała, Mikołaj Oettingen, Katarzyna Szarłowicz..... 128

Contemporary Trends of Using Hydrogen as an Energy Storage and Carrier in the Development of Sustainable Railway Transport

Magdalena Dudek, Andrzej Raźniak 130

Monte Carlo Simulation of Spallation Neutron Production in an Accelerator-Driven System

Eyvaz Teymurov, Mikołaj Oettingen 131

Numerical Investigation of Vortex Shedding and Heat Transfer from a Heated Circular Cylinder

Patrycja Bukowiec, Mateusz Marcinkowski, Jan Taler 133

Influence of PEM Electrolyzer Sizing and Part-Load Operation on Green Hydrogen Production from Residential PV Surplus

Szymon Wieteska, Olushola Olapade, Marek Jaszczur..... 134

Assessment of Sewage-Sludge-Derived Biochars for Mercury Removal from Coal Flue Gas

Karolina Kolarz, Dorota Makowska, Jerzy Górecki, Cezary Czosnek, Katarzyna Sztybel, Piotr Burmistrz 136

Numerical Analysis of Multiphase Flow Using Multifluid VOF Model and Gamma-Ray Absorption

Patryk Marczak, Marcin Zych, Marek Jaszczur.....137

Spatiotemporal Assessment of PM_{10} Oxidative Potential at Traffic-Influenced and Urban Background Sites in Kraków

Dominika Uchmanowicz, Agnieszka Orzechowska-Zięba, Eliza Wolak, Anna Nowak, Katarzyna Styszko.....139

Chemical Valorisation of Polyamide–Elastane Textiles through Alkaline Glycol Solvolysis

Lyudmila Slobodkina, Zuzanna Kusz, Roksana Muzyka, Marcin Sajdak,Szymon Sobek, Sebastian Werle.....141

Occurrence and Phase Distribution of selected OH-PAHs in Municipal Wastewater Treatment Plants

Zuzanna Prus-Frączek, Karolina Cwynar, Laura Węgrzyn, Justyna Pyssa, Katarzyna Styszko.....143

Effects of Europe's Energy Transition on Temporal and Interannual Variability in Equivalent Black Carbon (eBC) in Kraków, Poland

Rakshit Jakhar, Lucyna Samek, Katarzyna Styszko.....145

Application of Hydrotalcite-Derived Ni-Ce-Ca Catalysts for CO_2 Methanation

Tomasz Piechówka, Agnieszka Szymaszek-Wawryca, Konrad Świerczek, Monika Motak 147

Analysis of Concentrations and Environmental Mass Loads of Hydroxylated Polycyclic Aromatic Hydrocarbons (OH-PAHs) in Municipal Wastewater

Karolina Cwynar, Laura Węgrzyn, Zuzanna Prus-Frączek, Justyna Pyssa, Elżbieta Sochacka-Tatara, Agnieszka Pac, Katarzyna Styszko.....148

Cradle-to-Gate Life Cycle Assessment of a Multi-Fibre Composite Battery Housing System for a Solar Electric Vehicle: Environmental Hotspot Analysis and Eco-Design Implications

Oluwapelumi John Oluwalana, Katarzyna Grzesik.....150

Negative Thermal Expansion Materials: An Innovative Tool for TEC Adjustment in Solid Oxide Fuel Cells

Piotr Winiarz, Ming Chen, Kun Zheng, Konrad Świerczek.....152

Sustainable Urban Air Quality Monitoring: Determination of Equivalent Black Carbon Concentrations and Mass Absorption Cross Sections (MAC) Using Multi-Wavelength Absorption Black Carbon Instrument (MABI) in Athens and Krakow

Lucyna Samek', Rakshit Jakhar, Anna Ryś, Stefanos Papagiannis, Vassiliki Vassilatou, Stergios Vratolis, Evangelia Diapouli.....154

Tailoring SFM-Based Electrodes for Solid Oxide Cells: Effects of A-Site Deficiency, Morphology, and Nickel Substitution

Michał Gogacz, Kun Zheng 155

Effect of Aluminum Content on the Phase Stability, Microstructure and Hardness of $(TiZrHfNbV)_{100-x}Al_x$ Reduced-Activation Complex Concentrated Alloys

Agnieszka Buczkowska-Fertała, Amadeusz Łaszcz, Michał Biały, Mariusz Hasiak 157

From Fabric to Fuel: Pyrolysis and Co-Pyrolysis-Based Valorization of Textile Waste — Energy Properties versus Ecotoxicological Risk

Piotr Plata, Katarzyna Śpiewak, Grzegorz Czerski, Faustyna Wierońska-Wiśniewska 160

Iron(III)–ligand complexes as activators of peracetic acid in advanced oxidation processes

Patrycja Zawiślak, Justyna Kapelewska, Urszula Kotowska 162

Numerical Investigation of Aluminum Metal Foam Integration in a Sand-Based Thermal Energy Storage System

Homa Maksymilian', Sornek Krzysztof, Sergio Nardini, Bernardo Buonomo, Hala Salhab 164

Long-Term Transformation of Energy Demand in Poland's Service Sector to 2050

Marcin Pluta, Artur Wyrwa, Maciej Raczyński, Janusz Zyśk, Patrycja Rzeszut 166

From Marine Plastic Inventories to Valorisation Feedstock: Assessing the MPW Resource Base within the CUPOLA Project

Aleksandra Hudek-Pietras, Bartłomiej Kowal, Konrad Perzyński, Wenzhong Liu,Mariusz Wądrzyk, Marek Lewandowski, Aneta Magdziarz 168

Application of Design of Experiments (DoE) to methanation process design

Marek Inger, Karolina Grzęda, Agnieszka Dobrzyńska-Inger, Bogdan Samojeden 170

Innovative Two-Stage Blast Furnace Gas Cleaning Technology Implemented at Blast Furnace no 2 in ArcelorMittal Poland Dąbrowa Górnicza Plant

Marianna Czaplicka, Marian Niesler, Arkadiusz Ryfa, Michał Kocot 171

Hybrid Bio-Coke: A Route Towards Renewable Carbon Use for Blast Furnace Ironmaking

Michał Rejdak, Anna Rodź, Aneta Michałek, Małgorzata Wojtaszek-Kalaitzidi, Bartosz Mertas, Leszek Grudziński, Serhat Türkyılmaz, Erdal Ünal 172

Optimization of Infiltration Strategies for Enhanced Stability of Solid Oxide Electrolysis Cells Under SOE and Co-SOE Operation

Anna Niemczyk-Sobieszek, Julia Jeżewska, Alicja Lubańska, Krystian Machaj, Stanisław Szumowski 174

Voltage Assessment During Faults Occurring in the Vicinity of Photovoltaic Power Plants

Flaviu Mihai Frigura-Iliasa, Krzysztof Sornek, Mihaela Frigura-Iliasa, Doru Vatau 176

Design and Fabrication of MXene-Based Micro-Supercapacitors

Haibo Hu 177

Enhancing Metaheuristic Energy Management Systems with LargeLanguage Models for Smart Grid Optimization

Jakub Grela, Dominik Latoń 178

From Photovoltaic Generation to Battery Storage: The Power System of a Solar Racing Boat

Natalia Gałaś', Maciej Piofczyk, Kacper Sacha, Szymon Lenar, Michał Zieliński, Julia Czekańska, Krzysztof Sornek 180

Defect-Driven CO_2 Capture by Hydrotalcite-Derived Sorbents: Linking Surface Basicity with CO_2 Activation

Małgorzata Zimowska, Jerzy Podobiński, Jerzy Datka 182

Life Prediction and Degradation Diagnostics of Power System Equipment

Anna Jarosz-Kozyro 184

HAZOP-Based Qualitative and Semi-Quantitative Risk Assessment for Underground Hydrogen Storage (UHS) in Depleted Oil and Gas Reservoirs

Manal AlShafi, Canan Acar, Ahmad Abushaikha, Yusuf Bicer 185

Physics-Informed Digital Twins for Identifying Thermodynamic Flexibility in Heat Pump and Thermal Storage Systems

Adam Mroziński', Rafał Andrzejczyk, Jakub Grela, Belayneh Ayalew 187

Energy Data Analytics for Improving Industrial Energy Efficiency

Patrycja Zubień, Kamil Misiurek, Tadeusz Olkuski 190

From Wastewater to Public Health: Harnessing Water-Based Epidemiology for Community and Environmental Health Surveillance

Barbara Kasprzyk-Hordern 192

Comparative Methodologies for Structural and Hybrid Power-Market Price Modelling

Juliette A. van Delden, Arnoud P. Higler 193

Exergy Analysis of Hydrogen Supply Chains: Methods, Applications and a Framework for Consistent Assessment

Arnoud P. Higler 194

Techno-Economic and Environmental Assessment of a Hybrid Cogeneration and Heat Pump System for District Heating Modernization

Karol Sztekler, Mateusz Płatek, Witold Płatek, Łukasz Mika 195

Synthesis and Characterisation of Carbon Nanodots for CO_2 Capture Applications

Małgorzata Hasal, Izabela Rzeźnicka, Jakub Szczurowski 197

Influence of Accident-Tolerant Fuel Cladding Concepts on Hydrogen Accumulation and Mitigation in PWR Containments: A Reduced-Order Screening Assessmentment

Tomasz Bury, Kacper Bury, Sławomir Zdziebło 199

Circular Economy in Cementitious Systems: Valorization of Phosphogypsum and Slag in Low-Carbon Alkali-Activated Binders for Winter Decarbonized Construction

Povilas Telešius, Danutė Vaičiukynienė, Gabija Vinikaitė-Bačinskienė, Rėda Bistrickaitė 201

Impact of NaCl Contamination on the Durability and Performance of Reversible PEM Fuel Cells

Monika Piech, Bartosz Adamczyk, Magdalena Dudek, Adam Szurlej 203

Methane Pyrolysis as an Alternative Source of Hydrogen

Michał Wojtasik, Grażyna Żak, Wojciech Krasodomski 204

How Human Activity on Long Weekends Affect Air Pollution with Fine Particulate Matter (PM1 and PM2.5) in the Coastal Zone of the Baltic Sea (Gdynia Case Study)?

Eliza Wolak, Justyna Pyssa, Agnieszka Orzechowska-Zięba, Łukasz Nuckowski, Katarzyna Styszko, Anita Urszula Lewandowska 206

Variability of Hydroxylated Polycyclic Aromatic Hydrocarbons (OH-PAHs) in Raw and Treated Municipal Wastewater

Justyna Pyssa, Laura Węgrzyn, Zuzanna Prus-Frączek, Karolina Cwynar, Dominika Uchmanowicz, Katarzyna Styszko.....208

Effect of Cerium and Lanthanum Addition on Vermiculite-Supported Nickel Catalysts for CO2 Methanation

Michał Szymaszek', Agnieszka Szymaszek-Wawryca, Monika Motak 210

Influence of Oxidative Modification of Activated Carbon on the Removal of Organic Micropollutants from Water

Agnieszka Orzechowska-Zięba, Laura Węgrzyn, Eliza Wolak, Elżbieta Vogt, Dominika Uchmanowicz, Justyna Pyssa, Gabriela Kulka, Katarzyna Styszko 212

Experimental Investigation of Fuel-Cell Waste Heat Recovery for Thermal Management of a Metal-Hydride Hydrogen Storage Cylinder

Jakub Cebo, Ignacy Czajkowski, Jakub Ekes, Norbert Jamrozik, Kacper Wądołkowski, Stanisław Pilarski 214

Modular Reactor for Direct and Indirect Electrolysis Manufactured Using 3D Printing: From Dimensional Prototyping with Cost-Effective PETG to a Leak-Tight ABS Process Reactor

Aleksandra Chwała, Alekander Pizoń, Aleksander Piasecki, Wiktor Piekarski, Jacek Kowalczyk, Maciej Siekierski.....216

Heavy Industry Waste as an Alternative Means of Supporting Fire and Rescue Actions

Radosław Wójcik, Anna Magiera, Aneta Magdziarz.....218

PROZA: A Sectoral Econometric Model for Long-Term Energy Demand Forecasting in Poland

Wojciech Suwała, Janusz Zyśk, Artur Wyrwa, Marcin Pluta, Maciej Raczyński.....220

Modeling of Electrochemical Processes Occurring in Porous Materials by Means of a TLM-Based Impedance Model

Wiktor Piekarski, Jacek Kowalczyk, Maciej Siekierski 222

Weather-Related Price Patterns in the Polish Electricity Market

Patryk Garnek, Mikołaj Rzepka, Szymon Podlasek 224

Development of a Modular Dual-Atmosphere High-Temperature Electrochemical Furnace Insert

Aleksander Pizoń, Maciej Siekierski 225

1D Transient Heat Transfer Model for Inverse Thermal Conductivity Retrieval for Porous Materials

Mikołaj Woźny, Jakub Dworczyk, Mieszko Tokarski 227

Beyond Typical Weather: Assessing Residential HVAC Capacity Adequacy During Historical and Future Heatwaves Across Climate Zones

Majid Rafi, Muhammad Asif 228

Comparison of Model-Less and Model-Based Approaches to Multi-Phenomena Immittance Data

Jacek Kowalczyk', Paweł Kulesza, Wiktor Piekarski, Aleksander Pizoń, Aleksander Piasecki, Aleksandra Chwała, Maciej Siekierski 230

Photo-Oxidative Aging of Plastics in Indoor Environments: Chemical Emissions and Markers of Polymer Degradation in Airborne Particulette Matter

Anna Nowak, Katarzyna Styszko 232

Beyond Decarbonization: Reframing the Energy Transition Through Systems Modelling, Material Constraints and Economic Futures

Cesar Yalderrama, Sergi Yinardell, Sacha Dawid, Luke Quinn, Julia Otero, Francesca Stefanini . 233

Integrating Environmental Emissions and Pollution Control into Ghana's Mining Sector: Pathways to a Circular Economy and Sustainable Energy Transition

Kamal Razak 235

Electrochemical Performance and Intercalation Mechanism of Prussian Blue Analogues for Na-Ion Cells

Kamil Michalski, Marta Wolczko, Janina Molenda 236

Non-Euclidean Metrics of Similarity Applicable to Semi-Automated Analysis of Multicomponent Immittance Spectra of Electroactive Materials and Processes

Maciej Siekierski, Jacek Kowalczyk, Aleksandra Ossowska-Górzyńska, Wiktoria Zieńkowska, Władysław Wieczorek, Paweł Kulesza, Janusz Lewiński 237

Benchmarking Local Energy Market Mechanisms in a Virtual Power Plant

Oskar Antonik, Pablo Benalcazar 239

Electrospinning: Advanced Nanofiber Production

Marcin Moszczak 240

Research Tools for Energy Materials and Fuel Emissions

Mateusz Ścigaj 241

Methodology of Determination of Hydroxyl Derivatives of PAHs by LC-MS/MS

Laura Węgrzyn, Karolina Cwynar, Zuzanna Prus-Frączek, Justyna Pyssa, Katarzyna Styszko 243

Forecasting Prices for Balancing Services in the Balancing Market in Poland

Michał Rybiński, Piotr Dzierwa 245

Improving the Energy Efficiency of Natural Gas-Fired Cogeneration Systems: Energy and Economic Assessment

Piotr Dzierwa, Marcin Trojan, Karol Kaczmarski, Jan Taler, Dawid Taler, Patryk Peret 247

Emission Intensity of Hydrogen Production by Methane Pyrolysis and Steam Methane Reforming

Tomasz Chmielniak, Marek Ściążko, Wojciech Nowak, Leszek Stępień 250

Ni-Al-Co Hydrotalcites as Precursors of CO_2 Methanation Catalysts: Effect of Cobalt Substitution for Nickel

Bogdan Samojeden, Katarzyna Bania, Monika Motak 252

Assessment of Selected Valuable and Critical Elements in Metallurgical Wastes

Alicja Barczyk, Marta Seman, Katarzyna Król, Michał Szwamel, Natalia Skowrońska, Karolina Kolarz, Piotr Soprych, Dorota Makowska 253

Robust Regional Energy Planning under Data Uncertainty: A TIMES-Based Analysis of Sardinia to 2050

Roberto Ricciu, Pier Luca Maria Buonomo 254

Hollow-SiO_2@CuZnMgAl-LDH-derived Catalyst for Direct CO_2 Hydrogenation to Methanol

Tomasz Kondratowicz, Dermot O'Hare, Monika Motak 255

Material Requirements of the Polish Power Sector Transition: Linking Electricity Demand and Energy System Models

Patrycja Rzeszut, Artur Wyrwa, César Valderrama, Maciej Raczyński 257

From Carbon Dioxide to Alternative Fuels: Catalytic Routes for CO_2 Utilization

Bogdan Samojeden, Monika Motak 258

Identification of the Parameters of a Two-Zone Energy Balance Model of a Solar Domestic Hot Water Storage Tank Subject to Physical Constraints, Based on Field Operation Data

Wiktor Filipek, Barbara Tora, Krzysztof Broda, Stanisław Pietrzyk 259

Synthesis of GIS and LTA Zeolites from Fly Ash and Their Application as Adsorbents of Phosphate Ions from Aqueous Solution

Jakub Mokrzycki 261

Modernization of the Drivetrain for the "Zephyr AGH" Hybrid Vehicle

Maciej Kulawik, Przemysław Guziak, Mikołaj Miodoński, Jakub Ekes, Kamil Iwańczyk, Jakub Kurek, Tomasz Maciejowski, Joanna Michalik, Jafar Alijev, Piotr Miroń, Olaf Sulima, Joanna Domańska, Tadeusz Olkuski 263

In-Mold Embedding of Photovoltaic Cells in the Wings of an Unmanned Solar-Powered Aircraft

Izabella Rosikoń, Ignacy Kępa, Filip Gajda, Marta Łopusiewicz, Michał Pietrzykowski, Kacper Krempa, Filip Materowski, Jakub Konior, Krzysztof Sornek.....264

Contribution of Combustion to Ambient Particles in Different Parts of the World

Andre Prevot.....266

Experimental and Numerical Investigation of Micro-Wind Turbine Performance under Urban Airflow Conditions

Krzysztof Sornek, Flaviu Mihai Frigura-Iliasa, Maksymilian Homa, Zuzanna Topolska.....267

Co-creation between Local Authorities and Grassroots Initiatives in Sustainable Transitions: Evidence from Three Polish Case Studies

Aleksandra Komorowska, Wojciech Kowalik, Wit Hubert, Monika Pepłowska, Dominik Kryzia, Lidia Gawlik.....269

Numerical and Experimental Studies on the Limitations of Cold Starting an Anion-Exchange Membrane Electrolyser and the Optimization of Green Hydrogen Production in an Off-Grid System

Andrzej Raźniak, Łukasz Mazur, Magdalena Dudek.....271

Entropy- and Thermal-Driven Control of Local Structure in Disordered Rock Salt Cathodes

Yanxin Wang, Konrad Świerczek.....272

Nb-modified $Li_{1.02}Ni_{0.905}Co_{0.043}Al_{0.052}O_2$ Cathode for High-Energy-Density Li-ion Cells: Development, Optimization, and Degradation Studies with Transformer Based Model

Boya Fu, Boyang Fu, Marcin Kurdziel, Konrad Świerczek.....273

Rare-Earth Engineering of Oxygen-Electrode Materials for Solid Oxide Cells

Jacek Winiarski, Piotr Winiarz, Konrad Świerczek.....275

Temporal Spectral Analysis in Electrochemistry

Aleksander Piasecki, Jacek Kowalczyk, Maciej Siekierski.....277

Author Index.....279

Keyword Index.....287

Scientific Committee

Professor Monika Motak (AGH University of Krakow) – **Chair**
Professor Adam Smoliński (Central Mining Institute)
Professor Agnieszka Wiercińska-Nosal (Maria Curie-Skłodowska University)
Professor Aleksandra Komorowska (Mineral and Energy Economy Research Institute of the Polish Academy of Sciences)
Professor Ali Cemal Benim (Hochschule Düsseldorf)
Professor Andre Prevot (Paul Scherrer Institute)
Professor Andrzej Adamski (Jagiellonian University)
Professor Andrzej Szarata (Cracow University of Technology)
Professor Aneta Magdziarz (AGH University of Krakow)
Professor Anita Lewandowska (University of Gdańsk)
Professor Anna Białk-Bielińska (University of Gdańsk)
Professor Anne Kasper-Giebl (TU Wien)
Professor Artur Wyrwa (AGH University of Krakow)
Professor Barbara Kasprzyk-Hordern (University of Bath)
Professor Barbara Tora (AGH University of Krakow)
Professor Beatrice Castellani (University of Perugia)
Professor Cesar Alberto Valderrama Angel (Universitat Politècnica de Catalunya)
Professor Dawid Taler (Cracow University of Technology)
Professor Dorota Rutkowska-Żbik (Jerzy Haber Institute of Catalysis and Surface Chemistry)
Professor Duarte de Mesquita e Sousa (Instituto Superior Técnico)
Professor Flaviu Mihai Frigura-Iliasa (Polytechnic University of Timişoara)
Professor Francesco Calise (University of Naples Parthenope)
Professor Grzegorz Brus (AGH University of Krakow)
Professor Izabela Sówka (Wroclaw University of Science and Technology)
Professor Jacek Leszczyński (AGH University of Krakow)
Professor Jan Taler (Cracow University of Technology)
Professor Jerzy Lis (AGH University of Krakow)
Professor Joanna Gościańska (Adam Mickiewicz University)
Professor Jolanta Kumirska (University of Gdańsk)
Professor Józef Pacyna (NILU – Norwegian Institute for Air Research)
Professor Karol Sztekler (AGH University of Krakow)
Professor Katarzyna Styszko (AGH University of Krakow)
Professor Katarzyna Szarłowicz (AGH University of Krakow)
Professor Konrad Świerczek (AGH University of Krakow)
Professor Kun Zheng (AGH University of Krakow)
Professor Łukasz Mika (AGH University of Krakow)
Professor Maciej Paszyński (AGH University of Krakow)
Professor Magdalena Dudek (AGH University of Krakow)
Professor Magdalena Jaremkiewicz (Cracow University of Technology)
Professor Małgorzata Wilk (AGH University of Krakow)
Professor Małgorzata Wiśniewska (Maria Curie-Skłodowska University)
Professor Marcin Sosnowski (Jan Dlugosz University in Czestochowa)
Professor Marcin Trojan (Cracow University of Technology)
Professor Marek Inger (AGH University of Krakow)
Professor Maria Sozańska (Silesian University of Technology)
Professor Martin Ostoja-Starzewski (University of Illinois)
Professor Massimo Santarelli (Politecnico di Torino)
Professor Monika Wawrzkiewicz (Maria Curie-Sklodowska University in Lublin)
Professor Patrick Da Costa (Sorbonne University)
Professor Paweł Ocłoń (Cracow University of Technology)
Professor Paweł Rostkowski (NILU – Norwegian Institute for Air Research)

Professor Piotr Burmistrz (AGH University of Krakow)
Professor Piotr Dzierwa (Cracow University of Technology)
Professor Piotr Kuśtrowski (Jagiellonian University)
Professor Piotr Rutkowski (Wrocław University of Science and Technology)
Professor Robert Pietrzak (Adam Mickiewicz University)
Professor Roberto Ricciu (University of Cagliari)
Professor Sabina Dołęgowska (Jan Kochanowski University in Kielce)
Professor Sara Castiglioni (University of Milan)
Professor Sergio Nardini (The University of Campania "Luigi Vanvitelli")
Professor Tadeusz Dziok (AGH University of Krakow)
Professor Urszula Kotowska (University of Białystok)
Professor Verónica Cortés de Zea Bermudez (University of Trás-os-Montes and Alto Douro)
Professor Vincenzo Bianco (University of Naples Parthenope)

Organizing Committee

Professor Katarzyna Styszko (AGH University of Krakow) – Chair
Professor Artur Wyrwa (AGH University of Krakow) – Vice-Chair
Professor Jan Taler (Cracow University of Technology) – Vice-Chair

Professor Tadeusz Dziok (AGH University of Krakow) – Secretary
M.Sc. Wioletta Więcław (AGH University of Krakow) – Chief Financial Officer
Professor Magdalena Jaremkiewicz (Cracow University of Technology)
Professor Marcin Trojan (Cracow University of Technology)
Professor Piotr Dzierwa (Cracow University of Technology)
Professor Krzysztof Sornek (AGH University of Krakow)
Dr. Janusz Zyśk (AGH University of Krakow) coordination of publications
Dr. Andrzej Raźniak (AGH University of Krakow) coordination of partners and sponsors
Dr. Jakub Szczurowski (AGH University of Krakow) web of conference/ registration
Dr. Grzegorz Jodłowski (AGH University of Krakow) web of conference/ registration
Dr. Krzysztof Kogut (AGH University of Krakow) coordination of Microsymposium
Dr. Bogdan Samojeden (AGH University of Krakow) monography/proceedings of abstracts
M.Sc. Magdalena Starzec (AGH University of Krakow) coordination of foreign guests
M.Sc. Barbara Wolańska (AGH University of Krakow) administration
M.Sc. Wojciech Kalawa (AGH University of Krakow) administration
M.Sc. Maciej Skiba (AGH University of Krakow) administration
M.Sc. Olga Pidgorna (AGH University of Krakow) PR
M.Sc. Anna Nowak (AGH University of Krakow) administration
Iwona Pawłowska (AGH University of Krakow) administration

Preface

It is our great pleasure to present the Book of Abstracts of the 6th EFE Energy Fuels Environment International Conference (EFE 2026), held on 17-20 November 2026 at AGH University of Krakow, Poland. Over its six editions, EFE has established itself as an international forum for the exchange of scientific knowledge, the presentation of research achievements, and the development of cooperation in the fields of energy, fuels, and environmental protection.

The growing global demand for energy, the urgent need to address climate change, and the transition towards sustainable, low-emission economies pose significant challenges for science, industry, and society. Meeting these challenges requires technological innovation, interdisciplinary collaboration, responsible resource management, and integrated approaches that reconcile energy security, economic development, and environmental sustainability.

Building on the achievements of previous editions, EFE 2026 provides a platform for presenting recent scientific advances, discussing emerging technologies, and exploring innovative solutions to contemporary energy and environmental challenges. The conference brings together researchers, engineers, industry representatives, and other stakeholders, fostering scientific dialogue, knowledge transfer, and international cooperation.

The contributions collected in this volume encompass a wide range of scientific and technological topics, including advanced energy conversion processes, hydrogen production and storage, renewable energy technologies, fuel cells and electrochemical systems, catalysis, sustainable fuels, energy efficiency, environmental monitoring, pollution control, waste management, and circular economy strategies. Particular attention is also devoted to innovative materials, numerical modelling, digital technologies, and the environmental and socio-economic aspects of the energy transition.

This Book of Abstracts reflects the diversity of research conducted at universities, research institutions, and industrial organisations worldwide. The contributions range from fundamental investigations and experimental studies to numerical simulations, technological demonstrations, and interdisciplinary analyses, highlighting both the progress achieved and the opportunities for further scientific and technological development.

We hope that the findings presented at EFE 2026 will stimulate constructive discussions, encourage the exchange of ideas, and inspire new research initiatives and lasting international partnerships. We firmly believe that close cooperation between academia, industry, policymakers, and other stakeholders is essential for addressing complex energy and environmental challenges and accelerating the development of sustainable technologies.

We extend our sincere gratitude to all authors and participants for their valuable contributions to EFE 2026. We are particularly grateful to the members of the Scientific and Organising Committees for their commitment and dedication to preparing the conference. We also wish to acknowledge the generous support of our honorary patrons, institutional partners, sponsors, and media patrons, whose involvement has been instrumental in making this event possible.

Finally, we wish all participants an inspiring and productive conference, engaging scientific discussions, and an enjoyable stay in Kraków. May EFE 2026 strengthen existing partnerships, create new opportunities for collaboration, and contribute to the advancement of knowledge and technologies supporting a more sustainable energy future.

Bogdan Samojeden

Editor of the EFE 2026 Book of Abstracts
Kraków, November 2026

Hybrid type biosorbents - formulation and preparation

Grzegorz S. Jodłowski[1,*], Marta Wójcik

Keywords: biochars, pyrolysis, biosorbents, activation

ABSTRACT

The development of sustainable adsorbent materials from waste-derived feedstocks represents a promising approach to waste valorization and circular economy implementation. This study focuses on the formulation and preparation of a hybrid-type biosorbent based on spent coffee grounds and eggshell waste, with crude glycerol derived from fatty acid methyl ester (FAME) production incorporated as an additional waste-based component.

The proposed formulation consists primarily of spent coffee grounds, supplemented with approximately 10% ground eggshells, 7.5% crude glycerol, 14% water and 5% starch. [1-4] The eggshells were ground and sieved, and the fraction below 1 mm was selected for further processing. Starch was incorporated to improve the cohesion and mechanical properties of the mixture, while crude glycerol served as an additional component of the waste-based formulation. The prepared mixture was homogenized and extruded to obtain cylindrical pellets with an initial diameter of approximately 5 mm.

Following extrusion, the pellets were dried at 105 °C and subsequently subjected to pyrolysis at 800 °C under a nitrogen atmosphere (200 mL min^{-1}) for 90 min. [5] The pyrolysis process resulted in carbonization of the organic components and a reduction in pellet diameter to approximately 3 mm.

Physical activation was subsequently performed using carbon dioxide as the activating agent at 850 °C for 90 min, with nitrogen and carbon dioxide flow rates of 200 mL min^{-1} each. The activation process was based on the Boudouard reaction, which promotes carbon gasification and the development of a porous structure. [6]

Further research will investigate alternative modification strategies, including hydrochloric acid treatment and combined acid treatment followed by CO_2 activation. These approaches are intended to modify the mineral composition, surface chemistry and porous structure of the resulting materials.

The proposed approach combines waste valorization, pelletization and thermochemical conversion to produce hybrid carbon-based biosorbents. Particular attention will be paid to the influence of formulation and activation conditions on pellet integrity, textural properties and adsorption performance. The resulting materials are intended for potential application in water and wastewater treatment.

[1] Al Balushi, J et al., (2025) A Comprehensive Review on Sustainable Conversion of Spent Coffee Grounds into Energy Resources and Environmental Applications. Biomass, 5, 55. https://doi.org/10.3390/biomass5030055
[2] Babalola, B. M., Wilson, L. D. (2024) Valorization of Eggshell as Renewable Materials for Sustainable Biocomposite Adsorbents—An Overview. Journal of Composites Science, 8(10), 414. DOI: 10.3390/jcs8100414
[3] Cao, H. et al. (2020) Characteristics and mechanisms of phosphorous adsorption by rape straw-derived biochar functionalized with calcium from eggshell. Bioresource Technology, 318, 124063. DOI: 10.1016/j.biortech.2020.124063
[4] Zdanowicz, M. Et al. (2023) Study on Physicochemical Properties of Biocomposite Films with Spent Coffee Grounds as a Filler and Their Influence on Physiological State of Growing Plants. Int. J. Mol. Sci., 24, 7864. https://doi.org/10.3390/ijms24097864

[1] AGH University of Krakow, Faculty of Energy and Fuels, al. A.Mickiewicza 30, 30-059 Krakow, Poland, *jodlowsk@agh.edu.pl

[5] Jerzak, W.; Sokołowski, K.; Kalemba-Rec, I.; Magdziarz, A. (2026) Resource-Efficiency Assessment of Spent Coffee Grounds Valorization into Porous Biochars: Effect of KOH Activation Time on Pore Redistribution and Apparent CO2 Gasification Kinetics. Sustainability 2026, 18, 11117. https://doi.org/10.3390/su182111117

[6] Balla, A.; Marcu, C.; Mihet, M.; Kacsó, I.; Tripon, S.; Turza, A.; Szücs-Balázs, J.-Z. (2026) One-Step CO2-Assisted Pyrolysis of Spent Coffee Grounds: A Simpler Route to Highly Porous Biochar Compared with Two-Step Pyrolysis–CO2 Activation. ChemEngineering 10, 14. https://doi.org/10.3390/chemengineering10010014

[7] Vitoria S. Silveira et al. (2025) Demineralization of eucalyptus biochar with hydrochloric acid: A kinetic study, ENGINEERING SCIENCES • An. Acad. Bras. Ciênc. 97 (Suppl. 2) https://doi.org/10.1590/0001-3765202520250080

Research conducted with financial support from an IDUB AGH research grant: Activity 21, UB-696000-00001-Z02, application No 18399

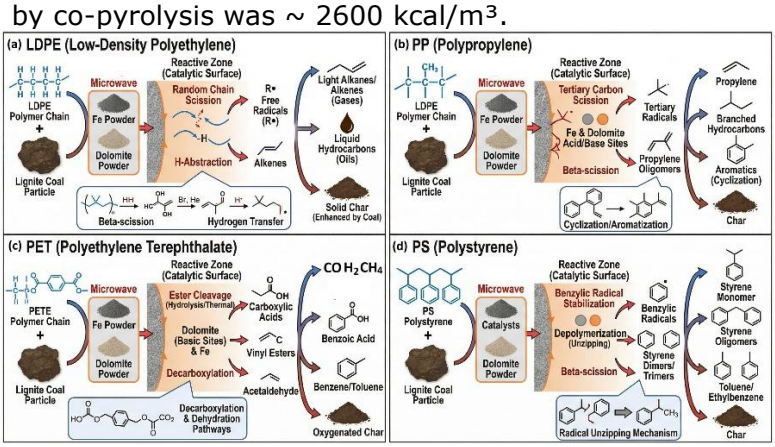
Enhanced Sustainable Production of Drop-in Fuel Precursors and High-Calorific Gas from Coal-Plastic Hybrids via Iron-dolomite Catalysed Microwave Thermochemical Conversion.

Kanak Kumar[1,*], B. Rajasekhar Reddy[1]

Keywords: Microwave-assisted co-pyrolysis, Mixed plastic waste, Iron-mediated catalysis, Drop-in fuel precursors, Energy recovery efficiency

ABSTRACT

Thermochemical conversion of plastic waste, comprising of LDPE, PP, PET and PS, the co-pyrolysis with coal, a cheap and abundant carbon-containing material, in a hybrid system is highly promising. The effects of various catalyst/susceptor systems on the energy recovery, product distributions and upgradeability of the pyrolysis oils were investigated. A total of twelve batch-type runs were carried out upto 600 °C maximum temperature and 630 W microwave power, and the runs were divided into three groups of four runs each. In the first group, dolomite was used in conjunction with activated carbon as the catalyst/susceptor. In the second group, the same dolomite was used in conjunction with iron. The third group of runs consisted of four runs, in which SiC powder was used as susceptor only to absorb the microwave energy. The quantitative distribution of the various product fractions resulting from co-pyrolysis of mixed plastics with coal, it was found that there was solid char (~ 45 wt. %) and condensable liquid (~ 49 wt. %) in large amounts, whilst the gaseous products also yielded substantial amounts (~ 57 wt. %). The liquid obtained from co-pyrolysis consisted largely of mono-aromatics and normal/iso-paraffins together with smaller amounts of naphthenes, olefins and polycyclic aromatic hydrocarbons. The distribution was found to be concentrated in the range C9 to C15 with ~ 70 wt. % of the liquid products having carbon numbers in this range. The fuel gases produced in the co-pyrolysis process consisted of H_2, CH_4 and CO, with the proportions of these various gaseous products affected to a marked extent by the catalysts used and the various types of feedstocks. The calculated higher heating value (HHV) of the gaseous products produced by co-pyrolysis was ~ 2600 kcal/m³.



[1] Department of Fuel, Minerals and Metallurgical Engineering, Indian Institute of Technology (Indian School of Mines) Dhanbad, India, * 22dr0110@iitism.ac.in

Flow Properties of Hydrophobized Fine Particulate Sorbents

Elżbieta Vogt[1]*, Eliza Wolak[1], Agnieszka Orzechowska-Zięba[1]

Keywords: powder sorbents, floodability index, flowability index, hydrophobization, flow properties

ABSTRACT

The article investigates the influence of hydrophobic surface modification on the sorption efficiency and powder flow properties of fine-grained mineral sorbents used for oil spill remediation. The study focuses on expanded perlite and expanded vermiculite, two lightweight and porous materials commonly applied for the removal of petroleum contaminants from water surfaces. The main objective was to determine whether hydrophobic treatment could improve oil sorption performance while maintaining acceptable handling and flow characteristics required for storage, transportation, and practical application.

The research involved four fractions of expanded vermiculite (VMed, VF, VSF, and VMic) and three grades of expanded perlite (EP100F, EP150, and EP180). In addition, a commercial hydrophobized perlite product, Hydroperl, was included for comparison. Hydrophobic surface modification was carried out using stearic acid and a silicone-based agent, Sarsil® H-15. The treatment was designed to create a water-repellent coating on the particle surface without altering the physical structure of the sorbents.

The effectiveness of the modified materials was evaluated through diesel oil sorption tests performed on water surfaces. The results showed a significant increase in oil sorption capacity after hydrophobic treatment. For expanded perlite, sorption capacity increased by 71–267%, whereas for vermiculite the improvement ranged from 117–467%, depending on the particle fraction and modifier used. The highest enhancement was observed for the finest vermiculite fraction (VMic), whose sorption capacity increased from 120 to 680 L/m³ after treatment with Sarsil® H-15. These findings demonstrate that hydrophobic modification effectively increases the affinity of mineral sorbents toward petroleum products while reducing water uptake.

To assess the influence of surface treatment on powder behavior, the materials were characterized using Carr's methodology. Measurements included bulk and tapped density, angle of repose, angle of fall, compressibility, dispersibility, and Hausner ratio. Based on these parameters, flowability and floodability indices were determined. These indices are widely used to evaluate the handling characteristics of powders during storage, transport, and processing operations.

The majority of hydrophobically modified sorbents maintained good powder flow properties. Flowability indices ranged from 70 to 89, corresponding to good or fairly good flowability according to Carr's classification. Hausner ratio values generally indicated low to moderate powder cohesion, suggesting that the surface treatment did not adversely affect handling performance. In some vermiculite samples, hydrophobic modification even improved powder mobility by reducing interparticle interactions.

The only significant exception was the finest perlite fraction, EP100F. After hydrophobic treatment, this material exhibited increased compressibility, stronger cohesive behavior, and reduced flowability. The authors attributed these effects to the high specific surface area of the fine particles, which promotes stronger particle interactions and agglomeration. Although such behavior may create difficulties during storage and handling,

[1] AGH University of Krakow, Faculty of Energy and Fuels, Krakow, al Mickiewicza 30, 30-059 Krakow, Poland, * vogt@agh.edu.pl

increased cohesion can reduce wind dispersion of sorbents during environmental cleanup operations.

All investigated materials showed relatively high floodability indices, indicating a tendency toward dispersion and dust formation. Therefore, appropriate precautions should be considered during industrial handling. Nevertheless, the modification process did not substantially increase floodability compared with untreated materials.

In conclusion, the study demonstrates that hydrophobic surface modification is an effective method for enhancing the performance of mineral sorbents used in oil spill remediation. The treatment significantly improves oil sorption capacity while generally preserving favorable powder flow and handling properties. Hydrophobically modified perlite and vermiculite therefore represent promising materials for environmental applications, particularly in humid conditions and on water surfaces where conventional sorbents may be less effective.

[1] R.L. Carr, Classifying flow properties of solids, Chem. Eng. 72 (1965) 69–72.
[2] H.H. Hausner, Friction conditions in a mass of metal powder, Int. J. Powder Metall. 3 (1967) 7–13.
[3] D. Schulze, Powders and Bulk Solids: Behavior, Characterization, Storage and Flow, Springer-Verlag, Berlin, Heidelberg, 2008. https://doi.org/10.1007/978-3-540-73768-1.
[4] L. Bandura, A. Woszuk, D. Kołodyńska, W. Franus, Application of mineral sorbents for removal of petroleum substances: A review, Minerals 7 (2017) 37. https://doi.org/10.3390/min7030037.
[5] M.O. Adebajo, R.L. Frost, J.T. Kloprogge, O. Carmody, S. Kokot, Porous materials for oil spill cleanup: A review of synthesis and absorbing properties, J. Porous Mater. 10 (2003) 159–170. https://doi.org/10.1023/A:1027484117065.

Acknowledgements:The authors acknowledge the financial support of AGH University of Krakow, grant number 501.00-210000-10000.

1

Natural Aluminosilicate-Supported Ni and NiCe Catalysts for CO_2 Methanation

Agnieszka Szymaszek-Wawryca[1]*, Tomasz Piechówka, Michał Szymaszek, Monika Motak

Keywords: CO_2 methanation, bentonite, kaolin, nickel, ceria

ABSTRACT

Methanation is a promising technology for the utilization of carbon dioxide (CO_2) and the production of synthetic natural gas. However, due to thermodynamic and kinetic limitations, it requires the use of efficient catalysts, with nickel being widely used as a cost-effective active phase [1]. Additionally, their performance can be further enhanced by promotion with CeO2, which improves Ni0 dispersion and surface basicity [2]. The overall cost of methanation catalysts can also be reduced by using natural aluminosilicates as supports, with particular attention to layered clays, such as bentonite and kaolin [2,3]. The structural and textural properties of these materials can be readily tailored using simple modification methods, such as thermal pretreatment [4] or chemical activation with acids or bases [5].

In this study, natural aluminosilicates (bentonite and kaolin) were investigated as environmentally friendly supports for Ni-based methanation catalysts. Prior to catalysts synthesis, the layered clays were either thermally or chemically activated to compare the effects of pretreatment routes on their physicochemical parameters. Subsequently, selected samples were modified with 15 wt.% Ni or 15 wt.% Ni and 15 wt.% Ce to determine the influence of CeO_2 promotion on the investigated systems. The samples were characterized by N_2 sorption at 77 K, XRD, H2-TPR, CO_2-TPD and evaluated in CO_2 methanation catalytic tests. The obtained results indicated that chemical activation with HNO_3 resulted in the development of a higher specific surface area compared with thermal activation. Moreover, CeO_2 promotion shifted the NiO reduction temperature towards lower values, improving the reducibility of the samples. Significantly higher CO2 conversion was observed for the Ce-promoted samples, particularly below 300 °C, resulting from not only improved redox properties, but also enhanced surface basicity, as confirmed by CO2-TPD.

Overall, the results demonstrated that layered clays can serve as promising, alternative, and environmentally friendly supports for CO_2 methanation catalysts.

[1] F. Hu, R. Ye, Z.H. Lu, R. Zhang, G. Feng, Structure–activity relationship of Ni-based catalysts toward CO_2 methanation: Recent advances and future perspectives, Energy Fuels 36 (2022) 156–169. https://doi.org/10.1021/acs.energyfuels.1c03645.

[2] K. Aimdate, A. Srifa, W. Koo-Amornpattana, C. Sakdaronnarong, W. Klysubun, S. Kiatphuengporn, S. Assabumrungrat, S. Wongsakulphasatch, W. Kaveevivitchai, M. Sudoh, R. Watanabe, C. Fukuhara, S. Ratchahat, Natural kaolin-based Ni catalysts for CO_2 methanation: On the effect of Ce enhancement and microwave-assisted hydrothermal synthesis, ACS Omega 6 (2021) 13779–13794. https://doi.org/10.1021/acsomega.1c01231.

[3] S. Tang, S. Qin, Z. Wang, L. Sang, J. Cheng, Z. Liu, Plasma-catalytic CO_2 methanation over NiO/bentonite catalysts prepared by solution combustion synthesis, Plasma Process. Polym. 21 (2024) 2400001. https://doi.org/10.1002/ppap.202400001.

Acknowledgements: Agnieszka Szymaszek-Wawryca gratefully acknowledges financial support from the National Science Centre, Poland, through the OPUS 29 grant (grant no. 2025/57/B/ST5/01462). The selected results presented herein were developed using equipment supported by the "Excellence Initiative – Research University" programme at AGH University of Krakow.

[1] AGH University of Krakow, Aleja Adama Mickiewicza 30, 30-059 Kraków, Poland, * agnszym@agh.edu.pl

Development of a One-Dimensional Transient Coking Model for Top-Charged and Stamp-Charged Systems

Mieszko Tokarski[1],*, Rafał Buczyński[1], Michał Ponikowski[2], Dariusz Zych[2], Paweł Cieślar[2]

Keywords: coke, coking, oven, numerical, model

ABSTRACT

Coking is a key sector of heavy industry, involving the thermal treatment of hard coal by pyrolysis. The main product of this process is coke, an essential substrate used in the metallurgical industry for smelting iron and steel. Furthermore, coking plants recover valuable byproducts such as coke oven gas, tar, and benzene, widely used in the chemical industry. Because coking is an energy-intensive process, proper operation is crucial, as it reduces energy consumption and release of pollutant to the environment, while maintaining high product quality and also positively impacting revenues. Therefore, computational models of the coking process are gaining significant attention, as they allow for identification of key optimal operating parameters and provide in-depth insight into the complex phenomena involved in the process [1,2,3].

The main objective of this study is to develop a one-dimensional transient model of a coking process that can predict coking time, coke-oven gas yield, and composition in relation to coal cake density, coal ultimate and proximate analysis, coke oven geometry, and thermal conditions inside heating flues. The model was developed in MATLAB to work for two coke production systems: top-charged and stamp-charged.

The most common type of coke oven is the slot-type oven, schematically shown in Figure 1 in cross-section. An average oven of this type is over 12 m long, 4-6 m high, and only 0.4-0.5 m wide. The model includes half of the oven width with a coal charge (D) in the center, heated from both sides, with the split (C) being a distance between the charge and the oven wall, and only half of one heating flue wall (B) with its corresponding heating flues (A). Only the charge is discretized (G), so the system of ordinary differential equations to be solved can be simplified, while the split and wall are both implicitly included in the boundary conditions (F). The model is based on a transient heat conduction equation as a system of ODEs using Crank-Nicholson scheme, which is then solved numerically. It is also extended with a convection matrix responsible for convective heat transfer during the movement of steam through the charge. Radiative heat transfer mechanism is accounted for be the effective thermal conductivity coefficient. The Merrick kinetic model is used for volatile species release [4], while the Ergun's equation with the continuity equation are used for steam transport (due to chemical release, evaporation, and condensation) inside the charge. The charge is assumed to be a porous material whose properties change over time as coking progresses [5,6].

The model has been successfully validated against literature data in top-charged mode. In the next step, its validity will be confronted with the design parameters of the newly built coke oven battery no. 4 by JSW KOKS S.A. in Koksownia Przyjaźń.

[1] AGH University of Krakow, Department of Fuels Technology, 30-059, Kraków, Poland, *mtokarski@agh.edu.pl
[2]Biuro Projektów KOKSOPROJEKT Sp. z o.o., 41-800 Zabrze, Poland

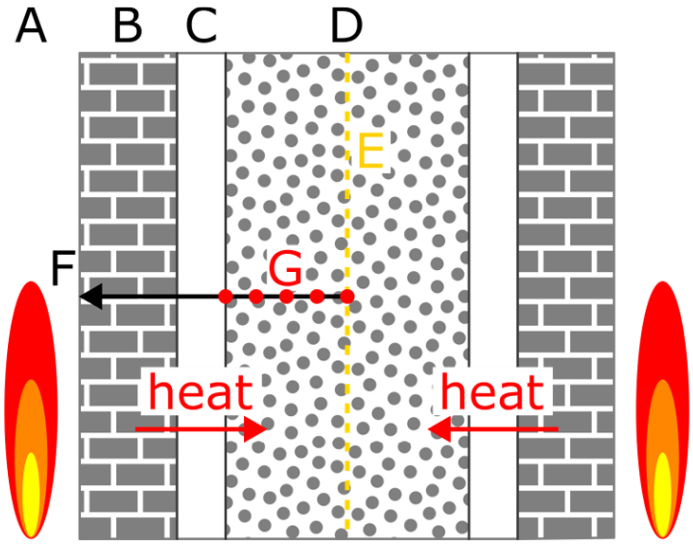


Figure 1. Scheme of the slot-type coke oven system: A – heating flues; B – heating flue walls; C – distance between the wall and charge; D – charge; E – symmetry; F – domain included in the model; G – discretized domain included in the ODE system actually solved. Red arrows indicate heat transfer direction towards axis (E)

[1] A. Karcz, Koksownictwo, część I, wyd. 2, Wydawnictwo AGH, Kraków, 1991.
[2] A. Karcz, Koksownictwo, część II, Wydawnictwo AGH, Kraków, 1991.
[3] R. Buczyński, R. Weber, R. Kim, P. Schwöppe, One-dimensional model of heat-recovery, non-recovery coke ovens. Part I: General description and hydraulic network sub-model, Fuel 181 (2016) 1097–1114. https://doi.org/10.1016/j.fuel.2016.01.085.
[4] D. Merrick, Mathematical models of the thermal decomposition of coal: 1. The evolution of volatile matter, Fuel 62 (1983) 534–539. https://doi.org/10.1016/0016-2361(83)90222-3.
[5] V.R. Voller, M. Cross, D. Merrick, Mathematical models of the thermal decomposition of coal: 5. Distribution of gas flow in a coke oven charge, Fuel 62 (1983) 562–566. https://doi.org/10.1016/0016-2361(83)90226-0.
[6] G. Wałowski, G. Filipczak, Hydrodynamika przepływu gazu przez złoże porowate, Oficyna Wydawnicza Politechniki Opolskiej, Opole, 2020.

Declining Energy Intensity Without Energy Savings? Hotspots And Rebound Effects Across The EU Agribusiness Production Chain

Kacper Mankowski[1],*, Bartłomiej Bajan[1],[2], Aldona Mrowczyńska-Kamińska[1]

Keywords: agribusiness, energy intensity, rebound effect, hotspots, input-output analysis

ABSTRACT

Declining energy intensity is commonly interpreted as progress towards lower energy demand. However, lower energy use per unit of economic output does not necessarily result in lower absolute energy consumption when production expands. This study examines whether reductions in energy intensity in European Union agribusiness translated into actual energy savings between 2014 and 2022. It also identifies energy-intensity hotspots, understood as countries and production stages characterized by disproportionately high energy use relative to economic output. Agribusiness is treated as a production subsystem consisting of four stages: agriculture provisioning, food-industry provisioning, agriculture, and food processing. By combining hotspot identification with an observed ex-post rebound assessment, the analysis distinguishes improvements in energy intensity from realized reductions in total energy use.

The empirical analysis combines EUROSTAT FIGARO input-output tables with Physical Energy Flow Accounts [1]. Consistent data are available for 21 EU countries, while comparisons beginning in 2014 cover 19 countries because energy end-use data for Czechia and Lithuania are unavailable for 2014–2015. Energy use and GDP for individual agribusiness stages are estimated using the Leontief input-output framework [2]. Energy intensity is measured as end-use energy consumption per unit of GDP expressed in constant prices and purchasing power standards. Hotspots are identified using three complementary thresholds: mean plus one standard deviation, median plus median absolute deviation, and the third quartile, together with a country-specific validation criterion [3]. For observations in which energy intensity declined, an observed ex-post rebound ratio is used to determine whether expected energy savings were realized, partially offset, or reversed. The measure is accounting-based and descriptive rather than a causal elasticity estimate [4].

Average agribusiness energy intensity declined by approximately 9.3%, from 4.46 MJ/EUR GDP PPS in 2014 to 4.04 MJ/EUR in 2022, but remained substantially higher than in the economy as a whole. Direct production stages, agriculture and food processing, accounted for 62.4% of average agribusiness energy use and generally exhibited higher energy intensity than provisioning activities (Fig. 1). Agribusiness-level hotspots were identified in Belgium, Czechia, Estonia, Lithuania, and Finland, with the strongest concentration in Northern and Eastern Europe. Agriculture was an important driver of hotspots in most of these countries, whereas Lithuania was distinguished by particularly high energy intensity in upstream provisioning stages (Fig. 1). Most importantly, declining energy intensity frequently failed to produce proportional reductions in energy use. Of 114 country-stage observations, energy intensity declined in 83 cases, of which 44 were classified as backfire effects, meaning that absolute energy consumption increased despite lower energy intensity. Backfire was particularly frequent for total agribusiness and agriculture. At the aggregate EU-19 level for 2014–2022, food-industry provisioning

[1] Faculty of Economics, Poznań University of Life Sciences, Poznań, Poland, * kacper.mankowski@up.poznan.pl
[2] Faculty of Economics and Management, Czech University of Life Sciences Prague, Czechia

exhibited a rebound effect, while all other agribusiness stages showed backfire. These patterns are consistent with production growth and structural expansion offsetting potential energy savings.

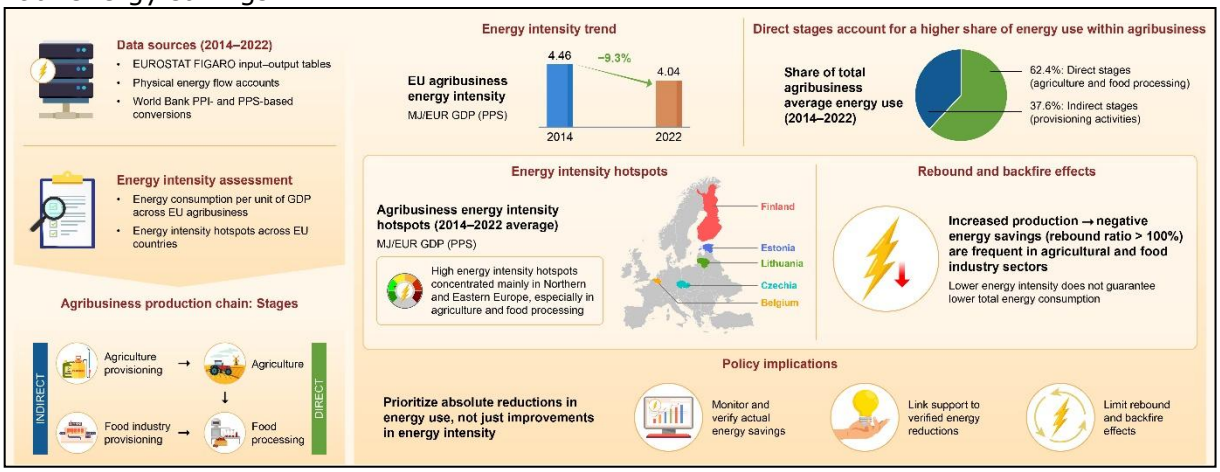


Figure 1. Key findings on energy intensity, hotspots and rebound/backfire effects in EU agribusiness, 2014–2022

The results demonstrate that declining energy intensity alone should not be treated as sufficient evidence of successful energy conservation. Agricultural and energy policies should therefore complement intensity indicators with monitoring of absolute energy use and verified energy savings. Public support for modernization, precision agriculture, and digital technologies may contribute to this objective, but its effectiveness should be assessed against measurable reductions in energy consumption rather than technology adoption alone. Energy-use baselines, standardized reporting, and ex-post monitoring could help identify cases in which efficiency improvements are offset by production expansion. Combining energy-intensity and absolute energy-use indicators would allow EU policy to distinguish structural hotspots from areas where expected savings are being eroded by rebound or backfire effects.

[1] I. Rémond-Tiedrez, J.M. Rueda-Cantuche (Eds.), EU Inter-country Supply, Use and Input-output Tables: Full International and Global Accounts for Research in Input-output Analysis (FIGARO), 2019 edition, Publications Office of the European Union, Luxembourg, 2019. https://doi.org/10.2785/008780.
[2] R.E. Miller, P.D. Blair, Input-Output Analysis: Foundations and Extensions, 2nd ed., Cambridge University Press, Cambridge, 2009. https://doi.org/10.1017/CBO9780511626982.
[3] B. Bajan, K. Mańkowski, A. Mrówczyńska-Kamińska, Energy intensity in European Union agribusiness: Identifying hotspots and rebound effects, Energy 360 (2026) 141434. https://doi.org/10.1016/j.energy.2026.141434.
[4] D.I. Stern, How large is the economy-wide rebound effect?, Energy Policy 147 (2020) 111870. https://doi.org/10.1016/j.enpol.2020.111870.

The Promotional Effect Of Ceria On Ni/Sba-15 Catalysts Prepared By The Solid-State Grinding For Co_2 Methanation

Dominika Książek[1,*], Jakub Mokrzycki[1], Agnieszka Szymaszek-Wawryca[1]

Keywords: SBA-15, CO_2 methanation, catalysts, Ni-based catalysts

ABSTRACT

The alarming rise of global temperature has intensified the search for technological pathways towards achieving carbon neutrality. Among the various strategies for mitigating carbon dioxide (CO_2) emissions, CO_2 methanation has emerged as one of the most promising approaches [1]. The reaction is thermodynamically favorable at low temperatures, while the produced methane can be readily stored and utilized as a fuel, making the process an attractive route for carbon utilization and emission reduction [2].

Noble metal catalysts, particularly Rn and Ru, exhibit outstanding catalytic performance in CO_2 methanation, especially at low temperatures. However, their high cost and susceptibility to sintering under reducing atmosphere significantly limit their large-scale industrial application [3]. Consequently, transition metal catalysts, especially Ni-based, have attracted considerable attention over the years, owing to their favorable balance between catalytic activity and economic viability [2,3].

The catalytic performance of Ni-based catalysts can be further enhanced through the incorporation of promoters. Ceria is widely recognized for promoting CO_2 adsorption and activation through the formation of oxygen vacancies. Due to the relatively high cost of rare-earth materials, ceria is more commonly employed as a promoter rather than as the catalyst support [3].

Among the various supports investigated for CO_2 methanation, including SiO_2, Al_2O_3, mesoporous silicas, and zeolites, SBA-15, has attracted particular interest. In catalysis it is widely recognized for its large surface area, pore size (5 to 10 nm), high thermal stability and chemical resistance. These properties promote high metal dispersion and suppress particle sintering during catalytic operation [1,2].

In the present work, Ni/SBA-15 catalysts promoted with ceria were prepared by a solid-state grinding method and investigated for CO_2 methanation. The investigated doses of Ni+Ce were: 20+2,5; 20+5; and 20+10 wt.% and the results were compared with a reference catalyst containing 20 wt.% Ni. The physicochemical properties of the obtained materials were characterized by means of: XRD, H_2-TPR, CO_2-TPD, N_2 physisorption and TEM. The catalytic performance was evaluated in CO_2 methanation. Among the investigated catalysts, the sample containing 20 wt.% Ni and 5% wt.% Ce exhibited the best catalytic performance, demonstrating the highest CO_2 conversion and CH_4 yield.

[1] N.T.T. Van, L.C. Loc, N.P. Anh, H.T. Cuong, N. Tri, Positive effects of CeO_2 promoter and co-reactant/CO on methanation of CO_2-rich gas over Ni/SBA-15 catalyst, Mater. Trans. 61 (2020) 1332–1338. https://doi.org/10.2320/matertrans.MT-M2020109.

[2] M.C. Bacariza, I. Graça, S.S. Bebiano, J.M. Lopes, C. Henriques, Micro- and mesoporous supports for CO_2 methanation catalysts: A comparison between SBA-15, MCM-41 and USY zeolite, Chem. Eng. Sci. 175 (2018) 72–83. https://doi.org/10.1016/j.ces.2017.09.027.

[3] C. Feng, H. Jiang, H. Gong, L. Wang, G. Yang, Enhancing low-temperature CO_2 methanation via a dual anchoring impregnation strategy for highly dispersed Ni-Ce/SBA-15 catalysts, J. Taiwan Inst. Chem. Eng. 183 (2026) 106640. https://doi.org/10.1016/j.jtice.2026.106640.

Acknowledgement: The financial support from the National Science Centre, Poland, through the OPUS 29 grant (grant no. 2025/57/B/ST5/01462) is gratefully acknowledged. The selected results presented herein

[1] AGH University of Krakow, Faculty of Energy and Fuels, Mickiewicza Ave. 30, 30-059 Kraków, *dksiazek@student.agh.edu.pl

were developed using equipment supported by the "Excellence Initiative – Research University" programme at AGH University of Krakow.

Nanomaterials as Additives Supporting Biogas Production: Effects on Microorganisms Involved in Anaerobic Digestion

Katarzyna Kapusta[1,*], Katarzyna Moskalewicz[1], Krzysztof Kogut[1]

Keywords: biogas, anaerobic digestion, fermentation, nanomaterials, nanoparticles

ABSTRACT

Biogas is a gaseous mixture composed mainly of methane (50–80%), carbon dioxide (20–50%), and trace amounts of hydrogen sulfide, nitrogen, oxygen, carbon monoxide, and ammonia [3]. It can be produced through anaerobic digestion of waste organic matter originating, among others, from landfills, agri-food production, and wastewater treatment plants. Through biogas cleaning and upgrading processes, biomethane is obtained, which can serve as a substitute for natural gas [4].

Table 1. Course of anaerobic digestion process, [2, 5]

Stage	***Description***	***Microorganisms***
Hydrolysis	Decomposition of fats, cellulose, starch, proteins, and other macromolecules into amino acids, fatty acids, and sugars.	Hydrolytic bacteria belonging to the genera Clostridium, Bacteroides, Bacillus, Staphylococcus, Micrococcus, Vibrio, Proteus, Peptococcus oraz Acetivibrio
Acidogenesis	Conversion of monomers into short-chain volatile fatty acids (VFAs).	Acidogenic bacteria belonging to the genera Lactobacillus, Escherichia, Clostridium, Bacillus, Pseudomonas, Eubacterium, Bifidobacterium, Acetobacterium, Staphylococcus, Micrococcus, Zymomonas oraz Syntrophomonas
Acetogenesis	Conversion of VFAs into acetic acid, carbon dioxide, and hydrogen.	Syntrophic bacteria belonging to the genera Syntrophobacter, Syntrophomonas, Pelotomaculum, Smithella oraz Clostridium
Methanogenesis	Production of methane through three main biochemical pathways: 1) acetotrophic pathway: $4CH_3COOH \rightarrow 4CO_2 + 4CH_4$; 2) hydrogenotrophic pathway: $CO_2 + 4H_2 \rightarrow CH_4 + 2H_2O$; 3) methylotrophic pathway: $4CH_3OH + 6H_2 \rightarrow 3CH_4 + 2H_2O$	Methanogenic archaea belonging to the genera Methanosaeta, Methanothrix, Methanosarcina, Methanobacterium, Methanobrevibacter, Methanococcus, Methanospirillum, Methanoplanus, Methanogenium oraz Methanocorpusculum

Nanomaterials may significantly affect the activity of microorganisms involved in anaerobic digestion. Their beneficial effects are mainly associated with the enhancement of interspecies electron transfer, particularly direct interspecies electron transfer (DIET) between syntrophic bacteria and methanogens. Owing to their conductive properties, selected nanoparticles may facilitate electron flow, improve metabolic cooperation between microorganisms, and increase the efficiency of methanogenesis. At the same time, the impact of nanomaterials depends on their type, dose, and physicochemical properties. Nanoparticles that are improperly selected or applied at excessive concentrations may exert toxic effects, disturb microbial activity, and reduce methane production [1].

The aim of this study is to provide a critical review of the current state of knowledge regarding the use of nanomaterials as additives supporting biogas production. The analysis includes selected groups of nanomaterials, such as metal and metal oxide nanoparticles, iron-based materials, carbon-based nanomaterials, and nanocomposites. Particular

[1] AGH University of Krakow, Faculty of Energy and Fuels, 30 Mickiewicz Av, 30-059 Krakow, Poland,
* kkapusta@agh.edu.pl

attention is paid to their effects on the activity of microorganisms involved in anaerobic digestion, process stability, methanogenesis efficiency, and potential environmental and technological limitations associated with their application.

[1] C.M. Ajay, S. Mohan, P. Dinesha, M.A. Rosen, Review of impact of nanoparticle additives on anaerobic digestion and methane generation, Fuel 277 (2020) 118234. https://doi.org/10.1016/j.fuel.2020.118234.
[2] T. Amani, M. Nosrati, T.R. Sreekrishnan, Anaerobic digestion from the viewpoint of microbiological, chemical, and operational aspects – a review, Environ. Rev. 18 (2010) 255–278. https://doi.org/10.1139/A10-011.
[3] D. Dimande, B. Mihalyi-Schneider, M. Harasek, W. Wukovits, Environmental assessment of enhanced biomethane production from biogas via membrane-based upgrading, Biomass Bioenergy 210 (2026) 109021. https://doi.org/10.1016/j.biombioe.2026.109021.
[4] Polska Spółka Gazownictwa, Gotowi na biometan – Czym jest biometan?, https://gotowinabiometan.pl/#biometan (accessed 1 September 2026).
[5] S.M. Tauseef, M. Premalatha, T. Abbasi, S.A. Abbasi, Methane capture from livestock manure, J. Environ. Manage. 117 (2013) 187–207. https://doi.org/10.1016/j.jenvman.2012.12.022.

Acknowledgment: This research was funded by AGH University of Krakow, within the „Excellence Initiative – Research University" program (Action 21).

Advanced Solid Oxide Electrochemical Technologies for Future Energy Systems: From Green Hydrogen Production to Carbon-Neutral Fuels

Zhihong Du[1,2]*, Tong Wang[1], Konrad Świerczek[3], Hailei Zhao[1,2]*

Keywords: Solid Oxide Electrochemical cells, Renewable Energy Storage and Conversion, Hydrogen, Carbon-Neutral Fuels

ABSTRACT

The global energy system is undergoing a profound transformation driven by the rapid deployment of renewable energy, the growing demand for electricity from artificial intelligence and data centers, and the urgent need to decarbonize hard-to-abate sectors. In this transition, solid oxide electrochemical technologies, including solid oxide fuel cells (SOFCs), solid oxide electrolysis cells (SOECs), and reversible solid oxide cells (rSOCs), offer a unique platform for highly efficient energy conversion, storage, and utilization.

This presentation will provide a general overview of the opportunities and challenges of solid oxide technologies from both energy-system and industrial perspectives. SOFCs can efficiently convert hydrogen, natural gas, biogas, and other fuels into electricity, while providing reliable and dispatchable power with high efficiency.[1] In particular, the rapidly growing electricity demand of artificial intelligence data centers is creating a strong need for high-density, reliable, and rapidly deployable onsite power generation. Recent commercial activities by companies such as Bloom Energy, including large-scale deployments for data centers, demonstrate the emerging market potential of SOFC technology.

SOECs provide another important pathway for the energy transition. By combining high-temperature electrolysis with renewable electricity and industrial waste heat, SOECs can achieve highly efficient hydrogen production and provide an attractive route for long-duration renewable energy storage.[2-3] Beyond hydrogen, the ability of SOECs to co-electrolyze H_2O and CO_2 into syngas opens a broader pathway toward carbon-neutral fuels and chemicals, including synthetic methane, methanol, ammonia-related fuels, and sustainable aviation fuels.[4] Recent advances are steadily improving the technological maturity and scalability of SOEC systems. Although large-scale electrolysis deployment is accelerating worldwide, SOEC remains at an earlier stage of commercialization than alkaline and PEM electrolysis. The presentation will also review the development status and challenges of solid oxide technologies in China. Although China has developed a strong manufacturing capability in conventional electrolysis technologies, high-performance SOFC/SOEC materials, cells, stacks, and long-term reliability remain important areas requiring further technological development.

Finally, recent research from our group at the University of Science and Technology Beijing will be presented, focusing on high-performance electrolytes, oxygen electrodes, fuel electrodes, and advanced single-cell architectures. Particular attention will be given to precursor and grain-boundary engineering, highly active perovskite electrodes, nanoscale exsolution, thin-electrolyte fabrication, and the development of high-performance

[1] School of Materials Science and Engineering, University of Science and Technology Beijing, Beijing 100083, China
[2] Beijing Municipal Key Lab for Advanced Energy Materials and Technologies, Beijing 100083, China
[3] Faculty of Energy and Fuels, AGH University of Krakow, al. A. Mickiewicza 30, Krakow 30-059, Poland
*corresponding author: zhihongdu@ustb.edu.cn, hlzhao@ustb.edu.cn

SOFC/SOEC single cells.[5] These advances have enabled enhanced power output in SOFC operation and high current density and efficiency in SOEC operation. The presentation will conclude with our perspectives on scaling up from materials and single cells toward reliable high-performance stacks, and on the role of solid oxide technologies in future data-center power supply, renewable-energy storage, green hydrogen production, and carbon-neutral fuel synthesis.

[1] N.S.M. Affandi, N. Osman, Short review on global trends in SOFC scenario and future perspective, Mater. Today Proc. 66 (2022) 3981–3984. https://doi.org/10.1016/j.matpr.2022.04.824.
[2] A. Hauch, R. Küngas, P. Blennow, A.B. Hansen, J.B. Hansen, B.V. Mathiesen, M.B. Mogensen, Recent advances in solid oxide cell technology for electrolysis, Science 370 (2020) eaba6118. https://doi.org/10.1126/science.aba6118.
[3] Y. Zheng, J. Wang, B. Yu, W. Zhang, J. Chen, J. Qiao, J. Zhang, A review of high temperature co-electrolysis of H_2O and CO_2 to produce sustainable fuels using solid oxide electrolysis cells (SOECs): Advanced materials and technology, Chem. Soc. Rev. 46 (2017) 1427–1463. https://doi.org/10.1039/C6CS00403B.
[4] S.R. Foit, I.C. Vinke, L.G.J. de Haart, R.-A. Eichel, Power-to-syngas: An enabling technology for the transition of the energy system?, Angew. Chem. Int. Ed. 56 (2017) 5402–5411. https://doi.org/10.1002/anie.201607552.
[5] Y. Liu, T. Wang, Z. Du, Y. Wang, Y. Gong, K. Świerczek, H. Zhao, Coherent exsolution of ultrafine Ru nanoparticles on double perovskite boosts CO_2 and H_2O electrolysis via strong metal-support interactions, Adv. Energy Mater. 16 (2026) e71314. https://doi.org/10.1002/aenm.71314.

Acknowledgement: The authors acknowledge financial support from the National Key R&D Program of China (2026YFE0150200) and the AGH Excellence Initiative - Research University program (IDUB AGH, Action 21, ID 17978).

Assessment of The Third-Party Access Potential in The Decarbonisation of The Polish District Heating Market: Lessons from Lithuania

Aleksandra Bałys[1,2]*, Aleksandra Komorowska[1]

Keywords: district heating, renewable energy, district heating prices, energy transition, third-party access

ABSTRACT

INTRODUCTION

Decarbonisation of the district heating and cooling sector is especially important due to its significant share in the European Union's final energy consumption (approximately 50% in 2025) and its potential to enable large-scale integration of renewable energy and waste heat. Dominant form of renewable energy used to produce district heat among Member States is biofuels. One of the countries with a high share of biofuels in district heating production is Lithuania, while Polish district heating systems are heavily dependent on fossil fuels [1,2]. The Lithuanian district heating sector has undergone a major transition, which mainly included shifting from natural gas to biofuels. An important factor contributing to the transition was the introduction of regulated third-party access (TPA), which led to an increase in the use of renewable energy sources in the district heating sector and to a decrease in district heating prices [3,4].

The main aim of this study is to assess the possibility of increasing the share of biofuels in Polish district heating systems, while decreasing district heating prices through the practical application of regulated TPA in Poland, using the Lithuanian district heating sector transition as a case study. The analyses also include an overview of Lithuanian and Polish district heating markets and an examination of the barriers to practical TPA implementation to Polish district heating systems. The study contributes to the existing body of literature by identifying TPA-related factors that facilitated Lithuanian district heating systems decarbonisation and that could also support a greater integration of renewable energy in the Polish district heating sector. The study also indicates strategic directions for overcoming the barriers to large-scale TPA implementation in Poland.

MATERIALS AND METHODS

The study was based on desk research, regulatory and institutional analysis, secondary data analysis and transferability assessment, covering official statistical databases, sector- and country-specific literature and reports, as well as legal acts. First, the research questions were formulated, and the data were collected conventionally, as well as with the assistance of AI-based tools. The data gathered concerned the basic characteristics of the Lithuanian and Polish district heating markets, the dynamics of the energy sources in district heating production, as well as detailed insights into the transition of the Lithuanian district heating sector and the legal provisions regarding TPA in Lithuania and Poland. After the data analysis, conclusions were derived with respect to the research questions.

RESULTS AND DISCUSSION

District heating production in Poland is significantly larger than in Lithuania. Nevertheless, in Lithuania district heat is produced primarily from biofuels, whereas in Poland it is produced from solid fossil fuels. Natural gas was the main energy source used

[1] Mineral and Energy Economy Research Institute of the Polish Academy of Sciences
ul. Wybickiego 7A, 31-261 Kraków, Poland
[2] AGH University of Krakow, Faculty of Energy and Fuels, al. Mickiewicza 30, 30-059 Kraków, Poland

to produce district heat in Lithuania until approximately 2012, that is, until its market prices increased significantly. In the case of Poland, solid fossil fuels have played a major role in district heating production in the past two decades, and their share has been decreasing gradually.

The introduction of regulated TPA in Lithuanian district heating systems fostered competition among producers and motivated them to lower their bids at the monthly heat auctions. Market competition contributed to investments in biomass-based generation units since biomass was more cost-competitive than natural gas. Consequently, the share of renewable energy in district heating production increased, while district heating prices decreased.

Polish law provides for the possibility of third-party access to district heating networks, but the complexity of the regulations is a barrier to the practical, large-scale development of this model [5]. Other provisions oblige district heating companies to purchase renewable heat, but they do not encourage price competition among heat suppliers.

Regulated TPA to Polish district heating systems could facilitate competition among district heat suppliers, leading to larger utilisation of renewable energy sources in district heating production, as well as lower district heating prices. Priority could be given to producers utilising renewable energy sources, especially biomass, since, according to [6], the price of district heat produced from biomass is lower compared to district heat produced from hard coal.

CONCLUSION

The Lithuanian district heating sector had been dependent on natural gas for many years. Following the implementation of regulated TPA and an auction system, market competition has supported biomass-based district heating production and a reduction in district heating prices. Adapting this regulatory framework to the conditions of the Polish district heating market could support the integration of renewable energy sources, and a reduction in district heating prices.

[1] Eurostat, Electricity and derived heat production by type of fuel (nrg_bal_peh), Eurostat Database, 2026. https://doi.org/10.2908/nrg_bal_peh (accessed 8 September 2026).
[2] A. Komorowska, T. Surma, Comparative analysis of district heating markets: Examining recent prices, regulatory frameworks, and pricing control mechanisms in Poland and selected neighbouring countries, Polityka Energetyczna – Energy Policy Journal 27 (2024) 95–118. https://doi.org/10.33223/epj/175328.
[3] A. Pažėraitė, V. Lekavičius, R. Gatautis, District heating system as the infrastructure for competition among producers in the heat market, Renew. Sustain. Energy Rev. 169 (2022) 112888. https://doi.org/10.1016/j.rser.2022.112888.
[4] D. Korsakaite, D. Bieksa, E. Bieksiene, Third-party access in district heating: Lithuanian case analysis, Competition and Regulation in Network Industries 19 (2018) 218–241. https://doi.org/10.1177/1783591719837410.
[5] I. Szwedziak-Bork, O rzeczywistej potrzebie stosowania zasady TPA w ciepłownictwie, Internetowy Kwart. Antymonop. Regulacyjny 4 (2015) 55–65. https://press.wz.uw.edu.pl/ikar/vol4/iss3/4/.
[6] Urząd Regulacji Energetyki, Energetyka cieplna w liczbach – 2025, URE, Warszawa, 2026. https://www.ure.gov.pl/pl/cieplo/energetyka-cieplna-w-l/13361,dok.html.

A Microporous Channel Anode Support Structure for the Efficient and Safe Conversion of Low-Concentration Coal Mine Methane in High-Temperature Fuel Cells

Yihan Ling[1],*

Keywords: Low Concentration-Coal Mine Methane; Solid Oxide Fuel Cell; Deoxygenation and Enrichment.

ABSTRACT

This report describes the safe and efficient utilization of low concentration-coal mine methane through the integration of micro-pressure vacuum pressure swing adsorption (PSA) technology with solid oxide fuel cells (SOFCs). Using micro-pressure vacuum pressure swing adsorption for deoxygenation and concentration enhancement, we safely and efficiently reduce the O_2 concentration in low concentration-coal mine methane while elevating methane concentration to levels suitable for direct utilization. SOFCs represent a green, high-efficiency energy conversion device featuring an all-solid-state ceramic structure, no precious metals, and broad fuel adaptability. This eliminates the multi-stage energy conversion losses inherent in traditional gas power generation technologies. SOFCs significantly reduce pollutant emissions, and their electrochemical reactions operate unrestricted by flammability limits. By optimizing SOFC cell configurations and developing anti-coking catalysts, we have enhanced electrochemical performance and extended operational lifespan under hydrocarbon fuels. This enables direct conversion of chemical energy from deoxygenated low concentration -coal mine methane into electricity, achieving resource utilization of low concentration -coal mine methane.

[1] China University of Mining and Technology, lyhyy@cumt.edu.cn

EFE2026 ENERGY FUELS ENVIRONMENT
INTERNATIONAL CONFERENCE
17-20 NOVEMBER 2026, KRAKÓW, POLAND

Analysis Of The Transient Temperature And Stress Fields In The Wall Of A Component During A Thermal Shock, Considering The Finite Heat Capacity Of The Coolant

Jan Taler[1,*], Dawid Taler[2]

Keywords: transient temperature, thermal shock, coolant's finite volume capacity, thermal stress reduction, attemperator

ABSTRACT

This paper determines the indeterminate field of temperature and thermal stresses in a flat wall during rapid cooling with a liquid of finite heat capacity. If the heat capacity of the coolant is significantly lower than the heat capacity of the component's wall, the coolant layer will heat up as the wall cools. Consequently, the temperature difference between the surface of the flat wall being cooled and the liquid decreases, resulting in significantly slower cooling of the wall and significantly lower thermal stresses.

Thermal shock, which occurs when a liquid's heat capacity is finite, is a common phenomenon in practice, for example, in horizontal pressure vessels in power plant units, in injection coolers (attemperators) for superheated steam in steam boilers, and in spray cooling or heating of solids [1].

The unsteady temperature and thermal stress fields in the wall of the component were determined using an approximate analytical method known as the heat flux integral method (HFIM) [2]. The same problem was solved using the finite volume method to evaluate the accuracy of the solution obtained using HFIM.

This paper presents the results of calculations of temperature and stresses in a flat wall for various Biot numbers characterizing heat transfer at the plate surface and various values of the ratio of the element's heat capacity to the heat capacity of the coolant.

Maximum thermal stresses on the plate surface were also determined as a function of the Biot number and the ratio of the plate's heat capacity to the heat capacity of the liquid. The analyses conducted show that the finite heat capacity of the coolant has a very significant effect on reducing maximum thermal stresses during a thermal shock.

[1] J. Taler, P. Dzierwa, D. Taler, M. Jaremkiewicz, M. Trojan, Monitoring of Thermal Stresses and Heating Optimization Including Industrial Applications, Nova Science Publishers, New York, 2016.
[2] J. Taler, D. Taler, An alternative formulation of the method of weighted residuals for the approximate solving of heat conduction problems, Arch. Thermodyn. 47 (2026) 25–41. https://doi.org/10.24425/ather.2026.158663

[1] Cracow University of Technology, Department of Energy, * jan.taler@pk.edu.pl
[2] Cracow University of Technology, Department of Thermal Processes, Air Protection and Waste Disposal

Designing Atmosphere-Adaptive Perovskite Nanofiber Electrodes for Symmetrical SOFCs

Jakub Lach[1,*], Kun Zheng[1,2], Michał Gogacz[1], Cristian Radu[3], Damian Kaufmann[1], Yihan Ling[4], Adam Rokosz[1]

Keywords: symmetrical SOFCs, perovskite oxides, nanofiber electrodes, surface reconstruction, core-shell nanoparticles

ABSTRACT

Symmetrical solid oxide fuel cells (S-SOFCs), employing the same material at both electrodes, offer simplified fabrication, lower manufacturing costs, and improved thermochemical compatibility. Their development, however, requires electrode materials that combine redox stability and mixed ionic-electronic conductivity with high catalytic activity toward both hydrogen oxidation and oxygen reduction [1,2]. In this work, a rational design strategy integrating compositional engineering, nanofibrous architecture, and atmosphere-responsive surface reconstruction is investigated using A-site-deficient Sm0.9Ba0.9Mn1.8−xFexCo0.1Ni0.1O5+δ perovskites.

Controlled thermal treatment under reducing conditions produces partially embedded multimetallic nanocatalysts on the perovskite surfaces. In the Sm-based series, increasing the Fe content from x = 0 to x = 0.9 increases the nanoparticle number density from 23.5 to 105.5 μm−2 while decreasing the average particle diameter from 39.3 to 35.2 nm. Comparison with the complementary perovskite system demonstrates that variations in nanoparticle population modify surface coverage, the density of accessible reaction sites, and the resulting electrochemical response. These findings indicate that electrode optimization requires a balance between high particle density, limited particle growth, uniform spatial distribution, and strong particle-support interactions [1].

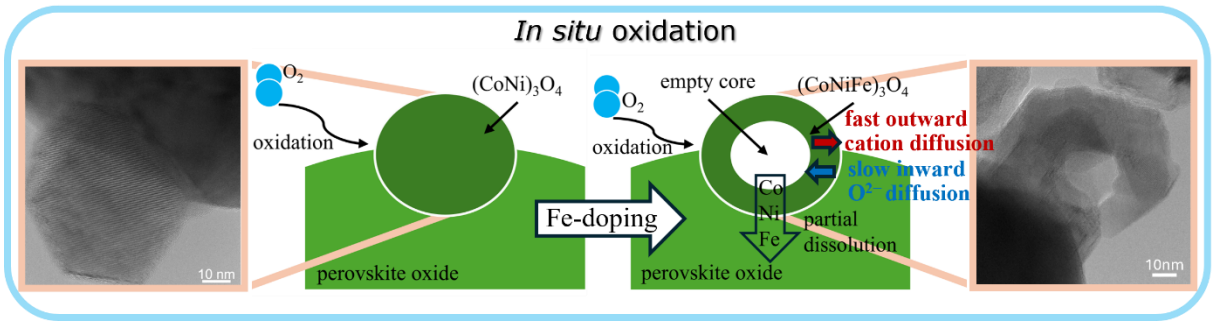


Figure 1. Schematic comparison of the oxidation behavior of Fe-free and Fe-containing nanocatalysts, illustrating the formation of a hollow core-shell structure through Kirkendall oxidation and partial dissolution into the perovskite lattice. Based on [1].

Fe substitution additionally stabilizes the double-perovskite structure and improves its compatibility with selected electrolytes. Under reducing conditions, partially embedded Co-Ni-Fe alloy nanoparticles provide active sites for hydrogen oxidation. In an oxidizing atmosphere, these nanoparticles transform into hollow $Fe_{3-x-y}Ni_xCo_yO_4$-type core-shell

[1] *Department of Hydrogen Energy, Faculty of Energy and Fuels, AGH University of Krakow, al. A. Mickiewicza 30, 30-059 Krakow, Poland, * jakublac@agh.edu.pl*
[2] *AGH Centre of Energy, AGH University of Krakow, ul. Czarnowiejska 36, 30-054 Krakow, Poland*
[3] *National Institute of Materials Physics, Atomistilor 405A, 077125, Magurele Romania*
[4] *School of Materials Science and Physics, China University of Mining and Technology, Xuzhou, Jiangsu Province, 221116, PR China*

oxides through a Kirkendall-type mechanism, enhancing oxygen reduction kinetics (see Fig. 1). The electrospun nanofiber architecture supports these processes by limiting grain coarsening and preserving an open porous network with a high density of accessible surface sites [1].

The optimized $Sm_{0.9}Ba_{0.9}Mn_{0.9}Fe_{0.9}Co_{0.1}Ni_{0.1}O_{5+\delta}$-30 wt.% GDC20 composite exhibits a polarization resistance of 0.046 Ω cm^2 at 800 °C. An electrolyte-supported symmetrical cell achieves a peak power density of 816 mW cm^{-2} at 800 °C and maintains stable operation without significant microstructural degradation. These results identify controlled nanoparticle population and atmosphere-adaptive surface nanostructuring as transferable design parameters for durable, high-performance symmetrical SOFC electrodes [1].

These results identify controlled nanoparticle population and atmosphere-adaptive surface nanostructuring as transferable design parameters for durable, high-performance symmetrical SOFC electrodes. Building on these findings, this approach has already been extended to multicomponent high-entropy Fe-Co-Ni-Cu-Pd nanoparticles, and ongoing research continues to investigate their population control, compositional uniformity, stability, and catalytic functionality under both fuel- and air-electrode conditions.

[1] J. Lach, K. Zheng, C. Radu, M. Kryński, M. Gogacz, Y. Ling, A. Klimkowicz, M. Łapiński, Controlled exsolution-dissolution in double perovskites enables symmetrical-capable high-performance SOFC electrodes, Chem. Eng. J. 532 (2026) 174527. https://doi.org/10.1016/j.cej.2026.174527.
[2] J. Lach, M. Gogacz, P. Winiarz, Y. Ling, M. Zhou, K. Zheng, A review of nanofiber electrodes and the in situ exsolution of nanoparticles for solid oxide cells, Materials 18 (2025) 1272. https://doi.org/10.3390/ma18061272.

Acknowledgement: The work was funded by the National Science Centre Poland (NCN) on the basis of the decision numbers UMO-2021/43/D/ST5/00824 and UMO-2025/57/N/ST11/01244. Jakub Lach acknowledges the financial support of research project supported by the program „Excellence Initiative – Research University" for the AGH University of Krakow.
HRTEM, EDS, and SAED results were a part of CERIC-ERIC grant no. 20232033 and were conducted in National Institute of Materials Physics, Măgurele in Romania.

EFE2026 ENERGY FUELS ENVIRONMENT
INTERNATIONAL CONFERENCE
17-20 NOVEMBER 2026, KRAKÓW, POLAND

Modeling of Syngas Production from Biomass Gasification Using Aspen Plus

Natalia Dulęba[1,2,*], Marcin Możdzierz[1], Alicja Klimkowicz[3]

Keywords: gasification, syngas, biomass, gasifier, process modeling

ABSTRACT

Biomass represents an attractive renewable energy source, which can be effectively utilized in the gasification process for syngas production. Syngas is a promising energy carrier due to its potential for clean and efficient energy production. The aim of this work is to provide recommendations for biomass gasification conditions based on their effect on syngas composition. This study models and analyzes a biomass gasification process shown in Figure 1 using Aspen Plus. The simulation starts with feedstock drying, after which thermal decomposition and pyrolysis generate gaseous products that are mixed with air. This mixture then enters a gasification reactor, which is partitioned into combustion and reduction zones. Each zone is modeled using kinetic reactions to predict syngas production. Finally, the raw gas passes through a cyclone for particulate removal, producing the final synthesis gas stream. The model was calibrated using literature data [1]. The calibration procedure considered an equivalence ratio ranging from 0.17 to 0.35 and gasification temperatures between 800 °C and 1200 °C, enabling an analysis of their influence on syngas composition. The simulations provided detailed results for the main gaseous components, including hydrogen, carbon monoxide, and carbon dioxide. The results demonstrate the formation of syngas with a suitable composition and favorable proportions, with H_2 reaching up to 17.5 vol%, CO up to 33 vol%, and CO_2 around 10 vol%. These findings demonstrate that process modeling can support the selection and optimization of operating parameters for real biomass gasification systems, thereby improving the efficiency of biomass utilization and syngas production.

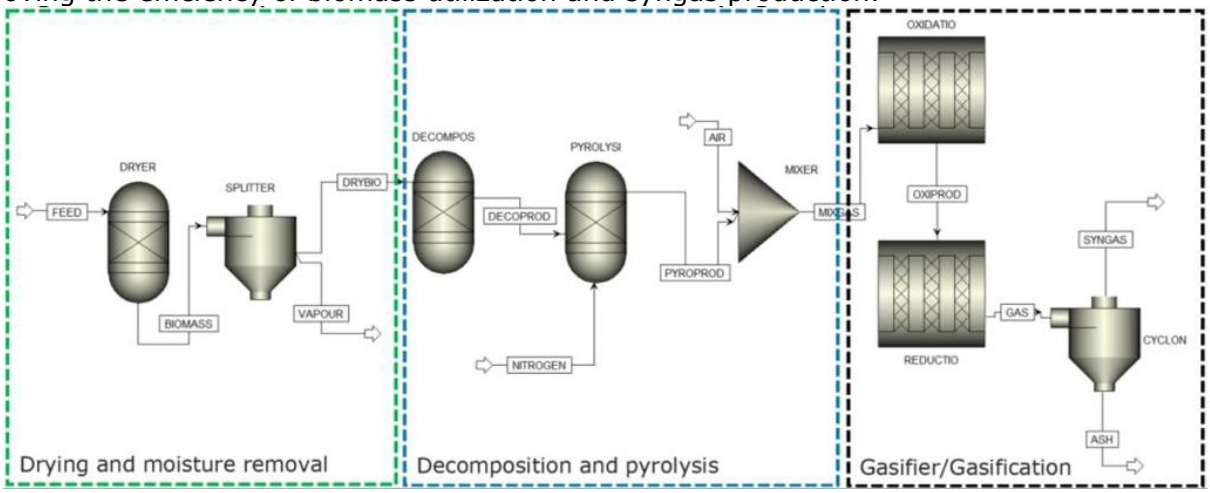


Figure 1. Gasification Process Model. Own elaboration

[1] M. Puig-Gamero, D.T. Pio, L.A.C. Tarelho, P. Sánchez, L. Sanchez-Silva, Simulation of biomass gasification in bubbling fluidized bed reactor using Aspen Plus®, Energy Convers. Manage. 235 (2021) 113981. https://doi.org/10.1016/j.enconman.2021.113981.

[1] Faculty of Energy and Fuels, AGH University of Krakow, Kraków, Poland, * nduleba@student.agh.edu.pl
[2] Graduate School of Engineering and Science, Shibaura Institute of Technology, Tokyo, Japan
[3] Faculty of Engineering, Shibaura Institute of Technology, Tokyo, Japan

Acknowledgments: This work was supported by the Polish National Agency for Academic Exchange (NAWA), within the Strategic Partnerships Programme, Project No. BPI/PST/2024/1/00046 (project title: Research and Educational Cooperation in the field of Energy and Environmental Engineering: AGH's strategic partnership with Japanese universities).

Critical Mineral Security and Macroeconomic Resilience after the EU Critical Raw Materials Act: A Multiple-Outcome Synthetic-Control Assessment

Atif Khan[1,]*, Artur Wyrwa[1]

Keywords: critical raw materials; Critical Raw Materials Act; import diversification; multiple-outcome synthetic control; macroeconomic resilience

ABSTRACT

Critical minerals link the energy transition to industrial competitiveness and macroeconomic stability. External disruptions to concentrated supplies of lithium, natural graphite, cobalt, and nickel can be transmitted through import prices, production costs, industrial output, investment, and economic growth. Regulation (EU) 2024/1252—the Critical Raw Materials Act (CRMA)—entered into force on 23 May 2024 to strengthen the security, sustainability, and diversification of the European Union's supply of strategic raw materials (European Parliament & Council of the European Union, 2024). However, the early economy-wide effects of the Act have not yet been adequately examined within an explicit counterfactual framework. This study evaluates whether the early post-CRMA period shows changes consistent with improved mineral import resilience and whether detectable industrial and macroeconomic responses accompany these changes.

A mixed-frequency panel is constructed for EU-27 and a donor pool of comparable non-EU economies from January 2015 to the latest complete observation available before estimation. Monthly UN Comtrade data on bilateral import values and quantities for selected lithium, natural graphite, cobalt, and nickel products measure supplier concentration, dominant supplier dependence, sourcing breadth, import volume, unit values, and import volatility. Eurostat provides data on industrial production, producer prices, inflation, unemployment, real GDP, manufacturing value added, and gross fixed capital formation. The EU-27 is treated as a single customs territory, intra-EU trade is excluded, and all external partners, including China, enter the diversification indicators according to their observed trade shares.

The primary estimator is the multiple-outcome synthetic control method proposed by Sun, Ben-Michael, and Feller (2025). Unlike conventional applications that estimate separate donor weights for individual outcomes, this method identifies a common set of nonnegative weights that jointly reproduce the EU's pre-CRMA trajectories across related mineral-security indicators. It therefore generates a coherent synthetic counterfactual while exploiting information shared across multiple outcomes. Post-intervention gaps are estimated separately for each mineral group and for a standardized import-resilience index.

Synthetic difference-in-differences, developed by Arkhangelsky et al. (2021), provides a complementary specification that combines unit and time weighting with fixed-effects adjustment. This estimator assesses whether the principal estimates are robust to imperfect pre-intervention fit and common time shocks. Credibility is further evaluated through in-space placebos, pseudo-intervention dates, leave-one-donor-out tests, alternative policy dates, alternative mineral baskets, and pre-treatment root-mean-square prediction errors. The synthetic business cycle approach proposed by Shi, Xi, and Xie (2025) is employed only as an exploratory sensitivity analysis for non-stationary macroeconomic outcomes because the method has not yet been published in a peer-reviewed journal.

This study contributes an integrated counterfactual assessment linking the CRMA's

[1] Faculty of Energy and Fuels, AGH University of Krakow, Kraków, Poland, *khan@agh.edu.pl

early mineral-trade effects to industrial and macroeconomic resilience. Its central novelty is the joint evaluation of multidimensional supply-chain adjustment and its potential transmission to prices, production, investment, and GDP within a unified policy-evaluation design. The analysis will determine whether early diversification is confined to trade composition or is already accompanied by broader economic adjustment. Given the short post-policy period, the findings will be interpreted as early reduced-form evidence rather than a definitive evaluation of the CRMA or the achievement of its 2030 benchmarks.

[1] D. Arkhangelsky, S. Athey, D.A. Hirshberg, G.W. Imbens, S. Wager, Synthetic difference-in-differences, Am. Econ. Rev. 111 (2021) 4088–4118. https://doi.org/10.1257/aer.20190159.
[2] European Parliament and Council of the European Union, Regulation (EU) 2024/1252 establishing a framework for ensuring a secure and sustainable supply of critical raw materials, Off. J. Eur. Union L (2024) 2024/1252. https://eur-lex.europa.eu/eli/reg/2024/1252/oj.
[3] Z. Shi, J. Xi, H. Xie, A synthetic business cycle approach to counterfactual analysis with nonstationary macroeconomic data, arXiv preprint arXiv:2505.22388 (2025). https://doi.org/10.48550/arXiv.2505.22388.
[4] L. Sun, E. Ben-Michael, A. Feller, Using multiple outcomes to improve the synthetic control method, Rev. Econ. Stat. (2025) 1–29. https://doi.org/10.1162/rest_a_01592.

Morphological Enhancement of A-Site Deficient and B-Site Substituted NdBa-Based Cobalites for High Performance IT-SOC Electrodes

Rameez Zafar[1], Amir Sultan[1,2], Laiba Amir[1], Kun Zheng[1,3,*]

Keywords: Double perovskite, A-site deficiency, Mn substitution, Oxygen electrode, Solid oxide cells

ABSTRACT

Sustainable energy production suffers from intermittent power generation due to natural weather variability, creating an urgent need for efficient and scalable energy storage technologies. Solid oxide cells (SOCs) offer a promising solution by enabling reversible energy storage in the form of hydrogen with high efficiency and fuel flexibility, but their commercialization is hindered by low durability and operating costs. Lowering the operating temperature to the intermediate-temperature range (600–800°C) is therefore essential for reducing cost and improving durability, although this inevitably slows the oxygen reduction reaction (ORR) and increases electrode polarization, imposing demanding requirements on electrode materials [1].

Barium-based layered double perovskites, $LnBaCo_2O_{5+\delta}$ (Ln = lanthanide), are attractive oxygen electrode candidates for IT-SOCs owing to their high mixed ionic-electronic conductivity and excellent intrinsic ORR activity [2-3]. However, the predominant presence of cobalt results in an elevated thermal expansion coefficient (TEC), arising from chemical expansion during Co^{4+}/Co^{3+} reduction and Co^{3+} spin-state transitions, which mismatches the electrolyte and causes electrode delamination and accelerated degradation. To counter this, B-site substitution with more thermally stable transition metals such as Mn and Fe can suppress chemical expansion and stabilize the lattice, while A-site deficiency promotes oxygen vacancy formation and enhances oxygen adsorption and surface exchange. Combining these strategies can simultaneously regulate oxygen defect chemistry, thermomechanical stability, and electrode kinetics, although their joint effect has remained largely unexplored [4-6].

In this work, a series of A-site-deficient and Fe-Mn co-substituted double perovskites, $(NdBa)_{2-\alpha}CoFe_{1-x}Mn_xO_{5+\delta}$ (α = 0, 0.1; x = 0, 0.25, 0.5, 0.75), were synthesized and comprehensively characterized by XRD, Rietveld refinement, TEM, XPS, BET, TGA, dilatometry, and EIS. Increasing Mn content progressively suppressed lattice oxygen release and lowered the TEC from $\sim 22\times10^{-6}$ K^{-1} towards below 16×10^{-6} K^{-1} through stronger Mn–O bonding and reduced Co-related chemical expansion, whereas A-site deficiency alone had limited influence on TEC. Among the single-phase electrodes, the undoped $(NdBa)_2CoFeO_{5+\delta}$ and A-site-deficient $(NdBa)_{1.9}CoFeO_{5+\delta}$ delivered the lowest area-specific resistances of 0.059 and 0.062 Ω cm^2 at 750°C (activation energies 0.77 and 0.88 eV), while increasing Mn substitution raised polarization resistance, revealing an intrinsic activity-stability trade-off. Incorporating 30 wt% Gd-doped ceria (GDC) into the Mn-rich $(NdBa)_{1.9}CoFe_{0.25}Mn_{0.75}O_{5+\delta}$ composition reduced its ASR nearly sevenfold to 0.067 Ω cm^2, matching the undoped electrode while retaining a substantially lower TEC.

[1] Faculty of Energy and Fuels, AGH University of Krakow, al. A. Mickiewicza 30, 30-059 Krakow, Poland, * zheng@agh.edu.pl
[2] Jerzy Haber Institute of Catalysis and Surface Chemistry, Polish Academy of Sciences, Niezapominajek 8, Krakow, PL-30239, Poland.
[3] AGH Centre of Energy, AGH University of Krakow, ul. Czarnowiejska 36, Krakow, 30-054, Poland

Oxygen partial pressure and DRT analyses showed that these strategies mainly modify the magnitude of individual polarization processes, chiefly oxygen adsorption/ionization and surface transport, without altering the intrinsic ORR pathway. Both $(NdBa)_{1.9}CoFeO_{5+\delta}$ and the GDC composite sustained stable operation over 100 hours at 700°C, corroborated by post-mortem SEM-EDS showing no interfacial delamination, in contrast to the stoichiometric $(NdBa)_2CoFeO_{5+\delta}$ electrode, which degraded under identical conditions. These results demonstrate that A-site deficiency and Mn substitution play distinct, complementary roles, and that composite electrode architecture can reconcile the resulting activity-stability trade-off, establishing a rational defect-engineering framework for durable, high-performance double-perovskite oxygen electrodes for IT-SOCs.

[1] A. Sultan, X. Xu, R. Zafar, L. Amir, R.T. Baker, M. Motola, P. Czaja, F. Jin, Y. Ling, K. Zheng, Coupled A-site regulation and multicomponent B-site substitution in $SrFeO_{3-\delta}$-derived perovskites for active and durable oxygen reduction, Appl. Catal. B Environ. Energy 402 (2027) 127439. https://doi.org/10.1016/j.apcatb.2026.127439.

[2] R. Zafar, A. Sultan, P. Czaja, K. Zheng, Balancing oxygen vacancy formation and thermal stability in A-site-deficient Mn-substituted NdBaCoFe-based double perovskite oxygen electrodes, J. Power Sources 695 (2026) 241358. https://doi.org/10.1016/j.jpowsour.2026.241358.

[3] A.I. Klyndyuk, D.S. Kharytonau, M. Mosiałek, E.A. Chizhova, A. Komenda, R.P. Socha, M. Zimowska, Double substituted $NdBa(Fe,Co,Cu)_2O_{5+\delta}$ layered perovskites as cathode materials for intermediate-temperature solid oxide fuel cells – correlation between structure and electrochemical properties, Electrochim. Acta 411 (2022) 140062. https://doi.org/10.1016/j.electacta.2022.140062.

[4] W. Zhang, Y. Zhou, E. Liu, Y. Ding, Z. Luo, T. Li, N. Kane, B. Zhao, Y. Niu, Y. Liu, M. Liu, A highly efficient and durable air electrode for intermediate-temperature reversible solid oxide cells, Appl. Catal. B Environ. 299 (2021) 120631. https://doi.org/10.1016/j.apcatb.2021.120631.

[5] G. Xue, J. Li, H. Wang, H. Sun, X. Guo, Q. Hu, $(Pr_{0.9}La_{0.1})_{1.9}(Ni_{0.7}Cu_{0.3})_{0.9}Mn_{0.1}O_{4+\delta}$ nanofiber cathode with Pr site cation defect prepared by electrospinning and its application in reversible fuel cells, J. Power Sources 552 (2022) 232220. https://doi.org/10.1016/j.jpowsour.2022.232220.

[6] S. Khan, A. Staykov, J. Matsuda, M. Kluczny, K.T. Wu, K. Ninomiya, M. Nishibori, J.T. Song, M. Watanabe, M. Inada, T. Ishihara, Effects of Ce co-doping at the A site of $Sm_{0.5-x}Sr_{0.5}CoO_{3\pm\delta}$ for a high-performance air electrode for solid oxide reversible cells, J. Mater. Chem. A 13 (2025) 6620–6630. https://doi.org/10.1039/D4TA08181A.

Acknowledgement: This work was financially supported by the „Excellence Initiative – Research University" program for the AGH University of Krakow, and the subvention of AGH University of Krakow, Faculty Energy and Fuels (project No. 16.16.210.476). The work is co-financed by the Polish National Agency for Academic Exchange grant nr BPN/BCH/2025/1/00043/U/00001.

Redox-Induced Exsolution in Multicomponent Perovskite Electrodes for Solid Oxide Cells

Zihao Chen[1], Kun Zheng[1, 2,*]

Keywords: Exsolution; Multicomponent perovskite; H_2-induced reconstruction; Solid oxide cells; Nanofibrous electrodes

ABSTRACT

The detrimental effects of fossil fuel consumption on the global climate are accelerating the transition toward carbon-neutral energy technologies and increasing interest in green hydrogen as a sustainable energy carrier. Solid oxide cells (SOCs), including SOFCs and SOECs, are promising technologies for efficient energy conversion and green hydrogen production. However, electrode activity and long-term stability remain key challenges[1].

Double perovskite oxides have emerged as promising electrode materials for solid oxide cells (SOCs), owing to their enhanced impurity tolerance, high redox stability, excellent coking resistance, and adequate ionic and electronic conductivity [2]. However, their practical application in SOCs is still limited by insufficient surface catalytic activity and sluggish electrode reaction kinetics, particularly under high-temperature operating conditions. Therefore, developing effective strategies to enhance surface catalytic activity while maintaining structural stability is highly desirable. In-situ exsolution has emerged as an effective strategy to address these challenges by generating catalytically active nanoparticles directly from the perovskite lattice [3]. This approach provides strong metal–support interactions, excellent nanoparticle anchoring, and high resistance to particle agglomeration [4]. Initially, exsolution research primarily focused on the formation of single-metal nanoparticles. Building on these advantages, bimetallic exsolution was subsequently developed to introduce synergistic effects between different metals, enabling tunable electronic structures and enhanced catalytic properties compared with monometallic nanoparticles. More recently, multicomponent exsolution has extended this concept to the simultaneous exsolution of three or more metallic species, offering greater compositional and structural flexibility. However, multicomponent alloy exsolution remains relatively scarce because of its intrinsic complexity. Previous studies have demonstrated the formation of Ni–Co–Fe [5] ternary and Ni–Fe–Co–Cu–Pd multicomponent nanoparticles [6], as well as diverse architectures such as Janus and core–shell nanoparticles. These studies highlight the considerable potential of multicomponent exsolution for enhancing the catalytic and electrochemical performance of perovskite electrodes. Nevertheless, the mechanisms governing multicomponent exsolution remain insufficiently understood. In particular, differences in the reducibility and cation diffusivity of individual elements may strongly influence cation migration, nanoparticle nucleation, and the final composition and structure of the exsolved nanoparticles.

In this work, a series of Mo-containing Fe-based multicomponent perovskite oxides, LaxSr1.8-xFe1.4Ti0.2Mo0.2(Co/Ni/Pd/Cu)0.2O5+δ (x = 0, 0.45, 0.9, 1.35, and 1.8), were systematically investigated to elucidate the effect of La/Sr composition on their redox-induced structural evolution and electrochemical performance. X-ray diffraction (XRD), scanning electron microscopy (SEM), and transmission electron microscopy (TEM) were employed to characterize the phase evolution, morphology, and nanoparticle exsolution/reincorporation behavior during reduction and reoxidation. Electrochemical

[1] Faculty of Energy and Fuels, AGH University of Krakow, al. A. Mickiewicza 30, 30-059 Krakow, Poland
[2] AGH Centre of Energy, AGH University of Krakow, ul. Czarnowiejska 36, 30-054 Krakow, Poland,
*zheng@agh.edu.pl;

impedance spectroscopy (EIS) was used to evaluate the electrochemical performance of the resulting electrodes. The structural evolution and electrochemical performance were then correlated to reveal the influence of A-site composition on the redox behavior and catalytic properties of the Mo-containing multicomponent perovskites.

[1] K. Zheng, J. Lach, P. Czaja, M. Gogacz, P. Czach, A. Brzoza-Kos, P. Winiarz, J. Luo, Designing high-performance quasi-symmetrical solid oxide cells with a facile chemical modification strategy for $Sr_2Fe_{2-x}W_xO_{6-\delta}$ ferrites electrodes with in situ exsolution of nanoparticles, J. Power Sources 587 (2023) 233707. https://doi.org/10.1016/j.jpowsour.2023.233707.
[2] A. Sultan, X. Xu, R. Zafar, L. Amir, R.T. Baker, M. Motola, P. Czaja, F. Jin, Y. Ling, K. Zheng, Coupled A-site regulation and multicomponent B-site substitution in $SrFeO_{3-\delta}$-derived perovskites for active and durable oxygen reduction, Appl. Catal. B Environ. Energy 402 (2027) 127439. https://doi.org/10.1016/j.apcatb.2026.127439.
[3] J. Lach, K. Zheng, C. Radu, M. Kryński, M. Gogacz, Y. Ling, A. Klimkowicz, M. Łapiński, Controlled exsolution-dissolution in double perovskites enables symmetrical-capable high-performance SOFC electrodes, Chem. Eng. J. 532 (2026) 174527. https://doi.org/10.1016/j.cej.2026.174527.
[4] L.B. Liu, S. Liu, M. Yang, Y. Li, B. Ouyang, P. Zhang, X.Z. Fu, Y. Sun, S. Liu, J.L. Luo, In situ exsolution of $NiFe@FeO_x$ core-shell nanoparticles with crosslinked oxygen-ion pathways from perovskite for efficient CO_2 electrolysis, Appl. Catal. B Environ. Energy 379 (2025) 125705. https://doi.org/10.1016/j.apcatb.2025.125705.
[5] A. López-García, L. Almar, S. Escolástico, A.B. Hungría, A.J. Carrillo, J.M. Serra, Tuning ternary alloyed nanoparticle composition and morphology by exsolution in double perovskite electrodes for CO_2 electrolysis, ACS Appl. Energy Mater. 5 (2022) 13269–13283. https://doi.org/10.1021/acsaem.2c01829.
[6] Y. Luo, D. Zhang, T. Liu, X. Chang, J. Wang, Y. Wang, X.K. Gu, M. Ding, In situ exsolution of quaternary alloy nanoparticles for CO_2–CO mutual conversion using reversible solid oxide cells, Adv. Funct. Mater. 34 (2024) 2403922. https://doi.org/10.1002/adfm.202403922.

Acknowledgements: This work was supported by the program "Excellence initiative – research university" for the AGH University of Krakow, grant number 17412. And it was supported by the STER NAWA Programme "International Space of the AGH Doctoral School", grant number 12.12.455.00710.

Commercial Fluid Catalytic Cracking Catalysts for Polymer Chemical Recycling

Oliwia Rogala[1,2], Karolina A. Tarach[1], Agata Kordek[1,2], Yuying Shu[3], Jean-Pierre Gilson[4], Louwanda Lakiss[4], Kinga Góra-Marek[1]*

Keywords: catalytic cracking, fluid catalytic cracking catalyst, operando FTIR, plastic waste, zeolite extrudates

ABSTRACT

The increasing production of plastic waste and the limitations of mechanical recycling have intensified the search for efficient chemical recycling technologies. Catalytic cracking over solid acid catalysts offers a promising route for converting polymers into valuable hydrocarbons at lower temperatures than thermal pyrolysis, while enabling control over product distribution through catalyst properties [1]. Fluid catalytic cracking (FCC) catalysts are particularly attractive for this purpose because they are industrially established and combine zeolite and matrix components that determine acidity, diffusion, and catalytic performance. However, the relationship between the physicochemical properties of commercial FCC catalysts and their performance in polymer cracking remains insufficiently understood.

In this work, fresh and equilibrium commercial FCC catalysts were systematically compared with laboratory-prepared USY/γ-Al_2O_3 extrudates. The catalysts were characterized in terms of their structural, textural, acidic, and diffusion properties and evaluated in the catalytic cracking of polypropylene (PP), low-density polyethylene (LDPE), and polystyrene (PS). Thermogravimetric analysis coupled with GC-MS was used to determine light-off behavior, product distributions, and coke deposition, while an operando FTIR&GC-MS approach enabled simultaneous monitoring of catalyst surface transformations and gaseous products under isothermal reaction conditions. Multivariate curve resolution–alternating least-squares (MCR-ALS) analysis was additionally applied to resolve spectroscopic features associated with polymer cracking and coke oxidation [2].

The results demonstrate that catalyst steaming substantially modifies the pore architecture and acid-site characteristics without eliminating catalytic functionality. The equilibrium catalyst treated at 800 °C (Cat-Eq800) exhibits enhanced secondary mesoporosity, efficient molecular transport, and a high Brønsted-to-Lewis acid site ratio. For PP cracking, the high acid-site density of the fresh catalyst promotes extensive secondary cracking and formation of lighter hydrocarbons, whereas Cat-Eq800 favors a higher olefinicity of the C4 fraction and reduced hydrogen-transfer reactions. Under operando conditions, the two commercial catalysts show comparable PP conversion but markedly different product selectivities, demonstrating the influence of micropore structure, acid-site density, and mass transport on polymer cracking pathways. LDPE cracking also shows a strong dependence on these properties, with Cat-Eq800 producing a higher fraction of C3–C5 hydrocarbons under the investigated operando conditions.

[1] Faculty of Chemistry, Jagiellonian University in Kraków, Kraków, Poland,
* kinga.gora-marek@uj.edu.pl
[2] Doctoral School of Exact and Natural Sciences, Jagiellonian University in Kraków, Kraków, Poland
[3] W. R. Grace, Columbia, Maryland, USA
[4] Laboratoire Catalyse & Spectrochimie, Normandie Université, ENSICAEN, CNRS, Caen, France

The catalyst–polymer interactions further depend on polymer structure. PS cracking follows a distinct pathway dominated by styrene formation at moderate temperatures, whereas polyolefin cracking produces broader hydrocarbon distributions governed by acid-site accessibility and hydrogen-transfer reactions. Coprocessing PP and LDPE results in enhanced formation of light hydrocarbons (C2–C5), reduced formation of C6+ products, and lower coke deposition compared with the individual polymers, indicating synergistic interactions between degradation intermediates originating from the two polyolefins. Notably, Cat-Eq800 shows substantially enhanced coke resistance, accumulating approximately twenty times less coke than Cat-F800 during PP cracking.

Overall, the combination of catalyst characterization, TGA&GC-MS, operando FTIR&GC-MS, and MCR-ALS provides a detailed picture of the relationships between FCC catalyst architecture, acidity, mass transport, product selectivity, and deactivation during polymer cracking. The results demonstrate that equilibrium FCC catalysts, despite their lower Brønsted acid-site concentration, can retain efficient mass transport and catalytic functionality due to their hierarchical pore structure. These findings provide a basis for understanding and further optimizing FCC catalyst formulations for the chemical recycling of individual and mixed plastic waste streams [3].

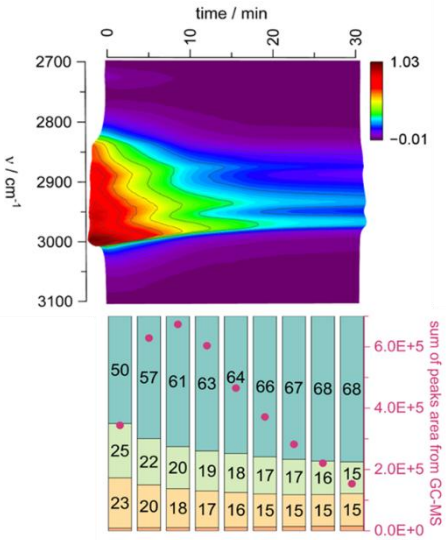


Figure 1. FTIR&GC-MS operando data for PP cracking.

[1] A. Rahimi, J.M. García, Chemical recycling of waste plastics for new materials production, Nat. Rev. Chem. 1 (2017) 0046. https://doi.org/10.1038/s41570-017-0046.
[2] A. de Juan, J. Jaumot, R. Tauler, Multivariate curve resolution (MCR). Solving the mixture analysis problem, Anal. Methods 6 (2014) 4964–4976. https://doi.org/10.1039/C4AY00571F.
[3] O. Rogala, K.A. Tarach, A. Kordek, Y. Shu, J.-P. Gilson, L. Lakiss, K. Góra-Marek, Commercial fluid catalytic cracking catalysts for polymers chemical recycling, ChemSusChem 19 (2026) e71002. https://doi.org/10.1002/cssc.71002.

Acknowledgment: This research was funded by the National Science Center, Poland [Grant No. 2021/43/B/ST4/00307].

Inclusion of Nuclear Energy in a Renewable Energy-Based Mix

Duarte M. Sousa[1,*], Maria Margarida Faustino Pinheiro[1], Bernardo Miguel Grilo Marçal[1]

Keywords: Nuclear Power, Energy Transition, Climate Change, Decarbonization, Carbon Neutrality

ABSTRACT

This work aims to analyze the feasibility of incorporating nuclear power into Portugal's energy mix to achieve carbon neutrality by 2050. Considering that the world is facing one of the greatest challenges in human history, and given the urgency of reducing CO_2 emissions, the main objective of this work is to present a feasible alternative to a renewable energy-based mix, using the Portuguese energy roadmap for 2050 (RNC2050) as a reference. The feasibility of introducing nuclear power as a low-carbon energy source and contributing to carbon neutrality by 2050 is assessed using energy data from recent years (Fig. 1) [1]. A modelling tool was used to assess how the energy mix would change if nuclear power were included, as well as to forecast electricity generation by 2050 (Fig. 2).

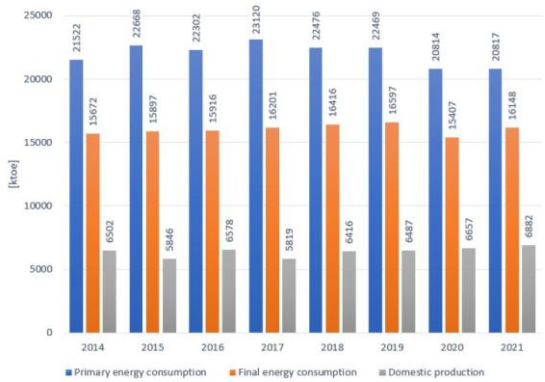


Figure 1. Primary energy consumption, final energy consumption, and domestic energy production from 2014 to 2021 (adapted from [1]).

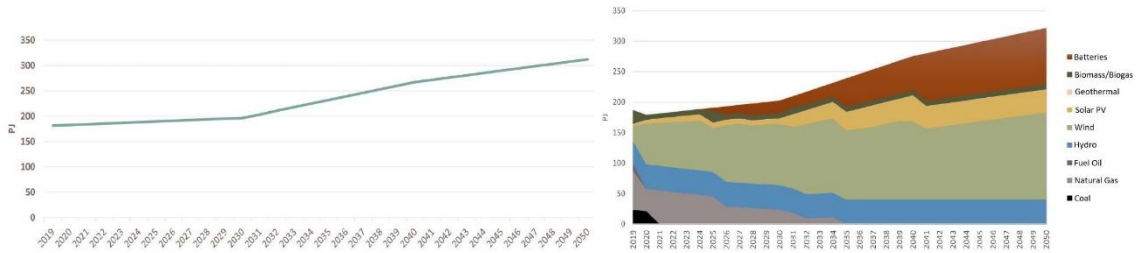


Figure 2. Forecast of final electricity consumption in Portugal (adapted from [2])

Based on the scenarios presented in Figs. 1 and 2, the feasibility of incorporating nuclear energy into the energy mix is analyzed. The potential nuclear power plant is dimensioned, and the simulation results for the installed capacity are presented in Tables 1 and 2, considering energy mixes without and with nuclear power generation, respectively.

[1] Instituto Superior Técnico/DEEC/AC Energia, Av. Rovisco Pais 1, 1049-001 Lisboa, Portugal
* duarte.sousa@tecnico.ulisboa.pt

Table 1. Evolution of installed capacity based on the simulation without nuclear power in the energy mix.

[MW]	2020	2030	2040	2050
Coal	1,76	0,00	0,00	0,00
Natural Gas	4,73	3,38	2,65	0,00
Fuel Oil	0,91	0,19	0,11	0,00
Hydro	6,99	7,10	7,10	7,10
Wind	2,28	9,60	16,91	17,42
Solar PV	1,90	7,10	16,95	26,20
Geothermal	0,03	0,02	0,02	0,02
Biomass	0,81	0,52	0,44	0,52
Batteries	0,00	1,67	5,79	11,54
Total	23,7	32,2	44,8	52,2

Table 2. Evolution of installed capacity based on the simulation with nuclear power in the energy mix

[MW]	2020	2030	2040	2050
Coal	1,76	0,00	0,00	0,00
Natural Gas	4,73	3,38	0,00	0,00
Fuel Oil	0,91	0,19	0,10	0,00
Hydro	6,99	6,26	6,76	7,10
Wind	6,24	9,19	9,32	11,80
Solar PV	2,28	3,23	3,06	0,18
Geothermal	0,03	0,02	0,01	0,01
Biomass	0,81	0,52	0,36	0,28
Batteries	0,00	0,63	1,24	3,25
Nuclear	0,00	4,00	6,00	6,00
Total	23,7	23,4	20,8	22,6

The addition of a nuclear power plant in Portugal would have a significant impact on the energy requirements forecast by the carbon neutrality roadmap. With the phase-out of natural gas plants, the use of fossil fuels could be eliminated by 2040. Dependence on hydropower would be reduced, and the modelling suggests that the required installed capacity could be lower than the current capacity.

Dam construction would continue to be relevant for energy storage and irrigation, and dams would play an important role in the energy mix during years with abundant water availability. The value of electricity generated in the future will depend on the ability of each generation technology to supply energy during critical periods. Nuclear power plants can generate electricity at any time of day on a consistent basis, regardless of weather conditions.

Nuclear energy is capable of producing both electricity and hydrogen. Generation IV nuclear reactors can contribute to hydrogen production by combining nuclear energy with thermochemical water splitting and electrolysis [5].

The compatibility of nuclear reactors with the majority of renewable energy sources remains an important consideration. Nuclear power plants have traditionally been considered relatively inflexible because they are designed to operate continuously at high output. Wind and solar power plants, on the other hand, produce electricity at variable levels depending on weather conditions.

As a final remark, despite the increased energy dependence resulting from uranium imports, the construction of a nuclear power plant could be economically viable and could also play an important role in the decarbonization process. However, several changes would be required, including a shift in public opinion, as well as reductions in investment costs and construction delays.

Achieving carbon neutrality by 2050 will require a secure and reliable energy supply while maintaining affordable electricity costs. The introduction of nuclear power into future energy mixes could therefore contribute to ensuring affordable electricity prices.

[1] Direção-Geral de Energia e Geologia (DGEG), Balanço Energético Nacional 2022, Lisbon, Portugal, 2023. https://www.dgeg.gov.pt/pt/destaques/balanco-energetico-nacional-2022/.
[2] Agência Portuguesa do Ambiente (APA), Roteiro para a Neutralidade Carbónica 2050 (RNC2050), Lisbon, Portugal, 2019. https://apambiente.pt/clima/roteiro-para-neutralidade-carbonica-2050.

[3] Y.A. Kazansky, Introduction to nuclear power technology, in: S.U.-D. Khan, A.V. Nakhabov (Eds.), Nuclear Reactor Technology Development and Utilization, Woodhead Publishing, 2020, pp. 1–26. https://doi.org/10.1016/B978-0-12-818483-7.10000-9.
[4] A. Berger, T. Blees, F.-M. Bréon, B.W. Brook, P. Hansen, R.B. Grover, C. Guet, W. Liu, F. Livet, H. Nifenecker, M. Petit, G. Pierre, H. Prévot, S. Richet, H. Safa, M. Salvatores, M. Schneeberger, S. Zhou, How much can nuclear energy do about global warming?, Int. J. Glob. Energy Issues 40 (2017) 43–78. https://doi.org/10.1504/IJGEI.2017.080766.
[5] S. Şahin, H.M. Şahin, Generation-IV reactors and nuclear hydrogen production, Int. J. Hydrogen Energy 46 (2021) 28936–28948. https://doi.org/10.1016/j.ijhydene.2020.12.182.

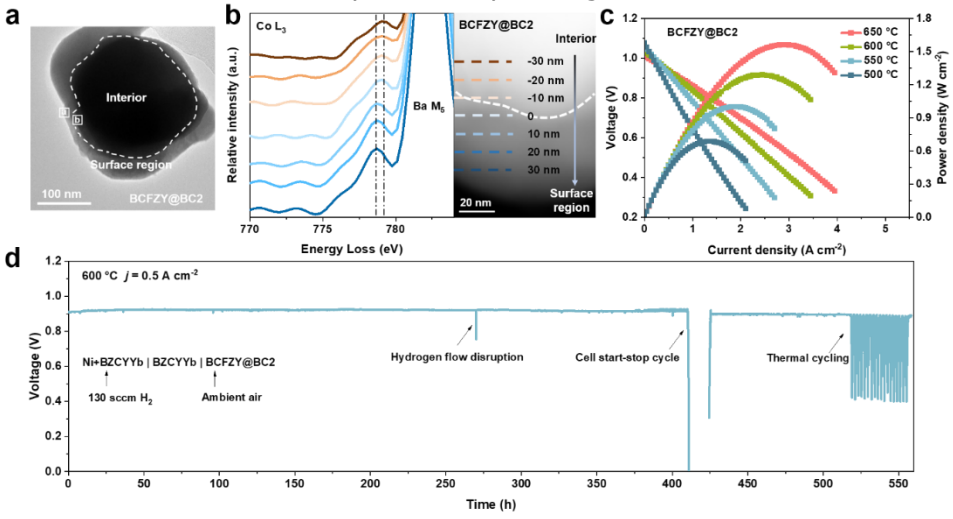
Surface Reconstruction Enables High-Performance and Fluctuation-Resistant Cathodes for Proton Ceramic Fuel Cells

Youmin Guo [1,*], Mengen Shao [1]

Keywords: Proton ceramic fuel cells; cathode; surface reconstruction; oxygen vacancies; oxygen reduction reaction; cycling stability

ABSTRACT

Proton ceramic fuel cells (PCFCs) are promising for efficient intermediate-temperature power generation, but their cathodes face two key challenges: sluggish oxygen reduction reaction (ORR) kinetics and structural instability under fluctuating operating conditions [1]. In this work, $BaCo_{0.4}Fe_{0.4}Zr_{0.1}Y_{0.1}O_{3-\delta}$ (BCFZY) was selected as the host cathode, and surface reconstruction was induced using barium nitrate and cobalt nitrate as Ba and Co precursors (Ba:Co = 1:1). BCFZY@BCx cathodes (x = 1, 2, and 3, with precursor concentrations of 0.01, 0.02, and 0.03 mol L^{-1}, respectively) were then prepared. Electron energy loss spectroscopy (EELS) revealed a Co-rich, Fe-depleted reconstructed layer on the surfac of BCFZY@BC2, accompanied by a lower Co valence state and an increased oxygen-vacancy concentration. X-ray absorption spectroscopy (XAS) revealed that the Co–O/Fe–O framework remained intact but became less ordered, preserving the bulk structure with introducing coordinatively unsaturated sites. O_2 temperature-programmed desorption (O_2-TPD) and X-ray photoelectron spectroscopy (XPS) confirmed the increase in oxygen-vacancy concentration. Electrical conductivity relaxation (ECR) measurements further showed the resulting oxygen-vacancies accelerate oxygen-ion transport and enhance hydration, while alleviating the H_2O/O_2 competitive adsorption. At 600 °C, a single cell with BCFZY@BC2 achieved a peak power density of 1.29 W cm^{-2}, compared with 0.70 W cm^{-2} for BCFZY. The cell operated for over 400 h without obvious voltage degradation, recovered after room-temperature shutdown/restart, and remained stable for over 100 h. Voltage and impedance showed no significant degradation after 18 thermal cycles and slow/rapid current cycling. These results demonstrate that precursor-induced surface reconstruction simultaneously improves cathode activity and durability, providing a promising strategy for long-life PCFC cathodes under practical operating conditions.



[1] School of Materials Science and Engineering, Anhui University, Hefei, 230601, China
*youminguo@ahu.edu.cn

Figure 1. (a) TEM image of BCFZY@BC2 particles; (b) Co L3-edge EELS spectra; (c) I–V and I-P curves of a BCFZY@BC2-based single cell at 500–650 °C; (d) Long-term stability under H2 interruption, start-up/shutdown, and thermal cycling at 600 °C and 0.5 A cm-2.

[1] S. Zhao, W. Ma, B. He, Y. Ling, Y. Huang, F. Hu, Z. Shu, L. Zhao, Single-atom enables reverse hydrogen spillover for high-performance protonic ceramic fuel cells, Adv. Mater. 37 (2025) 2501387. https://doi.org/10.1002/adma.202501387.

Mechanistic Insights into CO_x Methanation of CO_2/CO Mixtures over Nanostructured NiO–CeO_2

Ivan Martinez-Lopez[1,*], Juan Bueno-Ferrer[1], Iris Martin-Garcia[1], Esteban Guillen-Bas[1], Arantxa Davo-Quinonero[1], Virginia Perez-Dieste[2], Dolores Lozano-Castello[1], Agustin Bueno-Lopez[1]

Keywords: CO_x methanation; NiO–CeO_2; CO_2 hydrogenation; in situ DRIFTS; NAP-XPS

ABSTRACT

Decarbonization strategies increasingly rely on the conversion of carbon oxides into synthetic fuels that can be integrated into existing energy infrastructures. In this context, methanation of CO_2-containing streams is especially attractive, although the simultaneous presence of CO, as commonly encountered in industrial off-gases and process streams, can strongly modify catalyst behavior and reaction pathways. [1] Understanding how both carbon oxides compete and cooperate on the catalyst surface is therefore essential for moving from idealized single-reactant feeds toward more realistic gas compositions. Here, the methanation of CO_2, CO, and CO_2/CO mixtures over a nanostructured NiO–CeO_2 catalyst was investigated with particular emphasis on the interplay between catalytic performance, surface redox state, and reaction mechanism. The catalyst consists of uniform size 7 nm NiO–CeO_2 nanoparticles (Np), in which nickel oxide is finely dispersed within the ceria matrix, providing an intimate Ni–CeO_2 interface and pronounced redox functionality.

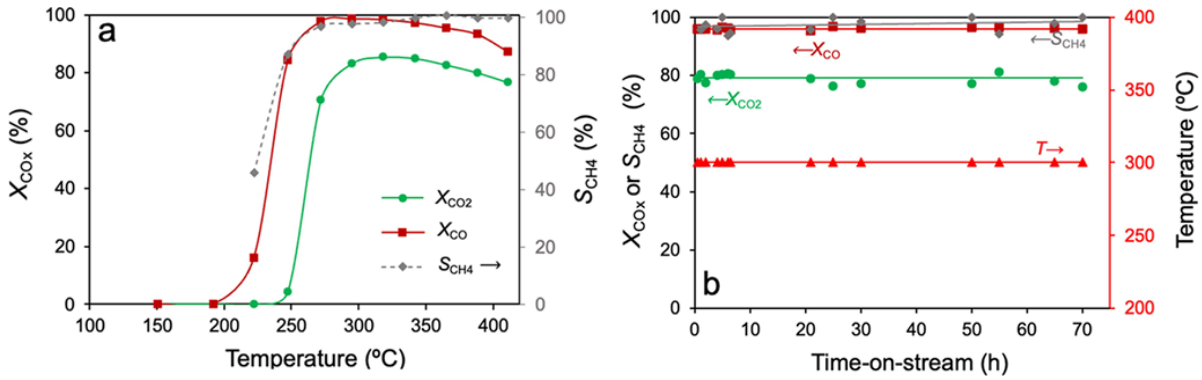


Figure 1. (a) CO_2 conversion profile (X_{CO2}, circles), CO conversion (X_{CO}, squares) and CH_4 selectivity (S_{CH4}, dashed line) in the fixed-bed activity test in the comethanation mixture with the NiO-CeO_2 (Np) catalyst. (b) 70 h isothermal (300 °C) comethanation test.

Catalytic tests showed that the material is highly active and selective for CO_2 methanation. CO_2 conversion reached 86% at 350 °C, close to the thermodynamic limit, while CH_4 selectivity remained near 100% throughout the investigated temperature range. Under simultaneous CO_2 + CO methanation conditions, CO was converted at lower temperature and reached 98% conversion at 300 °C. The presence of CO shifted the onset of CO_2 methanation to higher temperature, indicating competitive adsorption on the catalyst surface; nevertheless, above 300 °C the CO_2 conversion approached that obtained during standalone CO_2 methanation. The catalyst also displayed robust operation during a

[1] University of Alicante, Spain, * ivan.martinez1@ua.es
[2] ALBA Synchrotron Light Source, Spain

70 h isothermal comethanation test at 300 °C, maintaining high carbon-oxide conversion and methane selectivity. In contrast, methanation of CO in the absence of CO_2 was markedly less efficient. CO conversion reached only 41% at 250 °C and methane selectivity was approximately 80%, with CO_2 appearing as a competitive product. Differences between CO and CO_2 methanation over supported Ni catalysts, particularly the favorable behavior of CeO_2-supported systems, have also been reported previously. [2]

To elucidate these contrasting behaviors, fixed-bed activity measurements were combined with in situ diffuse reflectance infrared Fourier-transform spectroscopy coupled with mass spectrometry, isotopic pulse experiments using labeled carbon oxides, and near-ambient-pressure X-ray photoelectron spectroscopy at a synchrotron source. This multi-technique approach enabled the gas-phase activity trends to be directly related to adsorbed intermediates and changes in the Ni/Ce oxidation states under reaction environments. The spectroscopic results indicate that CO_2 methanation and CO_2/CO comethanation converge toward a common pathway in which CO_2 is transformed into adsorbed CO species prior to further hydrogenation to CH_4. Formate and carbonate species participate as surface intermediates, while transient nickel carbonyl species reveal the formation and rapid consumption of adsorbed CO. Isotopic experiments further support the role of CO as a key intermediate connecting the CO_2 and CO methanation pathways.

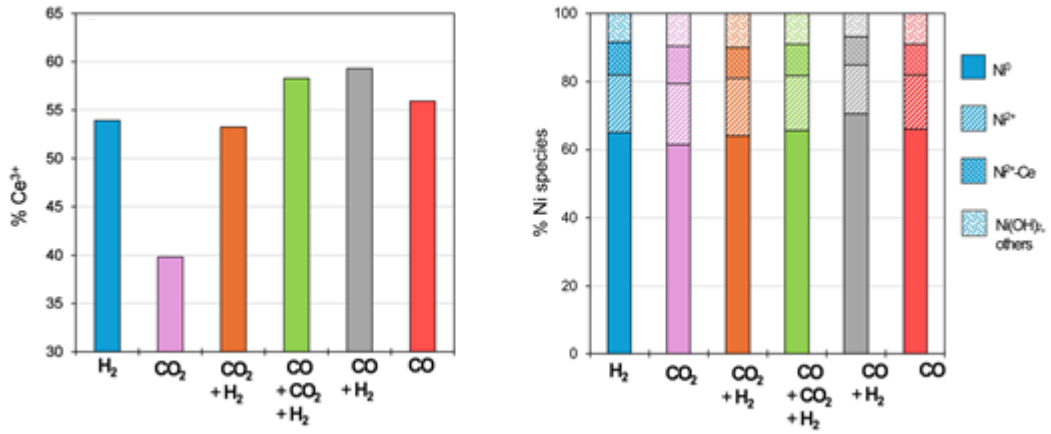


Figure 2. Quantification of surface reduced Ce3+ cations and Ni species distribution in NiO-CeO2 (Np) catalyst under different conditions.

Near-ambient-pressure XPS revealed that CO strongly affects the redox state of the catalyst. Under comethanation conditions, CO promotes ceria reduction, whereas the simultaneous presence of CO_2 provides an oxidizing counterbalance that stabilizes an effective redox cycle and favors selective methanation. [3] Conversely, under CO + H_2 without CO_2, excessive catalyst reduction and competing CO oxidation/disproportionation processes become significant, leading to CO_2 formation and limiting methane production. These findings demonstrate that the high activity of NiO–CeO_2 in mixed CO_2/CO feeds originates not simply from independent methanation of both reactants, but from a coupled reaction network governed by competitive adsorption and the dynamic redox response of the Ni–CeO_2 interface. The results highlight the potential of redox-active Ni–CeO_2 nanostructures for the valorization of realistic CO_x-containing streams into methane and provide mechanistic guidelines for designing catalysts for carbon recycling and sustainable synthetic-fuel production.

[1] L. Atzori, E. Rombi, D. Meloni, M.F. Sini, R. Monaci, M.G. Cutrufello, CO and CO_2 co-methanation on Ni/CeO_2-ZrO_2 soft-templated catalysts, Catalysts 9 (2019) 415. https://doi.org/10.3390/catal9050415.
[2] T.A. Le, M.S. Kim, S.H. Lee, T.W. Kim, E.D. Park, CO and CO_2 methanation over supported Ni catalysts, Catal. Today 293–294 (2017) 89–96. https://doi.org/10.1016/j.cattod.2016.12.036.
[3] S. López-Rodríguez, A. Davó-Quiñonero, E. Bailón-García, D. Lozano-Castelló, I.J. Villar-Garcia, V. Perez Dieste, J.A. Onrubia Calvo, J.R. González Velasco, A. Bueno-López, Monitoring by in situ NAP-XPS of active sites for CO_2 methanation on a Ni/CeO_2 catalyst, J. CO_2 Util. 60 (2022) 101980. https://doi.org/10.1016/j.jcou.2022.101980.

Natural Materials Powering Tomorrow's Buildings

Verónica de Zea Bermudez[1,*]

Keywords: net-zero energy buildings, optical and thermal comfort, smart windows, luminescent solar concentrators, natural materials

ABSTRACT

In recent years, the integration of natural materials as sustainable alternatives in energy devices has advanced rapidly, particularly within eco-friendly architecture. This shift is driven by the urgent need for greener alternatives to traditional materials—such as heavy metal oxides, toxic liquid electrolytes, and petroleum-based polymers—which are often scarce, hazardous, or difficult to recycle.

By prioritizing eco-friendly matrices and naturally derived fluorophores, this research addresses the environmental footprint of advanced light-harvesting technologies while simultaneously optimizing indoor daylighting and generating clean electricity on-site. Practical examples feature electrochromic and thermotropic smart windows, as well as luminescent solar concentrators, incorporating bio-based components derived from plants [1,2], polysaccharides [3-8], and proteins [9-12].

This work is a contribution to a scalable, green pathway for transforming static building envelopes into active, energy-positive systems, accelerating the transition toward net-zero energy buildings while maintaining the occupant's thermal and visual comfort.

[1] P.J. Nunes, M. Fernandes, V. de Zea Bermudez, Novel thermotropic system with UV-blocking ability for dynamic radiative cooling and synchronous visible/NIR tuning of windows in buildings in hot climate regions, J. Sci. Adv. Mater. Devices 10 (2025) 100907. https://doi.org/10.1016/j.jsamd.2025.100907.
[2] P.J. Nunes, R.F.P. Pereira, S.C. Nunes, S.F.H. Correia, L. Fu, R.A.S. Ferreira, M. Fernandes, V. de Zea Bermudez, POE-mediated tunable quantum yield of carbon dots derived from Agapanthus africanus (L.) Hoffmann leaves, Small 21 (2025) 2404717. https://doi.org/10.1002/smll.202404717.
[3] S.C. Nunes, T.A.G. Duarte, R.F.P. Pereira, L. Fu, R.A.S. Ferreira, P. Almeida, V. de Zea Bermudez, Eco-friendly innovation: Three-mode sun-actuated thermotropic devices integrating κ-carrageenan-based film doped with Arundo donax leaf-derived carbon dots and 1-butyl-3-methyl-1H-imidazolium chloride, J. Mater. Chem. A 13 (2025) 743–761. https://doi.org/10.1039/D4TA06890D.
[4] S.C. Nunes, S.M. Saraiva, R.F.P. Pereira, S. Pereira, M.M. Silva, L.D. Carlos, E. Fortunato, R.A.S. Ferreira, R. Rego, V. de Zea Bermudez, Sustainable dual-mode smart windows for energy-efficient buildings, ACS Appl. Energy Mater. 2 (2019) 1951–1960. https://doi.org/10.1021/acsaem.8b02041.
[5] F.M. Santos, T.A.G. Duarte, S.F.H. Correia, R.F.P. Pereira, A. Conde, Á.R. Ribeiro, S.S. Braga, S.P.M. Ventura, R.A.S. Ferreira, V. de Zea Bermudez, S.C. Nunes, Biphosphor carbon dots/chlorophyll system entirely derived from Chlorella microalgae for luminescent solar concentrators, ACS Nanosci. Au 5 (2025) 137–152. https://doi.org/10.1021/acsnanoscienceau.4c00048.
[6] F.M. Santos, S.C. Nunes, V. de Zea Bermudez, Looking beyond biology: Glycosaminoglycans as attractive platforms for energy devices and flexible electronics, Energy Adv. 3 (2024) 1766–1843. https://doi.org/10.1039/D4YA00155A.
[7] H.M.R. Gonçalves, R.F.P. Pereira, E. Lepleux, L. Pacheco, A.J.M. Valente, A.J. Duarte, V. de Zea Bermudez, Non-Newtonian thermosensitive nanofluid based on carbon dots functionalized with ionic liquids, Small 16 (2020) 1907661. https://doi.org/10.1002/smll.201907661.
[8] H.M.R. Gonçalves, R.F.P. Pereira, E. Lepleux, T. Carlier, L. Pacheco, S. Pereira, A.J.M. Valente, E. Fortunato, A.J. Duarte, V. de Zea Bermudez, Nanofluid based on glucose-derived carbon dots functionalized with [Bmim]Cl for the next generation of smart windows, Adv. Sustain. Syst. 3 (2019) 1900047. https://doi.org/10.1002/adsu.201900047.
[9] R.F.P. Pereira, R. Gonçalves, H.M.R. Gonçalves, D.M. Correia, C.M. Costa, M.M. Silva, S. Lanceros-Méndez, V. de Zea Bermudez, Plasma-treated Bombyx mori cocoon separators for high-performance and sustainable lithium-ion batteries, Mater. Today Sustain. 9 (2020) 100041. https://doi.org/10.1016/j.mtsust.2020.100041.
[10] T.C.D. Fernandes, H.M.R. Rodrigues, F.A.A. Paz, J.F.M. Sousa, A.J.M. Valente, M.M. Silva, V. de Zea

[1] Chemistry Department and CQ-VR, University of Trás-os-Montes e Alto Douro, 5000-801 Vila Real, Portugal; vbermude@utad.pt

Bermudez, R.F.P. Pereira, Highly conducting Bombyx mori silk fibroin-based electrolytes incorporating glycerol, dimethyl sulfoxide and [Bmim]PF_6, J. Electrochem. Soc. 167 (2020) 070551. https://doi.org/10.1149/1945-7111/ab8313.

[11] R.F.P. Pereira, F. Sentanin, A. Pawlicka, M.C. Gonçalves, M.M. Silva, V. de Zea Bermudez, Smart windows prepared from Bombyx mori silk, ChemElectroChem 3 (2016) 1084–1097. https://doi.org/10.1002/celc.201600095.

[12] T.A.G. Duarte, R.F.P. Pereira, B. Medronho, E.S. Maltseva, E.F. Krivoshapkina, A. Varela-Dopico, P. Taboada, L. Fu, R.A.S. Ferreira, V. de Zea Bermudez, A glance at novel ionanofluids incorporating silk-derived carbon dots, Chem. Mater. 36 (2024) 1136–1152. https://doi.org/10.1021/acs.chemmater.3c01370.

Acknowledgments: This work was funded by the RISE - Smart Cities, Sustainable Energy and Materials project (operation code NORTE2030-FEDER-02723100) financed by the European Regional Development Fund, through Incentives for Research, Development and Innovation, within the scope of the Northern Regional Program 2021-2027 [NORTE2030]. CQ-VR is also acknowledged for the support through projects UID/00616/2025 (https://doi.org/10.54499/UID/00616/2025) and UID/PRR/00616/2025 (https://doi.org/10.54499/UID/PRR/00616/2025).

Influence of Alkali Species on the Work Function of Cobalt Materials: Combined Experimental and Theoretical Insights

Mariia Bordulenko[1,2,*], Andrzej Wójtowicz[2,3], Filip Zasada[2], Witold Piskorz[2], Andrzej Kotarba[2], Gabriela Grzybek[2]

Keywords: cobalt catalyst, potassium promotion, thermal alkali desorption

ABSTRACT

The effect of alkali metal addition has been widely studied in various catalytic reactions. Alkali promotion can influence catalyst stability, activity, and selectivity. Due to their strong electron-donating character, alkali metals can alter the electronic structure of catalyst surfaces and may also enhance their structural and thermal stability [1].

Potassium promotion has proven particularly beneficial for cobalt-based catalysts used in ethanol steam reforming (ESR), improving hydrogen selectivity and catalyst durability under reaction conditions [2]. However, the exact mechanism of alkali promotion remains unclear due to the difficulties associated with characterizing alkali species on catalyst surfaces. This problem is related to their low concentration and elevated-temperature mobility. Alkali species may migrate, segregate, or desorb in different forms, such as atoms, ions, Rydberg atoms, and clusters [3]. Therefore, direct investigation of the surface state of alkali promoters is essential for understanding their promotional effects.

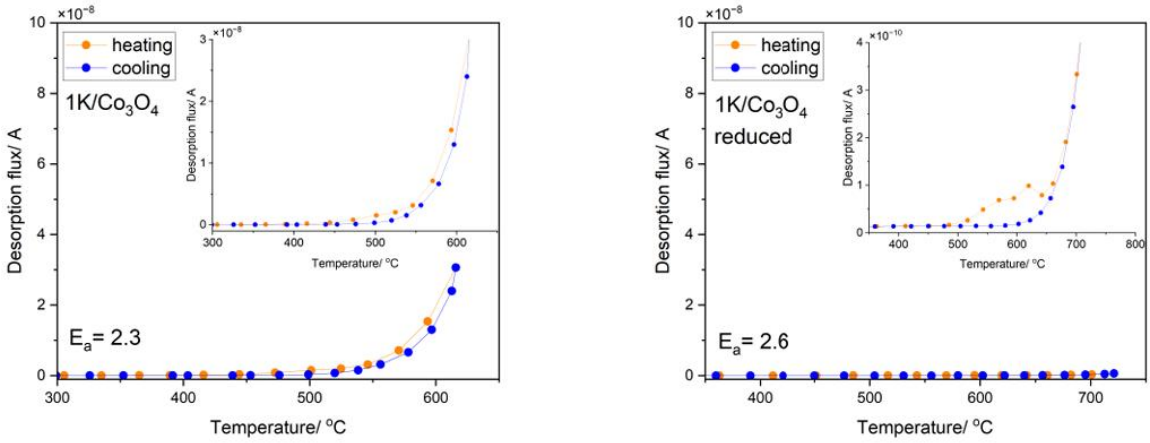


Figure 1. Potassium thermal desorption signals for K-doped (1 wt.% K) pristine and reduced Co3O4 catalysts.

In our studies, we employed a unique technique developed at the Jagiellonian University for thermal alkali desorption studies (TAD), which provides direct insight into alkali behavior by measuring the alkali desorbing from the catalyst surface. We studied cobalt oxide phases doped with potassium, which are considered promising and cost-effective catalyst materials for the ESR process and hydrogen production [2]. In this process, potassium promotion can improve catalyst selectivity toward hydrogen and enhance stability under reaction conditions [3]. As the starting material, we used cobalt

[1] Faculty of Physics, Astronomy and Applied Computer Science, Jagiellonian University in Kraków, prof. Stanisława Łojasiewicza 11, 30-348 Kraków, Poland, * mariia.bordulenko@student.uj.edu.pl
[2] Faculty of Chemistry, Jagiellonian University in Kraków, Gronostajowa 2, 30-387 Kraków, Poland
[3] Doctoral School of Exact and Natural Sciences, Jagiellonian University in Kraków, prof. S. Łojasiewicza 11, 30-384 Kraków, Poland

spinel prepared by a precipitation method and subsequently doped with potassium (0 – 2 wt. % K) via incipient wetness impregnation. Alkali desorption measurements were conducted for both pristine and *in situ* reduced (5% H_2/Ar, 500 °C, 1 h) samples, together with work function measurements performed using the Kelvin probe method, to elucidate the surface electronic properties. The thermal alkali desorption results were supported by complementary characterization techniques, including powder X-ray diffraction (XRD), transmission electron microscopy (TEM), Raman spectroscopy, and X-ray photoelectron spectroscopy (XPS). The results indicate that the surface state of potassium is affected by both the potassium concentration and the oxidation state of the cobalt phase. Additionally, we measured changes in work function upon potassium doping for both the oxidized and reduced cobalt phases. The experimentally observed changes in the electronic structure and electrostatic state of the catalyst surfaces induced by K-containing surface species, as evidenced by the work function measurements, were further investigated by periodic DFT calculations. The results indicate that the presence of potassium species on the surface reduces the work function, regardless of their chemical form, consistent with the formation of an outward-oriented surface dipole arising from electron donation by alkali species to the cobalt oxide surface.

[1] O.U. Osazuwa, K.H. Ng, A review to elucidate the influence of promoters on the acidity/basicity, reducibility, and metal-support interaction of catalysts in methane dry reforming, Alex. Eng. J. 127 (2025) 309–335. https://doi.org/10.1016/j.aej.2025.04.104.
[2] G. Grzybek, K. Góra-Marek, P. Patulski, M. Greluk, M. Rotko, G. Słowik, A. Kotarba, Optimization of the potassium promotion of the Co|α-Al_2O_3 catalyst for the effective hydrogen production via ethanol steam reforming, Appl. Catal. A Gen. 614 (2021) 118051. https://doi.org/10.1016/j.apcata.2021.118051.
[3] G. Grzybek, M. Greluk, P. Indyka, K. Góra-Marek, P. Legutko, G. Słowik, S. Turczyniak-Surdacka, M. Rotko, Z. Sojka, A. Kotarba, Cobalt catalyst for steam reforming of ethanol–Insights into the promotional role of potassium, Int. J. Hydrogen Energy 45 (2020) 22658–22673. https://doi.org/10.1016/j.ijhydene.2020.06.037.

Acknowledgments: The work was financed by Grant No. 2021/43/D/ST4/03016 from the National Science Centre, Poland.

From Microscale Pyrolysis Characterisation to Aspen Plus Process Modelling: Preliminary Pilot-Scale Assessment of Fuel-Range Hydrocarbon Separation and Recovery from Polypropylene Waste

Łukasz Korzeniowski[1,*], Mariusz Wądrzyk[1], Abul Hassan Quddusi[2], Chunfei Wu[2], Aneta Magdziarz[3]

Keywords: polypropylene, Py-GC-MS, process modelling, Aspen Plus, hydrocarbon separation.

ABSTRACT

Over the past decade, disruptions in global fuel, energy, and petrochemical markets have increased interest in securing feedstock supplies, diversifying hydrocarbon sources, and developing alternative supply routes. At the same time, the growing accumulation of plastic waste, including marine plastic waste, has intensified the need for technologies that combine effective waste management with the recovery of value-added chemical products.

Pyrolysis of polyolefins represents one such pathway, producing both a gaseous fraction and a liquid pyrolysis oil, each comprising a broad range of hydrocarbon compounds with different molecular weights and physicochemical properties [1]. The high compositional complexity of these products may limit their direct application and complicate their integration with existing refinery streams. Therefore, further fractionation and upgrading are required to obtain product streams with narrower boiling ranges and more uniform and stable physicochemical properties, thereby facilitating their subsequent utilization and potential blending with conventional refinery feedstocks.

In this study, experimental characterisation of waste polypropylene (PP) pyrolysis was combined with preliminary process modelling in Aspen Plus. Thermogravimetric analysis (TGA) and pyrolysis gas chromatography–mass spectrometry (Py-GC-MS) were used to investigate thermal degradation and the relative distribution of the main hydrocarbon groups released during thermal decomposition of raw material. Py-GC-MS data were interpreted as semi-quantitative information on the relative abundance of identified compounds rather than as direct measurements of absolute product yields. In the Aspen Plus model, polypropylene conversion was represented using an RYield reactor, with the product distribution and overall mass balance derived from the combined TGA and Py-GC-MS results. The model was developed for a nominal PP feed rate of 100 kg/h. The complex pyrolysis product mixture was represented by selected surrogate compounds (e.g. Propylene, 2-methyl-2-pentene) covering the main carbon-number ranges and chemical classes, including paraffins, olefins and aromatics.

The resulting model was used to investigate mass and energy balances across the main processing stages, including cooling, phase behaviour, gas–liquid separation, and sequential distillation of the pyrolysis products. Cooling temperature had a clear effect on the initial product split. Lower temperatures increased the recovery of the condensable C5+ fraction but also promoted the co-condensation of C1–C4 hydrocarbons. Deeper cooling therefore did not provide an unequivocal improvement in separation and instead shifted part of the separation duty to downstream fractionation. Nitrogen remained almost entirely in the gas phase, allowing the flash separator to remove most of the inert carrier

[1] AGH University of Krakow, Faculty of Energy and Fuels, Krakow, Poland, * lukkor@agh.edu.pl
[2] School of Chemistry and Chemical Engineering, Queen's University Belfast, Belfast, UK
[3] AGH University of Krakow, Faculty of Metals Engineering and Industrial Computer Science, Krakow, Poland

gas while providing an initial separation between light and condensable hydrocarbons. Residual C1–C4 hydrocarbons were subsequently removed from the liquid phase in the first distillation column, while the second column produced a C5–C10 light hydrocarbon fraction and a heavier wax-range fraction. The results indicate that effective recovery of compositionally distinct light-gas, C5–C10, and heavier fractions requires a combination of phase separation and sequential distillation rather than low-temperature condensation alone. Under the assumed process configuration, the simulated heating duty associated with feed heating and pyrolysis was approximately 3.5 MJ/kg PP. The two distillation stages required an additional 1.9 MJ/kg PP for their reboilers, resulting in a total simulated heating requirement of approximately 5.4 MJ/kg PP. In addition, approximately 2.2 MJ/kg PP of heat had to be removed upstream of the flash separator in the base case to achieve conditions favourable for C5+ condensation. These results show that downstream separation, particularly the combination of cooling and distillation, makes a substantial contribution to the overall process utility demand while also being essential for achieving the product purity required for the integration of PP pyrolysis-derived streams into conventional refinery processing.

Overall, the study demonstrates that combining microscale experimental characterisation with preliminary Aspen Plus modelling can provide a practical first step towards a more comprehensive assessment of hydrocarbon recovery from waste polypropylene. The approach enables key separation and energy trade-offs to be identified and supports the selection of process stages requiring more detailed investigation before pilot-scale development.

[1] G.G. Kombe, Global trends and strategic pathways for waste plastics depolymerization in the circular economy, Clean. Waste Syst. 11 (2025) 100292. https://doi.org/10.1016/j.clwas.2025.100292.

Acknowledgements: This project has received funding from the European Union's Horizon 2020 research and innovation programme under the Marie Skłodowska-Curie grant agreement No 101086071, project name "CUPOLA — Carbon-neutral pathways of recycling marine plastic waste".
Support was also provided by the Ministry of Science and Higher Education in Poland through the program "PMW grant no. 5863/HE/2024/2 (no. W52/HE/2024).
This research was partially funded by the Ministry of Science and Higher Education, Poland [AGH grant no. 16.16.110.663/501.00-110000-10000].

Reduction-Induced Changes in the Chemical State and Surface Dispersion of Potassium on Fe_2O_3

Andrzej Wójtowicz[1], Ivan Martinez Lopez[1], Andrzej Kotarba[1], Gabriela Grzybek[1,*]

Keywords: Fe_2O_3; potassium promotion; work function; potassium desorption; surface properties

ABSTRACT

Potassium is one of the most widely used promoters in iron-based catalysts for CO and CO_2 conversion processes [1]. Although its beneficial effect on catalytic performance is well established, considerably less attention has been devoted to understanding how the surface state of potassium evolves during catalyst activation. In particular, reduction of iron oxide may induce significant changes in the chemical form, distribution, and stability of potassium species, thereby modifying their electronic interaction with the catalyst surface and ultimately their promotional function.

In this work, the influence of reductive pretreatment on the surface state of potassium in Fe_2O_3 was investigated using work function measurements and thermal alkali desorption experiments under controlled vacuum conditions using the TADEK (*Thermal Alkali Desorption & Electronic Kelvin Probe*) station. A series of Fe_2O_3 samples containing 0-2 wt.% K was studied both in the fresh state and after reduction in order to track changes in potassium-derived surface species.

For the fresh materials, the work function decreased gradually from approximately 4.5 eV for unpromoted Fe_2O_3 to about 4.1 eV for the sample containing 2 wt.% K, indicating a moderate electronic effect associated with potassium incorporation. After reduction, however, a much stronger decrease was observed. While the reduced unpromoted sample exhibited a work function exceeding 4.2 eV, the K-containing samples displayed values between approximately 2.9 and 3.4 eV. The pronounced reduction in work function suggests that catalyst activation induces substantial changes in the surface state of potassium. These findings indicate that reduction does not simply preserve the promoter distribution established during synthesis, but instead drives a reorganization of potassium species at the catalyst surface.

Further evidence of potassium rearrangement was obtained from thermal alkali desorption measurements. Marked differences between fresh and reduced samples were observed (Figure 1). The modified desorption profiles demonstrate that reduction alters both the population and stability of surface potassium species. Rather than maintaining the initial promoter configuration, reductive treatment results in a redistribution of potassium accompanied by changes in the strength of K-surface interactions.

This conclusion is supported by the apparent activation energies derived from potassium desorption experiments (Figure 1). For the fresh samples, the activation energy increased strongly with potassium loading, from approximately 2 eV at low K content (0.2 – 0.5 wt.%) to values exceeding 5 eV at intermediate and high promoter concentrations. In contrast, the reduced materials exhibited considerably lower activation energies, ranging from approximately 1 to 2.3 eV over the entire composition range. The narrower distribution of activation energies observed after reduction points to the formation of a more uniform population of surface potassium species. These results reveal a substantial reorganization of the K-Fe surface interaction during catalyst activation and demonstrate

[1] Faculty of Chemistry, Jagiellonian University, Gronostajowa 2, 30-387 Kraków, Poland, * g.grzybek@uj.edu.pl

that reduction fundamentally modifies the chemical environment of potassium.

The combined work function and desorption data provide direct evidence that the surface state of potassium in Fe_2O_3-based catalysts is highly dynamic under reducing conditions. Reduction induces significant changes in the electronic character, and distribution of potassium species, indicating restructuring and redistribution of the promoter. [2] The evolution of potassium during activation, therefore, represents a critical factor governing promoter effectiveness in iron-based catalysts. These findings highlight the importance of considering the dynamic nature of alkali promoters when designing catalysts for CO and CO_2 conversion processes.

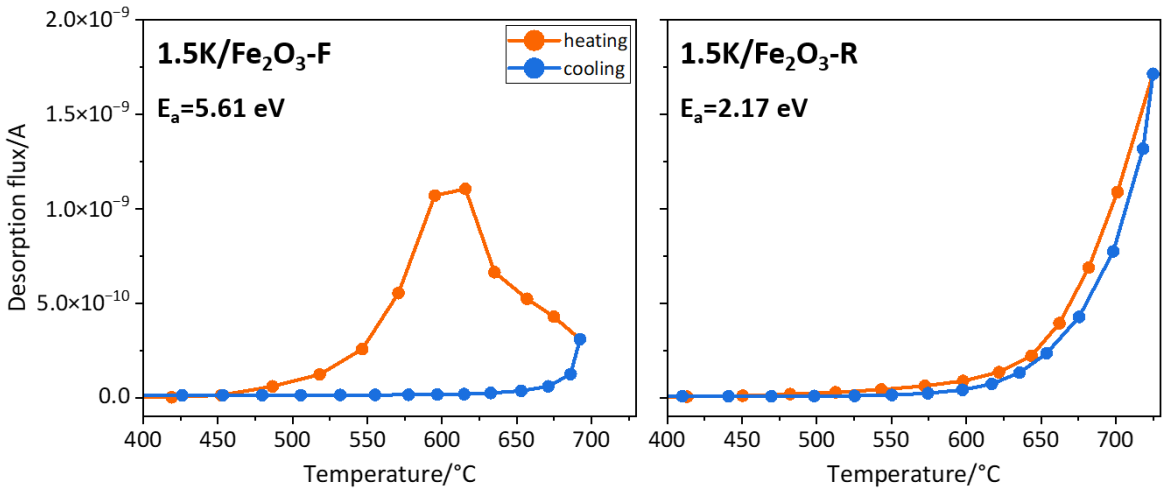


Figure 1. Potassium thermal desorption profiles for fresh (F) and reduced (R) 1.5 wt.%K sample together with the apparent activation energy for K desorption.

[1] A.P. Raje, R.J. O'Brien, B.H. Davis, Effect of potassium promotion on iron-based catalysts for Fischer–Tropsch synthesis, J. Catal. 180 (1998) 36–43. https://doi.org/10.1006/jcat.1998.2259.
[2] A. Kotarba, M. Hagström, K. Engvall, J.B.C. Pettersson, In situ characterization of an iron catalyst by potassium ion desorption and electron emission measurements, React. Kinet. Catal. Lett. 63 (1998) 219–224. https://doi.org/10.1007/BF02475391.

Acknowledgement: We thank the National Science Centre, Poland, for funding the research (grant no. 2024/55/B/ST5/02291).

Creating and Adjusting Iron-Based Perovskites for Potential Use in Waste Biomass Combustion Through Chemical Looping Processes

Ewelina Ksepko[1,*], Aleksandra Bobowska[1]

Keywords: oxide perovskites, synthesis, oxygen carriers, crystal structure, biomass, CO_2

ABSTRACT

A promising chemical looping combustion technique could provide a viable path toward carbon dioxide neutrality in energy production. It can generate a stream ready for carbon dioxide sequestration and greatly decrease nitrogen oxide emissions. This is achievable with an oxygen carrier (OC) that transfers oxygen between the fuel and air reactors during combustion. The OC should have suitable oxygen-transport capacity, high reactivity with fuel to combust it and regenerate with an air stream, and also adequate mechanical strength to maintain many redox cycles.

This work employs a family of iron-based perovskite monophasic oxygen carriers for selected biomass combustion. Perovskites are a class of materials with the general formula of ABX_3, in which the A site of the crystal lattice is occupied by a cation with a coordination number of 12, usually an alkaline or rare-earth metal. The synthesis method was discussed in detail to achieve the desired phase and quality. Inductively coupled plasma optical emission spectrometry (ICP-OES) to determine the exact chemical composition of the samples. Fourier transform infrared (FTIR) and X-ray powder diffraction (XRD), analyzed with FullProf, focused on structural properties and confirmed the materials' quality.

The OCs' reactivity toward the selected fuel was evaluated using a thermogravimetric analyzer coupled with a quadrupole mass spectrometer (TGA-QMS). We evaluated their regenerative ability and reuse potential using scanning electron microscopy (SEM).

The study indicates that using mixed metal oxides via chemical looping is a promising approach to achieving net carbon dioxide neutrality in power generation from waste biomass.

Acknowledgment: The work was financed by the National Science Centre Poland, Project No 2020/37/B/ST5/01259.

[1] Department of Engineering and Technology of Chemical Processes, Wroclaw University of Science and Technology, Wroclaw, Poland, * ewelina.ksepko@pwr.edu.pl

The Influence of Coal Ash on the Durability of Titanium-Containing Perovskite Oxygen Carriers

Aleksandra Bobowska[1], Ewelina Ksepko[1,*]

Keywords: coal, oxygen carriers, perovskites, combustion

ABSTRACT

Combustion of fuels in a Chemical Oxygen Loop enables flameless conversion of solid fuels without direct contact with oxygen from the air, allowing for the effective capture of emitted carbon dioxide (CO_2). In the energy context, fossil fuels such as coal remain the dominant raw materials in Poland.

Negative interactions between ash from solid fuels and the solid oxygen carrier can cause agglomeration or sintering of the carrier, as well as reactions between ash components and oxide materials, which reduce functionality and complicate separation of the carrier from the ash.

This work analyzed the properties of solid oxygen carriers with a perovskite structure, synthesized from iron and manganese oxides, which ensure oxygen transport. Additionally, these carriers were doped with titanium oxide as an inert component. The effect of ash on the properties of these solid oxygen carriers was investigated by conducting combustion tests on selected fuels, including Janina hard coal. Assessment of oxide materials included mechanical strength analysis, crystal structure and phase composition using X-ray diffraction (XRD), morphology change evaluation, and chemical composition study using scanning electron microscopy with energy-dispersive spectroscopy (SEM-EDS).

Acknowledgement:
The work was financed by the National Science Centre Poland, Project No 2020/37/B/ST5/01259.

[1] Department of Engineering and Technology of Chemical Processes, Wroclaw University of Science and Technology, Wroclaw, Poland, * ewelina.ksepko@pwr.edu.pl

Zn Sites in Zeolites During CH_4 and CO_2 Transformation – How the Zeolite Matrix Shapes the Catalytic Activity

Julia Sobalska[1,2,*], Agnieszka Kornas[3], Mathieu Vidal[3], Kinga Mlekodaj[3], Olena Tynkevych[1], Dalibor Kaucky[3], Dariusz Wardecki[3,4], Milan Bernauer[3,5], Miloslav Lhotka[5], Przemysław Rzepka[3], Kinga Góra-Marek[1], Edyta Tabor[3]

Keywords: Zn-containing zeolites, methane activation, CO_2 and CH_4 conversion, Zn speciation, framework dynamics

ABSTRACT

The direct conversion of methane and carbon dioxide into value-added chemicals is an attractive strategy for the utilization of two major greenhouse gases. Among the investigated catalytic systems, Zn-containing zeolites represent promising materials due to their ability to stabilize highly dispersed Zn species within well-defined microporous environments. However, the influence of zeolite topology on Zn speciation and its role in CH_4/CO_2 activation remains insufficiently understood. [1,2]

In this work, Zn-containing zeolites with FER, MFI (ZSM-5), and *BEA topologies and comparable Zn/Al ratios were investigated using complementary spectroscopic and structural techniques, including FTIR spectroscopy, UV-vis diffuse reflectance spectroscopy, mass spectrometry, and high-resolution X-ray powder diffraction. Particular attention was devoted to the relationship between framework topology, stabilization of Zn species, and their dynamic behavior during interaction with methane and carbon dioxide.

The results demonstrate that zeolite topology strongly governs Zn speciation. Zn/H-FER preferentially stabilizes highly dispersed isolated Zn^{2+} species located in exchangeable cationic positions, whereas Zn/H-ZSM-5 and especially Zn/H-*BEA contain increasingly heterogeneous Zn-oxo populations. FTIR studies confirmed the formation of methane-derived intermediates on Zn sites and revealed substantial differences in reaction pathways depending on the nature of Zn species. Isolated Zn^{2+} species in FER efficiently promote the formation of oxygenated intermediates and favor selective CH_4/CO_2 coupling toward acetic acid. In contrast, Zn-oxo species present in ZSM-5 and *BEA facilitate methane activation through methanol-related pathways and promote further transformations leading to hydrocarbons and olefinic products.

UV-vis spectroscopy revealed reversible perturbations of the electronic environment of Zn species during methane interaction. The strongest spectral response was observed for Zn/H-ZSM-5, whereas Zn/H-FER exhibited more subtle changes characteristic of highly dispersed cationic Zn species. Simultaneous CH_4/CO_2 treatment induced considerably smaller spectral perturbations than sequential exposure, indicating continuous consumption of methane-derived intermediates in the presence of CO_2.

Importantly, in situ high-resolution diffraction analysis revealed reversible changes in the zeolite lattice during CH_4 and CO_2 interaction. Methane exposure induced lattice expansion or anisotropic framework deformation, while subsequent CO_2 treatment resulted in framework contraction. These observations demonstrate the dynamic nature of thenteraction between Zn sites, adsorbed reaction intermediates, and the zeolite

[1] Faculty of Chemistry, Jagiellonian University in Kraków, * julia.sobalska@doctoral.uj.edu.pl
[2] Doctoral School of Exact and Natural Sciences, Jagiellonian University in Kraków
[3] J. Heyrovský Institute of the Czech Academy of Sciences, Prague, Czech Republic
[4] Faculty of Physics University of Warsaw, Warsaw, Poland
[5] Department of Inorganic Technology, University of Chemistry and Technology Prague, Czech Republic

framework under reaction conditions.

Overall, the study establishes a direct relationship between zeolite topology, Zn speciation, framework dynamics, and reaction pathways during CH_4/CO_2 conversion. The FER framework was identified as the most favorable environment for stabilization of highly reactive isolated Zn^{2+} species, which are responsible for enhanced formation of oxygenated products.

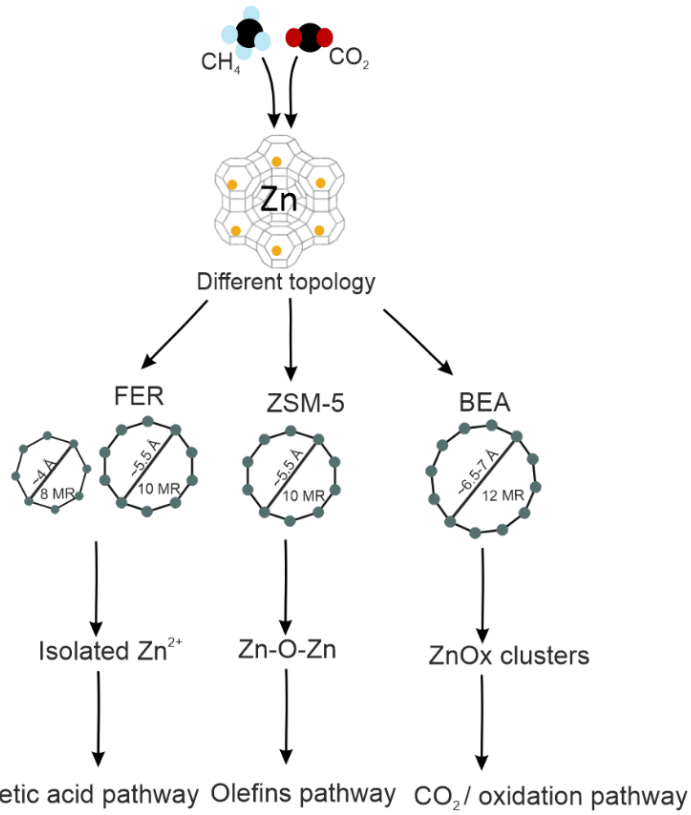


Figure 1. Schematic representation of CO_2 and CH_4 conversion over the studied zeolites.

[1] B.D. Montejo-Valencia, Y.J. Pagán-Torres, M.M. Martínez-Iñesta, M.C. Curet-Arana, Density functional theory (DFT) study to unravel the catalytic properties of M-exchanged MFI (M = Be, Co, Cu, Mg, Mn, Zn) for the conversion of methane and carbon dioxide to acetic acid, ACS Catal. 7 (2017) 6719–6728. https://doi.org/10.1021/acscatal.7b00844.

[2] G.F. Lopes, A.F. Lucrédio, L.H. Vieira, E.M. Assaf, Advances in the direct conversion of CH_4 and CO_2 into acetic acid over bimetallic catalysts supported on H-ZSM-5, Nanoscale Horiz. 10 (2025) 3051–3060. https://doi.org/10.1039/D5NH00496A.

Acknowledgement: The research was funded by the National Science Centre, Poland [2022/47/I/ST4/00607] and the Czech Science Foundation [project no. 24-14387L, 25-18196M, and 23-07616S]

Application of CO_2 and Manganite Mineral as Oxidants in Municipal Solid Waste Gasification

Ewelina Ksepko[1,*], Uzeru Haruna[1], Rui Zhang[2]

Keywords: MSW, gasification, mixed air-manganate-CO2, waste-to-energy conversion

ABSTRACT

Using carbon dioxide (CO_2) as a gasifying agent in municipal solid waste (MSW) gasification is a promising approach to waste valorization and enables CO_2 utilization in thermochemical conversion processes. CO_2 promotes gasification via the Boudouard reaction, thereby influencing syngas composition and carbon conversion.

This study uses a thermogravimetric analyzer coupled with quadrupole mass spectrometry (TGA-QMS) to evaluate the effects of CO_2-assisted gasification on syngas quality, particularly carbon monoxide (CO) production, and to further examine how temperature and concentration affect product yield.

The MSW was delivered from China and, before gasification, examined for proximate and ultimate analysis. The TGA-QMS approach enabled real-time monitoring of mass loss behavior and evolved gas species, providing insight into reaction pathways. The results indicate that syngas production is strongly temperature-dependent, with higher temperatures significantly increasing CO and H_2 formation through endothermic gasification and reforming reactions. Additionally, a moderate CO_2 concentration promoted syngas yield more effectively than higher concentrations, suggesting optimal reaction conditions in which CO_2 participation enhances carbon conversion without excessive dilution or kinetic limitations. Further, adding manganate as a gasification agent significantly improved gasification performance, as discussed in detail.

These findings highlight the critical role of process parameters in CO_2-assisted or solid gasification agent-assisted MSW gasification. Overall, the study shows that controlled CO_2 and manganate gasification, supported by TGA-QMS analysis, can improve syngas quality and support the development of low-carbon waste-to-energy systems.

[1] Department of Engineering and Technology of Chemical Processes, Wroclaw University of Science and Technology, Wroclaw, Poland, * ewelina.ksepko@pwr.edu.pl

[2] MIIT Key Laboratory of Thermal Control of Electronic Equipment, School of Energy and Power Engineering, Nanjing University of Science and Technology Nanjing, Jiangsu, China

Study on the Steam Gasification of Chars from the Pyrolysis of Polyester, Cotton and Their Mixtures

Piotr Soprych[1,*], Grzegorz Czerski[1], Katarzyna Śpiewak[1], Jarema Stańczyk[2]

Keywords: steam gasification, textile waste, thermochemical utilisation

ABSTRACT

Currently, due to environmental concerns and the principles of the circular economy, textile waste is subject to legislative regulations requiring, among other things, its selective collection. One method for its utilization is pyrolysis, which produces, among other products, char – an attractive material for the gasification process. The aim of this study was to evaluate the steam gasification of chars obtained through the pyrolysis of the main components of textile waste, i.e., polyester, cotton and their 60:40 blend. These materials were subjected to pyrolysis in a fixed-bed reactor and the resulting chars were characterized (ultimate and proximate analysis and ash composition) and then subjected to steam gasification using the thermovolumetric method under isothermal conditions (800, 850, 900 and 950 °C) and at a total pressure of 1.0 MPa. The formation rates of gaseous products were determined as well as the reactivity of the chars through the evaluation of conversion degree and partial conversion times ($t_{0.25}$, $t_{0.50}$ and $t_{0.75}$), the yields of gaseous products (CO, H_2, CO_2 and CH_4) were also determined. Furthermore, the kinetics of the gasification reaction were evaluated using the grain model. Cotton char is characterized by more favorable physicochemical properties (including ash composition) for gasification compared to polyester char. The experimental results demonstrated higher reactivity for cotton char and a favorable effect of adding cotton to the mixture on the gasification process (higher formation rates and higher yields of CO and H_2, as well as improved reactivity indices). The most beneficial effect and synergistic effect were obtained for temperatures of 900 and especially 950 °C. This is also confirmed by the kinetic parameter analysis; the best parameters were obtained for cotton char and although adding cotton to the mixture results in an increase in the E_a value compared to polyester, this is compensated for by a significantly higher pre-exponential factor value.

Acknowledgements
This research was funded by AGH University of Krakow, Faculty of Energy and Fuels, Research Subsidy, No. 501.00-210000-10000 and "Excellence initiative-research university" for the AGH University of Krakow, No. UB-696000-00001-Z01.

[1] AGH University of Krakow, Faculty of Energy and Fuels, al. Mickiewicza 30, 30-059, Krakow, Poland, *soprych@agh.edu.pl
[2] Reoil Sp. z o.o., ul. Przemysłowa 2, 32-400 Myślenice, Polska

Formation of Potassium Ferrites during Reduction of K/Fe_2O_3 Systems: A Study of Fischer-Tropsch Synthesis Catalysts

Andrzej Wójtowicz[1,2]*, Mariia Bordulenko[1,3], Iván Martínez López[1], Marcin Oszajca[1], Joanna Gryboś[1], Józef Korecki[4], Kinga Freindl[4], Nika Spiridis[4], Andrzej Kotarba[1], Gabriela Grzybek[1]

Keywords: Iron-based catalysts, Alkali promotion, Potassium ferrites, Thermal alkali desorption, Fischer-Tropsch synthesis

ABSTRACT

Fischer–Tropsch synthesis (FTS) is a catalytic process for converting syngas (a mixture of H2 and CO) into liquid hydrocarbons and other valuable chemicals [1]. In recent years, this technology has attracted renewed interest as a potential route to the sustainable production of synthetic fuels, particularly in the context of reducing dependence on finite crude-oil resources. A particularly promising concept involves using CO2 captured directly from the atmosphere. Following its conversion to CO, atmospheric CO2 can serve as an indirect carbon feedstock for the production of hydrocarbons, including industrially important olefins.

Iron-based materials are among the most extensively studied catalysts for FTS. Their widespread application stems from the relatively low cost and high natural abundance of iron, combined with their favourable selectivity towards desired products. Their catalytic performance can be further tailored by introducing alkali promoters, among which potassium is one of the most widely used. Potassium can improve catalyst stability and shift product selectivity towards more desirable hydrocarbons. However, both the magnitude and direction of its effects depend strongly on promoter loading [2]. Either too low or too high potassium contents may adversely affect catalytic activity, selectivity, or stability. Determining the optimum potassium loading is therefore essential for the development of efficient and selective FTS catalysts.

During activation and operation, iron-based FTS catalysts undergo complex phase transformations, including reduction and carburisation. Alkali promoters substantially influence these processes. However, elucidating their chemical state and promotion mechanism requires specialised analytical methods capable of monitoring low-concentration species exhibiting considerable mobility at elevated temperatures. One of such methods is thermal alkali desorption (TAD), a technique developed at the Jagiellonian University, allowing for the direct tracking of the stability and surface state of alkali admixtures [3].

In this study, commercial iron(III) oxide was modified with potassium by incipient-wetness impregnation using KNO3 as the precursor. A series of samples containing 0.2–2 wt.% of potassium was prepared to evaluate the effect of promoter loading. A combination of complementary characterisation methods was applied to monitor the structural, morphological, chemical, and electronic changes occurring during reduction. Thermogravimetric analysis was used to identify the individual stages of reduction. Temperature-programmed powder X-ray diffraction (XRD), performed under a reducing

[1] Faculty of Chemistry, Jagiellonian University in Kraków, Gronostajowa 2, 30-387 Kraków, Poland
[2] Doctoral School of Exact and Natural Sciences, Jagiellonian University in Kraków, prof. S. Łojasiewicza 11, 30-348 Kraków, Poland
[3] Faculty of Physics, Astronomy and Applied Computer Science, Jagiellonian University in Kraków, prof. S. Łojasiewicza 11, 30-348 Kraków, Poland
[4] Jerzy Haber Institute of Catalysis and Surface Chemistry, Polish Academy of Sciences, Niezapominajek 8, 30-239 Kraków, Poland

atmosphere of 10% H2 in He, enabled the phase composition to be followed at different stages of the reduction process. The morphology and chemical composition of the reduced samples were examined by transmission electron microscopy (TEM) coupled with energy-dispersive X-ray spectroscopy (EDS) mapping, electron energy loss spectroscopy (EELS) and selected area electron diffraction (SAED). The chemical state of iron in 1.5 wt.% K sample reduced at different temperatures was investigated by Mössbauer spectroscopy (MS).

The surface state of potassium was studied using the TAD technique. Measurements were conducted for both pristine samples and samples reduced in situ at 500°C for 1 h under a flow of 5% H2 in Ar (5 ml/min). The latter treatment was selected to approximate the state of activated FTS catalysts. In addition, changes in the electronic properties of the surface were assessed by work-function measurements performed before and after reduction of the oxide samples. This combined methodology provided complementary information on the evolution of the iron oxide phases, the state and location of potassium species, and promoter-induced changes in the surface electronic properties.

The results show that potassium addition significantly modifies the reduction behaviour of iron oxide and that the nature of this effect depends strongly on promoter loading. The combined XRD, TEM/EDX/EELS/SAED and MS results provide evidence for the formation of mixed potassium–iron oxide phases during the reduction of K/Fe2O3 systems. Consistent with this interpretation, the TAD measurements suggest the presence of K2Fe22O34 in the sample containing 0.2 wt.% K, whereas KFeO2 is identified for samples with higher potassium loadings. These findings show that potassium is not merely present as a surface additive, but actively participates in phase transformations under reducing conditions. The formation of distinct potassium–iron oxide species may therefore be an important factor governing potassium's influence on catalyst activation and, ultimately, on the performance of iron-based FTS catalysts.

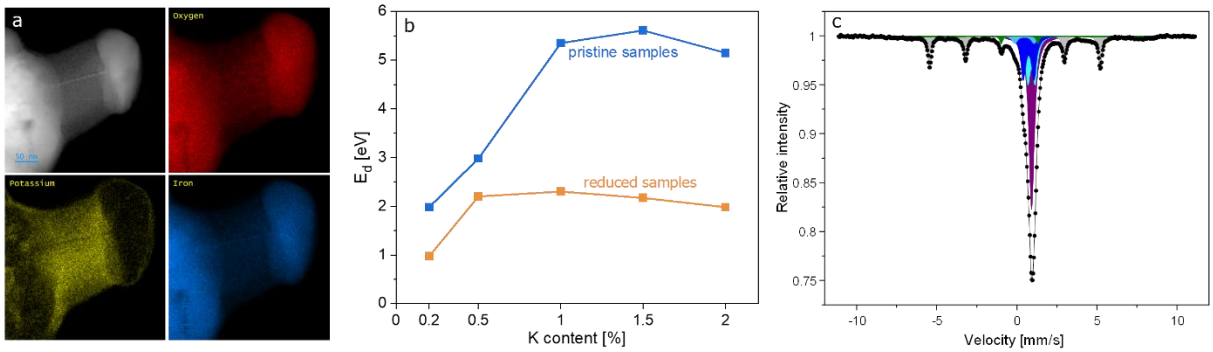


Figure 1. STEM/EDS images for the 1.5K/Fe_2O_3 sample reduced at 450°C (a), desorption activation energies of pristine and reduced K/Fe_2O_3 samples (b), and Mössbauer spectrum of the 1.5K/Fe_2O_3 sample reduced at 600°C (c).

[1] K. Jeske, T. Rösler, M. Belleflamme, T. Rodenas, N. Fischer, M. Claeys, W. Leitner, A.J. Vorholt, G. Prieto, Direct conversion of syngas to higher alcohols via tandem integration of Fischer–Tropsch synthesis and reductive hydroformylation, Angew. Chem. Int. Ed. 61 (2022) e202201004. https://doi.org/10.1002/anie.202201004.

[2] C.G. Visconti, M. Martinelli, L. Falbo, A. Infantes-Molina, L. Lietti, P. Forzatti, G. Iaquaniello, E. Palo, B. Picutti, F. Brignoli, CO_2 hydrogenation to lower olefins on a high surface area K-promoted bulk Fe-catalyst, Appl. Catal. B Environ. 200 (2017) 530–542. https://doi.org/10.1016/j.apcatb.2016.07.047.

[3] O.P. Ketlogetswe, M. Khasu, W. Marquart, C. Drivas, E.B. McShane, S.A. Kondrat, G. Grzybek, P. Stelmachowski, A. Kotarba, M. Claeys, N. Fischer, Tuning potassium concentration in empowered supports for Fischer–Tropsch synthesis, ChemCatChem 18 (2026) e01430 https://doi.org/10.1002/cctc.202501430.

Acknowledgement: We thank the National Science Centre, Poland, for funding the research (grant no. 2024/55/B/ST5/02291).

Efficient Nitrous Oxide Electrochemical Hydrogenation via Defect-Engineered Protonic Ceramic Electrolysis Cells

Zilin Ma, Yan Chen[1]*

Keywords: protonic ceramic electrolysis cells; nitrous oxide hydrogenation reaction; electrode materials; oxygen vacancy

ABSTRACT

Human-driven nitrous oxide (N_2O) emissions pose a significant threat to global systems. Although substantial efforts have been devoted to N_2O elimination, the removal of high-concentration N_2O (20-40 vol%) from industrial processes remains challenging due to the inefficiency of conventional catalytic methods. In this work, we demonstrate protonic ceramic electrolysis cells (PCECs) as an efficient strategy for electrochemical N_2O hydrogenation utilizing water vapor as a sustainable proton source. Symmetrical cells employing defective perovskite oxide electrodes $La_{0.6}Sr_{0.4}Co_{0.2}Fe_{0.8}O_{2.9-\delta}F_{0.1}$ (LSCF-F10) achieve a 65.4% conversion efficiency under 30 vol% N_2O atmosphere at 700 °C and 1.8 V, representing one of the highest N_2O conversion efficiencies reported for highly concentrated N_2O. Advanced spectroscopic characterization and density functional theory calculations reveal that the introduction of fluorine promotes oxygen vacancy formation, which enhances N_2O adsorption, accelerates proton transfer, and facilitates the generation of hydroxyl intermediates, thereby driving the N_2O hydrogenation reaction. The PCECs exhibit robust stability over 100 hours in simulated industrial off-gas, validating their potential for practical applications. The methodology presented here can be extended to other hydrogenation reactions, offering a promising pathway for efficient pollutant control and sustainable energy conversion.

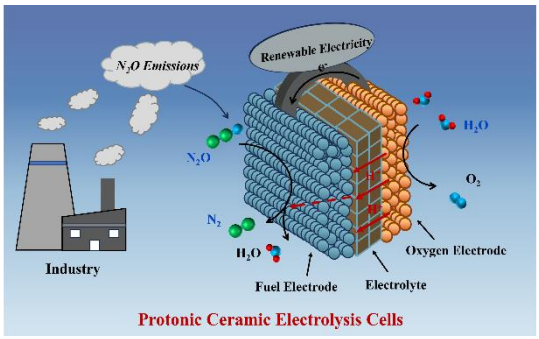


Figure 1. Schematic representation of PCEC-driven N_2O reduction reaction.

[1] Y. Ye, W. Lee, J. Pan, X. Sun, M. Zhou, J. Li, N. Zhang, J.W. Han, Y. Chen, Tuning the product selectivity of CO_2/H_2O co-electrolysis using CeO_2-modified proton-conducting electrolysis cells, Energy Environ. Sci. 16 (2023) 3137–3145. https://doi.org/10.1039/D3EE01468A.
[2] X. Xiang, Z. Ma, J. Zhang, Y. Li, Y. Ye, W. Lu, M. Zhou, S. Huang, H. Fu, B. Yu, S. Zhao, Z. Lin, Y. Chen, High-throughput DFT-assisted design of electrode for efficient high-temperature electrochemical dehydrogenation, Angew. Chem. Int. Ed. 64 (2025) e202502937. https://doi.org/10.1002/anie.202502937.

[1] South China University of Technology (SCUT), China, *escheny@scut.edu.cn

Dynamic Iron Sites in Ferrierite During CO_2 and CH_4 Conversion

Kinga Mlekodaj[1], Agnieszka Kornas[1], Julia Sobalska[2,3], Oliwia Rogala[2,3*], Karolina Tarach[2], Lukáš Grajciar[4], Carlos Bornes[4], Dariusz Wardecki[1,5], Przemysław Rzepka[1], Dalibor Kaucký[1], Olena Tynkevych[2], Kinga Góra-Marek[2], Edyta Tabor[1]

Keywords: greenhouse gases utilization, methane activation, ferrierite, iron sites, acetic acid

ABSTRACT

The direct co-conversion of carbon dioxide and methane into oxygenated products represents an attractive strategy for the simultaneous utilization of two major greenhouse gases [1,2]. However, the mechanism by which catalytic active sites coordinate the activation of these thermodynamically stable molecules remains poorly understood. In particular, little is known about the structural and electronic evolution of isolated iron sites during the reaction process. In this work, Fe-containing ferrierite (Fe-FER) was investigated using a combination of in situ FTIR spectroscopy coupled with mass spectrometry, Mössbauer spectroscopy, neutron powder diffraction (NPD), and density functional theory (DFT) calculations supported by machine-learning interatomic potentials. The objective was to establish the relationship between the structure of Fe active sites and their catalytic role in the direct conversion of CO_2 and CH_4 into oxygenates.

Spectroscopic characterization demonstrated that iron is present predominantly as isolated Fe(II) cations located in cationic positions of the FER framework. FTIR studies with CO and NO probe molecules together with Mössbauer spectroscopy revealed that only Fe(II) species located in β-sites are reactive toward CO_2 and CH_4, whereas Fe(II) species occupying α-sites remain largely inactive. Figure 1 shows the visualization of these sites.

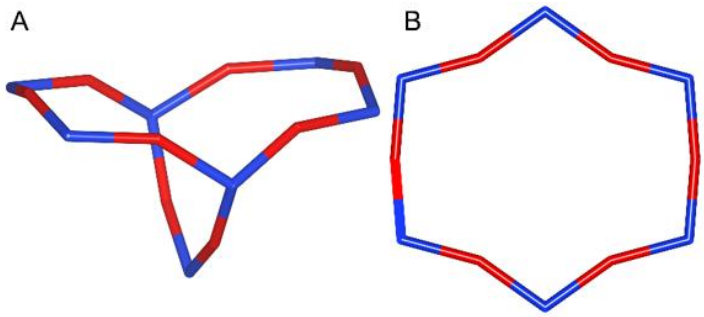


Figure 1. Visualization of α (A) and β (B) type sites in the FER topology (characteristic for pentasil zeolites).

In situ FTIR-MS experiments showed that exposure of Fe-FER to a CO_2/CH_4 mixture leads to the formation of oxygenated intermediates, including hydrocarbonate, methoxy, methanol, and acetate species. Methanol formation was detected at temperatures above approximately 170 °C, while acetic acid appeared at about 230 °C. At higher temperatures, methanol-derived intermediates underwent further transformation through methanol-to-olefin reactions, leading to the formation of light olefins. These observations demonstrate

[1] J. Heyrovský Institute of Physical Chemistry, Czech Academy of Sciences, Prague, Czech Republic
[2] Faculty of Chemistry, Jagiellonian University in Krakow, Poland, * oliwia.rogala@doctoral.uj.edu.pl
[3] Doctoral School of Exact and Natural Sciences, Jagiellonian University in Kraków
[4] Department of Physical and Macromolecular Chemistry, Charles University, Czech Republic
[5] Faculty of Physics University of Warsaw, Warsaw, Poland

the bifunctional nature of Fe-FER, where iron redox sites are responsible for reactant activation, whereas Brønsted acid sites promote carbonylation and subsequent hydrocarbon-forming reactions.

Mössbauer spectroscopy provided direct evidence for reversible changes in the oxidation state and coordination environment of iron during the reaction. Interaction with CO_2 induced partial oxidation of Fe(II) centers and formation of mixed-valence Fe(II)/Fe(III) species. Subsequent CH_4 exposure restored the original Fe(II) population, confirming a reversible redox cycle associated with catalytic turnover.

Neutron diffraction experiments revealed that CO_2 interaction causes displacement of Fe cations from the plane of the six-membered ring, whereas subsequent methane treatment restores their initial location. DFT calculations identified monodentate hydrocarbonate species as the most stable intermediates responsible for both partial Fe oxidation and local structural distortion. The calculated structural changes are consistent with diffraction and Mössbauer observations, providing a unified picture of catalyst behavior under reaction conditions.

Overall, the results demonstrate that Fe-FER operates through a cooperative redox-acid mechanism involving structurally flexible Fe(II)/Fe(III) centers and framework Brønsted acid sites. Reversible electronic and geometric changes of β-site Fe centers govern the activation of CO_2 and CH_4 and enable the selective formation of methanol and acetic acid under mild conditions. These findings provide new insight into the structure-activity relationships of Fe-zeolites and establish ferrierite as a promising catalyst for the atom-efficient valorization of greenhouse gases.

[1] L. Wang, L. Fan, Y. Wang, Q. Chen, Y. Zhu, Y. Yi, Tuning selectivity of acetic acid and alcohols by Brønsted and Lewis acid sites in plasma-catalytic CH_4/CO_2 conversion over zeolites, Appl. Catal. B Environ. Energy 350 (2024) 123938. https://doi.org/10.1016/j.apcatb.2024.123938.
[2] V. Havran, M.P. Duduković, C.S. Lo, Conversion of methane and carbon dioxide to higher value products, Ind. Eng. Chem. Res. 50 (2011) 7089–7100. https://doi.org/10.1021/ie2000192.

Acknowledgement: This research was funded by the National Science Centre, Poland [Grant No. 2022/47/I/ST4/00607].

Identification of Gas Phase Parameters in Water-Air Flow in A Horizontal Pipeline

Patryk Marczak[1],*, Marcin Zych[1], Andrzej Mrowiec[2], Artur Andruszkiewicz[3], Piotr Piechota[4], Ariel Dzwonkowski[4], Olena Ulitska[4], Anna Golijanek-Jędrzejczyk[4], Katarzyna Zbroja[1], Marek Jaszczur[1]

Keywords: two-phase flow, gamma-ray absorption radiometry, ultrasonic measurements, CFD, hybrid Eulerian-Volume of Fluid

ABSTRACT

Multiphase flows, particularly two-phase water-air systems, are fundamental to industrial sectors, including power generation, chemical processing, and petrochemicals. Accurately characterizing flow hydrodynamics is crucial for process optimization and operational safety. However, the inherent complexity of interfacial phenomena in such systems necessitates advanced, integrated investigative strategies.

To address this, the present study delivers a comprehensive experimental and numerical investigation of gas phase dynamics within a horizontal pipeline. The experimental framework integrates a robust suite of non-invasive method: gamma-ray absorption radiometry, ultrasonic measurements (Fig.1.), and advanced flow visualization. Concurrently, Computational Fluid Dynamics (CFD) simulations were executed utilizing the hybrid Eulerian-Volume of Fluid (Multi-Fluid VOF) framework to accurately model two-phase fluid flow.

Quantitative analysis was specifically targeted at resolving key gas phase parameters across three distinct flow regimes: bubbly, plug, and transitional plug-bubbly flows. By coupling empirical measurements with high-fidelity numerical predictions, the propagation velocity of gas structures and their localized and cross-sectional void fractions were precisely quantified.

The synergy between these approaches facilitated a critical evaluation of their suitability and accuracy for gas phase detection. Ultimately, this research provides actionable guidelines for the deployment of advanced process diagnostics, offering a foundational framework to optimize both instrumentation selection and computational modeling in horizontal two-phase pipe flow.



Figure 1. Experimetal set-up for two-phase flow analysis

[1] AGH University of Krakow, A. Mickiewicza 30, 30-059 Kraków, Poland, *pmarczak@agh.edu.pl
[2] University of Kalisz, Nowy Świat 4, 62-800 Kalisz, Poland
[3] Wrocław University of Science and Technology, Wybrzeże Wyspiańskiego 27, 50-370 Wrocław, Poland
[4] Gdańsk University of Technology, Narutowicza 11/12, 80-233 Gdańsk, Poland

Biopolymer-based Hydrogel Electrolytes for Energy-efficient Smart Windows

Ana Queijo[1], Yasmine Fernine[1], Tomé Júnior[1], Verónica de Zea Bermudez[2], Rosa Rego[2,*]

Keywords: alginate biopolymer, sustainable electrolytes, energy-efficient devices, electrochromic smart windows

ABSTRACT

Electrochromic devices (ECDs) reversibly modulate light absorption, reflection, and heat transmission by electrically controlling the redox states of their active materials. ECDs have a wide range of applications, including smart windows, e-paper displays, automotive roofs and windshields, and camouflage technologies, such as those used in drones [1].

Biopolymer-based gel electrolytes, derived from sustainable sources, combining the high ionic conductivity of liquid electrolytes with the mechanical stability of solid materials, have been proposed for ECDs. Using bio-based materials such as cellulose, chitosan, and alginate has opened new opportunities to enhance both device performance and environmental sustainability.

Alginate, derived from alginic acid found in the cell walls of brown algae, is an abundant marine biopolymer that can be recovered from seaweed by-products generated by the food and cosmetics industries. The sodiated form, sodium alginate (SA), can be readily gelled through interactions with multivalent cations, such as Ca^{2+} or Zn^{2+}, which promote hydrogel formation and the development of ion-conducting pathways [2].

Recently, we introduced an alginate-based hydrogel electrolyte strengthened with Ca^{2+} ions, denoted as ECD@Alg-Ca, employing polycarbonate (PC) as the transparent substrate due to its high optical transmittance (T). The ECD, with the configuration PC/IZO (indium zinc oxide)/a-WO_3 (amorphous tungsten oxide)/Alg-Ca/c-NiO (crystalline nickel oxide)/IZO/PC, exhibited T values of 72.7/97.1% and 21.1/20.1% at 620/1000 nm in the bleached (+3 V) and colored (-3 V) states, respectively (Figure 1). The device exhibited good cycling stability during chronoamperometry (CA) tests, with coloring and bleaching coloration efficiencies (CE_{in} and CE_{out}) values of -1497 and +1484 $cm^2\ C^{-1}$, respectively, at 620 nm, after the 205th cycle [3, 4].

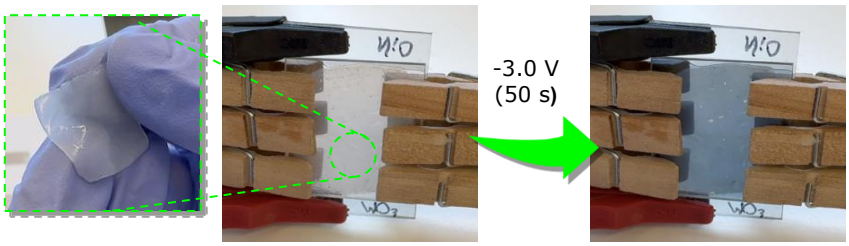


Figure 1. Inset: flexible Alg-Ca electrolyte film. The device was assembled with the Alg-Ca electrolyte between the a-WO_3 and c-NiO electrodes. Upon application of -3.0 V for 50 s, the device switches from the bleached (transparent) state to the colored (blue) state.

In this work, two new flexible alginate-based electrolytes containing Zn^{2+} ions were incorporated into ECDs with a five-layer sandwich configuration, namely ECD@Alg-Ca/Zn and ECD@Alg-Zn. Their electro-optical performance was evaluated and compared with that of the previously developed ECD@Alg-Ca.

[1] CQ-VR, University of Trás-os-Montes and Alto Douro, Quinta de Prados, 5000-801 Vila Real, Portugal
[2] Chemistry Department and CQ-VR, University of Trás-os-Montes e Alto Douro, Quinta de Prados, 5000-801 Vila Real, Portugal, * rrego@utad.pt

The electrolytes were characterized by POM, SEM/EDS, AFM, TGA, DTGA, and ionic conductivity measurements. After assembling the ECDs, visible-NIR spectra and color coordinates were recorded at each applied potential, ranging from +3 to -3 V. The CE was evaluated by CA. The influence of the scan rate on the electrochemical response of the devices was also investigated.

The PC/IZO/a-WO_3/Alg-Ca-Zn/c-NiO/IZO/PC device demonstrated good cycling stability and reached 6.8/5.0% at 620/1000 nm, in the colored state (Figure 2). These values are approximately three and four times lower, respectively, than those reported for the corresponding ECD@Alg-Ca, highlighting the enhanced light -and heat- blocking capability of the newly developed device.

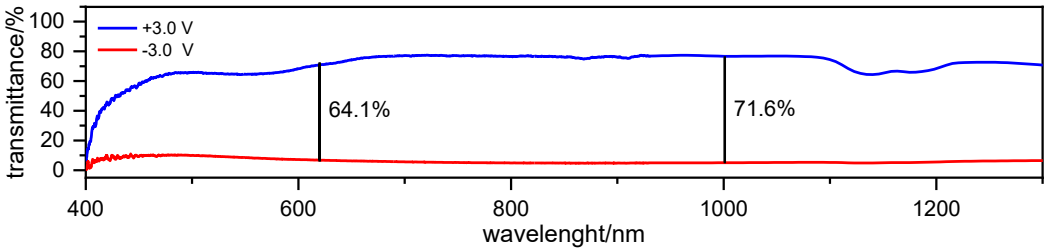


Figure 2. Transmittance spectra in the visible and NIR regions of ECD@Alg-Ca/Zn in the bleached and colored states.

[1] Z. Xiang, Y. Meng, X. Yang, Y. Yang, X. Li, Y. Gao, L. Wang, W. Lü, Low-temperature resistant plasticized polymer smart window based on phase change suppression mechanism: Enabling low-temperature stealth flight for drones, Chem. Eng. J. 539 (2026) 177036. https://doi.org/10.1016/j.cej.2026.177036.

[2] B. Belza, M.F. Palermo, E. García-Gaitán, I. Ruiz de Larramendi, N. Ortiz-Vitoriano, Biopolymer electrolytes for rechargeable zinc-air batteries: Advancements and challenges, Curr. Opin. Electrochem. 57 (2026) 101821. https://doi.org/10.1016/j.coelec.2026.101821.

[3] R. Rego, A.R. Queijo, T. Cá Júnior, V. de Zea Bermudez, Bio-derived alginate electrolytes for high-performance and sustainable electrochromic devices, 42nd Topical Meeting of the International Society of Electrochemistry, 23–26 June 2026, Espoo (Helsinki), Finland.

[4] D. Ji, J.M. Park, M.S. Oh, T.L. Nguyen, H. Shin, J.S. Kim, D. Kim, H.S. Park, J. Kim, Superstrong, superstiff, and conductive alginate hydrogels, Nat. Commun. 13 (2022) 3019. https://doi.org/10.1038/s41467-022-30691-z.

Acknowledgments: The authors are grateful for the support of the CQ-VR - through the projects UID/00616/2025, UID/PRR/00616/2025, and UID/PRR2/00616/2025, and the RISE project - Smart Cities, Sustainable Energy and Materials, operation code NORTE2030-FEDER-02723100, financed by the European Regional Development Fund (ERDF), through Incentives for Research, Development and Innovation, within the scope of the Northern Regional Program 2021-2027 [NORTE2030]. Yasmine Fernine thanks BI/UTAD/22/2026 RISE grant.

High-Entropy B-Site Engineering Coupled with *In Situ* Exsolution for High-Performance Sr-Free $LaCrO_3$-Based Fuel Electrodes in Reversible Solid Oxide Cells

Ziheng Yi[1,2], Hao Wang[1,2], Xu Xu[1,2,*], Linghong Luo[1], Liang Cheng[1], Leying Wang[2], Kun Zheng[3,*1]

Keywords: high-entropy perovskite; *in situ* exsolution; $LaCrO_3$; fuel electrode; reversible solid oxide cell; oxygen vacancies; density functional theory

ABSTRACT

Reversible solid oxide cells (RSOCs) require fuel electrodes that combine high electrocatalytic activity, efficient charge transport, and robust redox stability. $LaCrO_3$-based perovskites are attractive because of their good chemical stability under alternating oxidizing and reducing conditions, but their intrinsic catalytic activity and conductivity remain limited. Herein, a high-entropy B-site design is introduced into $LaCrO_3$ to regulate local structural and defect chemistry while incorporating multiple redox-active transition metals capable of reduction-induced exsolution. This design exploits the established effects of B-site composition, lattice distortion, and oxygen nonstoichiometry on the physicochemical properties of perovskite oxides, while avoiding Sr-related segregation pathways [1-3]. An equimolar $LaCr_{0.2}Mn_{0.2}Fe_{0.2}Co_{0.2}Ni_{0.2}O_{3-\delta}$ (LCMFCN) perovskite was composited with $Ce_{0.9}Gd_{0.1}O_{1.95}$ (GDC) to form the LCMFCN-GDC fuel electrode. Under reducing conditions, the composite undergoes spontaneous reconstruction into a reduced perovskite/GDC/FeCoNi-alloy three-phase heterostructure, with exsolved FeCoNi nanoparticles providing catalytically active sites and abundant metal/oxide heterointerfaces. The resulting reduced LCMFCN-GDC fuel electrode exhibits a polarization resistance of 0.13 $\Omega \cdot cm^2$ at 850 °C in SOFC operation, together with a peak power density of 592 $mW \cdot cm^{-2}$. In SOEC operation, a current density of 1.60 $A \cdot cm^{-2}$ is achieved at 850 °C and 1.5 V. The electrode also maintains stable performance over 10 consecutive SOFC/SOEC cycles for 20 h. To further elucidate the effects of B-site chemical disorder, DFT calculations based on a 150-atom equimolar special quasirandom structure [4] are employed to examine local structural distortion, oxygen-vacancy formation, electronic structure, and vibrational properties. The combined experimental and theoretical results clarify how high-entropy B-site disorder and *in situ* exsolution regulate defect chemistry and generate active FeCoNi/oxide interfaces, thereby enhancing catalytic activity and redox stability without Sr doping.

[1] T.X. Nguyen, Y.-C. Liao, C.-C. Lin, Y.-H. Su, J.-M. Ting, Advanced high entropy perovskite oxide electrocatalyst for oxygen evolution reaction, Adv. Funct. Mater. 31 (2021) 2101632. https://doi.org/10.1002/adfm.202101632.
[2] M. Singh, D. Zappa, E. Comini, Solid oxide fuel cell: Decade of progress, future perspectives and challenges, Int. J. Hydrogen Energy 46 (2021) 27643–27674. https://doi.org/10.1016/j.ijhydene.2021.06.020.
[3] R. Xu, S. Liu, M. Yang, G. Yang, Z. Luo, R. Ran, W. Zhou, Z. Shao, Advancements and prospects of perovskite-based fuel electrodes in solid oxide cells for CO_2 electrolysis to CO, Chem. Sci. 15 (2024) 11166–11187. https://doi.org/10.1039/D4SC03306J.

[1] School of Materials Science and Engineering, Jingdezhen Ceramic University, Jingdezhen 333403, China, *xuxu_80@163.com
[2] School of Energy Science and Engineering, Jingdezhen Ceramic University, Jingdezhen 333403, China
[3] Faculty of Energy and Fuels, AGH University of Krakow, al. A. Mickiewicza 30, 30-059 Krakow, Poland, *zheng@agh.edu.pl

[4] Z. Jiang, Y. Nahas, B. Xu, S. Prosandeev, D. Wang, L. Bellaiche, Special quasirandom structures for perovskite solid solutions, J. Phys. Condens. Matter 28 (2016) 475901. https://doi.org/10.1088/0953-8984/28/47/475901.

Design and Construction of Safe High-Energy-Density Zinc-Halogen Batteries

Panpan Zhu[1], Haibo Hu[1]

Keywords: Zinc-halogen batteries, Energy storage, High energy density

ABSTRACT

At present, battery systems for large-scale energy storage and consumer electronics power supply are faced with stringent requirements including low cost, ultra-long cycle life, high intrinsic safety, environmental friendliness and strong application adaptability. Conventional mainstream battery technologies generally suffer from prominent safety risks, limited cycling performance, high manufacturing costs and narrow application compatibility. Such drawbacks make it difficult to satisfy the scalable demands across diverse scenarios, which greatly hinders their large-scale deployment and commercialization for large-scale energy storage as well as flexible and smart consumer electronic devices.

In response to the above industrial bottlenecks and technical requirements, this report systematically summarizes the phased progress and preliminary explorations of our research group on new safe and high-energy-density zinc-halide energy storage battery systems over the past three years. Taking zinc-iodine batteries as the core research platform, our team targets the key challenges of battery performance enhancement and safety promotion. A series of studies on electrode structure design, mechanistic investigation and system construction of high-safety, high-efficiency zinc-halide batteries have been carried out, focusing on the fabrication of stable electrodes with high iodine loading, mechanistic elucidation and kinetic optimization of multi-electron halogen redox reactions, as well as electrolyte engineering.

Compared with traditional energy storage batteries, the newly developed rechargeable zinc-halide battery in this work exhibits remarkable merits such as high intrinsic safety, outstanding cycling stability, low raw material cost, simple fabrication procedure and wide applicability. It effectively breaks the technical bottlenecks of existing battery systems. This emerging battery chemistry can be adapted to multiple application scenarios, including grid-scale energy storage, distributed energy storage and integrated power supply for smart consumer electronics. It holds great promise for supporting renewable energy storage and powering intelligent electronic devices, and provides important technical references and theoretical foundations for the research, development and industrialization of next-generation low-cost, high-safety energy storage batteries.

[1] Anhui University

EFE2026 ENERGY FUELS ENVIRONMENT
INTERNATIONAL CONFERENCE
17-20 NOVEMBER 2026, KRAKÓW, POLAND

Do Municipal Advantages Persist? From Photovoltaics to Energy Storage in Poland's "Mój Prąd" Programme

Przemysław Grzelczyk[1,*], Aldona Mrówczyńska-Kamińska[1]

Keywords: energy transition, prosumers, photovoltaics, energy storage, subsidies

ABSTRACT

Poland's "Mój Prąd" (My Electricity) programme has been one of the main instruments supporting household energy transition since 2019. Its first three editions (MP1–MP3) subsidised rooftop photovoltaics (PV), while editions MP4–MP6 shifted support towards energy and heat storage. This study examines whether municipalities that led in the PV phase retained their advantage when support moved to a new technology, and whether their share of storage subsidies was disproportionate to their housing stock.

The analysis covers all six editions at the municipal level (2,321 municipalities/territorial units, with towns merged with surrounding rural municipalities of the same name). Subsidy intensity is measured as subsidised installations per 1,000 dwellings in one- and two-dwelling buildings (Census 2021). Persistence is assessed with Spearman rank correlations, retention of the top 10% of municipalities and quintile transition matrices. Disproportion is measured with a representation ratio R (share of subsidies divided by share of dwellings) with bootstrap confidence intervals.

Territorial advantages proved persistent, but probabilistic rather than deterministic. PV leaders were three to four times more likely than chance to remain in the top 10% for PV (44%) and energy storage (30%), but only weakly so for heat storage (17%). Leaders were over-represented in energy storage subsidies relative to housing (R = 1.40; 95% CI 1.31–1.49), yet this matched their over-representation in PV within the same phase. Relative to PV uptake, support was therefore proportional. Heat storage followed a distinct spatial logic, only weakly linked to earlier PV uptake.

The findings suggest that universal, application-based subsidy schemes tend to reproduce earlier territorial patterns when new technologies complement existing ones

[1] Uniwersytet Przyrodniczy w Poznaniu, Wydział Ekonomiczny,
* przemyslaw.grzelczyk@up.poznan.pl

Insights into the MTH Reaction over SSZ-13 by Operando Spectroscopy and MCR-ALS Analysis

Agata Kordek[1,2*], Anna Walczyk[1], Karolina Tarach[1], Kinga Góra-Marek[11]

Keywords: MTH reaction, operando spectroscopy, MCR-ALS

ABSTRACT

The conversion of methanol from biological sources is a promising route for producing hydrocarbons such as olefins and gasoline. However, process optimization requires a profound understanding of the reaction mechanism. In the case of such a complex reaction as methanol-to-hydrocarbons (MTH), in which simultaneous pathways occur, the spectral image is difficult to interpret. Operando spectroscopy has become one of the most powerful tools for obtaining mechanistic information while the catalytic reaction is taking place under conditions close to those of a working catalyst. The recorded FT-IR and UV-Vis spectra often contain contributions from a variety of compounds with similar chemical structures, including both active species and coke precursors accumulating within zeolite catalyst channels. To provide insights into the mechanism of the MTH reaction, we applied Multivariate Curve Resolution with Alternating Least Squares (MCR-ALS) to the obtained spectral data. This chemometric method deconstructs complex spectral data into distinct spectral components and their time-dependent concentration profiles.

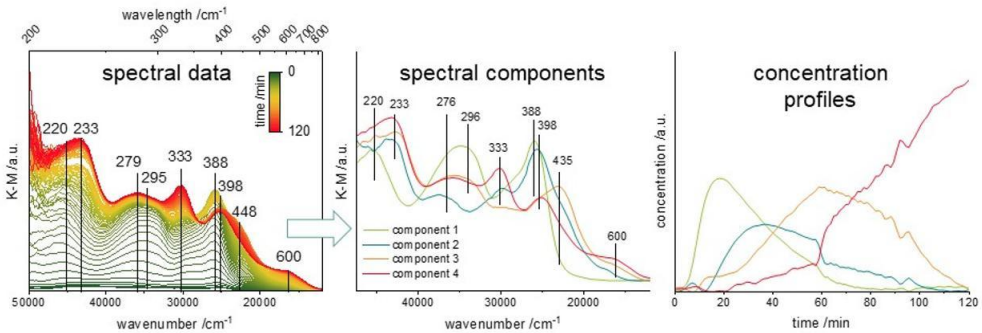


Figure 1. UV-Vis spectra obtained for the low-loading conditions experiments of the MTH reaction and results of MCR-ALS analysis: distinguished components and their concentration profiles.

Operando UV–Vis and FT-IR spectroscopy were used to monitor the catalyst surface during the MTH reaction over the SSZ-13 (CHA) zeolite catalyst under low- and high-loading conditions to emphasize the role of hydrocarbon pool initiating agent, i.e., formaldehyde. These measurements were complemented by GC and MS analysis to track the products released from the catalyst. The spectroscopic data were further analyzed using MCR-ALS, which enabled separation of the spectra into individual components and helped identify the different species contributing to the observed signals. High-loading conditions led to faster deactivation, a rapid decline in methanol conversion, and earlier dominance of aromatic and coke-forming species, whereas low-loading sustained higher conversion and delayed deactivation. This difference can be attributed to the higher HCHO formation rate at higher methanol loading, which promotes aromatic and coke precursor

[1] Faculty of Chemistry, Jagiellonian University in Kraków, Gronostajowa 2, 30-387 Kraków, Poland,
* kinga.gora-marek@uj.edu.pl
[2] Doctoral School of Exact and Natural Sciences, Jagiellonian University in Kraków, Łojasiewicza 11, 30-348 Kraków, Poland

formation via Prins-type reactions, thereby accelerating the aromatic HCP cycle. In contrast, lower methanol loading limits HCHO formation and favours the olefin cycle. Overall, the reaction mechanism remained unchanged, but reactant loading governed the balance between olefin- and aromatics-driven cycles as well as the rate of catalyst deactivation. The combined operando spectroscopic and following algorithmic analyses demonstrate that methanol loading plays a decisive role in governing both the evolution of hydrocarbon pool species and the deactivation pathway of SSZ-13 in the MTH reaction. The application of MCR-ALS proved particularly valuable in uncovering transient intermediates, such as cyclopentenyl cations, that are not directly evident from raw spectra. These findings provide deeper mechanistic insight into loading-dependent behaviour and highlight the importance of controlled reaction conditions for optimizing catalyst lifetime and selectivity in industrial MTH processes.

[1] J.F. Haw, W. Song, D.M. Marcus, J.B. Nicholas, The mechanism of methanol to hydrocarbon catalysis, Acc. Chem. Res. 36 (2003) 317–326. https://doi.org/10.1021/ar020006o.
[2] Z. Liu, J. Huang, Fundamentals of the catalytic conversion of methanol to hydrocarbons, Chem. Synth. 2 (2022) 21. https://doi.org/10.20517/cs.2022.26.
[3] J. Jaumot, A. de Juan, R. Tauler, MCR-ALS GUI 2.0: New features and applications, Chemom. Intell. Lab. Syst. 140 (2015) 1–12. https://doi.org/10.1016/j.chemolab.2014.10.003.

Acknowledgments: This work was financed by Grant No. 2023/49/B/ST4/02340 from the National Science Centre, Poland.

Zn-Modified Zeolites with Different Topologies for Catalytic Cracking of Polypropylene

Kamil Zawadziński[11,*], Shinya Kokuryo[2], Kinga Góra-Marek[1], Karolina A. Tarach[1], Edyta Tabor[3], Norikazu Nishiyama[2], Oliwia Rogala[1,4], Agata Kordek[1,4]

Keywords: zeolites, cracking, plastic waste, zinc, operando

ABSTRACT

The effective recycling and valorization of plastic waste remain significant global challenges. Despite the growing need for sustainable waste management, only 10% of discarded plastics is currently recycled [1], while the conversion of plastic waste into value-added chemicals and fuels remains particularly limited. Catalytic cracking seems to be a promising approach for transforming plastic waste into valuable hydrocarbons, including light olefins and fuel-range products. Zeolites are among the most promising catalysts for plastic conversion due to their well-defined microporous architecture, high thermal and hydrothermal stability, shape-selective properties, and tunable acidity. Their catalytic performance can be further modified through the incorporation of metal species. In particular, zinc incorporation can alter the acid properties of zeolites and introduce additional active sites, thereby affecting the reaction pathways and product distribution.

In this study, the catalytic performance of microporous Zn-modified beta and ZSM-5 zeolites was investigated in the catalytic cracking of polypropylene (PP). We investigated the effect of the Si/Al ratio at a similar zinc loading for the BEA-type structure and the impact of substituting aluminum with gallium atoms in the MFI-type structure (also at a similar zinc loading). The idea behind this study was to investigate the potential of zeolites from a different perspective, aiming at producing a hydrocarbon fuel, i.e. formed by saturated hydrocarbons, without the addition of external H_2 but using the self-generated hydrogen or hydrogen-transfer reactions. A detailed characterization of physicochemical properties was performed using methods such as X-ray diffraction, low-temperature nitrogen sorption, probe molecule sorption (CO, Py) with infrared detection, and inductively coupled plasma atomic emission spectrometry. Table 1 presents the acidity data of selected samples.

Table 1. Acidity results for selected zeolites with BEA (B) and MFI (M) frameworks. The first number indicates the Si/Al (Si/Ga) ratio, and the second - Zn/Al (Zn/Ga) ratio

Sample	cBAS / μmol·g^{-1}	cLAS / μmol·g^{-1}
B5	1621	103
B5-0.29	237	2356
B9.5-0.24	133	1172
B12-0.23	202	1439
M33-0.26	158	450
M25-0.31(Ga)	390	1322

The introduction of zinc ions causes a significant decrease in the concentration of Bronsted acid sites and an increase in the concentration of Lewis acid sites, which subsequently

[1]Faculty of Chemistry, Jagiellonian University in Kraków, Kraków, Poland,
*kamil.zawadzinski@student.uj.edu.pl
[2] Division of Chemical Engineering, Graduate School of Engineering Science, Osaka University, Osaka, Japan
[3] J. Heyrovsky Institute of Physical Chemistry, Czech Academy of Sciences, Prague, Czech Republic
[4] Doctoral School of Exact and Natural Sciences, Jagiellonian University in Kraków, Kraków, Poland

affects catalytic activity. Thermogravimetric analysis and operando FTIR spectroscopy were used to evaluate the catalytic properties of the materials.

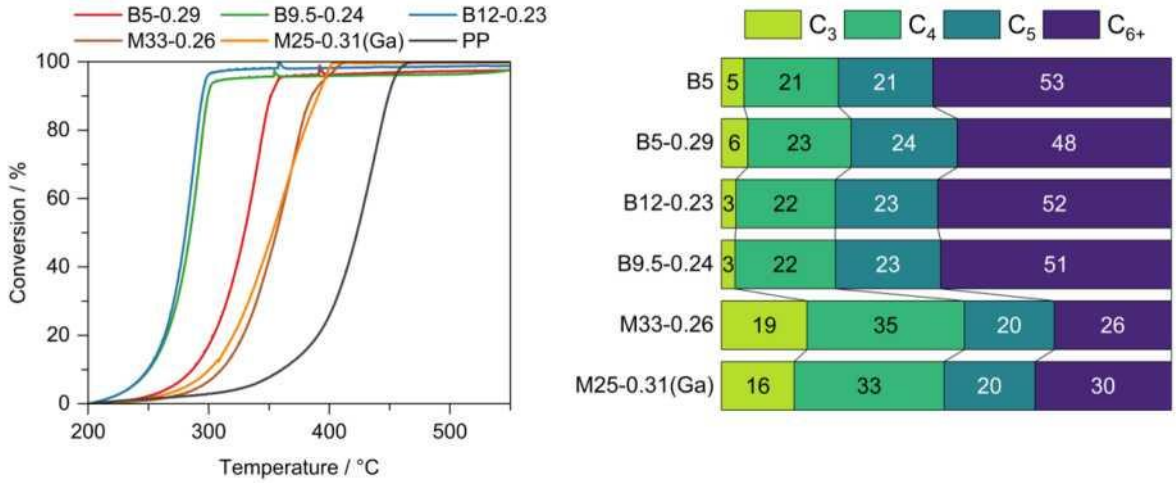


Figure 1. PP cracking conversion curves (left) and the corresponding average product selectivity (right).

The conversion profiles demonstrate a profound catalytic effect of all zeolite samples compared with non-catalytic polypropylene degradation. While thermal cracking of PP occurs mainly between approximately 400 and 480 °C, the presence of zeolite catalysts shifts the conversion to substantially lower temperatures, indicating efficient catalytic cracking. Among the catalysts studied, B12-0.23 and B9.5-0.24 exhibit the highest activity, reaching nearly complete conversion at around 290-300 °C. B5-0.29 requires slightly higher temperatures, whereas M33-0.26 and M25-0.31(Ga) achieve full conversion at approximately 380-400 °C. These results indicate that the catalytic activity is not solely determined by acid site density, but pore opening size (12-MR for B and 10-MR for M) plays an important role, showing pivotal role of the polymer chains' accessibility to the acid site.

The product distributions reveal a strong effect of zeolite structure on cracking pathways. The BEA-based catalysts (B5, B5-0.29, B12-0.23 and B9.5-0.24) predominantly produce heavier hydrocarbons (C6+), accounting for approximately 48-53% of the products. In contrast, the MFI-based catalysts (M33-0.26 and M25-0.31(Ga)) generate significantly larger amounts of C3 and C4 hydrocarbons, with a combined selectivity of about 50-55%. This behaviour suggests that PP cracking over the MFI catalysts proceeds through a greater extent of secondary cracking reactions, converting initially formed heavier fragments into lighter olefins. The BEA structure, characterized by larger pore channels, appears to facilitate the diffusion of primary cracking products from the zeolite pores before extensive secondary transformations occur, resulting in higher C6+ selectivity. Conversely, the more constrained MFI pore system promotes additional cracking of primary intermediates, increasing the yield of light hydrocarbons, particularly C3-C4 fractions.

[1] Plastics Europe, Plastics the Fast Facts 2025: Global and European Plastics Production and Economic Indicators, Plastics Europe AISBL, Brussels, 2025. https://plasticseurope.org/knowledge-hub/plastics-the-fast-facts-2025/.

This research was funded by the National Science Centre, Poland [Grant No. 2021/43/B/ST4/00307].

A General Metal Acetate-Assisted Alcohol Thermal Strategy to Fabricate Flexible Carbon Nanofiber Films for Supercapacitors

Helin Niu[1,*], Wei Song [1]

Keywords: Supercapacitor; flexible carbon nanofiber film; self-supporting electrode

ABSTRACT

Flexible carbon nanofiber films (CNFs) have drawn tremendous attention recently due to their fascinating properties. However, CNFs prepared by conventional methods are fragile and easily broken. Therefore, a general approach for synthesizing flexible CNFs is urgently needed [1]. Herein, we report a metal acetate-assisted alcohol thermal (MAA) method for the preparation of flexible CNFs. The MAA is a general and scalable method which can overcome the shortcomings of the pre-oxidation method, and more than 15 different flexible CNFs are successfully prepared. In this method, a polyacrylonitrile (PAN) film is first prepared through an electrostatic spinning process, and then a cyclized polyacrylonitrile (CPAN) film with a high-temperature-resistant trapezoidal structure is formed after MAA treatment. The unique structure of the CPAN will help in maintaining its flexibility to produce a flexible CNF during carbonization at an elevated temperature. To explore their potential in flexible devices, a supercapacitor made of flexible CNF-Zn (the specific surface area is 540 m^2 g^{-1}; the I_D/I_G ratio is 0.94) is investigated, and it shows an energy density of 11.5 W h kg^{-1} at 500 W kg^{-1} and has a capacitance retention rate of 97.2% even after 10 000 charge–discharge cycles. Our findings demonstrate that the MAA method could not only prepare flexible CNFs for energy storage devices, but also has potential application prospects in other fields.

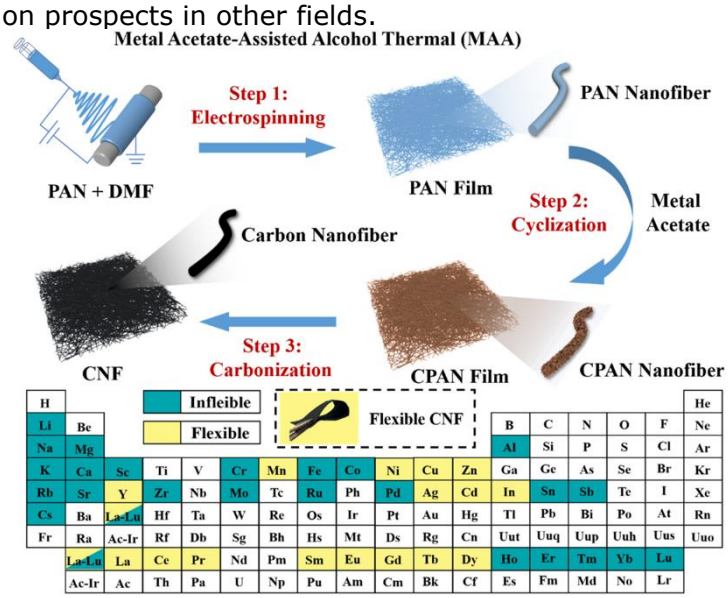


Figure 1. Schematic illustration of the metal acetate-assisted alcohol thermal (MAA) route to flexible carbon nanofiber films and its metal universality.

[1] P. Wang, Y. Sun, J. Li, G. Zhu, X. Zhang, H. Yang, B. Lin, Electrode materials for flexible supercapacitor with real-time visual monitoring of potential, Chem. Eng. J. 446 (2022) 137330. https://doi.org/10.1016/j.cej.2022.137330.

[1]Anhui University, Hefei, 230601, China

Cation-Driven Charge Modulation and In-Situ Exsolved Nanoparticles Enable a Self-Assembled Cathode for Proton Ceramic Solid Oxide Cells

Mengen Shao[1], Youmin Guo[1,*]

Keywords: Solid oxide cells; cathode; triple conductor; oxygen vacancy

ABSTRACT

Protonic ceramic fuel cells (PCFCs) offer considerable potential for clean and efficient energy conversion at intermediate temperatures [1]. However, their application is constrained by the trade-off between insufficient electrode activity and limited operational durability. Here, we develop a Zn/Yb B-site co-doping strategy combined with temperature-induced nanoparticle exsolution to construct a triple-conducting cathode. This approach introduces cation-driven charge modulation that enhances ionic diffusion and electronic conduction, while the exsolved secondary $BaCoO_{3-\delta}$ phase plays a pivotal role in increasing the density of active sites, optimizing interfacial charge transfer, and synergistically promoting oxygen reduction reaction (ORR) kinetics. The Zn/Yb co-doping redistributes local charge density, weakens metal-oxygen bonds, and reduces the energy required for oxygen vacancy formation, promoting oxygen vacancy generation. The increased oxygen vacancy concentration facilitates surface oxygen activation and lattice hydration, enhancing oxygen-ion and proton transport. Meanwhile, enhanced d-p orbital hybridization improves electronic conductivity and accelerates charge transfer kinetics. In addition, the optimized alkaline-earth sites suppress carbonate formation, thereby imparting excellent CO_2 tolerance. As a result, the optimized cathode delivers a peak power density of 0.99 W cm^{-2} at 600 °C and stable operation over 100 h, with a polarization resistance of 0.110 Ω cm^2 under 20% H_2O-air. This work provides a novel strategy for the optimization of activity, conductivity, and stability in PCFC cathodes.

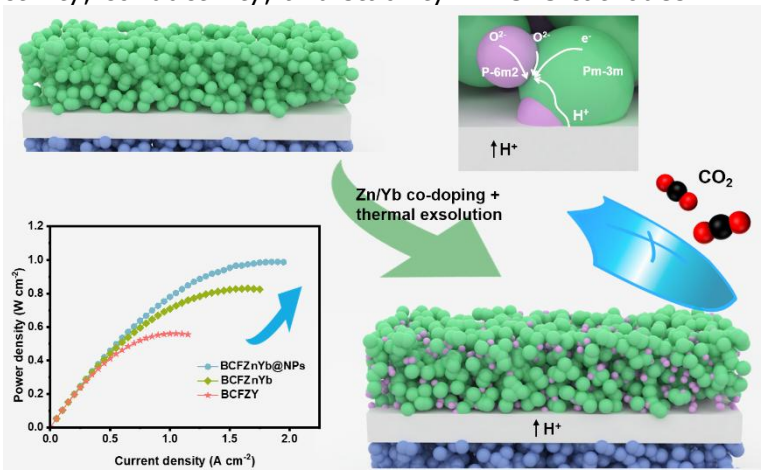


Figure 1. Graphical abstract: Zn/Yb co-doping and thermal exsolution strategy for high-activity and stable PCFC cathodes.

[1] S. Kim, D. Yoon, J. Chae, H. Kim, J. Hong, J.-W. Son, J.-H. Lee, S. Kang, H.-I. Ji, Elucidating the proton-coupled oxygen reduction pathway in protonic ceramic fuel cells, Energy Environ. Sci. 19 (2026) 1715–1731.

[1] School of Materials Science and Engineering, Anhui University, Hefei, 230601, China,
* youminguo@ahu.edu.cn

Estimation of Diffuse Solar Radiation Using a Machine Learning Approach

Olushola Olapade[1,*], Szymon Wieteska[1], Marek Jaszczur[1]

Keywords: solar radiation, photovoltaic systems, diffuse irradiance,machine learning

ABSTRACT

The rapid expansion of solar photovoltaic (PV) systems, with installed capacity reaching approximately 26.9 GW in Poland and more than 3.0 TW globally by the end of May 2026, places increasing demands on accurate solar resource assessment. Global PV capacity increased from approximately 946 GW at the end of 2021 to over 3.0 TW by the end of May 2026, representing more than a threefold increase in less than four and a half years [1].

Photovoltaic energy yield models require direct normal irradiance (DNI) and diffuse horizontal irradiance (DHI) rather than global horizontal irradiance (GHI) alone. However, standard meteorological networks routinely measure only GHI. Bridging this measurement gap requires irradiance decomposition models to estimate DNI and DHI using GHI and derived parameters, such as the clearness index [2].

This study evaluates and compares the performance of the traditional Erbs empirical model [3] with machine learning (ML) approaches to estimate DHI under the climatic conditions of Poland. The methodology relies on predicting the diffuse fraction (Kd) to reconstruct DHI using locally measured solar radiation data. Four ML methods, Artificial Neural Networks (ANN), Random Forest, XGBoost, and Support Vector Regression (SVR), are investigated. The models utilize a compact, physically meaningful input set: GHI, clearness index, extraterrestrial irradiance, solar zenith and azimuth angles, hour of the day, and day of the year.

Model performance is assessed at hourly and daily timescales using standard statistical metrics: R2, RMSE, MAE, MAPE, and NRMSE, to examine robustness and temporal generalization, the evaluation employs both chronological and random data-splitting strategies, along with independent validation using observations from a separate data period. By assessing predictive accuracy, this research provides a framework for selecting robust, data-driven methods to enhance photovoltaic energy system simulations and solar energy assessment.

[1] M. de l'Epine, G. Dominguez, I. Kaizuka, A. Jäger-Waldau, A Snapshot of Global PV Markets, IEA PVPS Task 1, Report No. T1-49:2026, 2026. https://doi.org/10.69766/WXLW1389

[2] J.A. Ruiz-Arias, C.A. Gueymard, Solar irradiance component separation benchmarking: The critical role of dynamically-constrained sky conditions, Renew. Sustain. Energy Rev. 202 (2024) 114678. https://doi.org/10.1016/j.rser.2024.114678

[3] M. Rynoson, S.M. Lu, J. Munkhammar, P.E. Campana, Evaluation of reverse transposition and separation methods for global tilted irradiance: Insights from high-latitude data, Sol. Energy 297 (2025) 113597. https://doi.org/10.1016/j.solener.2025.113597

[1] AGH University of Krakow, Faculty of Energy and Fuels, A.Mickiewicza 30, 30-059 Kraków, Poland
*olapade@agh.edu.pl

Dynamic Interface and Lattice Defect Engineering of Perovskite Electrodes for Intermediate-Temperature Solid Oxide Cells

Kun Zheng[1,2,*]

Keywords: solid oxide cells, perovskite electrodes, interface engineering, defect engineering, oxygen transport

ABSTRACT

Solid oxide cells (SOCs) provide efficient and reversible routes for electricity generation, hydrogen production, and renewable-energy storage. Lowering their operating temperature can reduce cost and degradation, but it also slows electrode reactions and intensifies the trade-offs among catalytic activity, mass and charge transport, thermomechanical compatibility, and long-term stability. This work presents a framework of interface- and defect-engineering for perovskite SOC electrodes, combining dynamic surface reconstruction, hierarchical architectures, functional heterointerfaces, and regulation of lattice oxygen defects [1-6]. First, catalytic interfaces were created by dynamically exsolving Fe nanoparticles from $Sr_2Fe_{2-x}W_xO_{6-\delta}$ double perovskites. The socketed metal nanoparticles provided stable active sites, improved carbon tolerance, and resisted agglomeration and detachment during operation [2]. The concept was then extended to electrospun $Sm_{0.9}Ba_{0.9}Mn_{1.8-x}Fe_xCo_{0.1}Ni_{0.1}O_{5+\delta}$ nanofibers, in which continuous porous networks enhanced gas diffusion and charge transport. Reducing conditions generated Co–Ni–Fe nanocatalysts, whereas subsequent oxidation produced hollow core–shell $Fe_{3-x-y}Ni_xCo_yO_4$ nano-oxides through a Kirkendall-type process [1]. The resulting multiscale interfaces enabled high activity in both fuel- and oxygen-electrode environments. Second, thermomechanical interfaces were engineered by incorporating negative-thermal-expansion phases into electrospun double-perovskite electrodes [3]. This approach reduced the effective thermal-expansion mismatch by approximately 50% and limited stress accumulation at the electrode–electrolyte interface. Multifunctional heterointerfaces were further constructed by combining electronically conducting $GdBa_{0.5}Sr_{0.5}CoCuO_{5+\delta}$ with ionically conducting $Ce_{0.9}Gd_{0.1}O_{1.95}$. The optimized 70:30 composite expanded the heterointerface area and triple-phase boundaries, producing a polarization resistance of approximately 0.05 Ω cm^2 after more than 480 h at 800 °C. Nanofibrous heterostructured electrodes delivered power densities above 1000 mW cm^{-2} at 700 °C.

Recent work extends this framework from interfaces into the perovskite lattice. Coupled A-site regulation and multicomponent B-site substitution were applied to $SrFeO_{3-\delta}$-derived oxygen electrodes [4]. $La_{0.5}Sr_{0.5}Fe_{0.7}Ti_{0.1}Co_{0.1}Mn_{0.1}O_{3-\delta}$ achieved a favorable balance between oxygen-vacancy formation and oxygen-ion migration while improving structural and thermomechanical stability. The electrode exhibited a polarization resistance of 0.071 Ω cm^2 at 700 °C, and an anode-supported cell reached 802 mW cm^{-2} at 800 °C with stable operation for more than 200 h. Density-functional-theory calculations showed that the intermediate La/Sr ratio optimizes the local electronic environment at the oxygen-migration bottleneck, demonstrating that maximum vacancy concentration does not necessarily produce the fastest oxygen transport. A complementary strategy combined A-site deficiency and Mn substitution in $(NdBa)_{2-\alpha}CoFe_{1-x}Mn_xO_{5+\delta}$ double perovskites [5].

[1] Faculty of Energy and Fuels, AGH University of Krakow, al. A. Mickiewicza 30, 30-059 Krakow, Poland, * zheng@agh.edu.pl
[2] AGH Centre of Energy, AGH University of Krakow, ul. Czarnowiejska 36, Krakow, 30-054, Poland

A-site deficiency promoted oxygen-vacancy formation and operational stability, whereas Mn–O bonding suppressed oxygen loss and Co-related chemical expansion. Because excessive Mn substitution reduced the activity of single-phase electrodes, 30 wt% GDC was introduced to extend ionic-transport pathways and enlarge the electrochemically active region. The optimized $(NdBa)_{1.9}CoFe_{0.25}Mn_{0.75}O_{5+\delta}$–GDC composite achieved an area-specific resistance of 0.067 Ω cm^2 at 750 °C and remained stable for more than 100 h.

These results show that interface structure and lattice defect chemistry must be coordinated across multiple length scales. Dynamic catalytic interfaces determine the availability and stability of reaction sites, hierarchical and heterostructured architectures regulate transport, and lattice engineering controls oxygen-vacancy thermodynamics, ion migration, and thermal expansion. Their combined regulation provides a practical materials-design framework for efficient and durable intermediate-temperature SOCs.

[1] J. Lach, K. Zheng, C. Radu, M. Kryński, M. Gogacz, Y. Ling, A. Klimkowicz, M. Łapiński, Controlled exsolution-dissolution in double perovskites enables symmetrical-capable high-performance SOFC electrodes, Chem. Eng. J. 532 (2026) 174527. https://doi.org/10.1016/j.cej.2026.174527.
[2] K. Zheng, J. Lach, P. Czaja, M. Gogacz, P. Czach, A. Brzoza-Kos, P. Winiarz, J. Luo, Designing high-performance quasi-symmetrical solid oxide cells with a facile chemical modification strategy for Sr2Fe2−xWxO6−δ ferrites electrodes with in situ exsolution of nanoparticles, J. Power Sources 587 (2023) 233707. https://doi.org/10.1016/j.jpowsour.2023.233707.
[3] P. Winiarz, J. Lach, Y. Ling, M. Gajewska, M. Chen, M. Marzec, K. Zheng, Stable and active nanofiber electrodes tuned via a negative thermal expansion strategy for designing high-performance solid oxide fuel cells, Appl. Catal. B 382 (2026) 125950. https://doi.org/10.1016/j.apcatb.2025.125950.
[4] A. Sultan, X. Xu, R. Zafar, L. Amir, R.T. Baker, M. Motola, P. Czaja, F. Jin, Y. Ling, K. Zheng, Coupled A-site regulation and multicomponent B-site substitution in SrFeO3−δ-derived perovskites for active and durable oxygen reduction, Appl. Catal. B 402 (2027) 127439. https://doi.org/10.1016/j.apcatb.2026.127439.
[5] R. Zafar, A. Sultan, P. Czaja, K. Zheng, Balancing oxygen vacancy formation and thermal stability in A-site-deficient Mn-substituted NdBaCoFe-based double perovskite oxygen electrodes, J. Power Sources 695 (2026) 241358. https://doi.org/10.1016/j.jpowsour.2026.241358.

Acknowledgements: This work was financially supported by the "Excellence Initiative – Research University" program for AGH University of Krakow and the subvention of the Faculty of Energy and Fuels (project No. 16.16.210.476). It was also supported by the Polish National Agency for Academic Exchange (grant No. BPN/BCH/2025/1/00043/U/00001) and the National Science Centre Poland (NCN, grant No. UMO-2021/43/D/ST5/00824).

Aminal- and Imine-Linked Covalent Organic Framework Thin Films for Solar Energy Conversion

Tomasz Polczyk,[*1], Jakub Ostapko,[2] Jan Nawrocki,[3] Sylwester Gawnikowki[3], Joanna Gryboś[1], Andrzej Adamski[1]

Keywords: covalent organic frameworks, photon upconversion, thin films, solar energy use

ABSTRACT

The development of materials for solar energy conversion requires novel strategies to improve the efficient utilization of the solar spectrum. One of the very effective methods is the conversion of low-energy into higher-energy photons. Covalent Organic Frameworks (COFs), with their modular architecture, a lack of the low-abundant metals, tunable electronic properties offer promising opportunities for the development of photoactive materials. In particular, aminal-linked COFs have recently demonstrated potential as promising solid-state platforms for triplet–triplet annihilation (TTA) photon upconversion.[1] However, their integration into photovoltaic technologies requires the development of reliable approaches for fabricating homogeneous thin films, maintaining structural order and exhibiting suitable optoelectronic properties.

This study is focused on the fabrication and characterization of COF thin films deposited on indium tin oxide (ITO) substrates by spin coating. Chosen methodology involves deposition of molecular building blocks (paraaminabenzene and 1,3,5-tris(4-formyl,3-hydroksyphenyl)benzene) from the dimethylacetamide solution followed by thermal treatment to promote framework formation. The resulting films were characterized in-depth using X-ray diffraction (XRD), Raman spectroscopy (RS), scanning electron microscopy (SEM) and UV/Vis spectroscopy to evaluate their structural characteristics, nature of chemical bonds formed, surface morphology and optical properties.

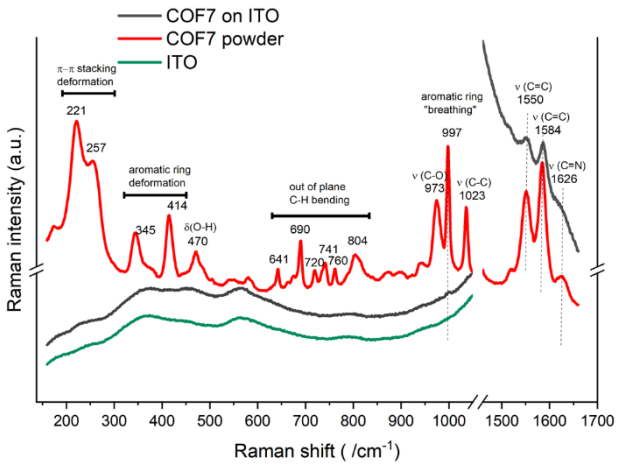


Figure 2 Comparison of the Raman spectra of the ITO support, COF on ITO and bulk crystalline COF.

Raman spectroscopy confirmed the presence of imine linkages within the COF thin

[1] Jagiellonian University, Faculty of Chemistry, Gronostajowa 2, 30-387 Krakow, Poland, * tomasz.polczyk@uj.edu.pl
[2] Centre of Excellence ENSEMBLE3 Sp. z o.o., Warsaw, Poland
[3] Institute of Physical Chemistry, Polish Academy of Sciences, Warsaw, Poland

films (Fig 1), supporting the formation of a chemically bonded stable framework. XRD analysis revealed very limited crystallinity, with a wide broadening at low diffraction angles, suggesting the presence of small, locally ordered crystalline domains. These findings indicate that, although the targeted chemical structure was formed, achieving long-range structural order in the ITO-supported thin films remains challenging. UV/Vis spectroscopy results show photoactive character of synthetized material.

The presented findings contribute to the development of COF-based thin-film materials for advanced solar energy conversion technologies. The study highlights, in particular, the potential of spin coating as a film fabrication strategy and identifies structural ordering and film quality as important aspects for further optimization.

[1] M. Brzeziński, A. Tyszka-Gumkowska, A. Gorski, M.J. Potrzebowski, T. Polczyk, W. Wegner, S. Gawinkowski, J. Ostapko, Aminal-linked covalent organic frameworks for light energy upconversion, Angew. Chem. Int. Ed. 65 (2026) e22521. https://doi.org/10.1002/anie.202522521.

Acknowledgements: participation in EFE 2026 has been supported from the Anthropocene Priority Research Area budget under the program "Excellence Initiative – Research University" at the Jagiellonian University.

Utilisation of Cenospheres as Support for CuO- and ZnO-Based Catalysts for Redox Processes of Environmental Importance

Tomasz Polczyk[1,*], Paweł Rybowicz[1], Allison Proszowska[1], Yana Vitushynska[1], Bogdan Samojeden[2], Monika Motak[2], Agata Łamacz[3], Andrzej Adamski[1]

Keywords: cenospheres, CuO, ZnO, environmental catalysis, fly ashes

ABSTRACT

The use of waste-derived materials like fly ashes (FAs), generated from industrial energy sector, as a source of valuable components that can be used as e.g. catalytic supports, offers an attractive opportunity to combine design of catalytic materials with the principles of circular economy. In this work, commercial cenospheres extracted from FAs were investigated as supports for CuO, ZnO and mixed CuO/ZnO systems, considered as catalysts for hydrogenation of CO_2 to methanol and SCR NO_x reactions. Catalysts with loadings of 0.5, 1, 3, 5 and 10 wt.% have been synthesized and characterized in-depth.

The materials obtained via wet impregnation were studied by XRF, XRD, RS and SEM techniques. XRF analysis revealed the presence of mainly Al and Si. Their occurrence was confirmed also by XRD as components of $Al_6Si_2O_{12}$ phase. The presence of copper and/or zinc was also confirmed by XRF in the supported materials, in accordance with the intended catalyst compositions and loadings. XRD measurements confirmed the presence of crystalline CuO and ZnO phases, demonstrating the formation of 3D oxide-like nanodomains stabilized on the cenosphere surfaces. RS and SEM provided additional information on the structural features and morphology of the prepared materials and their supported oxide phases.

The obtained results demonstrated quite high potential of fly-ash-derived cenospheres as supports for CuO, ZnO and CuO/ZnO to fabricate catalysts active in the redox reactions mentioned above. The formation of crystalline copper and zinc oxide (Fig.1) phases over a broad range of loadings indicated the structure-oriented effect of cenospheres used as waste-derived supports for catalytic systems of environmental importance.

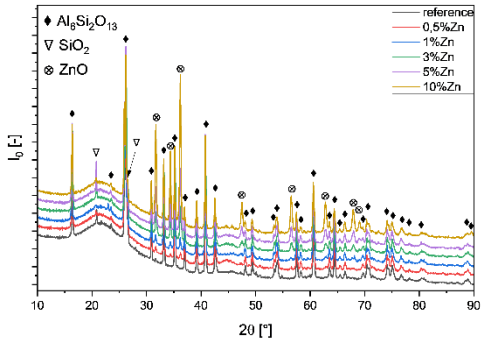


Figure 3 XRD of ZnO on cenosheres support samples.

Acknowledgements: this work has been supported from the Anthropocene Priority Research Area budget under the program "Excellence Initiative – Research University" at the Jagiellonian University.

[1] Jagiellonian University, Faculty of Chemistry, Gronostajowa 2, 30-387 Krakow, Poland, * tomasz.polczyk@uj.edu.pl
[2] AGH University of Krakow, Faculty of Energy and Fuels, Mickiewicza Ave. 30, 30-059 Krakow, Poland
[3] Wroclaw University of Science and Technology, Faculty of Chemistry, Wybrzeze Wyspianskiego 27, 50-370 Wroclaw, Poland

Tuning Hydrogen Sorption in $La_{1-x}Tb_xNi_{5-y}Sn_y$ Intermetallics: Effects of Tb and Sn Substitution on Structure and Storage Properties

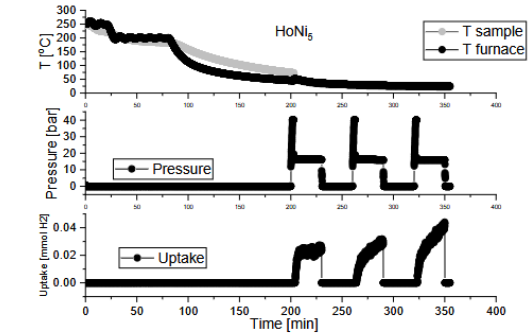
Andrzej Budziak[1,*], Julia Karweta[1], Maksymilian Skrzypiec[1]

Keywords: Hydrogen storage, intermetallic compounds, sorption properties

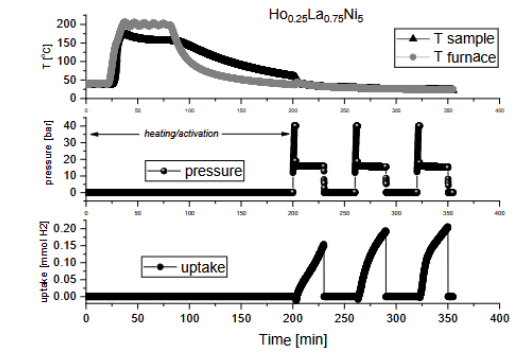
Abstract

Hydrogen is a promising energy carrier for a net-zero economy due to its exceptionally high gravimetric energy density (~142 MJ/kg), more than three times that of conventional hydrocarbon fuels. This potential has driven large-scale investments in hydrogen infrastructure and storage technologies. Efficient hydrogen storage remains a key challenge because of hydrogen's low volumetric energy density under standard conditions. Among solid-state storage approaches, AB-type intermetallic compounds are particularly attractive because they can reversibly absorb hydrogen at near-ambient temperatures and pressures. These materials typically exhibit low plateau pressures, high sorption reversibility, substantial hydrogen capacity under moderate conditions, and good cyclic stability. $LaNi_5$ is a classical representative of this family, and its properties can be tailored by partial substitution in the A- and B-sublattices (e.g., Pr, Ce, Nd in A; Al, Sn in B), which alters crystal structure, lattice parameters, and thermodynamic hydrogenation characteristics. This work investigates the $La_{1-x}Tb_xNi_{5-y}Sn_y$ system to determine how Tb and Sn content influences crystal structure, lattice parameters, and hydrogen sorption behavior. Samples with systematically varied Tb and Sn concentrations were synthesized and characterized by X-ray diffraction and hydrogen sorption measurements. Results demonstrate that targeted substitutions enable tuning of plateau pressure and sorption capacity while maintaining good reversibility and cyclic stability. The findings clarify the role of Tb and Sn in modifying structural and thermodynamic properties and assess the potential of these compositions for practical hydrogen-storage applications. Figure 1 below shows the hydrogen absorption kinetics for $HoNi_5$ and $Ho_{0.25}La_{0.75}Ni_5$ samples - representing, respectively, significant and minor deviations from the parent $LaNi_5$ compound. A high Ho content adversely affects the hydrogen absorption kinetics. Similar trends are observed in samples where lanthanum is substituted with terbium. A strong improvement in sorption properties was achieved through minor substitution of nickel with tin; these relationships will be presented during the presentation.

[1] Faculty of Energy and Fuels, AGH University of Krakow, al. Mickiewicza 30, 30-059 Kraków, Poland, *budziak@agh.edu.pl



a)



b)

Fig.1. Plots of activation pressure, hydrogen saturation of the sample, and sample temperature as a function of time for a) $HoNi_5$ and b)$Ho_{0.25}La_{0.75}Ni_5$.

Acknowledgments: This research was founded by AGH University, Poland (No.16.16.210.476). The authors would like to thank A. Dębski (IMIM PAN, Kraków) for pcT study.

EFE2026 ENERGY FUELS ENVIRONMENT
INTERNATIONAL CONFERENCE
17-20 NOVEMBER 2026, KRAKÓW, POLAND

Tailoring the Structural and Electrochemical Properties of Fe-based $La_{1-x}Sr_xFe_{0.7}Co_{0.2}Ni_{0.1}O_{3-\delta}$ Perovskite Oxides as Cathode Materials for IT-SOFCs

Laiba Amir[1], Amir Sultan[1,2], Rameez Zafar[2], Kun Zheng[1,3]*

Keywords: Sr-doping, Fe-basd perovskites, Oxygen electrode, IT-SOFCs, Polarization resistance

ABSTRACT

Solid oxide fuel cells (SOFCs) are among the most prominent energy conversion and storage technologies, converting the chemical energy of fuels directly into electricity with high efficiency. Conventional SOFCs operate at high temperatures, and this significantly limits their commercial marketability due to material degradation, high fabrication costs, and long start-up times. Lowering the operating temperature while maintaining high power output is therefore essential for SOFC technology. For intermediate-temperature SOFCs (IT-SOFCs), novel electrode materials with long-term stability and enhanced electrocatalytic activity are critical to achieving stable, high-performance cells [1]. A stable SOFC cathode requires both high catalytic activity for the oxygen reduction reaction (ORR) and excellent chemical stability under operating conditions. However, conventional Co-based perovskite oxides (such as LSCF), despite their widespread use, suffer from several drawbacks at intermediate temperatures, high thermal expansion coefficient (TEC) mismatch with common electrolytes, and gradual structural instability that leads to sluggish oxygen surface-exchange kinetics and long-term performance degradation. These limitations make LSCF prone to degradation in practical SOFC applications and motivate the search for compositional modifications that can improve both catalytic activity and stability [2-4].

In this study, Fe-based $La_{1-x}Sr_xFe_{0.7}Co_{0.2}Ni_{0.1}O_{3-\delta}$ (x = 0, 0.3, 0.5, 0.7, and 1) perovskites were fabricated to investigate the effect of A-site strontium doping, combined with minor B-site doping with Co and Ni cations, on their structural, microstructural, and electrochemical properties. These compositions represent non-Co-based perovskites combining with the La/Sr content optimization and B-site cations regulations for balancing catalytic activity and thermomechanical properties of perovskites. Fe serves as the principal B-site cation for structural stability, while Co content is limited to 0.2 to balance catalytic performance and thermomechanical compatibility, since higher Co levels enhance oxygen surface-exchange kinetics but also increase the TEC, risking mismatch with the electrolyte. Additional B-site substitution with Ni further modulates the catalytic activity, electronic and ionic transport properties, and defect chemistry. Partial substitution of Co by Ni has been reported to reduce the thermal expansion coefficient (TEC) and mitigate Sr segregation compared with unmodified LSCF. Moreover, the Ni^{2+}/Ni^{3+} redox couple provides additional charge carriers and alters the oxygen vacancy concentration, thereby affecting both bulk conductivity and surface oxygen exchange kinetics.

Phase formation and structural evolution were confirmed by X-ray diffraction (XRD), while scanning and transmission electron microscopy (SEM/TEM) were used to examine

[1] Faculty of Energy and Fuels, AGH University of Krakow, al. A. Mickiewicza 30, 30-059 Krakow, Poland, * zheng@agh.edu.pl
[2] Jerzy Haber Institute of Catalysis and Surface Chemistry, Polish Academy of Sciences, Niezapominajek 8, Krakow, PL-30239, Poland.
[3] AGH Centre of Energy, AGH University of Krakow, ul. Czarnowiejska 36, Krakow, 30-054, Poland.

particle morphology, grain size, and microstructural homogeneity. Thermogravimetric analysis (TGA) provided insight into thermal stability and oxygen non-stoichiometry, and Brunauer–Emmett–Teller (BET) analysis was used to determine specific surface area. Electrochemical impedance spectroscopy (EIS) studies showed a corresponding decrease in polarization resistance (Rp) with increasing Sr content, with the highest-Sr composition achieving the lowest Rp of 0.06 $\Omega \cdot cm^2$ at 750°C, indicating markedly improved electrocatalytic activity compared to the La-rich compositions. Overall, these findings highlight the LSFCNi electrode as an effective approach of addressing the inherent activity-stability trade-off in perovskite cathodes, providing a rational defect-engineering framework to guide the design of durable, high-performance oxygen electrodes for IT-SOCs.

[1] A. Sultan, X. Xu, R. Zafar, L. Amir, R.T. Baker, M. Motola, P. Czaja, F. Jin, Y. Ling, K. Zheng, Coupled A-site regulation and multicomponent B-site substitution in SrFeO3−δ-derived perovskites for active and durable oxygen reduction, Appl. Catal. B 402 (2027) 127439. https://doi.org/10.1016/j.apcatb.2026.127439.
[2] X. Han, Q. Shao, K. Li, Y. Gao, B. Wei, Z. Cai, K. Zheng, P. Feng, Z. Lv, Y. Ling, Constructing chromium-tolerance La0.6Sr0.4Co0.2Fe0.8O3−δ cathode for solid oxide fuel cells using entropy-assisted surface engineering, Chem. Eng. J. 503 (2025) 158480. https://doi.org/10.1016/j.cej.2024.158480.
[3] P. Feng, Q. Huang, N. Han, K. Yang, W. Yan, X. Xi, J. Zhang, Z.P. Li, Significant suppression of Sr segregation to substantially enhance performance of La0.6Sr0.4Co0.4Fe0.6O3−δ cathodes for SOFCs via thermodynamic-kinetic engineering, Adv. Funct. Mater. 36 (2026) e18931. https://doi.org/10.1002/adfm.202518931.
[4] R. Zafar, A. Sultan, P. Czaja, K. Zheng, Balancing oxygen vacancy formation and thermal stability in A-site-deficient Mn-substituted NdBaCoFe-based double perovskite oxygen electrodes, J. Power Sources 695 (2026) 241358. https://doi.org/10.1016/j.jpowsour.2026.241358.

Acknowledgements: This work was financially supported by the „Excellence Initiative – Research University" program for the AGH University of Krakow, and the subvention of AGH University of Krakow, Faculty Energy and Fuels (project No. 16.16.210.476). The work is co-financed by the Polish National Agency for Academic Exchange grant nr BPN/BCH/2025/1/00043/U/00001.

EFE2026 ENERGY FUELS ENVIRONMENT
INTERNATIONAL CONFERENCE
17-20 NOVEMBER 2026, KRAKÓW, POLAND

Pyrolysis of Oxidized Bitumen Residue: Preliminary Investigation of Gas and Solid Products

Małgorzata Cierpińska[1,*]

Keywords: Oxidized bitumen residue, Pyrolysis, Thermochemical conversion, Syngas composition, Circular economy

ABSTRACT

Bitumen is highly viscous petroleum derived material composed mainly of hydrocarbons (carbon content 83%, hydrogen content 10.6%), resins, asphaltenes, heteroatoms and trace metals [1]. Oxidized bitumen residue is formed through reactions with oxygen from air, which alter its composition by increasing the content of asphaltenes, sulfoxides, ketones and carboxylic acids [2].

Bitumen pyrolysis is a multi-stage process in which initial volatilization is followed by thermal cracking, dealkylation and aromatization at higher temperatures, resulting in the formation of gases and coke or pyrobitumen [3]. Pyrolysis enables the conversion of bitumen residues into potentially valuable liquid and gaseous products, supporting waste valorization and the recovery of resources within a circular economy concept. The product distribution is mainly influenced by temperature, residence time, heating rate, feedstock composition and reactor or catalyst type [3]. Therefore, the objective of this study is preliminary investigation of Oxidized Bitumen Residue (OBR) pyrolysis and assessment of temperature and residence time influence on the composition of gaseous products and solid residues. The obtained results provide a basis for further characterization of the liquid fraction to evaluate its potential for asphalt production within a circular economy framework.

The investigated material was obtained from an operating asphalt production plant. Pyrolysis experiments were conducted in a fixed-bed reactor under N_2 atmosphere (35 mL/min) at 450 and 500 °C temperature with a heating rate of 10 °C/min and a 20 minutes residence time, with an additional experiment at 500 °C for 40 minutes. Samples were named as OBR_process temperature_residence time, resulting in OBR_450_20, OBR_500_20 and OBR_500_40. The OBR feed was characterized by proximate and elemental analyses, including determination of moisture (M), ash (A), volatile matter (VM) and fixed carbon (FC) content as well as carbon (C), hydrogen (H), nitrogen (N) and oxygen (O) concentration. Obtained chars were subjected to elemental analysis. The gaseous products were collected in Tedlar bags and analysed by gas chromatography (GC) to determine the concentrations of H_2, CH_4, CO_2, CO, and higher hydrocarbons (C_nH_m).

Table 1. Proximate and ultimate analysis of Oxidized Bitumen Residue

Proximate analysis			
M, %	**A, %**	**VM, %**	**FC, %**
15.94	1.73	68.97	13.35
Ultimate analysis			
C, %	**H, %**	**N, %**	**O, %**
77.21	14.50	0.52	6.04

The results of the proximate and ultimate analyses presented in Table 1 confirm the hydrocarbon-rich nature of the feedstock and its potential for thermochemical conversion. As presented at Figure 1 gas composition varied substantially with pyrolysis temperature and residence time. Increasing the temperature from 450

[1] Department of Heat Engineering and Environment Protection, Faculty of Metals Engineering and Industrial Computer Science, AGH University of Krakow, 30 Mickiewicza Avenue 30-059 Krakow, Poland, msieradz@agh.edu.pl

to 500 °C for 20 min increased the CH_4 content from 38.29% to 47.39% and H_2 from 19.81% to 31.67%, while CO_2 decreased from 10.99% to 0.59%. This indicates enhanced thermal cracking and secondary reactions at higher temperature, favoring the formation of methane and hydrogen and promoting further conversion of oxygen-containing compounds. Extending the residence time at 500 °C to 40 min resulted in a decrease in H_2 and an increase in C_nH_m, suggesting that prolonged residence promoted secondary reactions and the formation of higher hydrocarbons. These changes were accompanied by an increase in the carbon content of the char from 66.80% for OBR_450_20 to 78.05% for OBR_500_20, indicating greater devolatilization and carbon enrichment at higher temperature. A slight decrease in char carbon content to 76.44% at 40 min may indicate the occurrence of secondary reactions and partial conversion of the carbonaceous residue. Overall, the results demonstrate that both temperature and residence time significantly affect the gas product distribution.

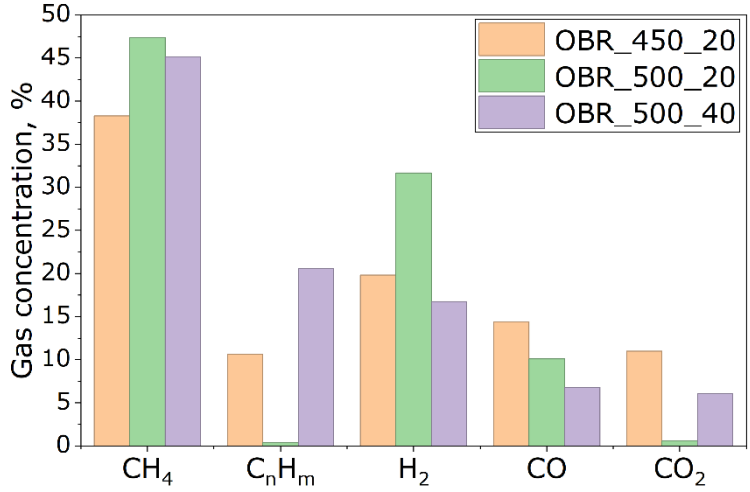


Figure 1. Syngas composition of pyrolysis products

The presented preliminary results demonstrate that pyrolysis temperature and residence time influence both gas composition and char characteristics. Further research will focus on the chemical composition, calorific value, and flash point of the liquid fraction to evaluate its potential for application in asphalt production within a circular economy framework.

[1] J.G. Speight, Feedstock types and properties, in: The Refinery of the Future, Elsevier, 2020: pp. 1–42. https://doi.org/10.1016/B978-0-12-816994-0.00001-4.
[2] S. Vassaux, V. Gaudefroy, L. Boulangé, A. Pévère, A. Michelet, V. Barragan-Montero, V. Mouillet, Assessment of the binder blending in bituminous mixtures based on the development of an innovative sustainable infrared imaging methodology, J. Clean. Prod. 215 (2019) 821–828. https://doi.org/10.1016/j.jclepro.2019.01.105.
[3] M. Maniscalco, L. Mistretta, P. Iannotta, G. Caputo, F. Scargiali, F. Grisafi, A. Brucato, Experimental study of the pyrolysis of waste bitumen for oil production, Journal of the Energy Institute 93 (2020) 2456–2463. https://doi.org/10.1016/j.joei.2020.08.003.

Acknowledgments: This research was funded by the Ministry of Science and Higher Education, Poland [AGH grant no. 16.16.110.663/501.00-110000-10000]. Research project was partly supported by program „Excellence initiative – research university" for the AGH University of Krakow, Action D21.

Mn-Co-Cu-Doped Potassium Silicate Glass as a Catalyst for Simultaneous Combustion of Soot and Ethylene

Piotr Legutko[1,*], Patrycja Przedwojska[1], Gabriela Grzybek[1], Michał Dziadek[2], Mateusz Marzec[3], Katarzyna Cholewa-Kowalska[2], Andrzej Adamski[1]

Keywords: potassium silicate glass, transition-metal doping, soot, ethylene, combustion

ABSTRACT

Despite increasingly stringent emission regulations, air pollution with carbonaceous particulate matter and volatile organic compounds (VOCs) remains a serious environmental and public-health concern. Catalytic total oxidation is considered one of the most effective approaches to the abatement of these pollutants. However, the simultaneous removal of solid soot and gaseous VOCs remains challenging because of their different nature, properties, and oxidation mechanisms. Their interactions with the catalyst surface and operating temperature requirements are also different. Therefore, the development of inexpensive multifunctional catalysts, capable of operating under mixed-pollutant conditions, is highly desirable.

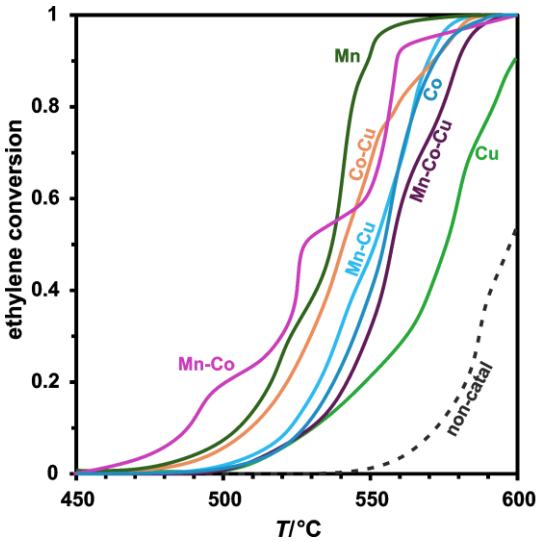


Figure 1. Ethylene conversion as a function of temperature without catalyst and over Mn-, Co-, and Cu-modified potassium silicate glasses

Potassium silicate glasses are promising materials for such catalytic systems because of their intrinsic activity in soot combustion, low production cost, available constituents, thermal stability, and ease of shaping [1,2]. Their composition can also be tailored, while the surface can be modified with transition metals of pronounced redox properties, able to provide catalytically active sites for VOC oxidation. In this study, the influence of Mn, Co,

[1] Jagiellonian University, Faculty of Chemistry, Gronostajowa 2, 30-687 Kraków, Poland,
* piotr.legutko@uj.edu.pl
[2] AGH University of Krakow, Faculty of Materials Science and Ceramics, Mickiewicza Ave. 30, 30-059 Kraków, Poland
[3] AGH University of Krakow, Academic Centre for Materials and Nanotechnology, Mickiewicza Ave. 30, 30-059 Kraków

and Cu (introduced individually and in binary or ternary combinations) on the physicochemical properties and catalytic performance of potassium silicate glass was investigated. In each studied formulation, the total loading of redox metals was kept constant at 10 mol.%, allowing the effect of metal composition to be assessed independently of the overall dopant content.

The parent $K_2O–SiO_2–CaO$ glass was synthesized by melt-quenching at 1345 °C, using K and Ca carbonates and SiO_2 as precursors. Mn, Co, and Cu were subsequently introduced by incipient wetness impregnation, using aqueous solutions of the corresponding nitrates. The materials were then dried and calcined at 500 °C for 4 h. Their structural, spectroscopic, morphological, and redox properties were examined by X-ray diffraction, Raman spectroscopy, FTIR spectroscopy, scanning electron microscopy, H_2 temperature-programmed reduction, UV/Vis diffuse reflectance spectroscopy, and X-ray photoelectron spectroscopy. Catalytic activity was evaluated in the separate combustion of soot and ethylene and under conditions suitable for their simultaneous oxidation.

Structural characterization confirmed that the amorphous character of the glass matrices was preserved after impregnation and subsequent calcination. The transition metal dopants have been quite well distributed within catalyst structures. Simultaneously, crystalline KNO_3 domains were detected. Spectroscopic and reduction temperature-programmed measurements revealed that the nature and combination of the deposited transition metals affected their coordination, oxidation states, and redox behavior, which was reflected in substantial differences in ethylene oxidation activity.

In separate ethylene combustion, the Mn–Co-modified glasses exhibited the highest activity, followed by that observed for Mn, Co–Cu, Mn–Cu, Co, Mn–Co–Cu, and Cu-containing samples. The temperature required to reach 50% ethylene conversion was approximately 520 °C for the most active catalyst and approximately 570 °C for the least active one, compared with about 595 °C for non-catalytic combustion. The differences between the mono-, bi-, and trimetallic systems clearly demonstrated that the catalytic performance is governed not only by the presence of a given metal but also by intimate interactions among the redox-active components.

At simultaneous soot and ethylene oxidation, the catalytic performance in ethylene combustion changed. The Mn–Co–Cu-, Mn–Cu-, and Mn-modified glasses showed the highest activity, followed by Mn–Co, Cu, Co, and Co–Cu samples. Importantly, the glasses modified with several transition metals retained their activity in soot combustion, while the characteristic temperature windows of soot and ethylene oxidation remained broadly similar in the separate and simultaneous experiments. The presence of ethylene therefore did not suppress the beneficial role of the potassium-containing glass matrix in soot oxidation, while the deposited metals provided the redox functionality necessary for VOC removal.

The results demonstrate that potassium silicate glass can serve as a low-cost, noble-metal-free, and shapeable matrix for multifunctional oxidation catalysts. By selecting an appropriate combination of Mn, Co, and Cu at a constant total metal loading, the activity toward ethylene can be tuned while preserving a satisfactory activity towards soot combustion. The developed materials are thus promising for the simultaneous abatement of soot and VOCs emitted in multicomponent exhaust streams.

[1] P. Legutko, M. Dziadek, G. Grzybek, M. Marzec, E. Jarosz, M. Michalik, M. Piumetti, K. Cholewa-Kowalska, D. Fino, A. Adamski, Catalytic removal of soot particles over potassium glasses – the effect of doping with aliovalent redox metals, Catal. Sci. Technol. 14 (2024) 2549–2562. https://doi.org/10.1039/D4CY00136B.
[2] P. Legutko, P. Przedwojska, M. Dziadek, G. Grzybek, M. Marzec, R. Fanselow, J. Czapla-Masztafiak, Z. Olejniczak, M. Piumetti, D. Fino, K. Cholewa-Kowalska, A. Adamski, Copper-dependent modification of structural and functional properties of potassium silicate glasses for catalytic applications, Ceram. Int. 52 (2026) 13728–13738. https://doi.org/10.1016/j.ceramint.2026.02.014.

The work was supported by Grant No. 2025/59/B/ST5/02932 from the National Science Centre, Poland.

EFE2026 ENERGY FUELS ENVIRONMENT
INTERNATIONAL CONFERENCE
17-20 NOVEMBER 2026, KRAKÓW, POLAND

An Energy Management Framework for Peer-to-Peer Energy Trading under Preference Uncertainty

Pablo Benalcazar[1,*], Maciej Kalka[1], Despoina Antoniadou[2]

Keywords: Peer-to-peer energy trading, Energy management system, Local energy markets, Distributed energy resources, Prosumer preferences

ABSTRACT

Peer-to-peer (P2P) energy trading can increase the value of distributed energy resources by enabling prosumers to exchange locally generated electricity within a community. By coordinating photovoltaic generation, battery storage, and electricity demand, P2P markets can increase local renewable energy utilization, reduce grid imports, and create additional value for participating prosumers. These benefits depend, however, on the ability of the energy management system (EMS) to translate prosumer preferences into appropriate trading decisions. As P2P trading becomes increasingly automated, preferences communicated through natural language may be converted into market orders with varying degrees of uncertainty, potentially affecting market efficiency and the benefits of local energy exchange.

This study develops an EMS framework for P2P energy trading that explicitly accounts for uncertainty in representing prosumer preferences. The framework integrates prosumer-level energy management, preference-based bid generation, P2P market clearing, and distribution network constraints. A rolling-horizon optimization model represents the operation of photovoltaic generation, battery storage, household electricity demand, and grid exchanges, and derives the marginal value of energy for each prosumer. These values are used to construct ordered bid blocks for the P2P market. A budget-balanced community market determines energy exchanges subject to distribution network constraints, while the resulting schedules are validated through AC power-flow analysis. The framework is evaluated using controlled preference scenarios and compared across accurate preference information, direct automated bidding, ambiguity-aware bidding, abstention, and a no-trading reference.

The results quantify how uncertainty in automated bidding affects the efficiency and value of P2P energy trading. The analysis evaluates local energy exchange, market surplus, prosumer outcomes, and the extent to which network congestion affects these benefits. It further identifies how the position of different preference dimensions relative to the market-clearing conditions determines their impact on trading outcomes. The results highlight the trade-off between protecting prosumers from uncertain bids and preserving the economic and operational benefits of local energy exchange.

Acknowledgments: The research was conducted as part of the CoEnerBuild project, funded by the Polish National Center for Research and Development and the European Union under the CETPartnership program (project code Cetp-FP2023-00014)

[1] Mineral and Energy Economy Research Institute of the Polish Academy of Sciences, Division of Energy Economics, Kraków, Poland, *benalcazar@min-pan.krakow.pl

[2] Aristotle University of Thessaloniki, School of Electrical and Computer Engineering, Thessaloniki, Greece

EFE2026 ENERGY FUELS ENVIRONMENT
INTERNATIONAL CONFERENCE
17-20 NOVEMBER 2026, KRAKÓW, POLAND

Ammonia Content as One of the Important Parameters Determining Pathways for the Efficient Valorization of Fly Ashes from the Energy Sector

Andrzej Adamski[1,*], Paweł Rybowicz[1], Michał Mochnaczewski[1], Stefania Wasiela[1], Michal Marko[2], František Šoukal[2]

Keywords: ammonia, fly ashes, valorization, energy sector, environmental hazard

ABSTRACT

Fly ashes (FAs), one of the main byproducts accompanying large scale energy generation in thermal power stations, are produced globally at a rate of approximately 500–700 million tons per year [1], with Poland accounting for about 4 million tons. In line with circular economy principles, effective methods for the management of fly ashes are being sought. Several physicochemical properties of FAs determine their potential applications. Primary conditions, strongly influencing properties of fly ashes, are controlled by both source and nature of the fossil fuels used for energy generation. Secondary conditions significantly affecting their properties are dependent on the course of combustion processes. Crucial variables here include the combustion technology itself, fuel pre-treatment, the type of boiler, and the combustion temperature. An additional factor that can strongly influence the composition and physicochemical properties of FAs is the application of flue gas purification technologies, particularly when additional reactants are introduced into the flue gas streams (which also carries fly ashes) - such as ammonia for nitrogen oxide removal via SCR or SNCR methods, or calcium for desulfurization.

Currently, the construction industry is the primary consumer of ashes from energy sector. However, it appears possible to develop much more advanced methods for fly ash management that allow for much better utilization of their potential [2]. FAs are usually characterized by high silicon and aluminum contents. These elements occur primarily in the form of aluminosilicate glasses, constituting e.g. the structural material of spherical grains known as cenospheres - as well as, in crystalline form, specifically occurring as quartz and mullite mineral phases. The use of ammonia in both SCR NO_x and SNCR NO_x technologies entails the risk of so-called ammonia slip - the passage of unreacted NH_3 beyond the denitrification systems (Fig. 1 below). The EU Best Available Techniques (BAT) recommendations introduced additional limits on ammonia emissions to the air from SCR NO_x and SNCR NO_x installations, ranging from below 3 to 10 mg/Nm³. It is thus important to take into consideration also ammonia content in fly ashes as an important parameter decisive (alongside the contents of iron and unburned fuel) for the efficient use of these byproducts of combustion processes.

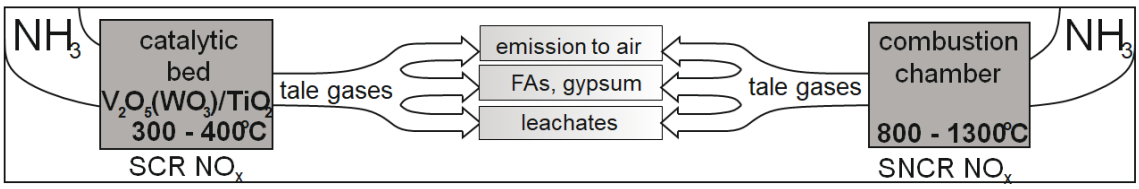


Fig. 1. Potential pathways for the release of unreacted ammonia into the environment from the flue gas denitrification technologies applied in conventional power plants.

This work presents a comparative analysis - with reference to SCR NOx and SNCR NOx

[1] Jagiellonian University, Faculty of Chemistry, Gronostajowa 2, 30-387 Krakow, Poland, * adamski@chemia.uj.edu.pl
[2] Brno University of Technology, Faculty of Chemistry, Purkyňova 464/118, 612 00 Brno, Czechia

technologies applied to denitrification of tale gases emitted from power stations - of the pathways by which ammonia from flue gas denitrification systems enters the environment: through direct emission with flue gas, via the power plant's water circuit, and following adsorption onto fly ash. Regarding the latter, our current study presents determination of ammonia concentrations in fly ash leachates, as well as the potential environmental implications of ammonia presence in power-sector fly ashes for their storage and subsequent utilization.

24 samples of fly ashes from coal- and lignite-fueled power plants in the Czech Republic and in Poland as well as from a commercial fly ash storage facility have been in-depth characterized among others by XRD, RS, DRIFT, porosimetry and analytical methods e.g. to identify and quantitatively assess potential hazard related to the presence of ammonia. A modified Berthelot method using a commercial test kit, the Nessler method, and the formalin titration method (so called Ronches' method) have been used to determine content of ammonia in FAs. The leachates were prepared by weighing 3 or 10 ± 0.1 g of each ash sample into Falcon-type centrifuge tubes. Approximately 30 or 100 ± 1 mL of distilled water was added to the weighed samples, and the resulting mixtures were agitated on a shaker for 24 hours at a speed of 180 rpm. Subsequently, the samples were centrifuged at a speed of 4000 rpm for 5 minutes. After removing the tubes from the centrifuge, the supernatant was separated from the solid ash phase by filtration through paper filters [3].

Currently, no specific EU legal regulations are imposed on the ammonia concentration in fly ashes, but usually 100 ppm is considered as an acceptable level of ammonia content. Our results showed that in several of the analyzed fly ash samples the content of ammonia exceeded the limit of 100 ppm. These samples originated mainly from power plants that utilized the SNCR NOx as denitrification method. A comparison of ammonia levels in ash samples from power plants using SCR NOx vs. those using SNCR NOx clearly revealed that higher ammonia slip occurred in the case of SNCR NOx method (with ammonia contents in the analyzed fly ashes being more than 200 times higher in some cases).

According to our operational algorithm proposed to determine the preferential methods of utilization of fly ashes [1], one of the possible ways of exploitation of fly ashes of a higher level of ammonia is their use as precursors for the synthesis of SiAlONs. Fly ashes as powders consisting of particles rich in Si and Al mixed sometimes with particles of unburned fuel can also be considered as very promising and cheap raw materials for the production of SiAlONs on a larger scale. Moreover, alternative methods for synthesis of SiAlONs require a nitrogen atmosphere at a relatively high temperature (1300 °C). In such a case, the naturally higher content of ammonia in the fly ashes may be beneficial.

Acknowledgements: participation in EFE 2026 has been supported from the Anthropocene Priority Research Area budget under the program "Excellence Initiative – Research University" at the Jagiellonian University.

[1] P. Rybowicz, M. Mochnaczewski, M. Kozieł, Ł. Uruski, A. Łagosz, M. Michalik, L. Chmielarz, A. Adamski, Key parameters of fly ashes generated from the industrial energy sector decisive for their pro-ecological applications, Energy Fuels 34 (2020) 6229–6238. https://doi.org/10.1021/acs.energyfuels.9b04426.
[2] P. Rybowicz, Y. Vitushynska, A. Kowalczyk, R. Panek, A. Łagosz, M. Michalik, W. Franus, A. Adamski, Crucial parameters determining efficient use of fly ashes from energy sector as raw materials for dedicated advanced applications, Sustain. Chem. Pharm. 27 (2022) 100637. https://doi.org/10.1016/j.scp.2022.100637.
[3] S. Wasiela, Master's thesis, Faculty of Chemistry, Jagiellonian University, 2022.

Research on the Effect of Solvent Processing on Changing the Low-Temperature Properties of Jojoba Oil

Stefan Ptak[1,*]

Keywords: vegetable waxes, oil jojoba, solvent dewaxing, low-temperature properties

ABSTRACT

Waxes of natural origin serve as renewable raw materials and are used in manufacturing to mitigate the negative environmental impacts associated with the emission and use of harmful, degrading substances. Plant waxes have diverse applications, including as ingredients in lubricants and paraffin-based products, as well as fuel components for compression-ignition engines. This presentation outlines the chemical composition, physicochemical properties, and applications of jojoba oil, which is derived from the fruit of the jojoba plant. It further presents the results of tests performed on a jojoba oil sample subjected to solvent dewaxing using a mixture of methyl ethyl ketone and toluene, alongside aggregated results from tests using other solvents. The study yielded modified jojoba oils with improved low-temperature properties, as well as a second product—termed "hardened wax"—consisting of the fraction retained on the filter cloth; after solvent removal, this fraction exhibited higher temperature-related performance characteristics compared to the raw jojoba oil feedstock. The solvent dewaxing process for jojoba oil proved efficient, requiring short filtration times and yielding modified oils characterized by significantly lower cloud, pour, and melting points—though without improvement in the Cold Filter Plugging Point (CFPP)—and an increased melting point for the recovered wax compared to the original oil. By using various solvents, the cloud point was reduced to a minimum of -11°C, the pour point to -12°C, and the melting point to -13°C. Conversely, the jojoba wax hardened in this process exhibited a maximum increase in cloud, pour, and solidification points to +10°C, +7°C, and +5°C, respectively.

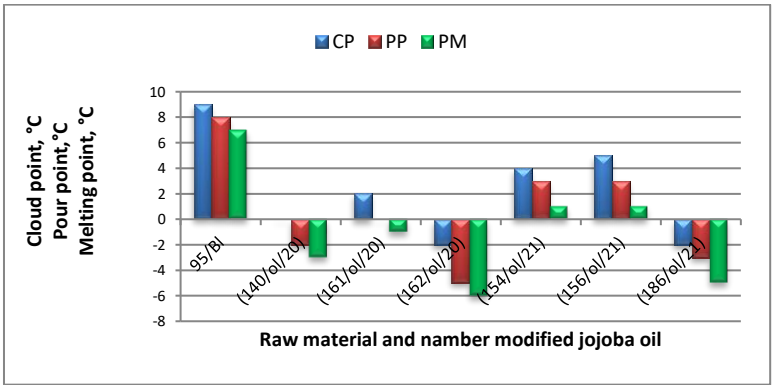


Figure 1. Low-temperature properties of 95/Bl jojoba oil and modified jojoba oils in the solvent dewaxing process using MEK-TOL

[1] Stefan Ptak; Oil and Gas Institute - National Research Institute, 25 A Lubicz Str.,31-503 Krakow, Poland,
* ptak@inig.pl

Real-World Emissions from Polish Waste-to-Energy Plants in the Context of Evolving EU Regulatory Requirements

Anna Korzeniewska[1,*], Katarzyna Szramowiat-Sala[1]

Keywords: waste incineration, BAT, air pollutant emissions, environmental transparency

ABSTRACT

Waste-to-energy (WtE) plants operate under stringent atmospheric emission requirements established through both regulatory emission limit values and Best Available Techniques (BAT) [1,2]. Publicly available monitoring data offer an opportunity to assess actual operating emission performance. However, differences in pollutant nomenclature, averaging periods, reference conditions and reporting formats may limit direct comparison between facilities. The aim of this study was to assess real-world emission performance and operating margins relative to BAT-associated emission levels (BAT-AELs) [3], while examining the extent to which publicly reported data allow meaningful comparison between municipal WtE facilities.

Publicly reported emission monitoring data from three municipal WtE facilities operating in Poland were analysed for particulate matter, HCl, HF, SO_2, CO, TOC and nitrogen oxides, reported as NO_x or NO_2 depending on the facility. Reported emission concentrations were compared with installation-specific reference values to assess the operating margin relative to applicable requirements. Where monitoring conditions allowed direct comparison, the data were additionally normalised to the upper BAT-AEL for existing plants to provide a common benchmark across facilities. Emission distributions were characterised using the median and 95th percentile (P95), representing typical and high-emission operating conditions, respectively.

The results showed clear pollutant-specific differences in operating margins. Mean particulate matter concentrations ranged from 0.16 to 0.86 mg/Nm³ and represented 0.55–3.82% of the applicable installation-specific reference values. For SO_2, mean concentrations ranged from 1.08 to 9.95 mg/Nm³, corresponding to 0.54–19.90% of the respective reference values. Nitrogen oxide concentrations were substantially closer to the applicable benchmarks, with mean values ranging from 120.20 to 156.78 mg/Nm³ and accounting for 30.05–67.21% of the installation-specific reference values. BAT-normalised P95 values for SO_2 remained within 4.6 and 35.3% of the upper BAT-AEL, whereas for NO_x/NO_2 they reached approximately 99.2–110.9%, indicating that the upper part of the nitrogen oxide emission distribution approached or slightly exceeded the upper BAT-AEL benchmark. Differences in pollutant definition, averaging structure and reporting conventions also limited direct comparison between the investigated facilities.

Overall, the analysis indicates that PM and SO_2 emissions remained well below applicable reference levels, whereas NO_x/NO_2 operated much closer to the upper BAT-AEL benchmark. At the same time, heterogeneity in public reporting constrained full cross-facility comparability.

[1] H.-W. Hsu, E. Binyet, R.A.A. Nugroho, W.-C. Wang, P. Srinophakun, R.-Y. Chein, R. Demafelis, N. Chiarasumran, H. Saputro, A.F. Alhikami, N. Sakulshah, T. Laemthong, Toward sustainability of Waste-to-Energy: An overview, Energy Convers. Manag. 321 (2024) 119063. https://doi.org/10.1016/j.enconman.2024.119063.

[2] J. Czerwińska, G. Wielgosiński, Functioning of the flue gas treatment system in Polish municipal waste incineration plants, Sci. Rev. Eng. Environ. Sci. 29 (2020) 108–119. https://doi.org/10.22630/PNIKS.2020.29.1.10.

[1] Faculty of Energy and Fuels, AGH University of Krakow, Al. A. Mickiewicza 30, 30-059 Kraków, Poland, *akorzen@agh.edu.pl

[3] European Commission, Commission Implementing Decision (EU) 2019/2010 of 12 November 2019 establishing the best available techniques (BAT) conclusions, under Directive 2010/75/EU of the European Parliament and of the Council, for waste incineration, Off. J. Eur. Union L 312 (2019) 55–91. http://data.europa.eu/eli/dec_impl/2019/2010/oj. [3] Commission Implementing Decision (EU) 2019/2010 of 12 November 2019 establishing the best available techniques (BAT) conclusions, under Directive 2010/75/EU of the European Parliament and of the Council, for waste incineration (notified under document C(2019) 7987)

The work was financed by subvention for the AGH University of Krakow (grant no. 501.00 210000 10000) and from funds of the "Excellence Initiative- Research University" program for AGH.

Waste-to-Energy Plants under Evolving Environmental and Climate Requirements: From Emission Control to Climate Neutrality

Anna Korzeniewska[1,*], Weronika Stępak[1], Katarzyna Szramowiat-Sala[1], Jerzy Górecki[1]

Keywords: waste incineration, BAT, atmospheric emissions, climate neutrality, dispersion modelling

ABSTRACT

Waste-to-Energy (WtE) plants operate at the intersection of waste management, air pollution control, and climate policy. Over recent decades, EU environmental requirements for municipal waste incineration have evolved from conventional emission limit values towards Best Available Techniques (BAT), resource efficiency, and decarbonisation goals [1,2]. This study evaluates the implications of this regulatory shift using atmospheric dispersion modelling (OPERAT FB) for a municipal WtE facility. Two emission scenarios were compared under identical operating and meteorological conditions: one representing earlier emission standards and the second based on current BAT-associated emission levels (BAT-AELs). The analysis covered major air pollutants, including PM10, PM2.5, SO_2, NOx, HCl, heavy metals, and PCDD/F, as well as dust and cadmium deposition.

The modelling results showed that the BAT-AEL scenario generally resulted in lower predicted ground-level concentrations, while the overall spatial dispersion pattern remained similar. Compared with the earlier emission-standard scenario, maximum one-hour concentrations decreased for PM10 (from 2.6 to 1.5 μg m^{-3}), SO_2 (24.9 to 21.0 μg m^{-3}), NOx as NO_2 (99.6 to 94.4 μg m^{-3}), and HCl (5.0 to 4.2 μg m^{-3}), whereas CO showed a slight increase (24.9 to 26.2 μg m^{-3}), reflecting pollutant-specific differences in the assumed emission levels.

These results indicate that the transition towards BAT-AELs can reduce predicted local air-quality impacts of WtE operation, while the broader environmental assessment of such facilities is increasingly expected to integrate air-pollutant control with climate-related aspects, including fossil CO_2 emissions, energy efficiency, and decarbonisation strategies [3,4].

[1] H.-W. Hsu, E. Binyet, R.A.A. Nugroho, W.-C. Wang, P. Srinophakun, R.-Y. Chein, R. Demafelis, N. Chiarasumran, H. Saputro, A.F. Alhikami, N. Sakulshah, T. Laemthong, Toward sustainability of Waste-to-Energy: An overview, Energy Convers. Manag. 321 (2024) 119063. https://doi.org/10.1016/j.enconman.2024.119063.

[2] European Commission, Commission Implementing Decision (EU) 2019/2010 of 12 November 2019 establishing the best available techniques (BAT) conclusions, under Directive 2010/75/EU of the European Parliament and of the Council, for waste incineration, Off. J. Eur. Union L 312 (2019) 55–91. http://data.europa.eu/eli/dec_impl/2019/2010/oj.

[3] J. Czerwińska, G. Wielgosiński, Functioning of the flue gas treatment system in Polish municipal waste incineration plants, Sci. Rev. Eng. Environ. Sci. 29 (2020) 108–119. https://doi.org/10.22630/PNIKS.2020.29.1.10.

[4] European Parliament and Council of the European Union, Regulation (EU) 2021/1119 of 30 June 2021 establishing the framework for achieving climate neutrality and amending Regulations (EC) No 401/2009 and (EU) 2018/1999 (European Climate Law), Off. J. Eur. Union L 243 (2021) 1–17. http://data.europa.eu/eli/reg/2021/1119/oj.

The work was financed by subvention for the AGH University of Krakow (grant no. 501.00 210000 10000) and from funds of the "Excellence Initiative- Research University" program for AGH.

[1] Faculty of Energy and Fuels, AGH University of Krakow, Al. A. Mickiewicza 30, 30-059 Kraków, Poland, * akorzen@agh.edu.pl

EFE2026 ENERGY FUELS ENVIRONMENT
INTERNATIONAL CONFERENCE
17-20 NOVEMBER 2026, KRAKÓW, POLAND

Advanced Materials and System Integration for Thermal and Electrochemical Energy Conversion

Ming Chen[1,*], Mehrdad Faraji[2], Emil Riis Hansen[1], Emil Frederik Tauris[1], Akhil Panicker[1], Rafael Nogueira Nakashima[1], Soheil Khosravi[1]

Keywords: thermal energy storage, electrochemical conversion, solid oxide cells, advanced materials, system integration

ABSTRACT

The increasing share of wind and solar power requires energy technologies that can connect electricity, heat and chemical fuels. Thermal energy storage, Power-to-Heat and Carnot battery concepts can provide flexibility for industrial heat supply, while solid oxide cells can convert electricity and heat into hydrogen or other fuels and convert these fuels back into electricity. These technologies may operate separately, but they can also be integrated through common heat sources, thermal storage units and industrial processes. Their practical performance depends not only on conversion efficiency, but also on the stability of materials and interfaces during long-term operation. This talk presents our recent work from materials and components to system integration, with examples covering both thermal and electrochemical energy conversion.

At the material level, thermal and electrochemical technologies share basic challenges. Both rely on stable interfaces and controlled transport of heat, mass and charge under demanding conditions. In molten-salt storage, reactions between the salt and containment alloy determine whether a protective surface layer can survive. Our studies of Fe-based alloys in Na_2CO_3-K_2CO_3 at 800 °C showed that Cr-rich oxides on SUS 441 and Crofer 22 APU reacted with the salt and did not provide effective protection, while Kanthal APM formed a more stable alumina layer [1]. In solid oxide cells, the Ni-YSZ fuel electrode is also controlled by the stability of its internal interfaces. Operating conditions, Ni redistribution and impurities can change the connected Ni network and reduce the active electrode structure. Three-dimensional reconstruction combined with phase-field simulation provides insight into Ni migration during long-term operation [2]. These examples raise a common question: how can composition, microstructure and surface chemistry maintain the required transport pathways?

At the component level, material properties must be transferred into manufacturable structures with sufficient lifetime. Storage tanks, pipes and heat exchangers must withstand molten salts and thermal cycling, while solid oxide cell electrodes and interconnects must remain stable under current load, gas gradients and redox conditions. Surface condition, processing history and local microstructure influence degradation. In molten nitrate salt, additively manufactured Inconel 718 showed different corrosion pathways after solution annealing and double aging because post-processing changed the microstructure and diffusion paths [3]. Machine-learning-assisted optimization of laser powder bed fusion also produced CuCrZr with a relative density of 99.8%, showing how process-structure-property relations can support complex heat-transfer components [4]. In SOC components, a similar approach links electrode processing and microstructure to electrochemical activity and durability.

At the system level, thermal and electrochemical components must be matched with renewable electricity, heat sources and industrial demand. High-temperature electrolysis

[1] Department of Energy Conversion and Storage, Technical University of Denmark
[2] Department of Industrial Engineering, University of Padova
*corresponding author: minc@dtu.dk

can use electricity and heat to produce hydrogen or synthetic fuels, while heat pumps and thermal storage can recover, upgrade and shift heat between different times and temperature levels. Their integration is governed by similar questions: when should electricity be consumed, where should heat be recovered, and how much storage is needed? For an eco-industrial cluster with variable wind power and waste-heat sources, integration of a high-temperature heat pump with thermal energy storage improved the use of renewable electricity and recovered heat [5]. Thermal storage decoupled heat generation from process demand, while the heat pump provided the required temperature lift. Storage size, temperature range, capital cost and control strategy determined the overall benefit.

Finally, our latest attempt to combine thermal energy storage with electrochemical conversion will be presented. In this study, flexible electrolysis was coupled with e-methanol production, reactor heat recovery and a two-tank sensible thermal energy storage system. The storage system acted as a buffer between variable electricity input, available process heat and the continuous heat demand of methanol distillation [6]. The results show that thermal storage can shift electricity consumption away from high-price periods and reduce operating costs. However, the overall benefit depends on the storage temperature range, the quality of the recovered heat and the additional investment. Overall, these studies show that advanced materials alone are not sufficient to achieve efficient and durable energy conversion. Materials, components and system operation must be designed together, and the integration of thermal storage with electrochemical conversion provides a promising route for improving the flexibility of future renewable energy systems.

[1] J. Wang, H. Liu, Y. Liu, M. Chen, Corrosion behavior of Fe based container alloys in molten Na2CO3-K2CO3 as thermal energy storage medium for reversible solid oxide cells, Corros. Sci. 225 (2023) 111616. https://doi.org/10.1016/j.corsci.2023.111616.
[2] S. Yang, J. Gao, Y. Shang, B. Li, P.S. Jørgensen, L. Zhang, M. Chen, Insights into Ni migration in long-term tested Ni-yttria stabilized zirconia electrodes by three-dimensional reconstruction aided phase-field simulations, Acta Mater. 317 (2026) 122588. https://doi.org/10.1016/j.actamat.2026.122588.
[3] M. Faraji, J. Weiss, T. Fluri, D. Cester, A. Yazdanpanah, T. Yu, M.R. Kraglund, A. Pepato, M. Bonesso, I. Calliari, M. Chen, Hot corrosion of additively manufactured Inconel 718 in molten solar salt: Effects of heat treatment and long-term exposure, J. Energy Storage 179 (2026) 124011. https://doi.org/10.1016/j.est.2026.124011.
[4] M. Faraji, O. Banapour Ghaffari, H. Elahikhah, M. Chen, V.M. Sglavo, I. Calliari, M. Bonesso, Machine learning-assisted defect control in LPBF CuCrZr: Unifying process, structure, and performance, J. Alloys Compd. 1079 (2026) 189868. https://doi.org/10.1016/j.jallcom.2026.189868.
[5] A.V. Panicker, H. Liu, E. Rattigan, K. Knobloch, M. Chen, Integration of high-temperature heat pump and thermal energy storage for enhancing energy flexibility in eco-industrial clusters, Energy Convers. Manag. 368 (2026) 122001. https://doi.org/10.1016/j.enconman.2026.122001.
[6] E.F. Tauris, System Modeling and Techno-Economic Evaluation of Sensible Thermal Energy Storage for Flexible E-Methanol Production, Bachelor's thesis, Technical University of Denmark, 2026.

Acknowledgements: The author gratefully acknowledges financial support from the Danish Energy Agency through the EUDP projects “Efficient Power2Gas Combining SOEC and Biomass Gasification” (No. 64017-0011), the Danish contribution to the Clean Energy Transition Partnership project LoCoMoSa (No. 640235-510582), and the Danish participation in IEA Energy Storage Task 44 (No. 134241-521072). The LoCoMoSa project was supported through CETP Call 2022 (Project No. CETP-2022-00044) and co-funded by national programmes in Denmark, Germany and Italy. Support from Villum Fonden through the project “Pump It Up – Raising the Temperature of Waste Heat with Thermally Integrated Heat Pumps” (Grant No. 40519), and DTU Energy is also gratefully acknowledged.

EFE2026 ENERGY FUELS ENVIRONMENT
INTERNATIONAL CONFERENCE
17-20 NOVEMBER 2026, KRAKÓW, POLAND

Effect of the Si/Al Ratio of Zeolite ZSM-5 on the Performance of Cu-Based NH_3-SCR of NO Catalysts Derived from HKUST-1

Jakub Mokrzycki[1,*], Katarzyna Rączka[1], Monika Motak[1]

Keywords: HKUST-1, MOF, catalysts, NH_3-SCR, zeolite

ABSTRACT

NO_x (~90% of NO, and ~10% of NO_2) are among the major air pollutants harmful to human health, contributing to environmental degradation, including ocean acidification, photochemical smog, and damage to infrastructure. Therefore, there is a continuous need to develop efficient, selective and sustainable catalysts for selective catalytic reduction of NO_x with ammonia (NH_3-SCR). NH_3-SCR is a well developed catalytic process, which is industrially operated by V_2O_5/TiO_2-based catalysts promoted with WO_3 [1]. However due to susceptibility of the active phase to sulfur poisoning and the potentially carcinogenic effects of V_2O_5, the development of efficient, and sustainable alternative catalysts remains a valid topic.

HKUST-1 (Hong Kong University of Science and Technology-1) is a type of copper-based metal-organic framework (MOF) consisting of 1,3,5-benzenetricarboxylic acid (trimesic acid) serving as the organic linker, and Cu^{2+} ions forming metal clusters. HKUST-1 is characterized by a high specific surface area (>1000 $m^2\ g^{-1}$), and pore size of approx. 0.9 nm. However, due to the presence of coordinatively unsaturated Cu^{2+} sites, HKUST-1 readily adsorbs water molecules from the vapor or liquid phase, which can cause significant structural degradation even after short-term exposure.

In present study, HKUST-1 (obtained using a dimethylformamide-free synthesis, 110 °C, 24 h) was utilized as a copper source for production of catalysts. Briefly, 20 wt.% of HKUST-1 was mixed with zeolite ZSM-5 in a mortar for 10 min and subsequently calcined at 650 °C for 4 h. Particular emphasis was placed on investigating the effect of the Si/Al ratio (23, 30, 80, 280) of zeolite ZSM-5. Materials were characterized by means of XRD, DR-UV-Vis, and NH_3-TPD. Catalytic tests were performed using 100 mg of catalyst (particle size: 0.2-0.4 mm) and feed gas consisting of 800 ppm NH_3, 800 ppm NO, 3.5 vol.% O_2 and He as balance gas, with a total flow of 100 mL min^{-1}. The concentrations of NO and N_2O were monitored to evaluate the catalytic performance and selectivity of the investigated catalytic systems.

The XRD patterns of the investigated materials are presented in Figure $1a_1$ and $1a_2$. HKUST-1 exhibited characteristic reflections (Figure $1a_1$), confirming the successful synthesis of the MOF [2]. Incorporation of HKUST-1 into the zeolite ZSM-5 (Figure $1a_2$) preserved the zeolite structure after calcination. Additional reflections attributed to CuO were observed at 2θ=35.5° and 38.7°, corresponding to (-111) and (111) planes, respectively. NH_3-TPD profiles (Figure $1b_1$-$1b_4$) revealed the generation of additional acid sites in both the medium and high temperature ranges, which was attributed to incorporation of copper species. With an increase in the Si/Al ratio, the intensities of all desorption peaks decreased, indicating a reduction in the concentration of both Lewis and Brønsted acid sites. From H_2-TPR profiles (Figure 1c) it can be seen, that the H_2 consumption was comparable among the series, however with an increase in the Si/Al ratio, the reduction peaks shifted toward higher temperatures, suggesting stronger interactions of metal with the support. DR-UV-Vis spectra (Figure 1d) revealed the differences in the copper speciation on the catalysts surface. Isolated Cu^{2+} ions (~220 nm) were the predominant copper species in the 23H and 30H samples, whereas $[Cu\text{-}O\text{-}Cu]^{2+}$

[1]AGH University of Krakow, Faculty of Energy and Fuels, Al. A. Mickiewicza 30, 30-059 Kraków, Poland; * jmokrzycki@agh.edu.pl

species were more prevalent in the 80H and 280H, at approx. 290 nm [1]. Such a differences in copper speciation impeded the catalytic performance of the catalytic systems (Figure 1e$_1$-1e$_2$). With an increase in the Si/Al ratio the NO conversion was significantly lowered. The temperature window corresponding to >90% NO conversion was the broadest for 23H and 30H samples, with simultaneous low N_2O production throughout the investigated temperature range, with concentrations <16 ppm.

Overall, the obtained results clearly indicate that HKUST-1 can serve as a promising copper precursor for the preparation of active catalytic systems in NO conversion. Optimization of the Si/Al ratio enables control over the copper speciation, and consequently the catalytic performance of the resulting catalysts.

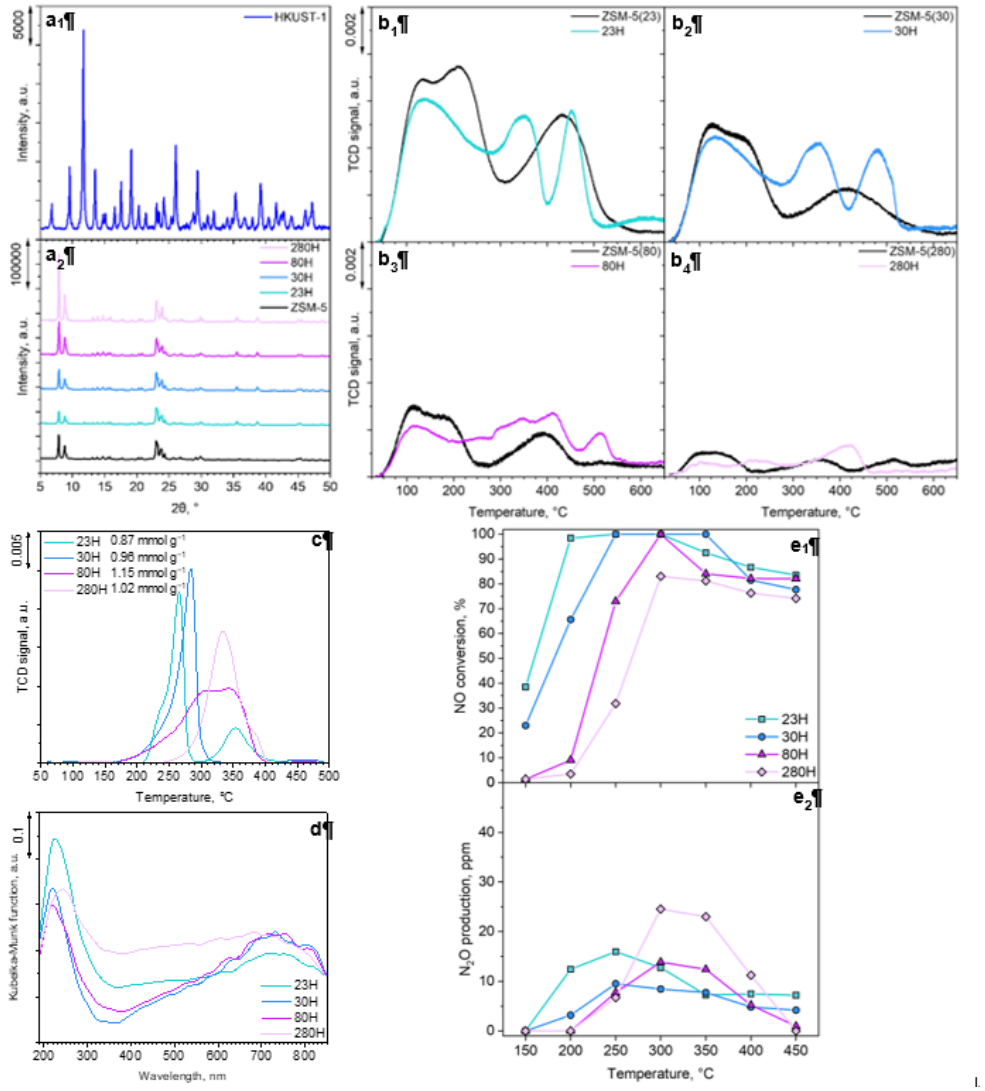


Figure 1. XRD pattern of HKUST-1 (a$_1$), and catalysts (a$_2$); NH_3-TPD profiles (b$_1$-b$_4$); H_2-TPR profiles (c); DR-UV-Vis spectra (d); NO conversion (e$_1$); N_2O production (e$_2$).

[1] M. Fedyna, P. Legutko, M. Marzec, Z. Sojka, Influence of zeolite framework, copper speciation, and water on NO_2 and N_2O formation during NH_3-SCR, Appl. Catal. B 361 (2025) 124632. https://doi.org/10.1016/j.apcatb.2024.124632.

[2] J. Mokrzycki, E. Wolak, A. Orzechowska-Zięba, K. Zheng, D. Duraczyńska, M. Marzec, M. Fedyna, The effect of copper(II) salt precursor on physicochemical properties of HKUST-1 MOFs and their application as adsorbents of Cr(III) ions from aqueous solutions, J. Water Process Eng. 64 (2024) 105761. https://doi.org/10.1016/j.jwpe.2024.105761.

The research was financed by AGH University of Krakow grant no. 501.00_210000_10000. Also, the research was supported by IDUB grant (Action 21, Application No. 18209).

EFE2026 ENERGY FUELS ENVIRONMENT
INTERNATIONAL CONFERENCE
17-20 NOVEMBER 2026, KRAKÓW, POLAND

Spatio-Temporal Complementarity of Photovoltaic Systems Across Poland

Erkin Jafarov[1,*], Marek Borowski[1], Marek Jaszczur[2]

Keywords: photovoltaic systems, spatial complementarity, grid stability, renewable energy, correlation analysis, PV energy yield

ABSTRACT

The installed photovoltaic (PV) capacity in Poland has experienced an unprecedented 85-fold expansion since 2015 (growing from 200 MW to over 17 GW) [1], driving the national transition toward a low-carbon economy [2]. However, the inherent stochastic nature of solar energy introduces significant challenges to national grid stability. This problem has led to a substantial increase in non-market generation curtailment by transmission system operators, reaching a record 731.4 GWh in 2024 [3]. To mitigate these disruptions and reduce dependency on costly physical energy storage, exploiting the spatio-temporal complementarity of distributed PV installations has emerged as a crucial mitigation strategy.

By addressing this issue through high-resolution analyses, this study investigates the comparative spatio-temporal complementarity of PV energy production across Poland. Based on 2024 data for a standardized 1.0 kWp system, the research evaluates system performance across varying seasonal and climatic conditions, focusing specifically on extreme weather patterns (the cloudiest and most stable sunny days). Various metric statistical framework including Pearson, Spearman, and Kendall correlation coefficients, was applied to analyze the PV production time series.

The results show statistically significant positive correlations between the PV yields across Poland demonstrating the locations with lowest and highest correlation values.

Seasonal assessments indicate that spring and summer periods achieve the strongest correlations and highest PV yields, whereas winter months exhibit distinct statistical decoupling. The comparative analysis isolates the boundaries of spatial complementarity, demonstrating that geographically distributed generation profiles effectively dampen overall output variability through a spatial smoothing effect.

Furthermore, the findings suggest that strategically optimizing the tilt and orientation of these installations can further enhance coordinated distributed generation, although this approach remains fundamentally constrained by the natural diurnal cycle and lack of production during the night.

These findings demonstrate that coordinating distributed multi-energy systems significantly minimizes supply volatility and power curtailment. The study provides highly localized, critical insights for regional grid balancing, microgrid planning and the optimization of Poland's energy infrastructure.

[1] D. Tomczyk, Z. Łapniewska, Solar panels on every rooftop? Photovoltaics boom in Poland and the role of the European Union funds, Energy Res. Soc. Sci. 125 (2025) 104107. https://doi.org/10.1016/j.erss.2025.104107.
[2] Instytut Energetyki Odnawialnej (IEO), Photovoltaic Market in Poland 2024, IEO, Warsaw, 2024.
[3] Forum Energii, Energy Transition in Poland. Edition 2025, Forum Energii, Warsaw, 2025.

[1] AGH University of Krakow, Faculty of Civil Engineering and Resource Management, A.Mickiewicza 30, 30-059 Krakow, Poland, * ejafarov@agh.edu.pl
[2] AGH University of Krakow, Faculty of Energy and Fuels, A.Mickiewicza 30, 30-059 Kraków, Poland

EFE2026 ENERGY FUELS ENVIRONMENT
INTERNATIONAL CONFERENCE
17-20 NOVEMBER 2026, KRAKÓW, POLAND

Pyrolysis of Wastewater Sludges: Yield and Composition Differences Between Municipal and Industrial Feedstocks

Dorota Makowska[1,*], Karolina Kolarz[1], Roksana Muzyka[2], Przemysław Grzywacz[1], Katarzyna Kapusta[1],

Keywords: pyrolysis, sewage sludge, biochar, bio-oil, pyrolytic gas

ABSTRACT

Pyrolysis has emerged as a promising method for the thermal utilization of wastewater sludge, offering the potential for economically viable recovery of energy and chemical products. Although industrial wastewater sludge accounts for a major portion of total sludge production, most existing studies have concentrated on municipal sludge. Given the substantial compositional differences between industrial and municipal sludge, this study investigates the pyrolytic behavior of three distinct sludge types: sludge from the food processing industry (FPM), oil refineries (REF), and municipal sewage (MS). The pyrolysis experiments were conducted in a horizontal tube furnace under quasi-isothermal conditions. Based on preliminary thermogravimetric analysis (TGA) and process optimization, the process was carried out at temperatures of 500 °C (for 5, 8, and 12 minutes) and 700 °C (for 5 and 8 minutes) in an argon atmosphere (1 dm^3/min). The resulting solid (char), liquid (bio-oil), and gaseous products were collected and subjected to comprehensive analysis. For the char products, proximate analysis (moisture, ash, volatile matter, fixed carbon, and high calorific value), elemental composition (C, H, S, Cl), FTIR spectroscopy, XRF spectrometry, and pH measurements were performed. The chemical composition of the pyrolytic gas was determined via gas chromatography (GC), while the bio-oil was analyzed using GC-FID. As anticipated, the char yield decreased with increasing pyrolysis temperature and residence time across all sludge types. Variations in char yield and composition were primarily attributed to differences in feedstock properties. Notably, bio-oil yields were highly dependent on sludge origin, with REF sludge producing the highest yield (up to 29.3%), significantly surpassing those of MS (7.8%) and FPM sludge (7.6%). The bio-oils contained a diverse range of organic compounds, including alkanes, fatty acids, fatty acid esters (FAME, FAEE), ketones, aldehydes, furans, phenolic compounds, and aromatics, suggesting their potential as feedstocks for chemical synthesis or fuel production. The pyrolytic gas mainly contained CO_2, CO, CH_4, and H_2. Pyrolysis temperature primarily influenced gas composition, with high temperatures substantially increasing H_2 and CH_4 yields. Our findings demonstrate that feedstock-specific pyrolysis optimization maximizes resource recovery. Industrial sludge, particularly REF, shows strong potential as a sustainable feedstock for circular bioeconomy applications, producing value-added products and chemicals.

Acknowledgment:
The research was financed from the Research Subsidy of the AGH University of Krakow for the Department of Energy and Fuels [No. 501.00-210000-10000].

[1] Department of Fuel Technology, Facutly of Energy and Fuel, AGH University of Krakow, Poland,
* makowska@agh.edu.pl
[2] Department of Air Protection, Faculty of Energy and Environmental Engineering, Silesian University of Technology, Poland

Development and Demonstration of an Intelligent Cooling System for Blast Furnace Cooling Circuit Integration and Increased Operational Reliability

Marek Berliński[1]

Keywords: Blast furnace cooling; Intelligent cooling system; Cooling circuit integration; Thermal management; Cooling stave; Operational reliability; Water efficiency; Numerical modelling.

ABSTRACT

The increasing demands for operational reliability, energy efficiency, and sustainable water management in the metallurgical industry require innovative approaches to cooling system design. This paper presents the development and demonstration of an intelligent cooling system for a blast furnace based on the integration and optimization of cooling water circuits. The project focused on improving the performance of blast furnace cooling elements through advanced modelling, monitoring, and control strategies while reducing cooling water consumption.

The study included a comprehensive analysis of the existing cooling system, development of thermal-fluid and thermo-mechanical models, implementation of additional measurement devices, and verification of multiple cooling circuit configurations. Particular attention was given to the design of an intelligent cooling stave incorporating a secondary cooling layer. Numerical simulations and industrial-scale validation demonstrated that the additional cooling layer significantly reduces stave temperatures and maintains effective heat removal even in the event of partial failure of the primary cooling channels.

Operational data from the demonstration installation confirmed the benefits of the proposed solution, including improved thermal stability, enhanced cooling system reliability, extended campaign life of blast furnace cooling elements, and more efficient utilization of industrial cooling water. The intelligent cooling concept enables better control of heat extraction from the furnace, contributing to improved process stability and optimized fuel utilization.

The results demonstrate that the integration of intelligent cooling technologies into blast furnace operation can support both production efficiency and sustainability objectives, providing a practical solution for modern metallurgical plants.

[1] ArcelorMittal Poland, *Marek.Berlinski@arcelormittal.com

EFE2026 ENERGY FUELS ENVIRONMENT
INTERNATIONAL CONFERENCE
17-20 NOVEMBER 2026, KRAKÓW, POLAND

Fibre-Dependent Thermal Decomposition Behaviour of Textile Materials

Marcelina Bury[1,*]

Keywords: textile waste; textile fibres; thermogravimetric analysis; thermal decomposition; thermochemical conversion

ABSTRACT

Textile waste represents a heterogeneous group of materials with considerably different chemical compositions and thermal characteristics, which directly influence their behaviour during thermochemical processing. This study investigates the fibre-dependent thermal decomposition behaviour of selected textile materials representing natural, regenerated and synthetic fibres. Thermogravimetric analysis was performed over a broad temperature range to determine changes in sample mass and identify characteristic differences in thermal decomposition profiles. The results revealed distinct fibre-dependent mass-loss profiles, with differences in both the temperature range and extent of thermal decomposition among the investigated materials. The findings indicate that fibre type is an important factor governing the thermal response of textile materials and should therefore be considered when selecting operating conditions for their thermochemical conversion. The results provide a basis for further assessment of textile waste in thermochemical valorisation processes.

Acknowledgment: the Research Subsidy of the AGH University of Krakow for the Department of Energy and Fuels [No. 501.00-210000-10000]; "Excellence initiative- research university" for the AGH University of Krakow, No. UB-696000-00001-Z01.

[1] AGH University of Krakow, Poland, * bury@agh.edu.pl

Electrochemical and Thermochemical Pathways to E-Chemicals and Solar-Chemicals

Massimo Santarelli[1]

Keywords: Synthetic chemicals; Defossilization; Solid oxide electrolysis; CO_2 reduction; Proton-conducting ceramic cells; Solar thermochemical cycles; Chemical looping; Perovskite oxides.

ABSTRACT

Synthetic chemicals can represent a necessary element of the defossilization pathways. Several processes can be used to obtain synthetic chemicals, and in this context we are particularly interested in the electrical—driven electrochemical one (ceramic cells) and in the solar-driven thermochemical one (chemical looping).

In electrochemical pathway, the research envisages the development of a solid oxide electrolytic system, which involves the co-ionic conduction of H^+ ions migrating from the anode to the cathode and available there in ionic form for the CO_2 reduction reaction, and of O^{2-} ions resulting from the cathodic reduction of CO_2 and removed from the cathode by migration towards the anode. In this context, the cathode electrode must be designed to develop CO_2 reduction mechanisms via H^+ protons for the direct production of totally deoxygenated hydrocarbons.

In solar-driven thermochemical pathway, two-step redox cycles driven by concentrated solar is considered a promising technology for clean energy production. The state-of-the-art process makes use of nonstoichiometric ceria as the redox oxygen carrier given its fast kinetics, crystallographic stability, cyclic durability, and abundance. However, reduction temperatures as high as 1500 °C are required to achieve a sufficient reduction extent. Currently, the most explored alternative to ceria are nonstoichiometric perovskites ($ABO_{3-\delta}$), allowing for a wide compositional space, doping strategies, stability at relatively high reduction extents, and more moderate reduction temperatures.

The talk will describe the running activities in these two domains of synthetic chemical production.

[1] Politecnico di Torino, Torino, Italy, massimo.santarelli@polito.it

EFE2026 ENERGY FUELS ENVIRONMENT
INTERNATIONAL CONFERENCE
17-20 NOVEMBER 2026, KRAKÓW, POLAND

Development of Numerical Models for Sodium-Cooled Fast Reactors for Thermal-Hydraulics, Neutronics, and Nuclear Data Library Preparation

Anna Bała[1]*, Mikołaj Oettingen[1], Katarzyna Szarłowicz[1]

Keywords: SFR, sodium-cooled reactor, thermal-hydraulics, neutronics, fast reactor

ABSTRACT

Sodium-cooled fast reactors (SFRs) are among the reactor concepts being developed within the Generation IV framework. They are of particular interest because of their potential to improve uranium resource utilization, facilitate the transmutation of long-lived minor actinides, and support operation within a closed nuclear fuel cycle [1]. The fast neutron spectrum, the use of liquid sodium as a coolant, and the temperature dependence of effective neutron cross sections necessitate coupled neutronic and thermal-hydraulic analyses. Although computational tools for such analyses are well established for conventional water-cooled reactors, their applicability to less widely deployed Generation IV systems, including SFRs, remains comparatively limited.

A key aspect of SFR modelling is the effect of temperature on reactor neutronics. Variations in fuel, cladding, and coolant temperatures alter thermophysical properties, material densities, and neutron interaction probabilities. In particular, changes in fuel temperature modify resonance absorption cross sections through Doppler broadening, while changes in coolant temperature affect sodium density and, consequently, neutron leakage and spectral characteristics. The spatial representation of the temperature field in a neutronic model may therefore influence calculated quantities such as the effective neutron multiplication factor, reaction-rate distributions, and local power density. A spatially resolved temperature representation may provide a more physically realistic description of reactor behaviour than assigning a single volume-averaged temperature to an entire material region.

The objective of this work is to develop a computational methodology for higher-fidelity thermal-hydraulic and neutronic analysis of SFR systems, with particular emphasis on the preparation of temperature-dependent nuclear data. Two temperature-mapping approaches are compared. In the simplified approach, a single representative temperature is assigned to each material. In the higher-fidelity approach, the spatial temperature distributions within the fuel, cladding, and coolant are explicitly represented. The reactor model, material specifications, and operating conditions are based on the Advanced Burner Reactor (ABR) design developed by Argonne National Laboratory [2].

The methodology employs two distinct computational models. The thermal-hydraulic model resolves heat transfer among the fuel, cladding, and coolant, as well as sodium flow through the fuel assembly. The neutronic model represents the corresponding geometry and material composition and is used to calculate neutron transport, criticality, and power-related parameters. Because these calculations are performed using separate numerical tools and discretizations, a consistent procedure is required to transfer data between the thermal-hydraulic and neutronic models. Particular attention is therefore given to spatial temperature mapping and to the generation of nuclear data corresponding to the calculated local thermal conditions.

Thermal-hydraulic calculations are performed using Ansys Fluent. Given the material properties, geometry, and boundary conditions, the software solves the governing

[1] AGH University of Krakow, Poland, Faculty of Energy and Fuels, Department of Nuclear Energy and Radiochemistry, * annabala@agh.edu.pl

conservation equations to obtain the temperature and flow fields [3]. The resulting temperature distributions in the fuel, cladding, and liquid-sodium coolant characterize the thermal state of the modelled fuel assembly with high spatial resolution. These fields are subsequently mapped onto a predefined set of spatial regions in the neutronic model.

The mapped temperatures are used in NJOY to process temperature-dependent neutron cross-section data [4]. This procedure enables nuclear data to be generated at temperatures corresponding to the thermal-hydraulic solution, thereby allowing temperature effects on neutron interaction probabilities to be represented more accurately. Neutron transport calculations are subsequently performed using OpenMC [5].

Several cases with different levels of thermal-field fidelity are analysed to quantify the influence of temperature representation on the calculated neutronic parameters. These include cases with uniformly prescribed temperatures, cases with material-specific volume-averaged temperatures, and cases in which the CFD-derived temperature distributions are represented by multiple axial regions. Calculations using cross sections explicitly processed with NJOY are also compared with calculations employing the temperature-interpolation treatment available in OpenMC. This comparison enables the effects of spatial temperature discretization to be distinguished from those associated with the nuclear-data processing methodology.

[1] International Atomic Energy Agency (IAEA), Fast Reactor Database: 2006 Update, IAEA-TECDOC-1531, IAEA, Vienna, 2006.
[2] E.A. Hoffman, W.S. Yang, R.N. Hill, Preliminary core design studies for the advanced burner reactor over a wide range of conversion ratios, Report ANL-AFCI-177, Argonne National Laboratory, 2006.
[3] ANSYS, Inc., Ansys Fluent Theory Guide, Release 2025 R1, ANSYS, Inc., Canonsburg, PA, USA, 2025.
[4] R.E. MacFarlane, D.W. Muir, R.M. Boicourt, A.C. Kahler, J.L. Conlin, W. Haeck, The NJOY Nuclear Data Processing System, Version 2016, Report LA-UR-17-20093, Los Alamos National Laboratory, 2017, updated 2019.
[5] P.K. Romano, N.E. Horelik, B.R. Herman, A.G. Nelson, B. Forget, K. Smith, OpenMC: A state-of-the-art Monte Carlo code for research and development, Ann. Nucl. Energy 82 (2015) 90–97. https://doi.org/10.1016/j.anucene.2014.07.048.

Acknowledgements: Partial financial support for this research was provided under the scientific subvention no. 501.00-210000-10000 by the Polish Ministry of Science and Higher Education. This research was also partly supported by the program "Excellence Initiative – Research University" of the AGH University of Krakow. We gratefully acknowledge the Polish high-performance computing infrastructure PLGrid (HPC Center: ACK Cyfronet AGH) for providing computational resources and support under computational grant no. PLG/2026/019581.

EFE2026 ENERGY FUELS ENVIRONMENT
INTERNATIONAL CONFERENCE
17-20 NOVEMBER 2026, KRAKÓW, POLAND

Contemporary Trends of Using Hydrogen as an Energy Storage and Carrier in the Development of Sustainable Railway Transport

Magdalena Dudek[1,]*, Andrzej Raźniak[1]

Keywords: hydrogen, storage energy, railway transport

ABSTRACT

Currently, the energy transition of the railway system is receiving considerable attention in the context of the objectives of European and international climate policy. Although railway transport produces fewer emissions compared with road transport, decarbonisation and improvement of the energy efficiency of rolling stock is the primary challenge today. One of the proposed approaches involves the gradual limitation of the use of diesel engines in rolling stock in favour of electrification of power units that utilise electrochemical energy sources (Li-ion batteries). This issue is more complex with the so-called non-electrified line networks, in which case it is proposed to develop ecological power units utilising hydrogen as a source of power for fuel cells or combustion engines. This approach is evidenced by the market presence of pilot passenger trains, the leading examples of which are solutions by Alstom and Siemens. There are also challenges related to making upgrades to and improving the energy efficiency of other rail vehicles (shunting locomotives, railbuses) and other components of the railway infrastructure, including buildings, stations, as well as other facilities and technical equipment.

The study presents the research results relating to the developed model of prediction of electric energy demand by electric power units of passenger trains, with particular emphasis on the use of hydrogen-oxygen generators with PEMFC fuel cells. Another topic discussed in the study concerns technical, logistical, and economic issues related to the provision of hydrogen and operation of refuelling stations. The results of research into energy efficiency of optimised electrochemical sources were implemented in the simulation of passenger trains running on the real-world railway routes. The results of the simulation tests of the operation of the hydrogen electrolyser were experimentally verified in a reduced scale.

The research was financed by project: Europe's Rail Joint Undertaking FP4-Rail4EARTH-101101917, and MEiN 5337/HE/2023/2

[1] AGH University of Krakow, Faculty of Energy and Fuels, Al. A. Mickiewicza 30, 30-059 Kraków, Poland; * potoczek@agh.edu.pl

Monte Carlo Simulation of Spallation Neutron Production in an Accelerator-Driven System

Eyvaz Teymurov[1,2], Mikołaj Oettingen[2,*]

Keywords: Accelerator-Driven System (ADS), Geant4, Monte Carlo, spallation target

ABSTRACT

Accelerator-Driven Systems (ADS) are subcritical nuclear systems coupled to high-energy particle accelerators and are being investigated for applications such as long-lived radioactive waste transmutation and advanced sustainable nuclear-energy concepts. A key component of an ADS is the spallation target, where high-energy protons interact with heavy nuclei and generate secondary neutrons that drive the subcritical reactor core [1]. Therefore, target material selection and proton-beam energy are important parameters in ADS design.

In this work, a comparative Monte Carlo simulation of proton-induced spallation neutron production was performed using the GEANT4 toolkit as part of the investigation of key parameters relevant to ADS design [2]. Five candidate target materials were investigated: tungsten (W), lead (Pb), lead-bismuth eutectic (LBE), depleted uranium (DU), and mercury (Hg) (Table 1). Simulations were conducted for incident proton energies of 350 MeV, 600 MeV, 1 GeV, 1.5 GeV, and 2 GeV to investigate the dependence of neutron production on target composition and beam energy [3],[4].

Table 1. The neutron yield per proton (n/p) obtained in the simulations.

Target material	350 MeV	600 MeV	1 GeV	1.5 GeV	2 GeV
Tungsten (W)	4.42	10.98	22.08	33.23	43.06
Lead (Pb)	4.54	10.9	20.99	30.47	38.7
Lead-Bismuth eutectic (LBE)	4.41	10.55	20.01	29.25	36.88
Uranium depleted (U)	12.97	29.26	56.04	81.67	104.9
Mercury (Hg)	4.38	10.72	21	30.98	39.54

The spallation target was modelled as a cylindrical geometry with a height of 675 mm and a radius of 45 mm. A proton pencil beam was directed along the Z-axis and characterized by a beam radius of 10 mm. The same target geometry and beam configuration were applied to the investigated target materials and proton energies to provide consistent conditions for comparison (Figure 1).

The FTFP_BERT_HP physics list was employed to model high-energy hadronic interactions, intranuclear cascade processes, secondary-particle production, and high-precision neutron transport at lower energies. The neutron yield per incident proton was calculated for each combination of target material and proton energy. The results demonstrate the dependence of neutron production on both target composition and incident proton energy and provide a basis for evaluating spallation-source characteristics within an ADS framework.

[1] Nuclear Research Department of the Innovation and Digital Development Agency, Baku, Azerbaijan
[2] AGH University of Krakow, Poland, Faculty of Energy and Fuels, Department of Nuclear Energy and Radiochemistry * moettin@agh.edu.pl

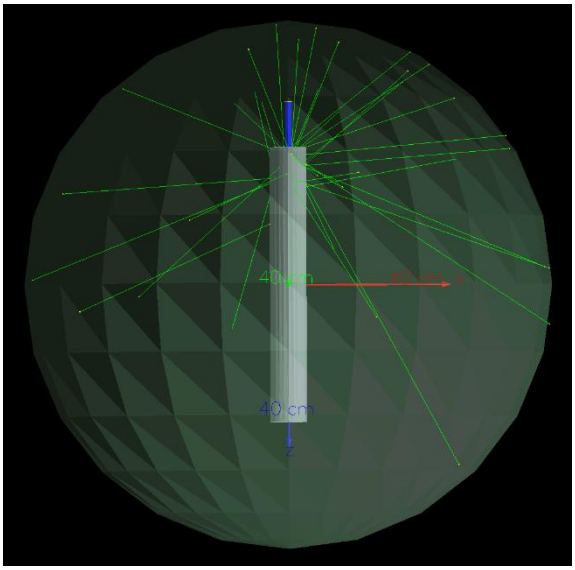


Figure 4. Develop numerical model for Geant4 simulation of ADS spallation target

The investigated target materials represent different classes of ADS spallation-target concepts, including solid heavy-metal, liquid-metal, and uranium-based targets. The obtained results contribute to the characterization of the neutron source in ADS and provide a basis for further studies of neutron transport, subcritical-core coupling, and the optimization of accelerator and target parameters for sustainable nuclear-energy applications.

[1] World Nuclear Association, Accelerator-driven nuclear energy, World Nuclear Association, 2026. https://world-nuclear.org/information-library/current-and-future-generation/accelerator-driven-nuclear-energy.
[2] S. Agostinelli, J. Allison, K. Amako, J. Apostolakis, H. Araujo, P. Arce, et al., Geant4—a simulation toolkit, Nucl. Instrum. Methods Phys. Res. A 506 (2003) 250–303. https://doi.org/10.1016/S0168-9002(03)01368-8.
[3] A. Bardane, A. Didi, E.M. Chakir, E.M.A. Ibrahmi, H.E. Bekkouri, Geant4-based optimization of spallation targets for high-intensity neutron production, Nucl. Anal. 5 (2026) 100230. https://doi.org/10.1016/j.nucana.2026.100230.
[4] T.A. Frolova, Optimization of breeding properties of the spallation neutron source target for ADS, Nucl. Energy Technol. 3 (2017) 60–64. https://doi.org/10.1016/j.nucet.2017.03.011.

Acknowledgements: Partial financial support for this research was provided under the scientific subvention no. 501.00-210000-10000 by the Polish Ministry of Science and Higher Education. This research was also partly supported by the program "Excellence Initiative – Research University" of the AGH University of Krakow. We gratefully acknowledge the Polish high-performance computing infrastructure PLGrid (HPC Center: ACK Cyfronet AGH) for providing computational resources and support under computational grant no. PLG/2026/019581.

EFE2026 ENERGY FUELS ENVIRONMENT
INTERNATIONAL CONFERENCE
17-20 NOVEMBER 2026, KRAKÓW, POLAND

Numerical Investigation of Vortex Shedding and Heat Transfer from a Heated Circular Cylinder

Patrycja Bukowiec[1], Mateusz Marcinkowski[1], Jan Taler[1]

Keywords: heated cylinder, vortex shedding, Strouhal number, heat- transfer coefficient, CFD

ABSTRACT

Flow around a circular cylinder is a classical problem in fluid mechanics and heat transfer. As air passes over the cylinder, the flow separates from its surface, causing vortices to be shed alternately from both sides and forming a von Karman vortex Street in the wake. The frequency of this process depends mainly on the Reynolds number and is commonly described by the Strouhal number. When the cylinder is heated, temperature-dependent changes in the properties of air may affect both the vortex-shedding process and convective heat transfer from the cylinder surface. This study numerically investigates these coupled flow and heat-transfer phenomena. Two-dimensional transient simulations are carried out in ANSYS Fluent for a circular cylinder with a diameter of 15 mm and Reynolds numbers ranging from 50 to 200. The inlet air temperature is maintained at 20 °C, while the cylinder surface is heated to 40, 80 and 300 °C. Two approaches to defining the flow conditions are compared. In the conventional approach, the Reynolds number is determined using constant air properties evaluated at the free-stream temperature. In the second approach, the influence of cylinder heating is represented using the effective-temperature concept proposed by Wang et al. [1]. The effective Reynolds number is calculated using the kinematic viscosity evaluated at the effective temperature, defined as $T_{eff} = T_\infty + 0.28(T_w - T_\infty)$. The shedding frequency is obtained from the periodic lift-coefficient signal using the oscillation period and fast Fourier transform, and the Strouhal number is calculated as $St = fD/U_\infty$. Results based on the conventional and effective Reynolds numbers are then compared. Finally, the local and average heat transfer coefficients will be determined on the heated cylinder surface and compared for cases based on the conventional nominal Reynolds number. The cylinder circumference will be divided into smaller angular segments, and the local heat transfer coefficient will be calculated for each segment from the wall heat flux and the corresponding temperature difference. Three reference fluid temperatures will be considered: the inlet air temperature, the mass-weighted outlet air temperature, and the local air temperature evaluated at a specified distance from the cylinder surface. In the third approach, this distance will be determined iteratively by changing the position of the temperature-sampling line until the average of the local heat transfer coefficients reaches a predefined target value. The target value will be defined as the arithmetic average of the heat transfer coefficients calculated using the inlet air temperature, the outlet air temperature, and the logarithmic mean temperature difference. The resulting local values will then be averaged over the entire cylinder circumference.

[1] A.-B. Wang, Z. Trávníček, K.-C. Chia, On the relationship of effective Reynolds number and Strouhal number for the laminar vortex shedding of a heated circular cylinder, Phys. Fluids 12 (2000) 1401–1410. https://doi.org/10.1063/1.870391.

[1] Department of Energy, Faculty of Environmental Engineering and Energy, Cracow University of Technology, Warszawska 24, 31-155 Kraków, Poland, *patrycja.bukowiec@pk.edu.pl

EFE2026 ENERGY FUELS ENVIRONMENT
INTERNATIONAL CONFERENCE
17-20 NOVEMBER 2026, KRAKÓW, POLAND

Influence of PEM Electrolyzer Sizing and Part-Load Operation on Green Hydrogen Production from Residential PV Surplus

Szymon Wieteska[1], Olushola Olapade[1], Marek Jaszczur[1]

Keywords**:** green hydrogen, PEM electrolyzer, photovoltaic system, part-load operation

ABSTRACT

As grid-export tariffs for residential photovoltaic systems in Poland become increasingly unfavourable, often yielding negligible or zero financial return for prosumers, converting surplus energy into green hydrogen using water electrolysis emerges as a potential alternative for decentralized energy storage. Proton exchange membrane (PEM) electrolyzers are well suited to photovoltaic (PV) integration because of their rapid response and broad operating range. Nevertheless, hydrogen yield is strongly affected by electrolyzer sizing, minimum load ratio, and part-load efficiency [1,2]. Recent studies therefore clearly show the need to represent dynamic electrolyzer operation and PV–electrolyzer sizing explicitly rather than relying only on nominal efficiency or annual-average energy balances [3–5].

This study evaluates green hydrogen production from surplus electricity generated by a small residential PV system, treating electrolysis as an alternative to low-value grid feed-in. A data-driven annual model was developed in HOMER Pro using measured 2024 global horizontal irradiance and ambient temperature for Krakow, Poland, together with an hourly residential electricity-demand profile. The system includes a 4 kWp PV generator, a 4 kW converter, a PEM electrolyzer, the electrical grid, and an unconstrained 1000 kg hydrogen tank so that storage capacity for research purposes does not limit production. The PV system generates approximately 4.53 MWh/year, while the annual residential demand is approximately 3.52 MWh. Electrolyzer power is varied from 0.5 to 4 kW, corresponding to electrolyzer-to-PV capacity ratios of 0.125 to 1.0, while minimum load ratios of 10%, 15%, and 20% are investigated. Part-load efficiency is represented by a literature-informed parametric curve, with assumed efficiencies of 55% at 10% load, a maximum of 69% near 30% load, and 60% at nominal power [6]. A constant-efficiency case is additionally considered to quantify the effect of model simplification. Annual hydrogen production, capacity factor (reflecting overall utilization of the installed capacity), operating hours, specific electricity consumption, and PV-surplus utilization are used as performance indicators.

Simulation results show diminishing returns with increasing electrolyzer capacity. At a 10% minimum load ratio, annual hydrogen production increases from 18.2 kg at 0.5 kW to 56.2 kg at 3 kW, reaching only 57.0 kg at 4 kW. This 33% capacity increase yields just 1.4% more hydrogen, while capacity factor drops from 13.3% to 9.9%. Specific electricity consumption decreases from approximately 65.0 to 60.8 kWh/kg H_2. For a 2 kW electrolyzer, raising the minimum load ratio from 10% to 20% reduces annual production from 48.6 to 46.9 kg and operating hours from 2,457 to 2,074. Overall, hydrogen production depends on matching electrolyzer capacity and minimum operating load to the timing of surplus PV electricity. Potential use of the hydrogen in fuel-cell vehicles is discussed, subject to conditioning, delivery, and vehicle-consumption assumptions.

[1] AGH University of Krakow, Faculty of Energy and Fuels, A. Mickiewicza 30, 30-059 Kraków, Poland
* wieteska@agh.edu.pl



Figure 1. Anode-side end plate of the laboratory PEM electrolyzer, showing the water inlet/outlet connections and positive electrical terminal (left side) and cathode-side end plate of the laboratory PEM electrolyzer, showing the hydrogen outlet and negative electrical terminal.

[1] H. Sayed-Ahmed, Á.I. Toldy, A. Santasalo-Aarnio, Dynamic operation of proton exchange membrane electrolyzers—Critical review, Renew. Sustain. Energy Rev. 189 (2024) 113883. https://doi.org/10.1016/j.rser.2023.113883.
[2] J. Wang, J. Wen, J. Wang, B. Yang, L. Jiang, Water electrolyzer operation scheduling for green hydrogen production: A review, Renew. Sustain. Energy Rev. 203 (2024) 114779. https://doi.org/10.1016/j.rser.2024.114779.
[3] M. Arunachalam, D.S. Han, Efficient solar-powered PEM electrolysis for sustainable hydrogen production: An integrated approach, Emergent Mater. 7 (2024) 1401–1415. https://doi.org/10.1007/s42247-024-00697-y.
[4] H. Renaudineau, N. Vergara-Rosales, A.M. Llor, S. Kouro, Green hydrogen production from off-grid photovoltaic: An assessment on optimal sizing, Renew. Energy 246 (2025) 122794. https://doi.org/10.1016/j.renene.2025.122794.
[5] B. Endrődi, C.A. Trapp, I. Szén, I. Bakos, M. Lukovics, C. Janáky, Challenges and opportunities of the dynamic operation of PEM water electrolyzers, Energies 18 (2025) 2154. https://doi.org/10.3390/en18092154.
[6] D. Virah-Sawmy, F.J. Beck, B. Sturmberg, Ignore variability, overestimate hydrogen production – Quantifying the effects of electrolyzer efficiency curves on hydrogen production from renewable energy sources, Int. J. Hydrogen Energy 72 (2024) 49–59. https://doi.org/10.1016/j.ijhydene.2024.05.360.

Acknowledgements:÷Work was partly funded by AGH University of Krakow, Faculty of Energy and Fuels (No. 500.00-210000-10000).

Assessment of Sewage-Sludge-Derived Biochars for Mercury Removal from Coal Flue Gas

Karolina Kolarz[1,*], Dorota Makowska[1], Jerzy Górecki[1], Cezary Czosnek[1], Katarzyna Sztybel[1], Piotr Burmistrz[1],

Keywords: waste-derived sorbents, mercury removal, sewage sludge biochar, coal flue gas

ABSTRACT

The aim of this study was to perform a preliminary assessment of sewage-sludge-derived biochars as sorbents for mercury removal from flue gas generated during coal combustion. The investigated materials were sewage sludges from a municipal wastewater treatment plant and from industrial wastewater treatment plants associated with refinery and food industry wastewater. Biochars were produced by pyrolysis at 500 and 700°C, with residence times of 5, 8 and 12 min. The obtained materials were characterized in terms of their basic physicochemical properties, including specific surface area, SBET, and pore structure parameters.

For each sludge type, the biochars with the highest surface area were selected for Hg sorption tests. These materials were produced at 700°C with pyrolysis times of 5 or 8 min. Mercury removal tests were carried out in a laboratory-scale system using flue gas from coal combustion at temperatures of 120–180°C. The highest Hg removal efficiency, reaching 82% at 120°C, was obtained for biochars derived from food-industry sludge. The lowest efficiency was observed for biochars produced from municipal sewage sludge. For all tested materials, Hg removal efficiency decreased with increasing flue gas temperature. Chemical activation did not improve the sorption performance of the biochars.

The results suggest that selected sewage-sludge-derived biochars may be promising waste-derived sorbents for mercury removal from flue gas. However, the study is preliminary and further optimization is required.

Acknowledgment: The research was financed from the Research Subsidy of the AGH University of Krakow for the Department of Energy and Fuels [No. 501.00-210000-10000].

[1] Department of Fuels Technology, Faculty of Energy and Fuels, AGH University of Krakow, 30-059 Krakow, Poland, * kolarz@agh.edu.pl

EFE2026 ENERGY FUELS ENVIRONMENT
INTERNATIONAL CONFERENCE
17-20 NOVEMBER 2026, KRAKÓW, POLAND

Numerical Analysis of Multiphase Flow Using Multifluid VOF Model and Gamma-Ray Absorption

Patryk Marczak[1,*], Marcin Zych[1], Marek Jaszczur[1]

Keywords: : CFD, Multiphase Flows, Multifluid VOF, Radiometric measurement, Gamma-ray absorption

ABSTRACT

Multiphase flows occur across a wide range of industrial applications, power generation systems, chemical processes and natural environments. To accurately analyze such complex flows, both experimental and numerical methods are employed. Among experimental approaches, radiometric techniques based on gamma-ray absorption frequently utilizing the Am-241 sealed sources coupled with scintillation probes remain highly effective. These methods enable the non-invasive measurement of dispersed phase velocities, void fraction and facilitate the identification of different flow regimes, such as bubbly, plug, and slug flows [1].

Despite their capabilities, gamma-ray absorption techniques require further development to optimize measurement precision and address inherent operational limitations. Furthermore, physical experiments with radioactive sources is constrained by strict radiation protection requirements, regulatory overhead, and high operational costs. Consequently, Computational Fluid Dynamics (CFD) provides a safe and robust alternative to empirical testing. In previous studies, the standard Volume of Fluid (VOF) model was used to simulate the transient air-water flows in a 50 mm horizontal pipe, and the resulting phase distribution data were subsequently applied to replicate the radiometric probe responses. Although the standard VOF is computationally efficient for distinct, large-scale interfaces, its reliance on a shared single-momentum equation inherently limits its accuracy and fails to provide a correct reference velocities for the modeled radiometric probes.

To overcome these limitations, this study investigates the application of the Multifluid VOF model [2,3]. By integrating an Eulerian multiphase formulation with robust interface-tracking algorithms, the Multifluid VOF approach resolves phase-specific momentum equations for each phase while maintaining sharp phase interfaces. The primary objective of this work is to simulate horizontal two-phase air-water flows, model the synthetic radiometric probe response, and conduct a comparative analysis against both experimental data and standard VOF predictions.

Table 1. Air velocity calculated using the synthetic probe model, numerical model with Standard VOF multiphase formulation and experimental data.

Velocity, m/s	**Plug flow**	**Bubbly flow**	**Slug flow**
Synthetic probe	2.06	2.77	1.03
Simulation	2.12	2.78	1.20
Experiment	1.99	1.93	1.82

[1]AGH University of Krakow, Faculty of Energy and Fuels, Al.Mickiewicza 30, 30-059 Kraków, Poland
* pmarczak@agh.edu.pl

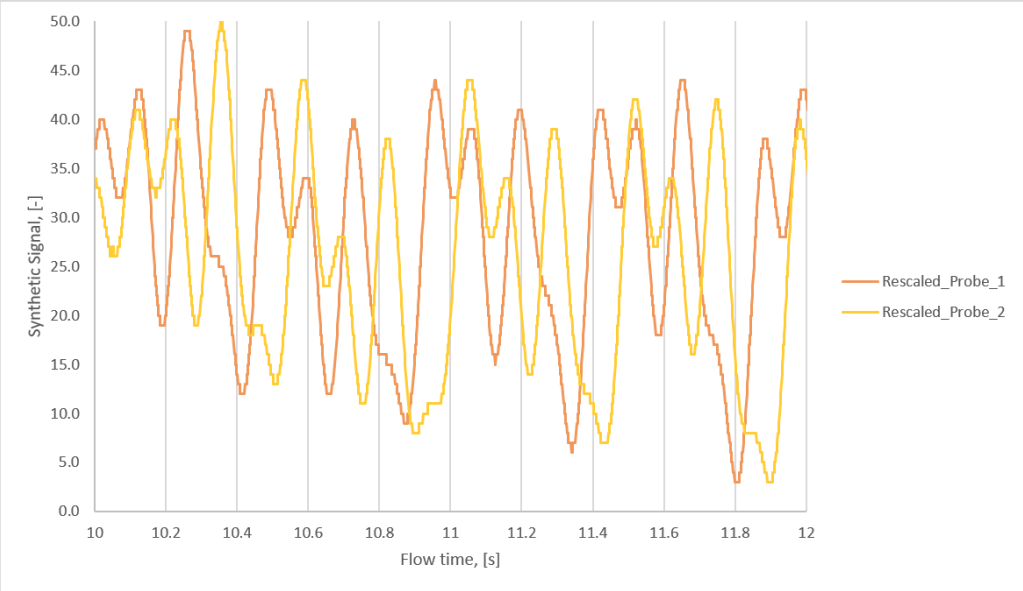


Figure 1. Synthetic signal of radiometric probe, generated using numerical simulation

[1] R. Hanus, M. Zych, M. Kusy, M. Jaszczur, L. Petryka, Identification of liquid-gas flow regime in a pipeline using gamma-ray absorption technique and computational intelligence methods, Flow Meas. Instrum. 60 (2018) 17–23. https://doi.org/10.1016/j.flowmeasinst.2018.02.008.
[2] M. Akhlaghi, V. Mohammadi, N.M. Nouri, M. Taherkhani, M. Karimi, Multi-Fluid VoF model assessment to simulate the horizontal air–water intermittent flow, Chem. Eng. Res. Des. 152 (2019) 48–59. https://doi.org/10.1016/j.cherd.2019.09.031.
[3] Y. Zhang, C. He, P. Li, Numerical investigation of gas-liquid two-phase flow in horizontal pipe with orifice plate, Prog. Nucl. Energy 138 (2021) 103801. https://doi.org/10.1016/j.pnucene.2021.103801.

Spatiotemporal Assessment of PM_{10} Oxidative Potential at Traffic-Influenced and Urban Background Sites in Kraków

Dominika Uchmanowicz[1,*], Agnieszka Orzechowska-Zięba[1], Eliza Wolak[1], Anna Nowak[1], Katarzyna Styszko[1]

Keywords: PM10, oxidative potential, dithiothreitol, ascorbic acid, urban aerosol

ABSTRACT

Mass concentration is the principal metric used to describe airborne particulate matter (PM), yet samples with similar PM10 concentrations may differ in chemical composition and reactivity [1]. Oxidative potential (OP) characterizes the capacity of PM constituents to participate in oxidative reactions, including processes that can promote the formation of reactive oxygen species (ROS) [3]. Cell-free assays estimate this capacity from the depletion of reducing agents or antioxidants in contact with particle extracts [1, 2]. These measurements describe chemical reactivity under defined laboratory conditions rather than directly measuring ROS production in the body or health effects. This study assessed the spatial and seasonal variability of PM10 oxidative potential at two urban sites in Kraków, Poland.

PM10 was collected during an approximately annual sampling campaign at a roadside site on Tkacka Street and at a rooftop site on the AGH University of Krakow campus. Sections of quartz-fibre filters were extracted in phosphate-buffered saline (PBS). The extracts were analysed using dithiothreitol (DTT) and ascorbic acid (AA) depletion assays, which can differ in their responses to redox-active PM constituents [1, 2]. Reaction mixtures were incubated at 37 °C, and absorbance was measured spectrophotometrically after 15, 30, and 60 min. Concentrations were determined using calibration curves, and depletion rates were calculated from their change over time. OP was expressed per unit volume of sampled air (OPv) and per unit mass of collected PM10 (OPm). The two metrics describe the oxidative activity associated with ambient air and the activity of the particle mass, respectively [2].

PM10 concentration and oxidative potential varied throughout the campaign, with distinct patterns at the two sites and for the two assays. Periods of elevated PM10 occurred mainly during the colder part of the campaign, but a single seasonal trend did not describe every OP measure. This was evident when air-volume- and mass-normalized results were compared within the same assay: their higher values sometimes occurred in different parts of the year. The contrast was observed at both sampling locations and was therefore relevant to the interpretation of seasonal differences. This contrast was illustrated by DTT: on 21 January 2026, the highest DTT-derived OPv values at both sites coincided with elevated PM10 concentrations of 132.06 μg/m³ at the roadside site and 112.77 μg/m³ at the rooftop site. In contrast, samples with some of the highest DTT-derived OPm values were collected during warmer months. Thus, days with high oxidative activity per volume of air were not necessarily those with the highest activity per unit mass of PM10.

AA-derived OP also changed over time. At the rooftop site, higher AA-derived OPv values were more frequent in the colder months, whereas the roadside series showed a less uniform pattern. DTT and AA did not consistently identify the same samples as having elevated OP, and neither assay yielded a fixed ranking of the roadside and rooftop sites across the campaign. These differences indicate that the interpretation of OP depends on the antioxidant used and on whether the result is normalized to air volume or particle

[1] AGH University of Krakow, Faculty of Energy and Fuels, Al. Mickiewicza 30, 30-059 Kraków, Poland, * duchmanowicz@agh.edu.pl

mass. For example, an elevated OPv may reflect the oxidative activity associated with more PM10 in a volume of air without implying that each unit of particle mass is more reactive. Considering OPm alongside OPv helps place such observations in context.

The results show temporal variation in PM10 oxidative potential and differences between the roadside and rooftop sampling environments in Kraków. The combined analysis of DTT and AA depletion, expressed as both OPv and OPm, offers a more detailed description of the samples than PM10 mass concentration alone. Further analysis linking OP to particle composition and environmental conditions may help explain the observed patterns. The cell-free assay results do not, by themselves, identify the emission sources responsible for the differences or quantify health effects.

[1] T. Fang, V. Verma, J.T. Bates, J. Abrams, M. Klein, M.J. Strickland, S.E. Sarnat, H.H. Chang, J.A. Mulholland, P.E. Tolbert, A.G. Russell, R.J. Weber, Oxidative potential of ambient water-soluble PM2.5 in the southeastern United States: contrasts in sources and health associations between ascorbic acid (AA) and dithiothreitol (DTT) assays, Atmos. Chem. Phys. 16 (2016) 3865–3879. https://doi.org/10.5194/acp-16-3865-2016.

[2] Á. Clemente, J. Gil-Moltó, E. Yubero, N. Juárez, J.F. Nicolás, J. Crespo, N. Galindo, Sensitivity of PM10 oxidative potential to aerosol chemical composition at a Mediterranean urban site: ascorbic acid versus dithiothreitol measurements, Air Qual. Atmos. Health 16 (2023) 1165–1172. https://doi.org/10.1007/s11869-023-01332-1.

[3] R. Jakhar, K. Styszko, L. Samek, K. Szramowiat-Sala, Oxidative potential of PM1, PM2.5, and PM10 collected in car and tram tunnels to analyse their impact on public health, Sci. Rep. 15 (2025) 21773. https://doi.org/10.1038/s41598-025-09037-4.

The research was financed by AGH University of Krakow grant no. 501.00_210000_10000. Also, the research was supported by IDUB grant (Action 21, Application No. 18209).

EFE2026 ENERGY FUELS ENVIRONMENT
INTERNATIONAL CONFERENCE
17-20 NOVEMBER 2026, KRAKÓW, POLAND

Chemical Valorisation of Polyamide–Elastane Textiles through Alkaline Glycol Solvolysis

Lyudmila Slobodkina[1,*], Zuzanna Kusz[1], Roksana Muzyka[2], Marcin Sajdak[2],Szymon Sobek[3], Sebastian Werle[1]

Keywords: textile waste, spandex, polyamide, solvolysis, chemical recycling

ABSTRACT

Elastane (spandex) is designed to provide high extensibility and shape recovery while remaining intimately integrated within the textile structure. These properties make it highly desirable in garments but also contribute to significant end-of-life recycling challenges. Once elastane is incorporated into a blended textile, the close physical integration of chemically dissimilar polymers makes their subsequent separation and recycling particularly difficult. This problem is especially relevant for polyamide/elastane (PA/EL) textiles widely used in hosiery, sportswear, and stretch garments. Recent recycling strategies have therefore concentrated predominantly on removing or selectively degrading the elastane component while attempting to preserve the polyamide fraction. Thermal degradation followed by washing [1], selective solvent dissolution [2–4], base-catalysed elastane disassembly [5], microwave-assisted glycolysis [6] and, more recently, deep-eutectic-solvent separation [7] have all been investigated. These approaches demonstrate that elastane can be isolated or chemically processed; however, direct short-term chemical treatment of PA/EL textiles in an alkaline glycol medium without prior separation of the polymer components remains relatively understudied.

In this study, a commercial textile containing approximately 92 wt% polyamide and 8 wt% elastane was investigated as a model PA/EL waste stream. The textile was subjected directly to alkaline solvolysis without prior separation of the elastane fraction. A binary mixture of ethylene glycol and propylene glycol (EG/PG) in a 1:1 ratio was used as the reaction medium, and potassium hydroxide was used as the alkaline catalyst. The experiments were conducted at 160-180 °C in an inert atmosphere using 1.5 wt% by weight of KOH relative to the solvent. The reaction time and the solid-to-liquid ratio were varied within the ranges of 10–20 min and 15–20 wt%, respectively. The selected conditions were used to evaluate whether relative short residence times and moderate reaction temperature could promote the chemical conversion of a polyamide-rich textile blends while avoiding a separate solvent-based elastane- removal step. The effectiveness of the process was evaluated using the total fiber decomposition (TFD) index. Statistical analysis of the experimental data was used to determine the influence and relative contribution of the investigated process variables to changes in TFD.

Chemical and structural changes occurring during solvolysis were chracterised using Fourier-transform infrared spectroscopy (FTIR), with particular emphasis on changes in the characteristic functional groups associated with the PA and EL components. In addition to the experimental, statistical, and analytical evaluation, the environmental performance of the proposed recycling route was assessed using life cycle assessment (LCA). The modelling was performed in openLCA 2.5 using the ecoinvent 3.12 database, while

[1] Silesian University of Technology, Department of Thermal Technology, Gliwice, 44-100, Poland, * lyudmila.slobodkina@polsl.pl
[2] Silesian University of Technology, Department of Air Protection, Gliwice, 44-100, Poland
[3] Silesian University of Technology, Department of Heating, Ventilation and Dust Removal Technology, Gliwice, 44-100, Poland

environmental impacts were evaluated using the Environmental Footprint (EF) 3.1 method. The assessment considers the principal material and energy inputs associated with the solvolysis process, including glycol consumption, potassium hydroxide demand, energy requirements, and management of the resulting process fractions. By targeting the valorisation of a difficult-to-recycle textile blend under relatively mild processing conditions, the proposed approach addresses the need for resource-efficient recycling technologies consistent with circular economy principles. Coupling experimental solvolysis data with LCA enables the process to be evaluated not only in terms of technical performance but also with respect to its broader environmental and energy-related implications.

The present work explores an alternative route to previously reported PA/EL recycling strategies. The integration of experimental decomposition measurements, statistical evaluation, FTIR characterisation, and life cycle assessment provides a broader framework for examining both the technical behaviour and environmental implications of the process. This combined approach provides a basis for future process optimisation, recovery and valorisation of products, and development of strategies for difficult-to-recycle polyamide and elastane textiles.

[1] Y. Yin, D. Yao, C. Wang, Y. Wang, Removal of spandex from nylon/spandex blended fabrics by selective polymer degradation, Text. Res. J. 84 (2014) 16–27. https://doi.org/10.1177/0040517513487790.
[2] K.T. Phan, S. Ügdüler, L. Harinck, R. Denolf, M. Roosen, G. O'Rourke, D. De Vos, V. Van Speybroeck, K. De Clerck, S. De Meester, Analysing the potential of the selective dissolution of elastane from mixed fiber textile waste, Resour. Conserv. Recycl. 191 (2023) 106903. https://doi.org/10.1016/j.resconrec.2023.106903.
[3] E. Boschmeier, V.-M. Archodoulaki, A. Schwaighofer, B. Lendl, W. Ipsmiller, A. Bartl, New separation process for elastane from polyester/elastane and polyamide/elastane textile waste, Resour. Conserv. Recycl. 198 (2023) 107215. https://doi.org/10.1016/j.resconrec.2023.107215.
[4] L. Vonbrül, M. Cordin, A.P. Manian, T. Bechtold, T. Pham, Solvent blends for selective elastane dissolution and recovery from mixed polyamide fabrics, Resour. Conserv. Recycl. 200 (2024) 107302. https://doi.org/10.1016/j.resconrec.2023.107302.
[5] M.B. Johansen, B.S. Donslund, M.L. Henriksen, S.K. Kristensen, T. Skrydstrup, Selective chemical disassembly of elastane fibres and polyurethane coatings in textiles, Green Chem. 25 (2023) 10622–10629. https://doi.org/10.1039/D3GC02994H.
[6] E. Andini, P. Bhalode, E. Gantert, S. Sadula, D.G. Vlachos, Chemical recycling of mixed textile waste, Sci. Adv. 10 (2024) eado6827. https://doi.org/10.1126/sciadv.ado6827.
[7] N. Depope, A. Depope, V.-M. Archodoulaki, A. Dabrowska, B. Lendl, A. Mautner, W. Ipsmiller, A. Bartl, DES formulation for recycling synthetic fibre textile waste containing elastane, Waste Manag. 224 (2026) 115736. https://doi.org/10.1016/j.wasman.2026.115736.

Acknowledgement: This work was supported by the Opus 26 project "Chemical recycling of textile waste by oxidative liquefaction and solvolysis - from waste to sustainable fashion" financed by the National Science Center (NCN), Poland [2023/51/B/ST8/02414].

EFE2026 ENERGY FUELS ENVIRONMENT
INTERNATIONAL CONFERENCE
17-20 NOVEMBER 2026, KRAKÓW, POLAND

Occurrence and Phase Distribution of selected OH-PAHs in Municipal Wastewater Treatment Plants

Zuzanna Prus-Frączek[1,*], Karolina Cwynar[2], Laura Węgrzyn[2], Justyna Pyssa[2], Katarzyna Styszko[2]

Keywords: activated sludge; wastewater treatment; hydroxylated PAHs; biomarkers; solid-water partitioning

ABSTRACT

Wastewater treatment plants (WWTPs) receive complex mixtures of organic contaminants originating from domestic activities, industrial inputs, urban runoff, and chemical transformations during treatment. Among these compounds, polycyclic aromatic hydrocarbons (PAHs) and their hydroxylated derivatives (OH-PAHs) are of particular interest because of their environmental persistence, potential toxicity, and ability to transform during biological and physicochemical treatment processes [1, 2]. OH-PAHs may also form as transformation products of parent PAHs and can exhibit different physicochemical properties and environmental behaviour than their non-hydroxylated counterparts. However, data on the occurrence of these compounds in wastewater are limited [3].

This study aimed to investigate the occurrence and distribution of selected OH-PAHs in activated sludge (AS) and corresponding supernatant water (SW) collected from two municipal wastewater treatment plants in a similar region. Particular attention was given to seasonal variability and the partitioning of target compounds between solid and aqueous phases to determine whether the concentration patterns observed in activated sludge were reflected in the corresponding aqueous phase and to assess how phase distribution may influence the interpretation of contaminant occurrence in wastewater treatment systems. Samples were collected from two municipal wastewater treatment plants located in southern Poland during two sampling campaigns representing different seasons (winter and summer). Sample preparation was performed using QuEChERS extraction, followed by solid-phase extraction (SPE) clean-up and pre-concentration. The target compounds were subsequently determined by liquid chromatography coupled with tandem mass spectrometry (LC-MS/MS). The investigated target compounds included 1-hydroxynaphthalene (1-OH-NAP), 2-hydroxynaphthalene (2-OH-NAP), 2-hydroxyfluorene (2-OH-FLU), 1-, 9-, 2-, 3-, and 4-hydroxyphenanthrene (1-, 9-, 2-, 3-, and 4-OH-PHEN), 1-hydroxypyrene (1-OH-PYR), and 3-hydroxybenzo[a]pyrene (3-OH-BaP). The concentrations of the investigated compounds varied substantially between the two wastewater treatment plants and between the analysed matrices.

Across both sampling seasons, individual OH-PAHs were detected over a broad concentration range, from approximately 3 to 8.9 × 10^3 ng/g dry matter in AS from WWTP 1 and from 2 to 9.9 × 10^3 ng/g dry matter in WWTP 2. In SW, concentrations ranged from approximately 2 to 3.6 × 10^3 ng/L and from 8 to 4.9 × 10^3 ng/L, respectively. The distribution coefficient ($\log_{10} Kd_{app}$) also varied between the investigated wastewater treatment plants. Across both sampling seasons, $\log_{10} Kd_{app}$ values ranged from c.a. 2.9-

[1] AGH University of Krakow, Department of Heat Engineering and Environment Protection, Faculty of Metals Engineering and Industrial Computer Science, A. Mickiewicza 30, Kraków 30-059, Poland, *zprus@agh.edu.pl

[2] AGH University of Krakow, Department of Fuel Technology, Faculty of Energy and Fuels, A. Mickiewicza 30, Krakow 30-059, Poland

5.0 in WWTP 1 and c.a. 1.8-7.1 in WWTP 2, indicating differences in the affinity of individual compounds for two phases.

The results demonstrate considerable variability in the occurrence and phase distribution of OH-PAHs in municipal wastewater treatment systems. Differences between WWTPs may reflect seasonal variation, catchment characteristics, organic matter sources, and treatment conditions. The dataset provides new information for wastewater monitoring and understanding the fate and phase partitioning of these compounds, supporting their integration with conventional wastewater parameters to better assess their sources and treatment-related transformations.

[1] M. Beygisangchin, J. Jakmunee, S.K. Kamarudin, A.H. Baghdadi, S. Saetang, S. Thipprasert, A critical review of polycyclic aromatic hydrocarbons and their adverse effects on human health: insights from the past six years, Environ. Sci. Eur. 38 (2026) 87. https://doi.org/10.1186/s12302-026-01367-y.
[2] K. Styszko, W. Bolesta, J. Worek, Z. Prus, K. Cwynar, J. Pyssa, D. Uchmanowicz, L. Frydel, A.P. Daso, B. Kasprzyk-Hordern, Tracking nonregulated micropollutants in sewage sludge: Antimicrobials, OH-PAHs, and microplastics—Environmental risks, fertilizer implications and energy considerations, Energy Rep. 13 (2025) 4756–4768. https://doi.org/10.1016/j.egyr.2025.04.013.
[3] L. Frydel, Z. Prus, K. Cwynar, J. Pamuła, J. Pyssa, R. Rego, K. Styszko, Determination of hydroxy derivatives of PAHs in sewage sludge by GC-MS/MS, Desalin. Water Treat. 321 (2025) 101015. https://doi.org/10.1016/j.dwt.2025.101015.
Acknowledgements: The project was funded by the Polish National Science Centre (grant no. 2022/45/B/ST10/02108).

Effects of Europe's Energy Transition on Temporal and Interannual Variability in Equivalent Black Carbon (eBC) in Kraków, Poland

Rakshit Jakhar[1], Lucyna Samek[2], Katarzyna Styszko[1]

Keywords: equivalent black carbon, seasonal variability, energy transition, regional transport, Kraków

ABSTRACT

Equivalent black carbon (eBC), a combustion-derived constituent of fine particulate matter ($PM_{2.5}$), has important implications for air quality, human health and climate. This study examines temporal variability and interannual differences in eBC in Kraków, Poland, against the background of Europe's changing energy policies and ongoing energy transition. Multi-wavelength optical measurements obtained between October 2023 and September 2024 were used to determine total eBC and estimate its fossil-fuel (eBCff) and biomass-burning (eBCbb) components. The results were compared with observations from 2020-2021 to assess changes in concentrations and temporal patterns. Pronounced seasonal differences were observed. Winter eBC concentrations averaged approximately 4.0 pg m^{-3}, reaching 5.5 pg m^{-3} in February, whereas summer minima ranged from 1.2 to 1.5 pg m^{-3}. Biomass-burning eBC remained relatively low, increasing from 0.1-0.2 pg m^{-3} in summer to 0.4-0.5 pg m^{-3} in winter. $PM_{2.5}$ displayed a comparable seasonal cycle, with winter concentrations of 24-31 pg m^{-3} and summer values of 8-12 pg m^{-3}. Severe winter episodes were characterised by $PM_{2.5}$ concentrations exceeding 120 pg m–3 and eBC concentrations approaching 13 pg m^{-3}. These patterns align with seasonal changes in heating emissions and meteorological conditions that govern pollutant dispersion and accumulation. Weekly variability was also evident. Average eBC concentrations were approximately 40% higher on weekdays than on weekends, at 3.1 and 2.2 pg m^{-3}, respectively. By contrast, eBCbb exhibited limited weekly variation, suggesting differences in the temporal behaviour of the contributing emission sources. The reported winter-to-summer eBC ratio of 2.2 further indicates a seasonal contrast, although its interpretation depends on the averaging periods used. Compared with 2020-2021, annual mean eBC concentrations were lower in 2023-2024, while substantial winter variability and short-term pollution episodes persisted. Annual average air quality improved, but periods of elevated particulate pollution persisted. The comparison does not establish that energy policy changes caused the observed variability or altered meteorological events. Persistently elevated wintertime eBC following Kraków's 2019 prohibition of coal and wood combustion is consistent with a contribution from emissions transported from neighbouring areas. Regional emissions and atmospheric conditions may therefore remain important determinants of local air quality alongside measures controlling emissions within the city. These findings support coordinated regional emission reductions to complement local interventions. They also underline the importance of incorporating seasonal variability and episodic extremes into air-quality evaluation and health-impact assessment, rather than relying exclusively on annual mean concentrations. This approach can provide a more complete assessment of persistent pollution burdens.

Table 1. Seasonal and annual eBC and BCbb concentrations in Kraków (mean ± standard deviation; pg m^{-3})

[1] Faculty of Energy and Fuels, AGH University of Krakow, 30-059 Krakow, Poland; *jakhar@agh.edu
[2] Faculty of Physics and Applied Computer Science, AGH University of Krakow, 30-059 Krakow, Poland

Period	eBC 20202021	eBC 20232024	BCbb 20202021	BCbb 20232024
Spring	3.0 ± 1.1	2.5 ± 1.1	0.30 ± 0.10	0.29 ± 0.10
Summer	2.2 ± 0.5	1.8 ± 0.9	0.20 ± 0.10	0.23 ± 0.10
Autumn	4.2 ± 1.6	2.3 ± 1.2	0.22 ± 0.16	0.34 ± 0.20
Winter	5.3 ± 1.8	4.1 ± 2.9	0.40 ± 0.30	0.36 ± 0.30
Annual	3.5 ± 1.5	2.7 ± 0.9	0.25 ± 0.15	0.25 ± 0.10

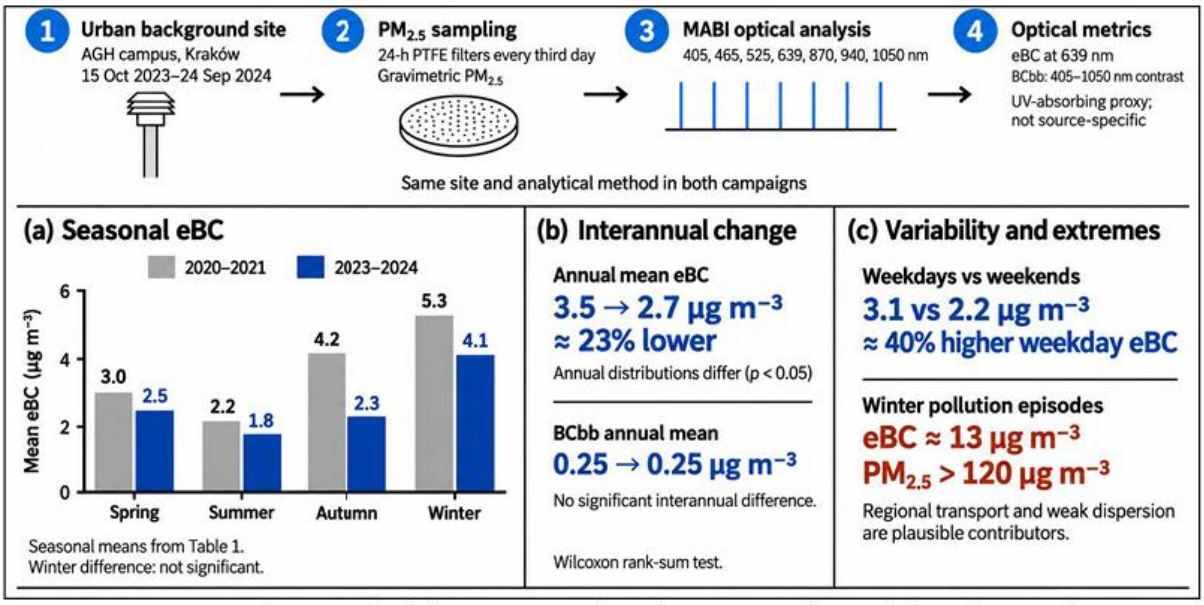


Figure 1. Sampling methodology, seasonal and interannual variability of equivalent black carbon (eBC), and winter pollution extremes in Kraków, Poland, comparing 2020– 2021 and 2023–2024.

[1] L. Samek, R. Jakhar, A. Ryś, S. Papagiannis, V. Vassilatou, S. Vratolis, E. Diapouli, Sustainable urban air quality monitoring: Determination of equivalent black carbon concentrations and mass absorption cross sections (MAC) using multi-wavelength absorption black carbon instrument (MABI) in Athens and Krakow, Sustainability 18 (2026) 8737. https://doi.org/10.3390/su18178737.

[2] R. Jakhar, L. Samek, K. Styszko, Influence of Europe's shifting energy conditions on the temporal variability and interannual changes in equivalent black carbon (eBC) in Kraków, Poland, Sustainability 18 (2026) 7850. https://doi.org/10.3390/su18157850.

[3] A. Ryś, L. Samek, Yearly variations of equivalent black carbon concentrations observed in Krakow, Poland, Atmosphere 13 (2022) 539. https://doi.org/10.3390/atmos13040539.

[4] A. Skiba, K. Styszko, A. Tobler, R. Casotto, Z. Gorczyca, P. Furman, L. Samek, D. Wideł, M. Zimnoch, A. Kasper-Giebl, J.G. Slowik, K.R. Daellenbach, A.S.H. Prévôt, K. Różański, Source attribution of carbonaceous fraction of particulate matter in the urban atmosphere based on chemical and carbon isotope composition, Sci. Rep. 14 (2024) 7234. https://doi.org/10.1038/s41598-024-57829-x.

[5] R. Casotto, A. Skiba, M. Rauber, J. Strähl, A. Tobler, D. Bhattu, H. Lamkaddam, M.I. Manousakas, G. Salazar, T. Cui, F. Canonaco, L. Samek, A. Ryś, I. El Haddad, A. Kasper-Giebl, U. Baltensperger, J. Necki, S. Szidat, K. Styszko, J.G. Slowik, A.S.H. Prévôt, K.R. Daellenbach, Organic aerosol sources in Krakow, Poland, before implementation of a solid fuel residential heating ban, Sci. Total Environ. 855 (2023) 158655. https://doi.org/10.1016/j.scitotenv.2022.158655.

EFE2026 ENERGY FUELS ENVIRONMENT
INTERNATIONAL CONFERENCE
17-20 NOVEMBER 2026, KRAKÓW, POLAND

Application of Hydrotalcite-Derived Ni-Ce-Ca Catalysts for CO_2 Methanation

Tomasz Piechówka[1,*], Agnieszka Szymaszek-Wawryca[1], Konrad Świerczek[1], Monika Motak[1]

Keywords: CO_2 methanation, hydrotalcite, nickel

ABSTRACT

Carbon dioxide (CO_2) emission represents one of the major environmental threats, leading to an intensification of the greenhouse effect and global climate change. An effective and promising method for the utilization of this gas is catalytic methanation, represented by the following reaction:

$$CO_2 + 4H_2 \rightleftharpoons CH_4 + 2H_2O,$$

which requires an appropriate catalyst to proceed efficiently [1]. Although noble metal catalysts exhibit the highest activity, their high cost requires replacement with much cheaper nickel. However, the metallic phase must be well-dispersed to ensure high catalytic activity and stability [2]. Excellent precursors for such active catalysts with well-dispersed active phase are layered double hydroxides, commonly known as hydrotalcites. The materials feature a unique brucite-like layered structure that allows for the highly uniform distribution and simultaneous accommodation of multiple metal cations within their crystal lattice. The advantage of such a solution is the seamless incorporation of metals, such as nickel, as well as cerium [2]. Furthermore, the final properties and catalytic performance of these materials strongly depend on the chosen promoters that can be incorporated using other methods, such as grinding.

Therefore, the aim of this study is to evaluate hydrotalcite-derived Ni and Ni-Ce catalysts promoted by Ca for CO_2 methanation, with a particular focus on the influence of calcium content. The experimental route was divided into three stages: (1) synthesis of a hydrotalcite-like phase containing nickel (20 wt. %), cerium (15 wt.%) and calcium promoter (1,2 or 5 wt. %) incorporated by grinding method, (2) determination of the structural and textural properties of the prepared materials, and (3) laboratory-scale CO_2 methanation catalytic tests, and stability tests for the best-performing sample.

Analysis of the spent catalysts using TGA and XRD allowed for an evaluation of the synergistic effect of calcium and cerium on the resistance to carbon deposition.

[1] P. Hongmanorom, J. Ashok, G. Zhang, Z. Bian, M.H. Wai, Y. Zeng, S. Xi, A. Borgna, S. Kawi, Enhanced performance and selectivity of CO2 methanation over phyllosilicate structure derived Ni-Mg/SBA-15 catalysts, Appl. Catal. B 282 (2021) 119564. https://doi.org/10.1016/j.apcatb.2020.119564.

[2] P. Marocco, E.A. Morosanu, E. Giglio, D. Ferrero, C. Mebrahtu, A. Lanzini, S. Abate, S. Bensaid, S. Perathoner, M. Santarelli, R. Pirone, G. Centi, CO2 methanation over Ni/Al hydrotalcite-derived catalyst: Experimental characterization and kinetic study, Fuel 225 (2018) 230–242. https://doi.org/10.1016/j.fuel.2018.03.137.

The authors gratefully acknowledge financial support from the National Science Centre, Poland, through the OPUS 29 grant (grant no. 2025/57/B/ST5/01462). The selected results presented herein were developed using equipement supported by the "Excellence Initiative – Research University" programme at AGH University of Krakow.

[1] AGH University of Krakow, Aleja Adama Mickiewicza 30, 30-059 Kraków
* tpiechowka@student.agh.edu.pl

Analysis of Concentrations and Environmental Mass Loads of Hydroxylated Polycyclic Aromatic Hydrocarbons (OH-PAHs) in Municipal Wastewater

Karolina Cwynar[1,*], Laura Węgrzyn[1], Zuzanna Prus-Frączek[2], Justyna Pyssa[1], Elżbieta Sochacka-Tatara[3], Agnieszka Pac[3], Katarzyna Styszko

Keywords: OH-PAHs, WBE, UHPLC-MS/MS, municipal wastewater

ABSTRACT

Polycyclic aromatic hydrocarbons (PAHs) are a group of ubiquitous environmental pollutants with proven toxicity. Upon absorpion into the human body, PAHs are metabolized and excreted in urine as hydroxylated derivatives (OH-PAHs), which ultimately enter the sewer system. The wastewater-based epidemiology (WBE) approach allows for the assessment of community-wide exposure and evaluation of population exposure profiles. However, the presence of OH-PAHs in treated wastewater also poses a potential threat to aquatic ecosystems. The aim of this study was to evaluate the concentrations of selected PAH metabolites in raw and treated wastewater, and to estimate the environmental loads of these pollutants discharged into the natural environment. To account for technological and seasonal variability, samples were collected from municipal wastewater treatment plants (Płaszów and Kujawy) during both summer and winter seasons. Analytical determinations were performed using ultra-high-performance liquid chromatography coupled with tandem mass spectrometry (UHPLC-MS/MS) [1-3] . A total of 8 OH-PAHs were targeted, of which 6 (including derivatives of naphthalene, fluorene and phenantherene) were confirmed in the analyzed wastewater samples. In contrast, neither 3-OH-BaP nor 1-OH-PYR was detected in any of the analyzed samples. The highest pre-treatment concentrations were recorded for fluorenols, reaching levels of up to 1100 ng/L during the winter season, and for 1-OH-NAP, with concentrations up to 614 ng/L during the summer season. The wastewater treatment process exhibited highly variable efficiency. While a substantial concentration reduction was observed for 1-OH-NAP at the Kujawy WWTP (decreasing from over 400 ng/L to 12-46 ng/L), a drastic increase in concentrations of 2-OH-NAP and fluorenols was noted in the treated effluent. During the winter period, effluent concentrations reached nearly 1200 ng/L for 2-OH-NAP in Płaszów WWTP and approximately 1120 ng/L for fluorenols in Kujawy WWTP. This phenomenon strongly suggests the occurence of deconjugation processes of conjugated metabolites or precursors transformations during biological wastewater treatment. Based on the measured concentrations and flow rates, the daily environmental mass loads discharged into the receiving water body were calulated, ranging for indiviual metabolites from approximately 0,0001 kg/day for the sum of 1- and 9-OH-PHEN to over 0,07 kg/day. The obtained results prove that standard municipal wastewater treatment systems do not completely eliminate PAH metabolites and, due to ongoing biochemical transformations, may even generate substantially elevated loads of certain forms released into surface waters. The discharge of treated wastewater represents a continuous emission source of

[1]AGH University of Krakow, Department of Fuel Technology, Faculty of Energy and Fuels, A. Mickiewicza 30, Krakow 30-059, Poland *kcwynar@agh.edu.pl
[2]AGH University of Krakow, Department of Heat Engineering and Environment Protection, Faculty of Metals Engineering and Industrial Computer Science, A. Mickiewicza 30, Kraków 30-059, Poland
[3]Jagiellonian University Medical College, Chair of Epidemiology and Preventive Medicine, Kraków, Poland

OH-PAHs into the environment, highlighting the critical need for advanced monitoring of this group of micropollutants.

[1] K. Styszko, W. Bolesta, J. Worek, Z. Prus, K. Cwynar, J. Pyssa, D. Uchmanowicz, L. Frydel, A.P. Daso, B. Kasprzyk-Hordern, Tracking nonregulated micropollutants in sewage sludge: Antimicrobials, OH-PAHs, and microplastics—Environmental risks, fertilizer implications and energy considerations, Energy Rep. 13 (2025) 4756–4768. https://doi.org/10.1016/j.egyr.2025.04.013.
[2] L. Frydel, Z. Prus, K. Cwynar, J. Pamuła, J. Pyssa, R. Rego, K. Styszko, Determination of hydroxy derivatives of PAHs in sewage sludge by GC-MS/MS, Desalin. Water Treat. 321 (2025) 101015. https://doi.org/10.1016/j.dwt.2025.101015.
[3] K. Styszko, L. Węgrzyn, K. Cwynar, Z. Prus, D. Uchmanowicz, E. Sochacka-Tatara, A. Pac, B. Kasprzyk-Hordern, Assessment of population exposure to polycyclic aromatic hydrocarbons using wastewater-based epidemiological analysis, in: SETAC Europe 36th Annual Meeting: Embrace the Outlier: In Science, Regulations and Networks, Maastricht, The Netherlands, 17–21 May 2026, conference abstract.

Cradle-to-Gate Life Cycle Assessment of a Multi-Fibre Composite Battery Housing System for a Solar Electric Vehicle: Environmental Hotspot Analysis and Eco-Design Implications

Oluwapelumi John Oluwalana [1],*, Katarzyna Grzesik [1]

Keywords: life-cycle assessment, vehicle-integrated photovoltaics, solar electric vehicle, battery housing, multi-fibre composite.

ABSTRACT

The transition from internal combustion engine vehicles (ICEVs) to battery electric vehicles (BEVs) can reduce use-phase greenhouse-gas emissions, but it transfers a substantial share of environmental burden to vehicle and battery manufacturing. This issue is particularly important for vehicle-integrated photovoltaic (VIPV) systems, in which the additional mass and material demand of photovoltaic modules, electrical components and structures must be balanced against electricity generated during operation. For lightweight solar vehicles, the battery housing can influence structural performance, battery protection, vehicle mass and energy efficiency. This study investigates the cradle-to-gate environmental profile of a multi-fibre composite battery housing developed for the Perla solar electric vehicle prototype of the AGH Solar Team.

The objective is to quantify the housing's environmental impacts, identify dominant processes and materials, and derive eco-design recommendations. The assessment uses experimentally and technically documented primary data collected in the authors' laboratory, including the masses and composition of reinforcement fibres, matrix and auxiliary materials, component geometry, manufacturing operations, energy consumption and production yields. The life-cycle model is implemented in SimaPro. The system boundary covers input-material production and manufacture of the composite housing up to the factory gate. Laboratory data are complemented, where necessary, by background inventories for material production and energy supply. The functional unit is one battery housing system meeting the Perla prototype's structural and dimensional requirements. Midpoint indicators include climate change, cumulative energy demand, resource use and selected emissions-related categories. Contribution, hotspot, sensitivity and uncertainty analyses are used to evaluate the results and their robustness.

Existing studies have examined the life-cycle impacts of electric-vehicle batteries, aluminium and polymeric enclosures, fibre-reinforced automotive components and VIPV systems. They indicate that battery-cell production, energy-intensive metals, resin systems, fibre production and manufacturing electricity can be important contributors. However, replacing a metallic structure with a composite does not automatically provide an environmental benefit. Outcomes depend on fibre type, matrix content, production efficiency, electricity mix, component mass, service requirements and end-of-life assumptions. Natural or bio-based fibres may reduce production impacts in some applications, whereas carbon or glass fibres can provide higher mechanical performance at potentially greater embodied impact. Hybrid multi-fibre architectures may therefore offer a compromise between performance, mass and environmental impact, but their application to solar-electric-vehicle battery housings remains insufficiently documented using detailed primary data.

[1] Faculty of Geo-Data Science, Geodesy and Environmental Engineering AGH University of Krakow,
* ojoluwalana@agh.edu.pl

The analysis distinguishes material-related impacts from manufacturing impacts. Particular attention is given to reinforcement fibres, polymer matrix, inserts, coatings, joining elements and process energy. Alternative scenarios examine reduced component mass, fibre-ratio changes, increased recycled or bio-based content, improved production yield, lower-carbon electricity and alternative matrix or end-of-life assumptions. These scenarios are interpreted alongside the functional requirements of a battery housing, including mechanical integrity, dimensional stability, thermal resistance, impact protection and manufacturability. Lightweighting is considered both as a direct reduction in material demand and as a possible enabler of improved solar-vehicle efficiency; any use-phase benefit is kept separate from the cradle-to-gate inventory.

The study provides a transparent, primary-data-based environmental baseline for a multi-fibre composite battery housing designed for a solar electric vehicle. The results will identify the dominant contributors within the housing supply chain and the design parameters that most strongly influence the selected impact categories. Linking hotspot results with feasible design changes supports the selection of fibre–matrix combinations, reduction of process losses, specification of electricity requirements and planning of future recycling strategies. More broadly, the research demonstrates how component-level LCA can support VIPV eco-design and more consistent comparisons of solar electric vehicles, BEVs and ICEVs under defined life-cycle assumptions.

Negative Thermal Expansion Materials: An Innovative Tool for TEC Adjustment in Solid Oxide Fuel Cells

Piotr Winiarz[1,*], Ming Chen[2], Kun Zheng[1], Konrad Świerczek[1]

Keywords: negative thermal expansion, thermal expansion coefficient, cathode materials, solid oxide fuel cells

ABSTRACT

Solid oxide fuel cells (SOFCs) are electrochemical devices producing clean electrical energy through simple chemical reactions without combustion, at elevated temperatures, e.g., 600°C – 900°C. Despite dozens of years of different improvements in their electrodes or performance, long-term stability is still probably one of the most limiting factors, which slows down their wider commercialization. Since the thermal expansion coefficient (TEC) of the electrolyte and cathode are very different, there is a so-called thermal mismatch. Hence, upon heating, we can expect different degradation mechanisms that damage the device, lowering its performance. Therefore, the novel idea is to use state-of-the-art negative thermal expansion materials (NTEs) to adjust the TEC of the cathode to match the chosen electrolyte material [1,2].

In this work, several NTEs were prepared, optimized, and used as an additive to previously obtained double-perovskite $SmBa_{0.5}Sr_{0.5}CoCuO_{5+\delta}$ (SBSCCO) cathode material [3]. The main purpose of the work was to find as many materials as possible with different negative TECs in different temperature ranges, to have a TEC-adjusting tool for cathodes in electrochemical devices such as LT-SOFCs, IT-SOFCs, and typical SOFCs/SOECs. To address this, materials from the $Ln_{1-x}A_xMnO_{3-\delta}$ group, where Ln = chosen lanthanides, A = chosen 3d metals, and $x \leq 0.15$, were synthesized using the solid-state reaction method with final annealing at 1300°C for 10 h. The obtained samples were single-phase, with the majority crystallizing in an orthorhombic structure with Pnma symmetry (Fig.1a). The relative elongation was estimated using dilatometry, where the TECs of the measured materials ranged from $-9 \cdot 10^{-6}$ 1/K to $-5 \cdot 10^{-6}$ 1/K, between 100°C and 800°C (Fig.1b). Interestingly, there is a dependence between the negative TEC and its range and the average A-site ionic radius. Moreover, registered Raman spectra as a function of temperature revealed that the coexistence of in-phase stretching and out-of-phase bending of Sm-O polyhedra is responsible for lowering each other's energy, which in effect may cause the negative expansion. The total conductivity of the chosen NTE material, $Sm_{0.85}Zn_{0.15}MnO_{3-\delta}$ (SZM15), is thermally activated and reaches ~20 $S \cdot cm^{-1}$, whereas the conductivity of the SBSCCO cathode material is around 100 $S \cdot cm^{-1}$. The addition of SZM15 to SBSCCO does not visibly change the conductivity. To evaluate the electrochemical properties, symmetrical cells were constructed based on $La_{0.8}Sr_{0.2}Ga_{0.8}Mg_{0.2}O_{3-\delta}$ (LSGM) electrolyte. Between 700°C and 900°C, the polarization resistance (R_p) of the composite cathode (SBSCCO + 10wt.%SZM15) was lower when compared to pristine SBSCCO. For further optimization, the electrospinning method was utilized to obtain the composite cathode in the form of nanofibers. The electrospun SBSCCO + 10wt.% SZM15_ES composite cathode exhibits around 60% lower R_p compared to pristine SBSCCO. Therefore, for this material, the long-term stability test was performed at 600°C (Fig.1c-inset). The result showed that degradation mechanisms were visibly diminished, hence, this composite cathode was used in an anode-supported cell. The peak power density reached

[1] AGH University of Krakow, al. Adama Mickiewicza 30, 30-059 Krakow, Poland, *pwiniarz@agh.edu.pl
[2] Technical University of Denmark, Kongens, Lyngby 2800, Denmark

850 mW·cm^{-2} at 800°C.

The obtained results show that the addition of the NTE phase to the chosen cathode materials improves the electrochemical properties, fuel cell performance, and long-term stability.

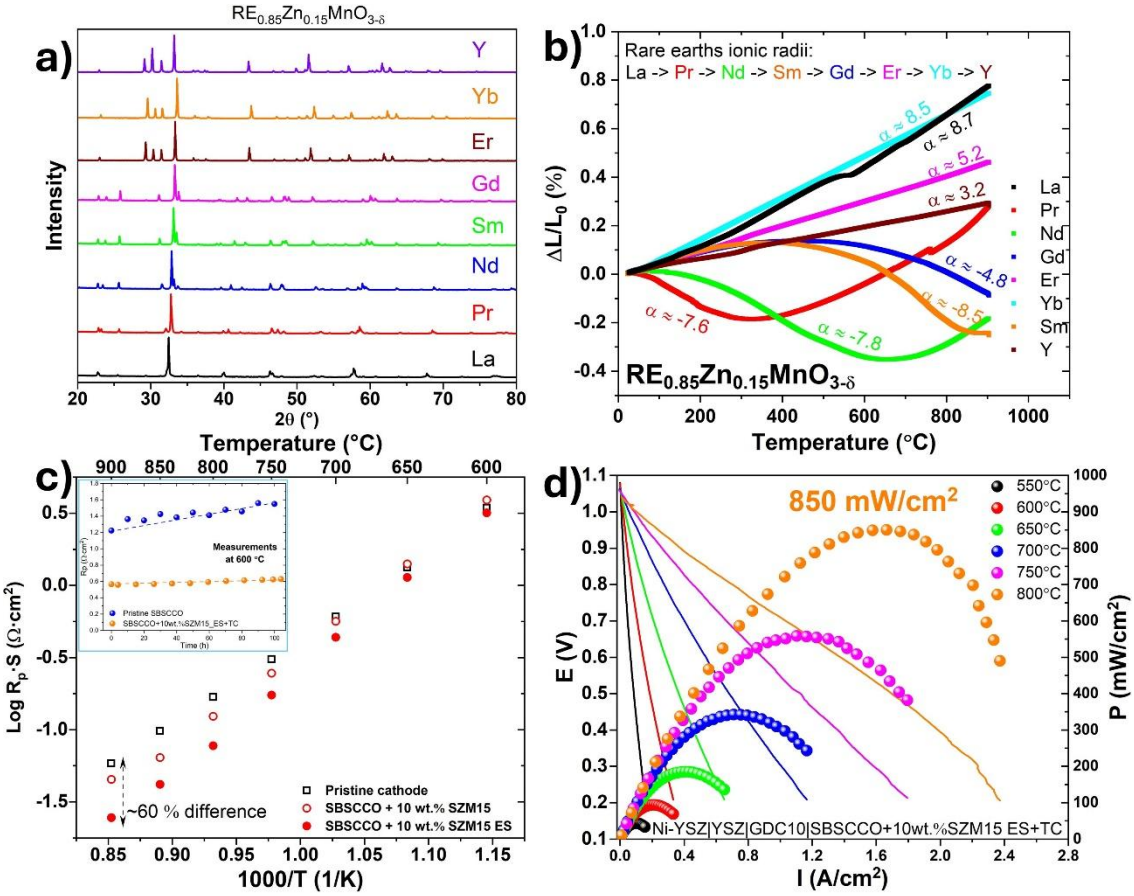


Figure 1. Structural, thermal, and electrochemical properties of the obtained NTEs and composites: a) exemplary X-ray diffraction patterns for $RE_{0.85}Zn_{0.15}MnO_{3-\delta}$ NTE materials recorded at room temperature, b) relative elongation vs. temperature with estimated TECs, c) polarization resistance vs. temperature (inset: long-term stability), d) I-V characteristics for an anode-supported cell with the best-chosen composite as a cathode

[1] P. Winiarz, A. Sultan, Y. Ling, K. Zheng, Negative thermal expansion coefficient materials: From basics to applications, recent advances in solid oxide cells and future perspectives, Sustain. Mater. Technol. 45 (2025) e01442. https://doi.org/10.1016/j.susmat.2025.e01442.

[2] P. Winiarz, J. Lach, Y. Ling, M. Gajewska, M. Chen, M. Marzec, K. Zheng, Stable and active nanofiber electrodes tuned via a negative thermal expansion strategy for designing high-performance solid oxide fuel cells, Appl. Catal. B 382 (2026) 125950. https://doi.org/10.1016/j.apcatb.2025.125950.

[3] P. Winiarz, E.A. Sroczyk, A. Brzoza-Kos, P. Czaja, K. Kapusta, K. Świerczek, SmBa0.5Sr0.5CoCuO5+δ and Sm0.5Ba0.25Sr0.25Co0.5Cu0.5O3−δ oxygen electrode materials for Solid Oxide Fuel Cells: Crystal structure and morphology influence on the electrocatalytic activity, Acta Mater. 277 (2024) 120186. https://doi.org/10.1016/j.actamat.2024.120186.

This project was funded by the National Science Centre, Poland, based on the decision number UMO-2025/59/D/ST11/03011

EFE2026 ENERGY FUELS ENVIRONMENT
INTERNATIONAL CONFERENCE
17-20 NOVEMBER 2026, KRAKÓW, POLAND

Sustainable Urban Air Quality Monitoring: Determination of Equivalent Black Carbon Concentrations and Mass Absorption Cross Sections (MAC) Using Multi-Wavelength Absorption Black Carbon Instrument (MABI) in Athens and Krakow

Lucyna Samek[1,*], Rakshit Jakhar[2], Anna Ryś[1,3], Stefanos Papagiannis[4], Vassiliki Vassilatou[4], Stergios Vratolis[4], Evangelia Diapouli[4]

Keywords: $PM_{2.5}$, PM_{10}, Black Carbon, MABI, Elemental Carbon

ABSTRACT

Black carbon is an important light-absorbing component of atmospheric particulate matter, with significant implications for urban air quality, climate forcing, human health, and sustainable urban development. Reliable monitoring of black carbon is therefore essential for assessing combustion-related pollution and supporting sustainable air quality management and emission-reduction strategies. This study evaluated the performance of the Multi-Wavelength Absorption Black Carbon Instrument for the offline determination of aerosol light absorption and equivalent black carbon under contrasting urban conditions. PM2.5 and PM10 samples were collected at urban-background sites in Krakow, Poland, and Athens, Greece, during winter and summer 2024, thereby covering heating and non- heating periods and a broad range of aerosol concentrations. Samples were collected in parallel on Quartz-fibre and Teflon filters. Their light absorption was measured offline using the Multi-Wavelength Absorption Black Carbon Instrument at 870 nm. Elemental carbon concentrations were independently determined on Quartz-fibre filters by thermo-optical transmittance using the EUSAAR_2 protocol, while continuous absorption measurements from an AE33 Aethalometer operated in Athens were used to assess the comparability of offline and online measurements. The consistency of two independent Multi-Wavelength Absorption Black Carbon Instruments operated in Krakow and Athens was also examined using a common set of filters. Strong linear relationships were observed between the offline absorption coefficients and elemental carbon concentrations, with coefficients of determination exceeding 0.90 for the investigated datasets. The offline measurements also reproduced the variability observed by the AE33, although they systematically yielded higher absorption coefficients than the continuous instrument. Quartz-fibre filters produced higher absorption values and higher apparent mass absorption cross-sections than Teflon filters, demonstrating a pronounced substrate-dependent effect. The differences in the quartz-based relationships between Krakow and Athens indicated that aerosol composition, source characteristics, ageing, and mixing state may also affect the relationship between optical absorption and elemental carbon concentration. These findings confirm that the instrument is suitable for offline and retrospective assessment of equivalent black carbon, particularly where continuous monitoring is unavailable. Reliable quantitative application requires filter-specific calibration and, where necessary, site-specific mass absorption cross-section values. By enabling the use of archived and routinely collected filter samples for black carbon assessment, this approach can complement continuous monitoring networks and support more accessible and sustainable air quality monitoring. Such measurements can contribute to the evaluation of pollution trends, emission-control measures, and evidence-based strategies aimed at improving urban environmental quality and advancing sustainability goals.

Acknowledgements: This research project was supported by the program "Excellence initiative—research university" for the University of Science and Technology and the ATMO ACCESS TNA project.

1

EFE2026 ENERGY FUELS ENVIRONMENT
INTERNATIONAL CONFERENCE
17-20 NOVEMBER 2026, KRAKÓW, POLAND

Tailoring SFM-Based Electrodes for Solid Oxide Cells: Effects of A-Site Deficiency, Morphology, and Nickel Substitution

Michał Gogacz[1,*], Kun Zheng[1]

Keywords: solid oxide cells, SFM, A-site deficiency, nanofibers

ABSTRACT

Solid oxide cells (SOCs) are a promising technology for reversible energy conversion and storage, enabling hydrogen production from renewable electricity in electrolysis mode and its subsequent use for electricity and heat generation in fuel cell mode. However, conventional operation above 800°C promotes thermomechanical stresses and material degradation, increasing system costs and limiting widespread implementation [1]. Lowering the operating temperature, particularly towards 600°C and below, is therefore attractive, but is accompanied by slower electrode reaction kinetics and increased polarization losses. Developing electrodes that maintain sufficient electrochemical activity at reduced temperatures remains a key challenge. Compositional modification and morphology engineering offer complementary approaches to electrode development. Transforming conventional powder-based materials into nanofibrous architectures provides opportunities to modify the available reaction surface and transport pathways. In parallel, *in situ* exsolution of nanoparticles offers a route to surface functionalization with catalytically active species [2,3]. Combining these approaches motivates an investigation of how electrode composition and morphology jointly influence material properties and electrochemical performance, rather than considering either factor in isolation.

This work investigates $Sr_2Fe_{1.5}Mo_{0.5}O_{6-\delta}$ (SFM)-based electrode materials, focusing on A-site nonstoichiometry, morphology, and partial substitution of Fe by Ni. The compositions are described by the nominal formula $Sr_{2-a}Fe_{1.5-x}Ni_xMo_{0.5}O_{6-\delta}$. Materials with nominally stoichiometric and Sr-deficient A-site compositions are compared across different Ni contents, while morphology engineering involves conventional powders and electrospun nanofibers. The comparison addresses both the individual effects of these modifications and their combined influence on electrode behavior.

The material characterization focuses on the relationships between composition, crystal structure, phase composition, oxygen nonstoichiometry, thermal expansion, and electrical conductivity. Particular attention is given to the interplay between compositional changes and microstructural development during thermal processing, including the retention of nanofibrous morphology. The possible role of A-site deficiency and Ni substitution in reduction induced surface modification via *in situ* nanoparticle exsolution is also considered, with emphasis on how powder and nanofiber morphologies may influence this process. The comparison assesses whether Sr deficiency, Ni substitution, and nanofibrous morphology provide individual or combined advantages over the corresponding SFM reference materials. By linking composition and morphology to the electrochemical response, the study aims to identify a favorable balance between structural, thermal, and transport properties and cell-level performance at reduced operating temperatures.

[1] S. Zarabi Golkhatmi, M.I. Asghar, P.D. Lund, A review on solid oxide fuel cell durability: Latest progress, mechanisms, and study tools, Renew. Sustain. Energy Rev. 161 (2022) 112339. https://doi.org/10.1016/j.rser.2022.112339.
[2] K. Kousi, C. Tang, I.S. Metcalfe, D. Neagu, Emergence and future of exsolved materials, Small 17 (2021)

[1] Department of Hydrogen Energy, Faculty of Energy and Fuels, AGH University of Krakow, al. A. Mickiewicza 30, 30-059 Krakow, Poland, *migogacz@agh.edu.pl

2006479. https://doi.org/10.1002/smll.202006479.
[3] Z. Gao, L.V. Mogni, E.C. Miller, J.G. Railsback, S.A. Barnett, A perspective on low-temperature solid oxide fuel cells, Energy Environ. Sci. 9 (2016) 1602–1644. https://doi.org/10.1039/C5EE03858H.

Acknowledgements: This work was funded by the National Science Centre Poland (NCN) under decision number UMO-2025/57/N/ST5/04955. Michał Gogacz acknowledges the financial support of research project supported by the program "Excellence Initiative - Research University" for the AGH University of Krakow.

Effect of Aluminum Content on the Phase Stability, Microstructure and Hardness of $(TiZrHfNbV)_{100-x}Al_x$ Reduced-Activation Complex Concentrated Alloys

Agnieszka Buczkowska-Fertała[1], Amadeusz Łaszcz[1], Michał Biały[1], Mariusz Hasiak[*,1]

Keywords: Reduced-activation complex concentrated alloys, high-entropy alloys, nuclear materials.

ABSTRACT

Reduced-activation complex concentrated alloys (RACCAs) based on refractory elements are promising candidate materials for advanced nuclear energy systems due to their potential irradiation tolerance and the possibility of limiting the formation of long-lived radioactive products [1]. The presence of multiple elements in these alloys enables the control of phase stability and microstructure through appropriate selection of the chemical composition [2-4]. In this study, the effect of Al addition on the phase constitution, microstructure and hardness of $(TiZrHfNbV)_{100-x}Al_x$ alloys (x = 0, 5, 10, 15 and 20 at.%) denoted as Al5-Al20 (Table 1), was investigated to determine the compositional range promoting the formation of a BCC solid solution and limiting the formation of secondary intermetallic phases.

The alloys were synthesized by arc melting of high-purity elements under an argon atmosphere and remelted five times to improve chemical homogeneity. The thermodynamic and empirical parameters (Table 1), including configurational entropy DS_{conf}, mixing enthalpy DHmix, atomic size mismatch d, valence electron concentration (VEC), and the parameter Ω, representing the ratio of entropic to enthalpic contributions were calculated to predict the formation of solid-solution and intermetallic phases. Considering calculated parameters materials were characterized in the as-cast condition using X-ray diffraction (XRD), scanning electron microscopy coupled with energy-dispersive X-ray spectroscopy (SEM/EDS), and Vickers microhardness tester. Phase identification and lattice parameters were determined by Rietveld refinement of the XRD data.

The equiatomic TiZrHfNbV base alloy exhibits a single BCC solid solution with a lattice parameter of 3.355 Å. The single-phase BCC structure is preserved at Al contents of 5 and 10 at.%, with the lattice parameter decreasing to 3.350 and 3.337 Å, respectively. At higher Al contents of 15 and 20 at.%, the BCC lattice parameter further decreases to 3.328 and 3.316 Å, respectively, however a C14-type Laves phase was observed alongside the BCC matrix. SEM observations are in good agreement with XRD analysis (Figure 1). Alloys containing up to 10 at.% Al exhibit a relatively homogeneous microstructure, whereas at 15 and 20 at.% Al, regions with distinct contrast are observed, corresponding to the secondary phase.

The observed phase evolution correlates with changes in the calculated thermodynamic parameters. Increasing Al content results in a progressively more negative mixing enthalpy, from 0.040 kJ/mol for the base alloy to -4.653 kJ/mol for Al20, accompanied by a substantial decrease in the Ω parameter. These changes promote the formation of intermetallic phases, which is consistent with the transition from a single BCC phase to a two-phase BCC+C14 microstructure at higher Al contents.

The structural changes are accompanied by a pronounced increase in microhardness.

[1] Department of Mechanics, Materials and Biomedical Engineering, Wrocław University of Science and Technology, Poland, * mariusz.hasiak@pwr.edu.pl

The base TiZrHfNbV alloy exhibits a hardness of 356±6 HV1. For Al5 and Al10, the hardness increases to 379±6 and 421±4 HV1, respectively, and the single-phase BCC structure is preserved. It demonstrates that the hardness increases with rising Al content within the compositional range corresponding to the single-phase BCC structure. For Al15 and Al20, the hardness further increases to 492±11 and 559±7 HV1, respectively. This behavior coincides with the formation of the C14 Laves phase, suggesting its additional contribution to alloy hardening. Above results indicates that Al content strongly affects the phase stability and hardness of $(TiZrHfNbV)_{100-x}Al_x$ RACCAs. The addition of Al up to 10 at.% preserve the single-phase BCC structure and substantially increase hardness, whereas higher Al contents promote the formation of the C14 Laves phase and further hardening. These results identify a compositional transition between single- and multiphase microstructures and provide a basis for further optimization of TiZrHfNbV-based reduced-activation alloys.

Table 1. Thermodynamic and empirical parameters of RACCAs, where: ΔS_{conf} – configurational entropy of mixing, VEC – valence electron concentration, δ – atomic size mismatch, ΔH_{mix} – enthalpy of mixing, Ω – ratio of entropic to enthalpic contributions.

Alloy	**Short name**	**$DS_{conf}·R^{-1}$ (–)**	**VEC (–)**	***d*** **(%)**	**DH_{mix} (kJ/mol)**	***W*** **(–)**
$Ti_{20}Zr_{20}Hf_{20}Nb_{20}V_{20}$	Al0	1.609	4.400	6.30	0.040	769.935
$Ti_{19}Zr_{19}Hf_{19}Nb_{19}V_{19}Al_5$	Al5	1.727	4.330	6.21	-1.353	23.709
$Ti_{18}Zr_{18}Hf_{18}Nb_{18}V_{18}Al_{10}$	Al10	1.774	4.260	6.12	-2.599	12.281
$Ti_{17}Zr_{17}Hf_{17}Nb_{17}V_{17}Al_{15}$	Al15	1.791	4.190	6.02	-3.669	8.437
$Ti_{16}Zr_{16}Hf_{16}Nb_{16}V_{16}Al_{20}$	Al20	1.788	4.120	5.90	-4.653	6.479

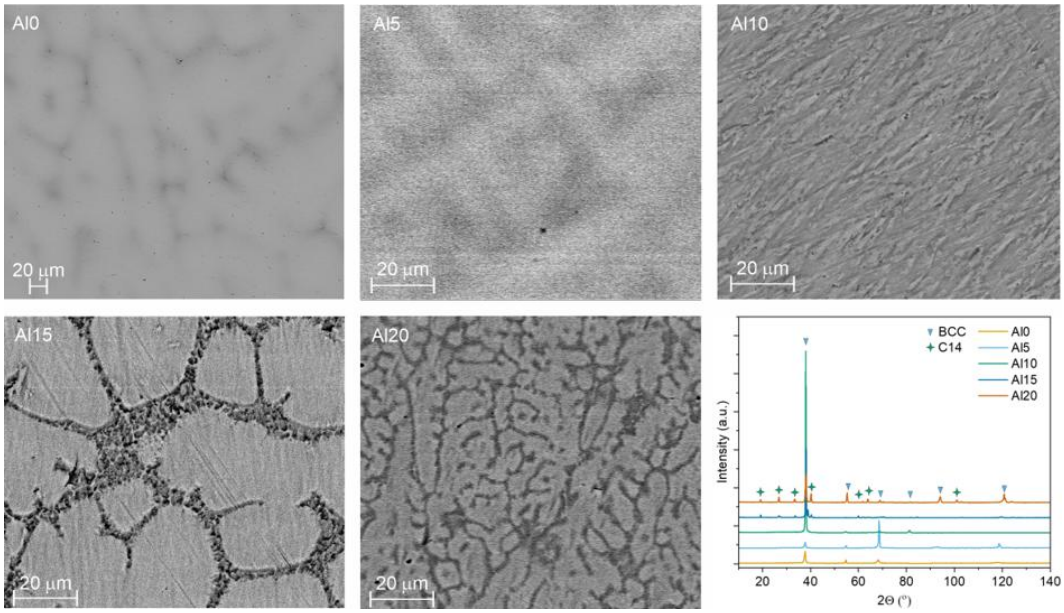


Figure 1. SEM micrographs and XRD patterns of as-cast (TiZrHfNbV)100−xAlx alloys showing microstructural and phase evolution with increasing Al content.

[1] Ayyagari A, Salloom R, Muskeri S and Mukherjee S 2018 Low activation high entropy alloys for next generation nuclear applications. Materialia (Oxf), 4 99–103.
[2] Yeh J.W., Chen S.K., Lin S.J., Gan J.Y., Chin T.S., Shun T.T., Tsau C.H., Chang S.Y. (2004). Nanostructured high-entropy alloys with multiple principal elements: Novel alloy design concepts and outcomes. Advanced Engineering Materials, 6(5), 299–303.
[3] Cantor B., Chang I.T.H., Knight P., Vincent A.J.B. (2004). Microstructural development in equiatomic multicomponent alloys. Materials Science and Engineering: A, 375–377, 213–218.

[4] Senkov O.N., Wilks G.B., Miracle D.B., Chuang C.P., (2010). Refractory high-entropy alloys. Intermetallics, 18(9), 1758–1765.

The work was supported by the project Minigrants for doctoral students of the Wroclaw University of Science and Technology.

From Fabric to Fuel: Pyrolysis and Co-Pyrolysis-Based Valorization of Textile Waste — Energy Properties versus Ecotoxicological Risk

Piotr Plata[1,*], Katarzyna Śpiewak[1], Grzegorz Czerski[1], Faustyna Wierońska-Wiśniewska[1]

Keywords: textile waste, co-pyrolysis, energy recovery, thermochemical recycling ecotoxicity

ABSTRACT

Rising global production of textile fibers (>130 Mt/year), coupled with a negligible fiber-to-fiber recycling rate (<1%), generates a massive waste stream comprising natural, regenerated, and synthetic materials [1]. The fashion sector has been estimated to generate more than 92 Mt of waste annually, much of which is landfilled or incinerated [2]. The diverse chemical composition of textile waste, along with the presence of dyes, finishes, and multifiber blends, limits the effectiveness of mechanical and chemical recycling [3]. These limitations justify further research into alternative management pathways, particularly for blended textiles that cannot be effectively separated. Pyrolysis has been proposed as a route to valorize this difficult-to-manage fraction, transforming the heterogeneous feedstock into a more homogeneous carbon-rich product with higher calorific value, better bulk density, and potentially usable as gasification fuel, sorbent or soil amendment [4,5]. Previous studies have often focused on yield and energy value - a justified priority when assessing fuel potential - yet this should be paired with an evaluation of environmental safety.

This study evaluated whether pyrolysis of four fibers (cotton, viscose, polyester, and acrylic) and their blends (natural–synthetic) in a 50:50 ratio at 400°C and 500°C (5°C/min) improves fuel properties, and to what extent this involves chemical and ecotoxicological risk. The produced chars were characterized by mass yield, CHS ultimate analysis, proximate analysis, EDR/EY ratios, ash composition, and Hg and chlorine content. Preliminary ecotoxicity of aqueous extracts from the five chars with the highest EY was assessed using three bioassays: Microtox® (bacterial bioluminescence inhibition), *Daphnia* (immobilisation), and duckweed (growth inhibition).

The char yield ranged from 20.2% (PET, 400°C) to 59.4% (acrylic, 400°C), and the highest energy efficiency was achieved for acrylic and its blends (EY up to 55.9%). Blends containing PET showed clear synergy - the actual EY exceeded the additive value by 7–9 percentage points (single determinations), whereas at 500 °C the difference did not exceed 2 percentage points, suggesting a possible interaction between PET and cellulose that may be relevant for unsorted waste streams. PET alone increased in EY with rising temperature (24.7%→32.3%), unlike all other materials. Pyrolysis decreased the H content in all materials and increased the C content of cotton, viscose and PET; acrylic showed only minor change in carbon content - likely due to early PAN cyclization [6]. Additionally viscose stood out due to its elevated sulfur content (0,20% and 0.34% at 500°C and 400°C, respectively).

The key finding concerns the trade-off between energy efficiency and safety. Despite their favorable EY, acrylic-containing chars showed the highest ecotoxicological effects: pure acrylic strongly affected all bioassays, while its cellulosic blends were classified as toxic primarily due to their Microtox® responses; cotton and viscose chars remained non-toxic. The toxicity of the acrylic char did not follow its ash content (1.7 wt.% for AC400

[1] Department of Fuel Technology, Faculty of Energy and Fuels, AGH University of Krakow
* pplata@agh.edu.pl

against 2.5–3.5 wt.% for the non-toxic CC400 and VC400) or the composition of the feedstock ash, which was dominated by Ti and showed no obvious enrichment of toxic elements; it is therefore more likely related to water-soluble organic or nitrogen-containing pyrolysis by-products, which are known to form during PAN pyrolysis [7,8]. Additionally, in blends containing cellulose, the Hg content increased with temperature (e.g., cotton + acrylic: 0.59→4.23 µg/kg), whereas in pure PET it decreased - suggesting that higher temperature does not always improve safety despite improving energy performance, as blend interactions may promote retention of inorganic contaminants. These findings show that energy performance alone is insufficient to assess textile-char valorization. Because the composition of real textile waste varies considerably, energy properties, elemental composition, leachability, and ecotoxicity should be evaluated jointly.

[1] Textile Exchange, Materials Market Report 2025, Textile Exchange, 2025. https://textileexchange.org/app/uploads/2025/09/Materials-Market-Report-2025.pdf.
[2] K. Niinimäki, G. Peters, H. Dahlbo, P. Perry, T. Rissanen, A. Gwilt, The environmental price of fast fashion, Nat. Rev. Earth Environ. 1 (2020) 189–200. https://doi.org/10.1038/s43017-020-0039-9.
[3] R.B. Baloyi, O.J. Gbadeyan, B. Sithole, V. Chunilall, Recent advances in recycling technologies for waste textile fabrics: A review, Text. Res. J. 94 (2024) 508–529. https://doi.org/10.1177/00405175231210239.
[4] P. Athanasopoulos, A. Zabaniotou, Post-consumer textile thermochemical recycling to fuels and biocarbon: A critical review, Sci. Total Environ. 834 (2022) 155387. https://doi.org/10.1016/j.scitotenv.2022.155387.
[5] A. Hanoğlu, A. Çay, J. Yanık, Production of biochars from textile fibres through torrefaction and their characterisation, Energy 166 (2019) 664–673. https://doi.org/10.1016/j.energy.2018.10.123.
[6] M.S.A. Rahaman, A.F. Ismail, A. Mustafa, A review of heat treatment on polyacrylonitrile fiber, Polym. Degrad. Stab. 92 (2007) 1421–1432. https://doi.org/10.1016/j.polymdegradstab.2007.03.023.
[7] Y. Tsuchiya, K. Sumi, Thermal decomposition products of polyacrylonitrile, J. Appl. Polym. Sci. 21 (1977) 975–980. https://doi.org/10.1002/app.1977.070210411.
[8] M. Nielsen, P. Jurasek, J. Hayashi, E. Furimsky, Formation of toxic gases during pyrolysis of polyacrylonitrile and nylons, J. Anal. Appl. Pyrolysis 35 (1995) 43–51. https://doi.org/10.1016/0165-2370(95)00898-O.

Iron(III)–ligand complexes as activators of peracetic acid in advanced oxidation processes

Patrycja Zawiślak[1,2]*, Justyna Kapelewska[2], Urszula Kotowska[2]

Keywords: iron complexes, ligand-assisted oxidation, peracetic acid, advanced oxidation processes

ABSTRACT

Microplastics (MPs) are persistent environmental pollutants whose chemical stability and resistance to natural degradation pose significant challenges to their removal. Advanced oxidation processes (AOPs) based on peracetic acid (PAA) are currently being considered as a promising alternative to conventional peroxide-based processes. PAA can be activated by transition metals, including iron, thereby generating reactive species capable of transforming a wide range of organic pollutants. However, the conventional Fe(III)/PAA system is limited by the hydrolysis and precipitation of Fe(III) under near-neutral conditions, which reduces the availability of dissolved iron and thereby limits its catalytic efficiency [1,2]. A potential solution to this limitation is the introduction of organic ligands that modify the coordination environment and redox properties of iron. Ligand complexes can enhance the stability of dissolved Fe(III), influence the Fe(III)/Fe(II) redox cycle, modify PAA activation pathways, and promote the formation of high-valent iron species. Consequently, the choice of ligand should not be viewed merely as a method to prevent iron precipitation, but rather as a means to control the mechanism and selectivity of the oxidation process [3].

Available studies indicate that the effect of complexing agents is strongly dependent on ligand structure and cannot be generalized. It has been demonstrated that picolinic acid (PICA) significantly enhanced the oxidation efficiency of several organic micropollutants—including methylene blue, naproxen, sulfamethoxazole, carbamazepine, trimethoprim, diclofenac, and bisphenol A—in the Fe(III)/PAA system, particularly at higher pH values. Mechanistic studies pointed to the dominant role of high-valent iron species, Fe(IV) and/or Fe(V), rather than classical radical pathways. The same study showed that EDTA, nitrilotriacetic acid (NTA), proline, and nicotinic acid did not enhance micropollutant degradation under the tested conditions. In contrast, 2,6-pyridinedicarboxylic acid resulted in a moderate improvement in process efficiency [4]. These results indicate that the mere presence of a ligand does not guarantee enhanced PAA activation. Different ligands can promote different reaction pathways. Citric acid has been shown to enhance the degradation of oxytetracycline in the Fe(III)/PAA system by complexing Fe(III) and facilitating its reduction to Fe(II). In this instance, hydroxyl and organic radicals played a significant role in the process [5]. Conversely, salicylic acid, when used in the Fe(III)-salicylic acid/PAA system, significantly accelerated the oxidation of bisphenols and extended the effective pH range compared to the ligand-free Fe(III)/PAA system. The study indicated a significant contribution of Fe(IV) species to the oxidation of contaminants [5]. Thus, different ligands can channel iron into distinct catalytic cycles, leading to the formation of various reactive species, ranging from radical-driven processes to oxidation involving highly oxidized iron species (Table 1).

[1] Doctoral School, University of Bialystok, Ciolkowskiego 1K, 15-245 Bialystok, Poland
[2] Laboratory of Environmental Chemistry, Faculty of Chemistry, University of Bialystok, Ciolkowskiego 1K, 15-245 Bialystok, Poland, * p.zawislak@uwb.edu.pl

Table 1. Selected ligands used to enhance Fe-based advanced oxidation processes.

Ligand	Example pollutants	Main function/mechanism
Picolinic acid (PICA)	Organic micropollutants, BPA	Stabilization of Fe(III), promotion of Fe(IV)/Fe(V) species
Citric acid (CA)	Oxytetracycline	Facilitation of the Fe(III)/Fe(II) cycle, involvement of •OH and organic radicals
Salicylic acid (SAc)	Bisphenols	Fe(III) stabilization, extended pH range, significant contribution of Fe(IV)
EDTA, NTA, proline, nicotinic acid	Organic micropollutants	No significant improvement in efficiency in the studied systems

In the context of microplastics, this approach is particularly significant because polymer oxidation occurs within a heterogeneous solid–water system and entails not only the modification of surface functional groups but also the progressive scission of polymer chains, fragmentation, and the conversion of oxidation products into lower-molecular-weight compounds. Research conducted to date on the oxidation of materials such as polystyrene using the Fe(III)/PAA system has demonstrated that the process leads to polymer surface modification, the formation of hydroxyl groups, and the gradual fragmentation of the material's structure. Further studies involve using an Fe(III)-SAc complex as a novel catalytic system to stabilize iron ions in solution and enhance process reactivity. The application of this complex for microplastic degradation has not previously been described. These studies will enable a direct comparison of the efficacy of the conventional Fe(III)/PAA system versus the modified Fe(III)–SAc/PAA system in polystyrene degradation. This will allow for an assessment of how Fe(III) complexation influences the oxidation rate, the degree of polymer surface oxidation, particle fragmentation, and the mineralization of degradation products. The results obtained will provide valuable insights into the role of highly oxidized iron species in the depolymerization and oxidative aging processes of plastics.

[1] K. Rizwan, M. Bilal, Developments in advanced oxidation processes for removal of microplastics from aqueous matrices, Environ. Sci. Pollut. Res. 29 (2022) 86933–86953. https://doi.org/10.1007/s11356-022-23545-0.
[2] C. Shi, C. Li, Y. Wang, J. Guo, S. Barry, Y. Zhang, N. Marmier, Review of advanced oxidation processes based on peracetic acid for organic pollutants, Water 14 (2022) 2309. https://doi.org/10.3390/w14152309.
[3] A.K.N. Souza, J. Paggiaro, W.S. Martins, A.K.S. Pereira, D.H. Pereira, G.S. Cavallini, Theoretical–experimental evaluation of the effects of Fe3+ ions in the disinfection of water supply by peracetic acid, Discov. Water 4 (2024) 70. https://doi.org/10.1007/s43832-024-00126-5.
[4] J. Kim, J. Wang, D.C. Ashley, V.K. Sharma, C.-H. Huang, Enhanced degradation of micropollutants in a peracetic acid–Fe(III) system with picolinic acid, Environ. Sci. Technol. 56 (2022) 4437–4446. https://doi.org/10.1021/acs.est.1c08311.
[5] D. Kiejza, J. Karpińska, A. Leszczyńska, E. Olchowik-Grabarek, K. Makarova, U. Kotowska, Acceleration of the bisphenols oxidation in the Fe(III)/peracetic acid system with salicylic acid, J. Mol. Liq. 411 (2024) 125697. https://doi.org/10.1016/j.molliq.2024.125697.

EFE2026 ENERGY FUELS ENVIRONMENT
INTERNATIONAL CONFERENCE
17-20 NOVEMBER 2026, KRAKÓW, POLAND

Numerical Investigation of Aluminum Metal Foam Integration in a Sand-Based Thermal Energy Storage System

Homa Maksymilian[1], *, Sornek Krzysztof[1], Sergio Nardini[2], Bernardo Buonomo[2], Hala Salhab[2]

Keywords: energy storage, CFD, RES, sand, TES

ABSTRACT

The increasing share of renewable energy sources in modern energy systems creates a growing demand for efficient and cost-effective energy storage technologies. One promising solution is thermal energy storage using sand beds, which offer low material cost, high availability, and the ability to operate at elevated temperatures. However, a major limitation of sand-based storage systems is the relatively low thermal conductivity of sand, which can lead to significant temperature gradients within the bed and consequently prolong the charging and discharging processes.

This study investigates the possibility of enhancing heat transfer in a sand-based thermal energy storage system by incorporating aluminum porous metal foam structures (Fig. 1).

The research was based on numerical simulations performed in the ANSYS Workbench environment. The developed numerical model was validated against experimental results, providing a basis for the subsequent comparative analysis. The analyzed storage unit is equipped with an internal tubular heat exchanger, in which air, heated by electric heaters is used as the heat transfer fluid. The experimental setup is shown in Figure 2. A comparative analysis was performed for three different metal foam configurations: a solid cylindrical insert located in the central region of the storage bed, a cylindrical insert with an axial hollow channel, and a metal foam layer surrounding the tubular heat exchanger (Fig. 3). Throughout the analyses, dimensions of metal foam sections were changed in the search of optimum amount of metal foam used. The performance of these configurations was compared with a reference case consisting of a sand bed without metal foam.

The following key output parameters were selected for analysis: the charging and discharging times of the storage and the amount of energy stored during the analysis. The results demonstrated that the application of aluminum metal foam can significantly enhance heat transfer within the storage medium. Depending on the considered configuration, the charging and discharging times were reduced by up to approximately 50% compared with the reference case. Furthermore, the use of metal foam increased the amount of energy that could be stored by approximately 30%. In addition, it was observed that different approaches to positioning the metal foam within the bed result in a progressively smaller amount of metal foam required to achieve similar results (Fig. 4). These findings indicate that appropriately designed porous metallic structures can provide an effective method for improving heat transfer and enhancing the overall performance of high-temperature sand-based thermal energy storage systems.

[1] AGH University of Krakow, Faculty of Energy and Fuels, Department of Sustainable Energy Development, Krakow, Poland, * maksymilian.homa@agh.edu.pl
[2] Università degli Studi della Campania Luigi Vanvitelli, Department of Engineering, Aversa, Italy

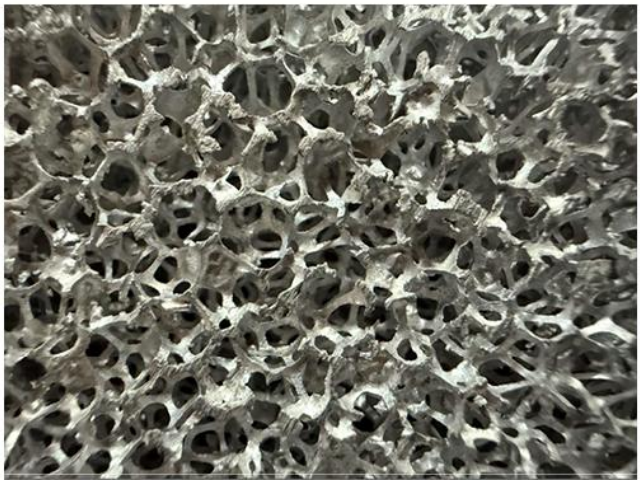


Figure 1. Porous structure of aluminum



Figure 2. Half-filled sand bed with heat

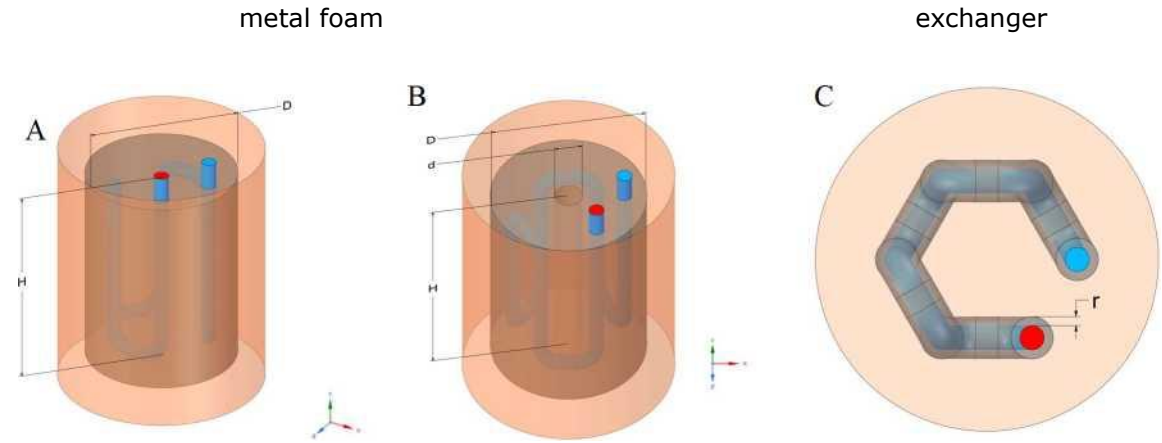


Figure. 3. Presentation of various variant analyses. A - metal foam cylinder, B - hollowed metal foam cylinder, C - metal foam jacket on the heat exchanger tubing. D [m] - diameter of the cylinder cross-section, d [m] - diameter of the hollow section, H [m] - height of the cylinder, r [m] - thickness of the layer on the tubing.

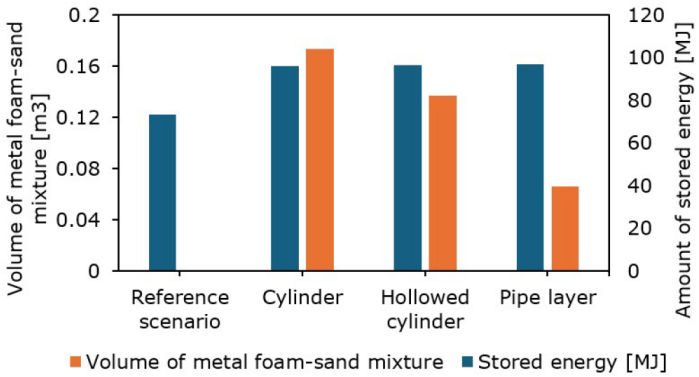


Figure 4. A comparison of the required volume of metal foam to the amount of stored energy for the best variant from each analysis and for the reference configuration.

EFE2026 ENERGY FUELS ENVIRONMENT
INTERNATIONAL CONFERENCE
17-20 NOVEMBER 2026, KRAKÓW, POLAND

Long-Term Transformation of Energy Demand in Poland's Service Sector to 2050

Marcin Pluta[1,*], Artur Wyrwa[1], Maciej Raczyński[1], Janusz Zyśk[1], Patrycja Rzeszut[1]

Keywords: service sector, energy demand, energy system modelling, electrification, decarbonisation

ABSTRACT

The service sector is an important component of long-term energy transition analysis because it combines building-related thermal demand with rapidly changing electricity uses and heterogeneous activity drivers. Using the TIMES model generator, this study develops a detailed bottom-up representation of energy use in the Polish service sector and analyses its transformation to 2050. Seven subsectors are distinguished: healthcare, hotels and restaurants, sport and recreation, large and small retail, offices, and education. Energy demand is represented separately for space heating, water heating, cooking and space cooling, as well as for non-thermal electricity uses including ICT and multimedia, building lighting, commercial refrigeration, other building technologies, street lighting, and ventilation. Such a structure makes it possible to capture differences in activity levels, energy-service intensities and energy carrier use across service activities rather than treating the service sector as a single aggregated category.

The model is calibrated to 2024 using a combination of Eurostat energy statistics, GUS data on useful floor area by building category, and JRC-IDEES information on end-use structure and electricity-use characteristics [1-3]. The total useful floor area represented in the base year amounts to about 456.5 million m². The calibrated demand includes approximately 193.8 PJ of useful energy for thermal processes and 76.8 PJ of non-thermal electricity use. For building-related thermal services, useful energy demand is determined by activity and service intensity, with useful floor area acting as the main activity driver. Long-term projections differentiate the development of individual subsectors and include updated floor-area trajectories and changes in energy-service intensities. Fuel and technology shares evolve over time to reflect increasing electrification, renewable heat deployment and the gradual phase-out of more carbon-intensive energy carriers. Thermal and non-thermal uses are modelled separately, allowing their distinct demand drivers and transition patterns to be represented consistently.

The results indicate a substantial transformation of the service-sector energy balance by 2050. Space-heating demand declines markedly despite changes in sector activity, while electricity-based technologies gain importance and fossil fuel use decreases. Coal is ultimately phased out from both space and water heating, while water-heating demand changes more moderately, with an increasing contribution from electricity, district heat and solar energy. Cooling demand grows over the projection period and remains almost entirely electrified. Cooking shows a gradual shift from natural gas and LPG towards electricity. Aggregate non-thermal electricity demand remains relatively stable, although its internal structure changes considerably: electricity use for building and street lighting declines, whereas demand associated with ICT, commercial refrigeration, ventilation and other building-related applications increases. The results therefore indicate that relatively stable aggregate electricity demand may coexist with pronounced changes in the composition of end uses.

The analysis demonstrates the importance of representing the service sector at the

[1] Faculty of Energy and Fuels, AGH University of Krakow, 30-059 Kraków, Poland.*mpluta@agh.edu.pl

level of individual subsectors and energy services. Changes in useful floor area, activity levels, service intensities and fuel structure jointly determine the long-term evolution of energy demand. The adopted approach also makes it possible to distinguish the effects of structural change in the sector from changes in the intensity and composition of energy use. The developed framework provides a consistent basis for analysing electrification, fuel substitution and changing energy-use patterns in the Polish service sector to 2050. In a subsequent stage, the service-sector module can be integrated with the full TIMES-PL energy system model, enabling assessment of interactions between service-sector demand and the transformation of the wider Polish energy system.

[1] European Commission, Joint Research Centre (JRC), JRC-IDEES-2023: Integrated Database of the European Energy System, JRC Data Catalogue, 2025. https://doi.org/10.2905/JRC.JPXYRT8.
[2] Główny Urząd Statystyczny (GUS), Efekty działalności budowlanej w 2024 r., GUS, Warszawa–Lublin, 2025. https://stat.gov.pl/files/gfx/portalinformacyjny/pl/defaultaktualnosci/5478/3/20/1/efekty_dzialalnosci_budowlanej_2024.pdf.
[3] Eurostat, Services energy consumption by NACE Rev. 2 activity – quantities (nrg_d_serq_n) and Simplified energy balances (nrg_bal_s), Eurostat Database, 2026. https://ec.europa.eu/eurostat/databrowser/view/nrg_d_serq_n/default/table?lang=en; https://doi.org/10.2908/nrg_bal_s.

From Marine Plastic Inventories to Valorisation Feedstock: Assessing the MPW Resource Base within the CUPOLA Project

Aleksandra Hudek-Pietras[1],*, Bartłomiej Kowal[2], Konrad Perzyński[2], Wenzhong Liu[3],Mariusz Wądrzyk[1], Marek Lewandowski[1], Aneta Magdziarz[2]

Keywords: marine plastic waste, valorisation, waste characterisation, plastic recycling, CUPOLA

ABSTRACT

Marine plastic waste (MPW) represents a highly heterogeneous material stream whose potential for recycling and valorisation depends not only on the quantity of plastic present in the marine environment, but also on its origin, polymer composition, physical form, condition and accessibility for collection. Assessing this potential is particularly challenging because available quantitative estimates are based on different system boundaries, source pathways, particle-size ranges and modelling approaches. Consequently, reported quantities of marine plastic cannot always be directly compared or translated into the amount of material potentially available as a secondary resource.

This study was conducted within the CUPOLA - Carbon-neutral Pathways of Recycling Marine Plastic Waste project, which investigates sustainable approaches to the characterisation, sorting, pre-treatment and conversion of MPW into value-added materials. The aim of the present work is to characterise the MPW resource base relevant to subsequent processing, with particular attention to polyethylene terephthalate (PET), polyolefins (PO) and polyamides (PA). Scientific and technical literature was critically analysed with regard to plastic inputs to seas and oceans, accumulated stocks, source pathways, environmental compartments, waste forms, regional variability and polymer composition. Particular attention was given to the comparability of available data and to the distinction between the total quantity of plastic present in the marine environment and the fraction that may realistically constitute a recoverable feedstock.

The analysis highlights substantial differences between published estimates of plastic entering the marine environment. For example, annual inputs of approximately 0.5 Mt/y have been reported for riverine export of macro- and microplastics [1], whereas a broader mass-balance assessment estimated land-to-sea transfer at approximately 17 Mt/y [2]. These values should not be interpreted as directly comparable lower and upper estimates of the same quantity. They reflect different system definitions, pathways, particle-size ranges and assumptions, illustrating the difficulty of deriving a single estimate of the MPW resource potentially available for valorisation. A similar distinction applies to accumulated marine plastic stocks, since material present in different environmental compartments varies considerably in its accessibility for collection. Thus, the environmental inventory of marine plastic does not directly represent the amount of material that can be supplied to recycling or conversion processes.

[1]AGH University of Krakow, Faculty of Energy and Fuels, Department of Fuel Technology, al. A. Mickiewicza 30, 30-059 Krakow, Poland, * hudek@agh.edu.pl
[2]AGH University of Krakow, Faculty of Metals Engineering and Industrial Computer Science, Department of Heat Engineering and Environment Protection, al. A. Mickiewicza 30, 30-059 Krakow, Poland
[3]Department of Measurement Science and Instruments, School of Artificial Intelligence and Automation, Huazhong University of Science and Technology, 1037 Luoyu Road, Wuhan, Hubei 430074, China

The potential use of MPW as a feedstock is additionally influenced by its source and composition. Land-derived streams include consumer and packaging waste that may contain PET- and polyolefin-rich fractions, while other sources may generate substantially different material profiles. Transport and residence in marine and coastal environments can further modify the physical form and condition of plastics through fragmentation, weathering, biofouling and mixing with other materials. Geographic and seasonal variability may also affect the composition of collected waste. These factors influence the requirements for sorting and pre-treatment and should be considered when defining representative MPW streams for further processing.

By integrating quantitative information with waste characteristics and accessibility considerations, the study provides a basis for a more realistic assessment of the MPW resource base. This framework can support the selection of representative feedstocks within the CUPOLA project and contribute to a more robust evaluation of available MPW management and valorisation technologies by linking technological assessment to the characteristics and potential availability of the material to be processed.

[1] M. Strokal, P. Vriend, M.P. Bak, C. Kroeze, J. van Wijnen, T. van Emmerik, River export of macro- and microplastics to seas by sources worldwide, Nat. Commun. 14 (2023) 4842. https://doi.org/10.1038/s41467-023-40501-9.
[2] J.E. Sonke, A. Koenig, T. Segur, N. Yakovenko, Global environmental plastic dispersal under OECD policy scenarios toward 2060, Sci. Adv. 11 (2025) eadu2396. https://doi.org/10.1126/sciadv.adu2396.

Acknowledgements: This work was carried out within the CUPOLA project — *Carbon-neutral pathways of recycling marine plastic waste.* The project has received funding from the European Union under the HORIZON TMA MSCA Staff Exchanges programme (HORIZON-MSCA-2021-SE- 01), Grant Agreement No. 101086071. Support was also provided by the Ministry of Science and Higher Education in Poland through the programme "PMW", grant No. 5863/HE/2024/2 (No. W52/HE/2024). The authors also acknowledge Huazhong University of Science and Technology (HUST) for facilitating international scientific cooperation and knowledge exchange within the scope of the CUPOLA project.

EFE2026 ENERGY FUELS ENVIRONMENT
INTERNATIONAL CONFERENCE
17-20 NOVEMBER 2026, KRAKÓW, POLAND

Application of Design of Experiments (DoE) to methanation process design

Marek Inger[1,*], Karolina Grzęda[2], Agnieszka Dobrzyńska-Inger[2], Bogdan Samojeden[1]

Keywords: Design of Experiments, response surface methodology methanation, SNG

ABSTRACT

The catalytic methanation of carbon dioxide using green hydrogen, enabling the production of synthetic natural gas (SNG) within Power-to-Gas (PtG) systems [1]. A significant technological challenge of this process is its highly exothermic nature (ΔH^o = -165 kJ/mol). The released reaction heat increases the temperature of the reaction mixture, which can lead to thermal deactivation of the catalyst (e.g., through sintering of the active phase) and decrease the equilibrium conversion of carbon dioxide to methane. To address this, efficient heat removal is crucial. In the analyzed system, evaporative cooling was implemented, utilizing the reaction heat to generate saturated steam, thereby combining reactor temperature control with effective energy recovery.

This study presents the results of methanation process simulations conducted using CHEMCAD software. The effects of key operating parameters were investigated, including reaction temperature, operating pressure, and molar ratio of the substrates. The evaluated output variables were methane yield, the mass flow rate of the generated saturated steam, and the maximum temperature in the nickel catalyst bed [2].

Based on the simulation data, second-order regression models describing the process performance were developed using Design-Expert software. The statistical significance of the models and their components was verified via analysis of variance (ANOVA). The application of Design of Experiments (DoE) methodologies allowed for a precise evaluation of the interactions between the parameters. This procedure is adopted for the analysis of the methanation process [3].

Finally, a multi-criteria optimization was performed to determine the optimal operating conditions. The results indicated that a high methane yield could be achieved while maintaining the catalyst bed temperature below 500°C, effectively mitigating the risk of thermal degradation of the catalyst. The findings enhance the understanding of the relationships between operating parameters and methanation efficiency, providing a valuable foundation for parameter selection, design, and scaling of methanation reactor.

[1] C. Bassano, P. Deiana, L. Lietti, C.G. Visconti, P2G movable modular plant operation on synthetic methane production from CO2 and hydrogen from renewables sources, Fuel 253 (2019) 1071–1079. https://doi.org/10.1016/j.fuel.2019.05.074.
[2] E. Mancusi, P. Bareschino, A. Forgione, C. Tregambi, F. Pepe, CO2 methanation: Reactor modelling and parametric analysis, Comput. Aided Chem. Eng. 50 (2021) 585–590. https://doi.org/10.1016/B978-0-323-88506-5.50093-0.
[3] N.N. Zulkefli, W.M. Wan Ramli, N. Muda, R.M. Jais, A.L. Omar, M.Z. Muda, M.A. Phang, M.S. Ahmad Fauzi, K. Mazlan, J. Adv. Res. Appl. Sci. Eng. Technol. 56 (2026) 68–79.

Acknowledgments: This work was carried out under an IDUB subsidiary – Action 21, Application 18209

[1] Faculty of Energy and Fuels, AGH University of Krakow, Poland, * inger@agh.edu.pl
[2] Łukasiewicz – New Chemical Syntheses Instutute, Puławy, Poland

Innovative Two-Stage Blast Furnace Gas Cleaning Technology Implemented at Blast Furnace no 2 in ArcelorMittal Poland Dąbrowa Górnicza Plant

Marianna Czaplicka[1], Marian Niesler[2], Arkadiusz Ryfa[3], Michał Kocot[4,*]

Keywords: blast furnace, numerical model, CFD, waste reduction, noise reduction, energy recovery, energy efficiency

ABSTRACT

Paper presents the development of an innovative two-stage blast furnace gas cleaning technology aimed at minimization of the amount of waste generated in the form of sludge, increasing the degree of dust recycling and allows for further energy utilization of blast furnace gas.

The technology consists of a cyclone separator and a wet scrubber. Designed modern cyclone separator is tailored to catch as much iron and coal in dust while keeping the zinc and lead at low level, so that dust can be reverted to blast furnace. The efficiency of a cyclone separator is above 90%. Second part of an installation is a wet scrubber enabling most efficient gas cleaning process with reduced water consumption and reduced noise emissions. Both devices were designed with the use of numerical modelling. Developed models were validated with experimental data in laboratory and full industrial scale.

Such system will be available for the first time in Polish blast furnaces. The result of the project is a demonstration technology that has a positive impact on the environment through a cleaner production process of hot metal while recovering the energy of blast furnace gas pressure. As a result, the following benefits are to be obtained: firstly reduce the amount of waste generated in the form of sludge, and secondly, increase energy efficiency blast furnace process.

[1] Institute of Environmental Engineering of the Polish Academy of Sciences in Zabrze, Poland
[2] Upper Silesian Institute of Technology, Poland
[3] Silesian University of Technology, Poland
[4] ArcelorMittal Poland, * michal.kocot@arcelormittal.com

Hybrid Bio-Coke: A Route Towards Renewable Carbon Use for Blast Furnace Ironmaking

Michał Rejdak[1,*], Anna Rodź[1], Aneta Michałek[1], Małgorzata Wojtaszek-Kalaitzidi[1], Bartosz Mertas[1], Leszek Grudziński[2], Serhat Türkyılmaz[3], Erdal Ünal[3]

Keywords: biocarbon, biochar, coke, biocoke, decarbonization

ABSTRACT

The blast furnace–basic oxygen furnace route continues to be the principal route for crude steel production worldwide and remains strongly dependent on metallurgical coke, which acts as a fuel, reducing agent and structural support ensuring gas permeability within the blast furnace. The BioCoke4BF project aims to decrease the consumption of fossil carbon through the development of hybrid bio-coke produced from coking coal and biochar used as a renewable carbon component.

The proposed approach is based on the partial replacement of coking coal with biochar derived from woody and waste biomass, followed by carbonization under conditions representative of conventional coke production. This presentation summarizes the current research activities focused on assessing how biochar origin, addition rate and feedstock preparation influence the quality and performance of the resulting hybrid bio-coke.

Laboratory carbonization trials were performed in a 4 kg Karbotest furnace using two different biochars introduced at levels of 3, 6 and 9% (Fig. 1). The biochars were added either directly in loose form or incorporated into partially briquetted coal blends. The produced bio-cokes were characterized in terms of CO_2 reactivity (CRI), coke strength after reaction (CSR) and optical texture.

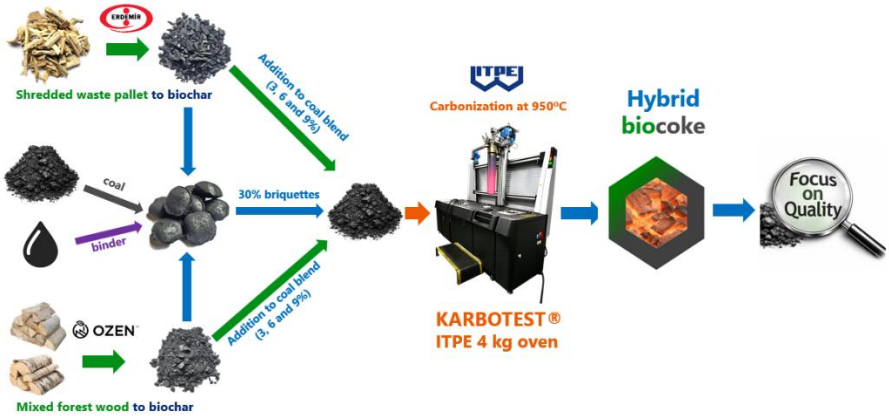


Figure 1. Graphical representation of BioCoke4BF research procedure in bench-scale.

The results confirm that biochar can be successfully incorporated into the coke structure, although its effect on coke quality depends strongly on both the addition level and the method of blend preparation. Partial briquetting was found to improve the ability to retain properties comparable with those of conventional metallurgical coke. The results obtained so far indicate that this approach may enable the substitution of approximately

[1] ITPE – Institute of Energy and Fuel Processing Technology, Zabrze, Poland, *mrejdak@itpe.pl
[2] OZEN sp. Z o.o., Wałcz, Poland
[3] Erdemir, Karadeniz Ereğli, Turkey

5–7% of the fossil carbon feed with biochar while maintaining hybrid bio-coke properties compatible with blast furnace requirements (Fig.2).

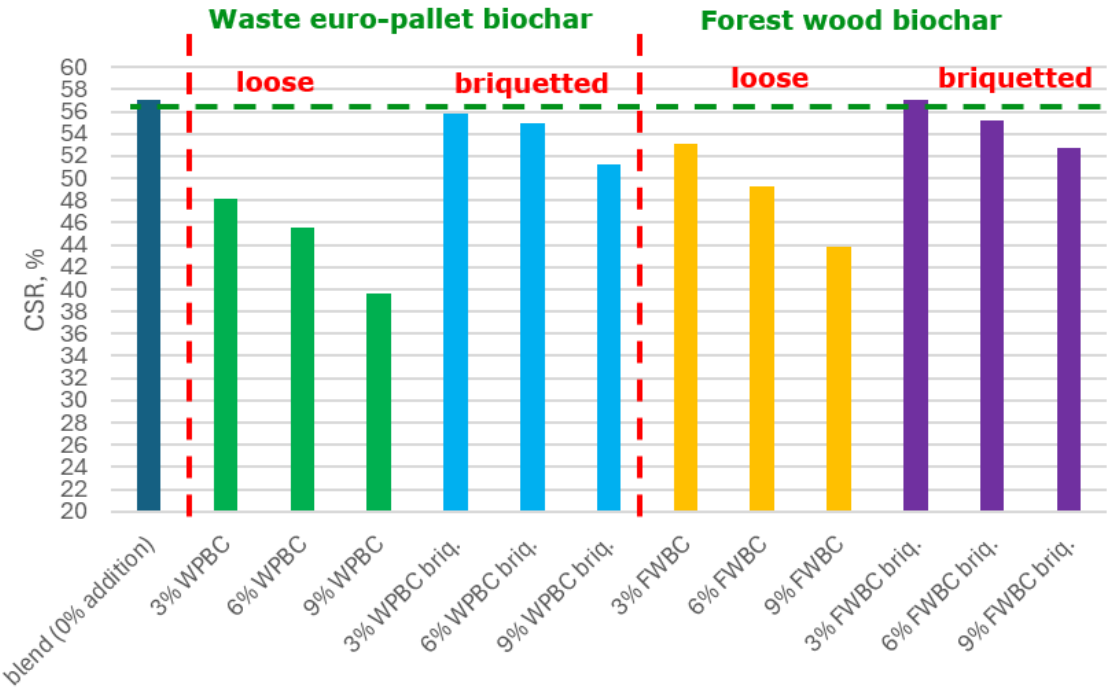


Figure 2. The results of CSR results of hybrid bio-cokes produced.

Acknowledgement

The project is co-funded by the National Centre for Research and Development under the 6th call for proposals for joint bilateral projects within the framework of Polish-Turkish cooperation. Contract number: POLTUR/2024/39/Biocoke4BF/2025.

Optimization of Infiltration Strategies for Enhanced Stability of Solid Oxide Electrolysis Cells Under SOE and Co-SOE Operation

Anna Niemczyk-Sobieszek[1,2,*], Julia Jeżewska[1], Alicja Lubańska[1], Krystian Machaj[1,2], Stanisław Szumowski[1]

Keywords: solid oxide electrolysis, co-eletrolysis, degradation, electrode infiltration, Ni-YSZ

ABSTRACT

Solid oxide electrolysers (SOE) are among the most promising technologies for efficient hydrogen and syngas production. However, their widespread implementation is still limited by progressive degradation phenomena occurring during long-term operation, particularly within the fuel electrode. Microstructural evolution of the Ni-based electrode, including nickel coarsening, loss of active triple-phase boundaries, redox instability, and increased susceptibility to carbon-related degradation under co-electrolysis conditions, may significantly reduce cell lifetime. Therefore, the development of effective electrode modification strategies capable of improving both electrochemical performance and durability remains a key research challenge.

This work presents recent advances in fuel-electrode engineering conducted at the Institute of Power Engineering – National Research Institute. Particular emphasis was placed on the optimization of infiltration methodology and the development of tailored ceria-based infiltrates dedicated to SOE and co-SOE applications. The study included preparation of precursor solutions, optimization of solvent composition, infiltration and calcination protocols aimed at ensuring homogeneous catalyst distribution throughout the electrode volume.

Two groups of modifiers were investigated. The first consisted of CeO_2-based formulations doped with transition metals (Ni, Fe and Cu) the second group comprised ceria modified with alkaline-earth elements (Ca, Sr and Ba), both, designed to improve catalytic activity, influence surface chemistry, electrode reactivity and resistance to degradation processes. The developed infiltration procedures were applied to anode-supported SOC architectures with Ni-YSZ as a fuel electrode. The modified electrodes were extensively characterized using SEM, SEM-EDS, XRD, current-voltage measurements and electrochemical impedance spectroscopy under both steam electrolysis and co-electrolysis operating conditions. The investigations demonstrated that infiltration effectiveness strongly depends on the chemical composition of the modifier. Optimized infiltration procedures enabled uniform distribution of catalytic phases within the porous electrode while minimizing pore blockage and preserving gas transport pathways.

Electrochemical testing revealed reduced polarization resistance and improved performance for selected infiltrated cells compared with non-modified references. Post-test microstructural analyses indicated improved preservation of electrode morphology and reduced evidence of microstructural degradation after operation. Furthermore, the influence of fuel-electrode modification on operational stability under carbon-prone co-electrolysis conditions was evaluated using a gas mixture containing 45% CO_2, 45% H_2O and 10% H_2 at 680°C. While thermodynamic calculations predicted a carbon-deposition threshold corresponding to approximately 7.4 A, all tested cells remained operational above this boundary. The most effective modification extended stable operation to current

[1] Institute of Power Engineering – National Research Institute, Mory 8, 01-330 Warsaw, Poland
[2] Center for Hydrogen Technologies CTH2, Institute of Power Engineering – National Research Institute, Augustówka 36, 02-981 Warsaw, Poland, * anna.niemczyk@ien.com.pl

loads exceeding 11 A, whereas the reference cell exhibited a noticeable increase in degradation rate at approximately 9.3 A. Simultaneous voltage monitoring and outlet-gas analysis demonstrated that changes in degradation behaviour were closely correlated with shifts in reaction pathways occurring at high conversion levels.

The results confirm that both infiltration chemistry and process optimization play a crucial role in determining the long-term behaviour of SOC fuel electrodes. The developed modification strategies provide a promising route towards enhanced durability and wider operating windows for next-generation SOEC and co-SOEC systems dedicated to efficient hydrogen and syngas production.

Acknowledgments: The research are financially supported by the National Science Center, Poland within the no. 2023/51/D/ST11/01792.

EFE2026 ENERGY FUELS ENVIRONMENT
INTERNATIONAL CONFERENCE
17-20 NOVEMBER 2026, KRAKÓW, POLAND

Voltage Assessment During Faults Occurring in the Vicinity of Photovoltaic Power Plants

Flaviu Mihai Frigura-Iliasa[1,2], Krzysztof Sornek[3], Mihaela Frigura-Iliasa[1], Doru Vatau[1]

Keywords: Voltage Assessment, Power Faults, Photovoltaic Plants

ABSTRACT

In the event of polyphase or three-phase faults occurring near power sources from photovoltaic (PV) installations, it is observed that the residual voltage can reach levels capable of sustaining an electric arc at the fault location, even after the distribution substation circuit breaker has tripped on the line where the renewable energy generation facility is connected. This observation highlights a significant challenge in integrating photovoltaic systems into electrical distribution grids. Residual voltage—the voltage that persists after a fault occurs and the distribution line circuit breaker trips—can sustain a dangerous electric arc, potentially causing fires or damaging equipment.

The integration of high-capacity photovoltaic (PV) systems can affect line voltage in several ways. Voltage rise and voltage variations caused by fluctuations in solar output are two of the most significant and potentially problematic impacts of integrating large-scale PV generation capacity into the grid.

These effects are particularly pronounced when large amounts of PV power are connected near the end of long, lightly loaded lines. The active and reactive power output of the PV system can influence the circuit's voltage equilibrium, while increases and decreases in PV generation can lead to voltage fluctuations along the circuit.

This paper presents some measured waveforms and simulations concerning some overvoltage faults and overloading incidents occurring near a real PV plant.

[1] POLITEHNICA University, Timisoara, Romania, flaviu.frigura@upt.ro, mihaela.frigura@upt.ro
[2] National Institute for Research and Development in Electrochemistry and Condensed Matter, Timisoara, Romania
[3] AGH University of Krakow, Krakow, Poland, ksornek@agh.edu.pl

Design and Fabrication of MXene-Based Micro-Supercapacitors

Haibo Hu[1]

Keywords: Micro-Redox Capacitors; MXene; Energy Density; Power Output Stability

ABSTRACT

The rapid advancement of wearable electronics has driven the demand for monolithically integrated micro power sources combining mechanical flexibility and high energy density. Accordingly, micro-supercapacitors with outstanding rechargeable cycling performance and high power density are gaining increasing importance for powering flexible wearable devices. Nevertheless, their low energy density and unstable power output severely restrict the practical deployment of most supercapacitor systems in flexible wearable power supplies. In this report, I will present my group's preliminary explorations over the past three years on new systems of MXene-based micro-supercapacitors with high energy density. Special focus is placed on the design and construction of novel micro-redox capacitor device systems that simultaneously deliver high energy density and stable power output. Featuring excellent safety, high energy density and robust power output stability, the newly developed MXene-based micro-redox capacitors hold great promise for applications in flexible wearable power supply systems.

[1] School of Materials Science and Engineering, Anhui University, Hefei 230601, P. R. China; haibohu@ahu.edu.cn

EFE2026 ENERGY FUELS ENVIRONMENT
INTERNATIONAL CONFERENCE
17-20 NOVEMBER 2026, KRAKÓW, POLAND

Enhancing Metaheuristic Energy Management Systems with LargeLanguage Models for Smart Grid Optimization

Jakub Grela[1],*, Dominik Latoń

Keywords: Energy Management System, Large Language Models, Smart Grid, Metaheuristic Optimization, Battery Energy Storage System

ABSTRACT

The massive integration of Renewable Energy Sources (RES) has introduced unprecedented volatility into Wholesale electricity markets. In Day-Ahead Markets (DAM), peak solar and wind production frequently creates severe supply-demand imbalances, leading to negative electricity prices. Consequently, commercial prosumers operating behind-the-meter Photovoltaic (PV) installations and Battery Energy Storage Systems (BESS) require agile Energy Management Systems (EMS). Traditional optimization methodologies based on Model Predictive Control (MPC) and metaheuristics such as Genetic Algorithms (GA) and Particle Swarm Optimization (PSO) excel at handling non-linear hardware constraints. However, conventional numerical solvers are fundamentally market-unaware. Confined to rigid penalty formulations and local search, they struggle to capture broader market contexts, frequently falling into suboptimal local minima, suffering economic penalties, or inducing detrimental battery micro-cycling.

To address these limitations, this paper proposes an edge-deployed hybrid EMS architecture integrating a GA-PSO optimizer with a Large Language Model (LLM) serving as a cognitive supervisory layer. In this cascaded framework (Figure 1), the GA-PSO algorithm first synthesizes a physically feasible baseline schedule governing BESS charging/discharging trajectories across a rolling 33-hour horizon. This baseline is subsequently evaluated and refined by a locally hosted, quantized LLM (Qwen-3.6-35b running via Ollama, orchestrated by LangChain and Apache Airflow). By translating complex techno-economic guidelines into structured prompt rules, the supervisory layer enforces strategic market behaviors: (i) mitigating cell degradation by restricting operation to a maximum of two full cycles per day; (ii) proactive State of Charge (SoC) management by discharging the BESS during pre-valley peak prices to maximize absorption during negative price events; (iii) dynamic PV curtailment flags (cut_pv) to prevent injection penalties; and (iv) strict compliance with Point of Common Coupling (PCC) throughput limits.

The proposed architecture was empirically validated using a seven-month operational dataset (April 1 to October 31) from an active commercial facility equipped with a 60 kWp rooftop PV array and a 100 kWh / 50 kW lithium-ion BESS. Deep learning models (LSTM in PyTorch) provided 15-minute resolution forecasts of solar generation and facility load. Three control strategies were evaluated: a fixed schedule, standalone GA-PSO, and the proposed hybrid system. Under a realistic 50 kW grid connection limit, a competitive 'Tournament Mode' with a physical hardware simulator and median-price residual SoC valuation was implemented to ensure robust convergence and eliminate myopic end-of-day battery depletion.

As presented in Table 1, the proposed cognitive tournament architecture achieved superior economic performance, reducing total electricity expenses to 22,799.40 EUR, representing a 10.6% cost reduction compared to the baseline (25,503.80 EUR) and outperforming standalone GA-PSO (24,473.81 EUR). In an unconstrained grid configuration, the LLM supervisory control achieved a net negative operational balance in June (-335.23 EUR), converting power consumption into financial profit during extreme negative price events. Trajectory analysis showed that the cognitive layer eliminated

erratic micro-cycling, producing smooth operations that preserve battery State of Health (SoH). The findings prove that integrating generative AI reasoning within edge EMS provides a robust, scalable paradigm for smart grid optimization in volatile renewable-dominated markets.

Table 1. Monthly operational electricity costs [EUR] under a 50 kW grid connection limit

Month	Fixed schedule	GA-PSO	Tournament mode (LLM)
April	2,940.38	3,427.09	3,125.37
May	3,198.85	2,635.10	2,319.95
June	1,407.70	775.57	197.79
July	3,444.62	2,688.51	3,006.63
August	2,155.32	2,260.13	1,721.51
September	2,668.23	3,549.38	3,303.95
October	9,689.19	9,137.10	9,124.19
Total	**25,503.80**	**24,473.81**	**22,799.40**

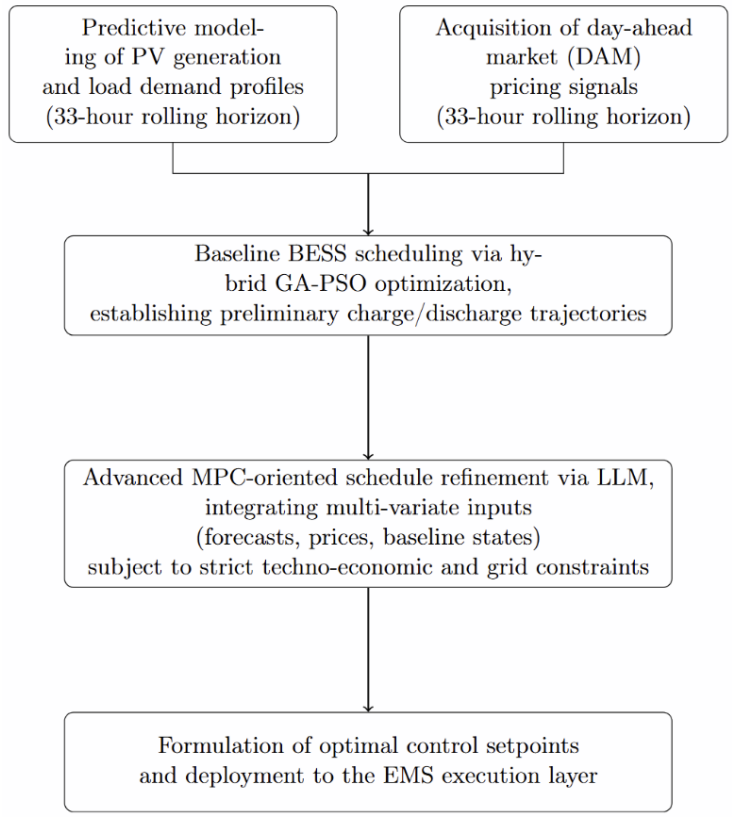


Figure 1. Architecture of the proposed hybrid GA-PSO and cognitive LLM Energy Management System

From Photovoltaic Generation to Battery Storage: The Power System of a Solar Racing Boat

Natalia Gałaś[1,*], Maciej Piofczyk[2], Kacper Sacha[2], Szymon Lenar[2], Michał Zieliński[3], Julia Czekańska[2], Krzysztof Sornek[1]

Keywords: electric boat, solar boat, photovoltaic panels, lithium-ion battery

ABSTRACT

Water transport accounted for 13% of total transport emissions in the European Union in 2023. Notably, this share has remained relatively constant since 1990, indicating a clear need for further development [1]. Moreover, it is estimated that in 2017 electric and hybrid watercraft accounted for at most 2% of the global fleet [2]. One of the most significant challenges in developing environmentally friendly transport is achieving a lightweight power system while maintaining an optimal vehicle operating range. This requires both minimizing the vessel's energy losses and providing a mobile, sustainable source of electricity. In our latest project, Delta (Fig. 1), this challenge is addressed by deck-mounted photovoltaic cells. This not only extends the boat's range but also eliminates reliance on grid electricity, the majority (about 59%) of which in the EU still originates from non-renewable sources [3].

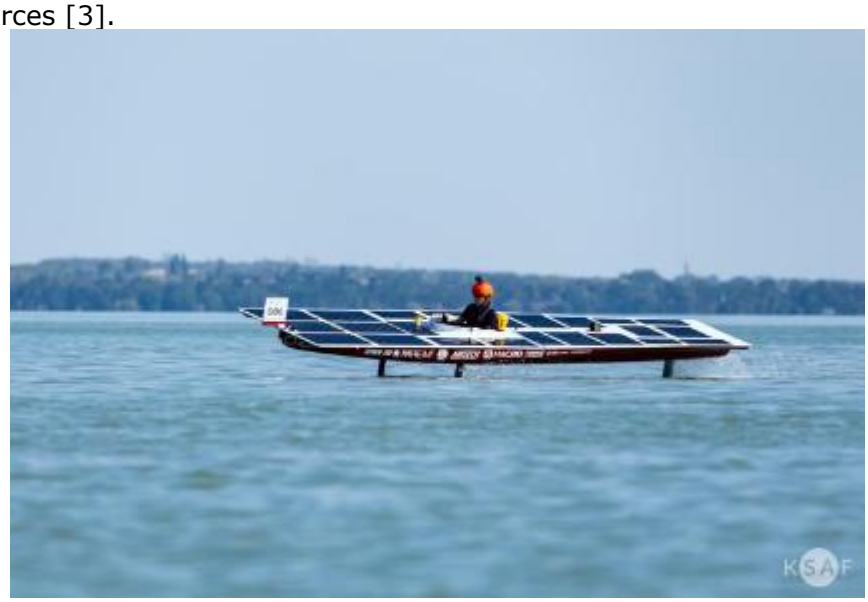


Figure 1. Delta solar racing boat operating on hydrofoils. Photograph by Aurelia Ciekalska, 2026

To achieve these objectives, we developed lightweight photovoltaic panels using Maxeon Gen 3 Me3 monocrystalline silicon solar cells, selected for their high conversion efficiency of 24% [4]. The cells were assembled in-house and laminated with a highly transparent ETFE film, providing protection against environmental exposure, including ultraviolet radiation and water, while maintaining high optical performance [5]. The resulting photovoltaic array covers 6 m^2, has a rated power of 1.4 kWp, and weighs 12 kg.

[1] Faculty of Energy and Fuels, AGH University of Krakow, Al. Mickiewicza 30, 30-059 Krakow, Poland, *Natalia.galas@solarboat.agh.edu.pl
[2] Faculty of Electrical Engineering, Automatics, Computer Science and Biomedical Engineering, AGH University of Krakow, Al. Mickiewicza 30, 30-059 Krakow, Poland
[3]The Faculty of Computer Science, Electronics and Telecommunications, AGH University of Krakow, Al. Mickiewicza 30, 30-059 Krakow, Poland

A Maximum Power Point Tracking (MPPT) controller with an efficiency of 98% maximizes the harvested solar power. During CoreComm Solar Boat Challenge 2026, the system achieved a peak power output of 1.1 kW, with an estimated photovoltaic conversion efficiency of approximately 20%.

The harvested energy is stored in a lithium-ion battery pack assembled in a 14S7P configuration using Molicel INR-21700-P45B cells, selected for their high energy density [6]. The measured capacity was 1,487 Wh, with a mass of 7.53 kg. The battery serves as an energy buffer, supplying additional power during high-demand operating conditions, such as high-speed sections. When propulsion power demand is lower, surplus solar energy can be used to charge the battery while the vessel continues operating. To ensure safe operation, an in-house battery management system (BMS) protects the pack against overcharging and excessive discharge and balances individual cells, helping to maintain reliable performance and prevent premature degradation. The battery is housed in a lightweight glass-fiber-reinforced composite enclosure and cooled by fans to manage operating temperatures while minimizing the mass of the energy storage system.

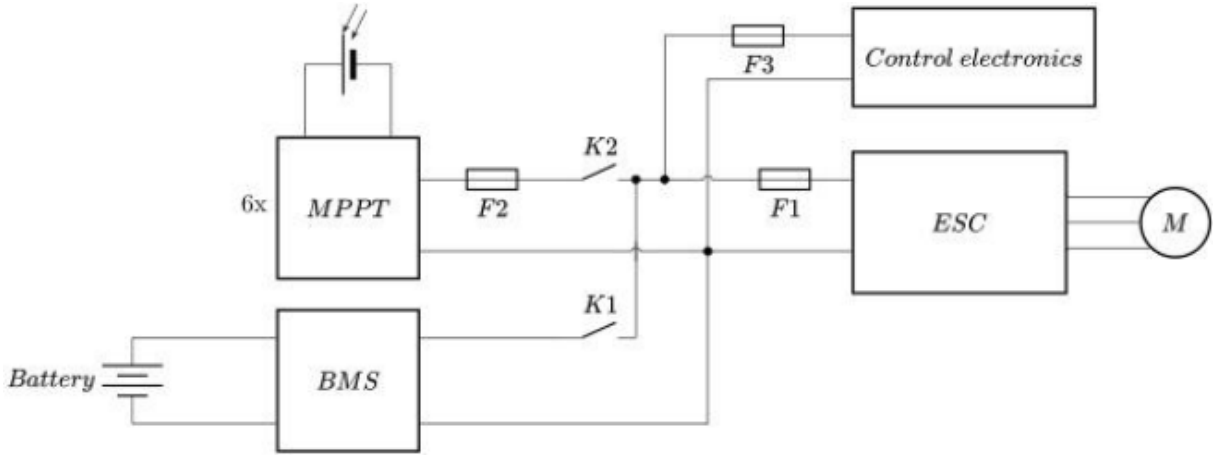


Figure 2. Simplified electrical architecture of the Delta power system, showing the photovoltaic array and MPPT converters, BMS, electronic speed controller (ESC), control electronics, and propulsion motor.

A key advancement in our research is the improved manufacturing technology of photovoltaic panels, which significantly reduced their weight. At the same time, reducing the battery mass contributed to a substantial decrease in the boat's overall mass. Through these enhancements, we improved energy efficiency, thereby increasing the vessel's energy autonomy and reducing the environmental impact associated with external energy use. The presented approach holds broad potential for application in the development of modern boats and ships.

[1] European Environment Agency (EEA), Sustainability of Europe's Mobility Systems 2025, EEA Web Report 02/2025, 2026. https://doi.org/10.2800/4890019 (accessed 24 September 2026).
[2] IDTechEx, Electric Boats and Ships 2017–2027, IDTechEx Research Report, 2017. https://www.idtechex.com/en/research-report/electric-boats-and-ships-2017-2027/509 (accessed 23 September 2026).
[3] Eurostat, Electricity production, consumption and market overview, Statistics Explained, 2025. https://ec.europa.eu/eurostat/statistics-explained/index.php?title=Electricity_production,_consumption_and_market_overview (accessed 30 September 2026).
[4] Maxeon, Maxeon Gen 3 High Efficiency Solar Cell, Technical Datasheet. https://oceanplanetenergy.com/wp-content/uploads/2023/11/Maxeon_3_Solar_Cell_ds_en_a4_166_519452E-final.pdf (accessed 26 September 2026).
[5] Aluminium Féron GmbH & Co. KG, transluX EC Frontsheets, Product Information. https://www.feron.de/en/feron-solar/frontsheet-translux-ec-and-ecc/ (accessed 30 September 2026).
[6] Molicel, INR-21700-P45B Ultra-High Power Cell, Product Specifications. https://www.molicel.com/inr-21700-p45b/ (accessed 27 September 2026).

Acknowledgement: This work was financed by the AGH University of Krakow within the Rector's Grant programme.

EFE2026 ENERGY FUELS ENVIRONMENT
INTERNATIONAL CONFERENCE
17-20 NOVEMBER 2026, KRAKÓW, POLAND

Defect-Driven CO_2 Capture by Hydrotalcite-Derived Sorbents: Linking Surface Basicity with CO_2 Activation

Małgorzata Zimowska[1,*], Jerzy Podobiński[1], Jerzy Datka[1]

Keywords: CO_2 capture, Hydrotalcite-Based Sorbents, in situ FTIR measurments, quantum-chemical modelling of CO_2 interactions

ABSTRACT

Nature rarely favors structurally perfect surfaces: defects and low-coordinated sites often determine the reactivity of functional materials and their interactions with adsorbates. In this study, we investigate the role of structural imperfections in controlling CO_2 capture by hydrotalcite-like (Htlc) materials and their derived mixed oxides. A combination of in situ FTIR spectroscopy, structural and textural characterization, temperature-programmed CO_2 desorption, and quantum-chemical modelling was employed to establish the relationship between defect chemistry, surface basicity, and CO_2 adsorption.

Quantum-chemical calculations on MgO surfaces demonstrate that regular terrace sites containing five-coordinated O^{2-} centers interact only weakly with CO_2, whereas defect-rich, low-coordinated oxygen sites strongly stabilize adsorbed CO_2 species and promote surface carbonate formation. These results indicate that CO_2 capture is governed not simply by the abundance of surface oxygen, but by the accessibility and energetic characteristics of structurally heterogeneous adsorption sites. The role of surface water in modifying CO_2 adsorption was also examined.

In this study, defect engineering of the MgO structure was achieved through octahedral substitution of basic cations in Htlc precursors with more acidic ones, promoting the formation of low-coordinated surface sites and increasing the density of basic sites available for CO_2 adsorption. To experimentally probe these effects, Mg–Al and Mg–Al–Fe hydrotalcite-like nanostructures with tunable cation compositions were synthesized and subsequently transformed into mixed oxides. Changes in composition and thermal treatment resulted in pronounced modifications of crystallinity, morphology, surface area, and basic-site distribution. In situ FTIR measurements using CO_2 as a molecular probe revealed the formation of carbonate and bicarbonate species associated with surface O^{2-} and OH^- groups, enabling differentiation of adsorption sites according to their chemical environment and strength. Complementary temperature-programmed desorption confirmed preferential occupation and release of energetically distinct CO_2 adsorption centers.

[1] Jerzy Haber Institute of Catalysis and Surface Chemistry Polish Academy of Sciences, Poland
* malgorzata.zimowska@ikifp.edu.pl

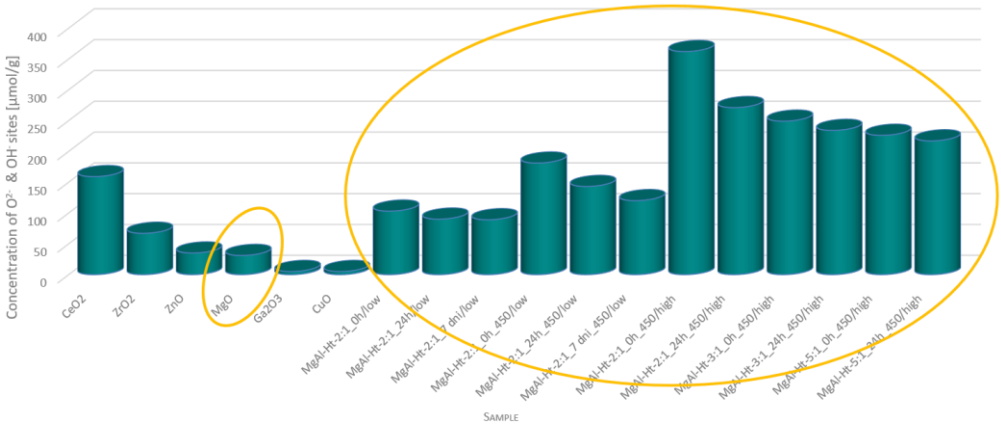


Figure 1. Concentration of O^{2-} & OH^- centers/ [µmol/g]

Increasing the Mg ratio in Htlc, enhanced the concentration of basic surface sites from 103 to 292 µmol g^{-1}. Calcination of the Htlc precursors nearly doubled the concentration of basic sites, with a pronounced contribution from O^{2-} centers. Transformation into mixed oxides further increased surface basicity, particularly in materials with higher Al content, where the concentration of basic sites exceeded 400 µmol g^{-1}. Incorporation of Fe additionally promoted the development of these surface features.

Overall, the results demonstrate that defect engineering is a key strategy for controlling CO_2 capture in hydrotalcite-derived sorbents. Rather than maximizing structural perfection, tailoring the concentration, accessibility, and strength of defective surface sites provides a route toward optimizing CO_2 adsorption. The combined spectroscopic and theoretical approach offers a molecular-level understanding of CO_2 activation and provides guidelines for the rational design of tunable sorbents relevant to carbon-capture and environmental energy technologies.

Acknowledgment: The research supported by the ICSC PAS development project No./PR-MZ/2024-2026

Life Prediction and Degradation Diagnostics of Power System Equipment

Anna Jarosz-Kozyro[1]

Keywords: Power equipment degradation, Service life prediction, Predictive maintenance, Machine learning, Condition monitoring

ABSTRACT

The escalating complexity of modern energy systems demands robust asset management to ensure uninterrupted power supply and grid security. This chapter analyzes the primary degradation pathways—mechanical, thermal, chemical, environmental, and operational—affecting critical infrastructure like transformers, photovoltaics, and energy storage devices. It details various mathematical and prognostic modeling techniques, including statistical regressions, finite element simulations, and machine learning algorithms, utilized for accurate lifetime prediction. Emphasizing the role of digital transformation, the chapter demonstrates how IoT-enabled sensor systems and real-time analytics shift maintenance strategies from rigid schedules to predictive, condition-based operations.

[1] AGH University of Krakow, anjarosz@agh.edu.pl

EFE2026 ENERGY FUELS ENVIRONMENT
INTERNATIONAL CONFERENCE
17-20 NOVEMBER 2026, KRAKÓW, POLAND

HAZOP-Based Qualitative and Semi-Quantitative Risk Assessment for Underground Hydrogen Storage (UHS) in Depleted Oil and Gas Reservoirs

Manal AlShafi[1,*], Canan Acar[2], Ahmad Abushaikha[1], Yusuf Bicer[1]

Keywords: Risk assessment; Hydrogen; Underground gas storage; leakage

ABSTRACT

Underground hydrogen storage (UHS) in depleted oil and gas reservoirs offers a potential solution for large-scale and seasonal hydrogen storage, but its operation involves risks related to high pressure, hydrogen leakage, well integrity, and material compatibility. This study presents an integrated risk assessment combining Hazard and Operability (HAZOP), Low–Medium–High (LMH) classification, and semi-quantitative multi-criteria scoring. The assessment covers the principal UHS process components and evaluates deviations in pressure, temperature, flow, phase, and gas purity. Five parameters—Likelihood, Consequence, Detectability, Exposure, and Robustness—are used to quantify deviation risk. Four critical nodes were identified: the cushion-gas injector, H_2 compressor, H_2 injector well, and H_2 production well. Each obtained a risk score of 3.6 and was classified as High risk, primarily due to overpressure. The findings highlight pressure control, well and equipment integrity, leakage detection, and emergency response as key safety considerations for UHS implementation.

1. Introduction

Large-scale hydrogen (H2) storage is essential for balancing H2 supply and demand and enabling its integration into future low-carbon energy systems. Underground storage can provide substantially larger capacities than many aboveground alternatives, with depleted oil and gas reservoirs offering advantages including existing infrastructure, geological characterization, and potentially large storage volumes [1–3]. Nevertheless, H2 storage in porous reservoirs presents technical and safety challenges related to leakage, well integrity, geochemical and microbial interactions, and pressure-induced risks [2–4]. Consequently, systematic risk assessment is required to identify critical hazards and prioritize appropriate safeguards. This study develops an integrated HAZOP-LMH and semi-quantitative framework for assessing risks associated with UHS in depleted oil and gas reservoirs.

2. Methodology

The assessment was structured around the HAZOP methodology in accordance with IEC 61882:2016 [5]. The UHS system was divided into principal process and subsurface nodes, including cushion-gas compression and cooling, cushion-gas injection, the storage reservoir, H2 compression and cooling, H2 injection, H2 production, and gas separation. Deviations were evaluated for parameters including pressure, temperature, flow, phase, and gas purity. For each deviation, potential causes, consequences, existing safeguards, LMH risk classification, and mitigation measures were identified.

Following the qualitative HAZOP assessment, a semi-quantitative multi-criteria scoring

[1] College of Science and Engineering, Hamad bin Khalifa University, Qatar Foundation, Doha, Qatar, * dr.manalshafi7@gmail.com

[2] Faculty of Engineering Technology, University of Twente, 7500 AE Enschede, The Netherlands

approach was applied to further prioritize the identified hazards. Five parameters—Likelihood (L), Consequence (C), Detectability (D), Exposure (E), and Robustness (Rb)—were scored from 1 to 5. The overall risk index was calculated as Ri = (L + C + D + E + Rb) / 5. Risk levels were classified as Low (1.0–2.5), Medium (2.6–3.5), and High (3.6–5.0). Node-level scores represent the average of the associated deviation scores.

3. Results and Discussion

The HAZOP-LMH assessment identified four critical nodes (3, 5, 7, and 8), with high-pressure deviations representing the dominant contributors to risk. These deviations may compromise well or equipment integrity and increase the potential for H2 leakage.

To further quantify and compare the relative significance of the identified hazards, the semi-quantitative scoring results were evaluated at the node level. The results were consistent with the HAZOP-LMH classification and provided a numerical basis for prioritizing risk-control measures.

Table 1. Semi-quantitative node-level risk scores for the assessed UHS system.

UHS node	Risk score (Ri)	Level
Cushion-gas compressor	2.6	Medium
Cushion-gas cooling	2.6	Medium
Cushion-gas injector	3.6	High
Storage reservoir	3.2	Medium
H_2 compressor	3.6	High
H_2 cooling	3.0	Medium
H_2 injector well	3.6	High
H_2 production well	3.6	High

The highest scores were associated with H2 injection, compression, and production operations. The consistency between the HAZOP-LMH findings and semi-quantitative results indicates that high-pressure operations constitute the principal areas requiring attention within the assessed UHS system.

4. Conclusion

An integrated HAZOP-LMH and semi-quantitative risk assessment framework was applied to UHS in depleted oil and gas reservoirs. The assessment identified four high-risk nodes, each obtaining a risk score of 3.6, while the remaining assessed nodes were classified as Medium risk. High-pressure deviations were the principal contributors to the identified critical hazards. Combining qualitative hazard identification with semi-quantitative prioritization provides a structured basis for identifying critical UHS components, prioritizing safeguards, and supporting risk-informed design and operation.

[1] M. S. A. Perera, "A review of underground hydrogen storage in depleted gas reservoirs: Insights into various rock-fluid interaction mechanisms and their impact on the process integrity," Fuel, vol. 334, p. 126677, Feb. 2023, doi: 10.1016/j.fuel.2022.126677.
[2] N. S. Muhammed et al., "Hydrogen storage in depleted gas reservoirs: A comprehensive review," Fuel, vol. 337, p. 127032, Apr. 2023, doi: 10.1016/j.fuel.2022.127032.
[3] M. Delshad, Y. Umurzakov, K. Sepehrnoori, P. Eichhubl, and B. R. Batista Fernandes, "Hydrogen Storage Assessment in Depleted Oil Reservoir and Saline Aquifer," Energies (Basel)., vol. 15, no. 21, p. 8132, Oct. 2022, doi: 10.3390/en15218132.
[4] B. Uliasz-Misiak, J. Lewandowska-Śmierzchalska, and R. Matuła, "Selection of Underground Hydrogen Storage Risk Assessment Techniques," Energies (Basel)., vol. 14, no. 23, p. 8049, Dec. 2021, doi: 10.3390/en14238049.
[5] "IEC 61882:2016 | IEC." Accessed: Aug. 05, 2025. [Online]. Available: https://webstore.iec.ch/en/publication/24321.
[6] M. L. Malki, H. Chellal, K. C. Bijay, A. Indro, V. Rasouli, and M. Mehana, "Risk assessment of wellbore leakage during underground hydrogen storage," Gas Science and Engineering, vol. 140, p. 205661, Aug. 2025, doi: 10.1016/j.jgsce.2025.205661.

EFE2026 ENERGY FUELS ENVIRONMENT
INTERNATIONAL CONFERENCE
17-20 NOVEMBER 2026, KRAKÓW, POLAND

Physics-Informed Digital Twins for Identifying Thermodynamic Flexibility in Heat Pump and Thermal Storage Systems

Adam Mroziński[1,*], Rafał Andrzejczyk[2], Jakub Grela[3], Belayneh Ayalew[2]

Keywords: thermodynamic flexibility, digital twin, heat pump, thermal energy storage, model predictive control

ABSTRACT

The integration of variable renewable electricity with electrified heating requires flexibility that can be quantified without violating comfort or equipment constraints [1]. Buildings with heat pumps and thermal energy storage (TES) can shift electricity consumption by using structural thermal inertia and dedicated storage. Research on latent TES in building HVAC motivates consideration of optional phase-change material (PCM) modules [2]. However, nominal storage capacity alone does not determine the available service: usable flexibility depends on the current thermal state, weather, occupancy, operating limits and the selected prediction horizon [3].

This paper proposes a physics-informed digital twin framework for identifying thermodynamic flexibility in residential heat-pump-TES systems. Here, thermodynamic flexibility denotes the time-dependent ability to modify electrical demand by changing thermal energy flows and stored energy while satisfying comfort and operational constraints. It is represented by feasible trajectories conditional on the initial state and boundary conditions. The methodological contribution is a joint identification procedure that quantifies state-dependent flexibility envelopes and their uncertainty for the coupled heat-pump-storage-building system over complete activation-recovery cycles.

The proposed architecture combines synchronized measurements with reduced-order resistance-capacitance (RC) building models [4], storage energy balances and heat-pump performance maps. Optional PCM modules can use enthalpy-based dynamic models informed by experimentally validated modular TES studies [5]. Temperatures, water flow rates and electrical power are used to estimate latent thermal states and model parameters. Outdoor conditions, solar gains and occupancy-related disturbances enter the dynamic balance [6]. Heat output is linked to electrical input through an operating-condition-dependent coefficient of performance (COP), with auxiliary loads and relevant compressor limits included. The twin is updated through data assimilation and supports feedback to the physical system, providing a synchronized model-measurement connection [7].

Flexibility envelopes describe admissible electrical-power and thermal-state trajectories over a specified horizon (Fig. 1). Their indicators include allowable compressor suspension time, useful thermal energy within operating temperature limits, load-shifting duration and electrical peak reduction relative to an explicit reference operation. Post-event recovery demand and rebound peaks are evaluated together with the activation period. Separate storage balances distinguish building thermal mass from the water buffer and avoid double counting.

The proposed Identification protocol combines normal-operation monitoring with

[1] Faculty of Mechanical Engineering, Bydgoszcz University of Science and Technology, Al. Prof. S. Kaliskiego 7, 85-796 Bydgoszcz, Poland. *Adam.Mrozinski@pbs.edu.p
[2] Faculty of Mechanical Engineering and Ship Technology, Gdańsk University of Technology, ul. G. Narutowicza 11/12, 80-233 Gdańsk, Poland.
[3] Faculty of Electrical Engineering, Automatics, Computer Science and Biomedical Engineering, AGH University of Krakow, al. A. Mickiewicza 30, 30-059 Kraków, Poland

controlled heating interruptions, set-point changes and storage charge-discharge tests. Excitation is constrained by comfort and equipment limits. State observability and practical parameter identifiability are assessed before increasing model complexity. Heat-pump response and buffer dynamics are identified separately where measurements permit, and then coupled to the building model. For optional PCM modules, ultrasound and image-based phase-fraction measurements can inform state estimation [8]. Sensitivity to measurement noise, parameter uncertainty, model structure and unobserved disturbances is propagated to prediction intervals.

The validation protocol withholds independent time blocks and complete activation - recovery cycles from calibration. Performance is assessed using temperature and power prediction errors, energy-balance consistency, prediction-interval coverage and comfort-constraint violations. Benchmark models comprise a fixed-parameter RC representation and a data-driven predictor. Comparisons with the reference operation use identical initial thermal states, external conditions and comfort constraints. Net electrical-energy changes are assessed over the complete activation-recovery cycle, including recovery to equivalent terminal thermal states of the building and storage. Residual differences in stored thermal energy are quantified and included in the energy balance. Transfer between building classes is treated as a testable hypothesis requiring further data.

The intended output is an interpretable, uncertainty-aware representation of flexibility that can be embedded in model predictive control (MPC) to coordinate heat pumps and storage with renewable generation [9-11]. This contribution presents the research framework and its experimental validation protocol; quantitative gains in renewable self-consumption or peak reduction remain to be established. The approach provides a basis for investigating the operating conditions under which distributed thermal storage can deliver reliable demand-side flexibility.

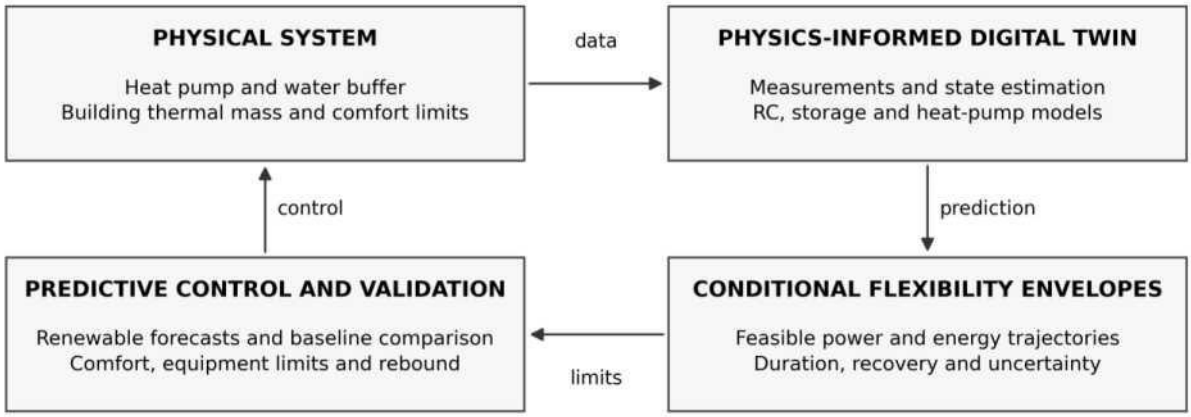


Figure 1. Proposed framework linking thermal states, flexibility envelopes and control.

[1] S.Ø. Jensen, A. Marszal-Pomianowska, R. Lollini, W. Pasut, A. Knotzer, P. Engelmann, A. Stafford, G. Reynders, IEA EBC Annex 67 Energy Flexible Buildings, Energy Build. 155 (2017) 25–34. https://doi.org/10.1016/j.enbuild.2017.08.044.

[2] B.S. Ayalew, R. Andrzejczyk, Recent advancements in latent thermal energy storage and their applications for HVAC systems in commercial and residential buildings in Europe—Analysis of different EU countries' scenarios, Energies 18 (2025) 4000. https://doi.org/10.3390/en18154000.

[3] G. Reynders, J. Diriken, D. Saelens, Generic characterization method for energy flexibility: Applied to structural thermal storage in residential buildings, Appl. Energy 198 (2017) 192–202. https://doi.org/10.1016/j.apenergy.2017.04.061.

[4] P. Bacher, H. Madsen, Identifying suitable models for the heat dynamics of buildings, Energy Build. 43 (2011) 1511–1522. https://doi.org/10.1016/j.enbuild.2011.02.005.

[5] M. Rogowski, M. Fabrykiewicz, D. Kuhn, E. Schröder, R. Andrzejczyk, Development and experimental investigation of a modular, honeycomb shell-and-coil PCM-based latent heat thermal energy storage unit assisted with heat pipes. Dynamic simulation of melting process by using object-oriented modeling, Int. Commun. Heat Mass Transf. 167 (2025) 109379. https://doi.org/10.1016/j.icheatmasstransfer.2025.109379.

[6] F. Durlik, J. Grela, D. Latoń, A. Ożadowicz, L. Wisniewski, User activity detection and identification of energy habits in home energy-management systems using AI and ML: A comprehensive review, Energies 19 (2026) 641. https://doi.org/10.3390/en19030641.

[7] D. Jones, C. Snider, A. Nassehi, J. Yon, B. Hicks, Characterising the digital twin: A systematic literature review, CIRP J. Manuf. Sci. Technol. 29 (2020) 36–52. https://doi.org/10.1016/j.cirpj.2020.02.002.

[8] R. Andrzejczyk, R. Drelich, M. Pakuła, Experimental investigations of the melting/solidification of coconut oil using ultrasound-based and image processing approaches, Energies 18 (2025) 5455. https://doi.org/10.3390/en18205455.

[9] J. Drgoňa, J. Arroyo, I. Cupeiro Figueroa, D. Blum, K. Arendt, D. Kim, E.P. Ollé, J. Oravec, M. Wetter, D.L. Vrabie, L. Helsen, All you need to know about model predictive control for buildings, Annu. Rev. Control 50 (2020) 190–232. https://doi.org/10.1016/j.arcontrol.2020.09.001.

[10] I. Rojek, D. Mikołajewski, A. Mroziński, M. Macko, T. Bednarek, K. Tyburek, Internet of Things applications for energy management in buildings using artificial intelligence—A case study, Energies 18 (2025) 1706. https://doi.org/10.3390/en18071706.

[11] F. Durlik, J. Grela, D. Latoń, A comprehensive literature review of optimization algorithms for intelligent load scheduling in home energy management systems, Energies 19 (2026) 2517. https://doi.org/10.3390/en19112517.

EFE2026 ENERGY FUELS ENVIRONMENT
INTERNATIONAL CONFERENCE
17-20 NOVEMBER 2026, KRAKÓW, POLAND

Energy Data Analytics for Improving Industrial Energy Efficiency

Patrycja Zubień[1], Kamil Misiurek[2,*], Tadeusz Olkuski[3]

Keywords: industrial energy efficiency, energy data analytics, anomaly detection, idle consumption, data-driven energy management

ABSTRACT

Industrial facilities generate large volumes of energy, production, machine, process, and environmental data. However, the availability of such data alone does not directly translate into improved energy efficiency. Recent studies suggest that data-driven methods can support industrial energy management through energy-performance assessment, baseline modelling, anomaly detection, forecasting and process optimization [1-5]. However, their practical application depends on data quality, availability and integration of energy data with production and process information.

This study presents a conceptual framework demonstrating how data analytics can support the identification of industrial energy inefficiencies and energy-saving opportunities. The proposed approach includes data acquisition, preprocessing, calculation of energy performance indicators, baseline modelling, anomaly detection, and identification of excessive or unnecessary energy consumption. The conceptual framework organizes the analytical process into five stages: data acquisition, data processing, analytics, identification of inefficiencies and energy-saving actions. This approach assumes that energy data should be interpreted together with production, machine, process and environmental variables in order to distinguish expected variations in energy consumption from deviations that may indicate inefficiencies.

The framework is illustrated using synthetic datasets comprising a 15-minute industrial load profile and a 30-day production-energy dataset. The synthetic load profile represents variations in power demand over a 24-hour operating cycle, including production and idle periods. The production-energy dataset was constructed to represent a reference relationship between daily production output and energy consumption. Twenty-four observations were used to represent reference operating conditions, while six excess-consumption events were introduced to illustrate deviations from the expected energy baseline. An illustrative alert level was applied above the baseline to demonstrate how abnormal consumption can be identified.

The analyses focus on detecting energy consumption during idle periods and identifying deviations from production-adjusted energy baselines. In the modelled scenario, reducing idle power demand from 40 to 20 kW for eight hours per day decreases daily energy consumption from 2,560 to 2,400 kWh. This corresponds to a potential saving of 160 kWh per day, or 6.25%, without changing production output. Figure 1 illustrates the synthetic production-adjusted baseline together with the introduced excess-consumption events.

The illustrative analyses demonstrate three complementary uses of industrial energy data. First, a time-based load profile can reveal persistent electricity demand during non-production periods. Second, a production-adjusted baseline provides a reference for distinguishing expected changes in energy consumption from abnormal deviations. Third, scenario analysis can be used to quantify the potential effect of selected operational changes while maintaining the same production output.

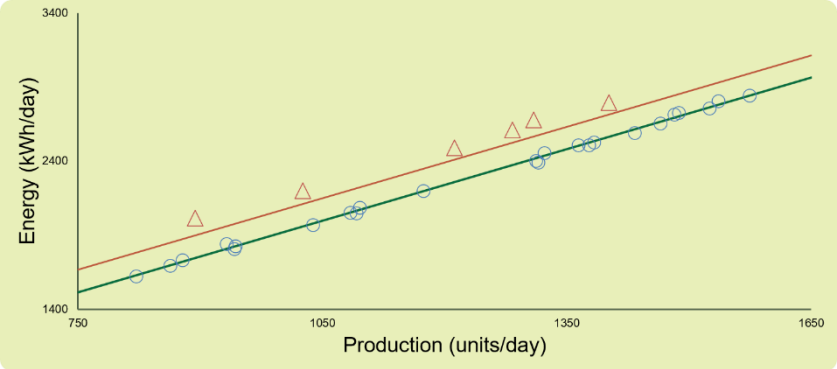


Figure 1. Synthetic production-adjusted energy baseline and excess-consumption events.

The illustrative analyses demonstrate three complementary uses of industrial energy data. First, a time-based load profile can reveal persistent electricity demand during non-production periods. Second, a production-adjusted baseline provides a reference for distinguishing expected changes in energy consumption from abnormal deviations. Third, scenario analysis can be used to quantify the potential effect of selected operational changes while maintaining the same production output.

The results demonstrate the potential of energy data analytics to reveal hidden inefficiencies and support operational decisions related to scheduling, equipment operation, maintenance, and process optimization. The framework therefore provides a structured basis for transforming heterogeneous industrial data into information that may support operational and energy-management decisions. As the presented examples are based on synthetic data, further validation using measurements from industrial facilities is required.

[1] May G., Psarommatis F. (2026). Advancing Industrial Energy Efficiency with Data-Driven Methods: A Systematic Review and Roadmap for Research and Practice. Journal of Sustainability Research, 8(2), e260036. (accesed on: 8.09.2026 r.) https://doi.org/10.20900/jsr20260036 (on-line)
[2] Keramati Feyz Abadi M.M., Liu C., Zhang M., Hu Y., Xu Y. (2025). Leveraging AI for energyefficient manufacturing systems: Review and future prospectives. Journal of Manufacturing Systems, 78, 153-177. (accesed on: 8.09.2026 r.) https://doi.org/10.1016/j.jmsy.2024.11.017 (on-line)
[3] Song B., Ao Y., Xiang L., K.Y.Ng Lionel (2018). Data-driven Approach for Discovery of Energy Saving Potentials in Manufacturing Factory. Procedia CIRP, 69, 330-335. (accesed on: 8.09.2026 r.) https://doi.org/10.1016/j.procir.2017.11.143 (on-line)
[4] Diogo A.C. Narciso, F. G. Martins (2020). Application of machine learning tools for energy efficiency in industry: A review. Energy Reports, 6, 1181-1199 (accesed on: 8.09.2026 r.) https://doi.org/10.1016/j.egyr.2020.04.035 (on-line)
[5] Teng S.Y., Touš M. Leong W.D., How B.S., Lam H.L., Máša V. (2021). Recent advances on industrial data-driven energy savings: Digital twins and infrastructures. Renewable and Sustainable Energy Reviews, Volume 135, 110208 (accesed on: 8.09.2026 r.) https://doi.org/10.1016/j.rser.2020.110208 (on-line)

From Wastewater to Public Health: Harnessing Water-Based Epidemiology for Community and Environmental Health Surveillance

Barbara Kasprzyk-Hordern[1]

Keywords: Wastewater-based epidemiology (WBE), Population health surveillance, Data triangulation, Early-warning systems, One Health

ABSTRACT

Water-based epidemiology (WBE) has emerged as a powerful tool for monitoring population health, providing objective, near real-time information on community exposure to chemicals, pharmaceuticals, infectious diseases, lifestyle factors, and environmental stressors. Recent advances in analytical chemistry, high-resolution mass spectrometry, biomarker discovery, and computational approaches have significantly expanded the scope and utility of WBE, enabling more comprehensive assessments of population health and environmental risk.

This talk will present recent developments in WBE and demonstrate how the integration of diverse data streams, including environmental monitoring, clinical datasets, demographic information, public health records, and other epidemiological indicators, can strengthen community health early-warning systems. Particular emphasis will be placed on data triangulation approaches that enhance the interpretation, validation, and actionability of WBE-derived evidence.

Drawing on examples from large-scale surveillance programmes and environmental and public health studies, the presentation will illustrate how WBE can support the detection of emerging health threats, track population-level exposures and behaviours, assess intervention effectiveness, and inform policy and public health decision-making.

The talk will also critically examine the advantages, limitations, and current knowledge gaps associated with WBE and discuss the challenges of achieving meaningful integration with established epidemiological approaches. Finally, it will explore future opportunities for embedding WBE within wider public health surveillance frameworks to support more holistic, timely, and equitable health monitoring under a One Health perspective.

[1] Centre of Excellence in Water Based Early Warning Systems
Department of Chemistry, University of Bath, bkh20@bath.ac.uk

EFE2026 ENERGY FUELS ENVIRONMENT
INTERNATIONAL CONFERENCE
17-20 NOVEMBER 2026, KRAKÓW, POLAND

Comparative Methodologies for Structural and Hybrid Power-Market Price Modelling

Juliette A. van Delden [1,*], Arnoud P. Higler [1]

Keywords: electricity price formation, economic dispatch, merit order, cross-border coupling, hybrid modelling, battery storage

ABSTRACT

Power-market price models must balance structural interpretability, empirical accuracy, temporal robustness, and fitness for downstream applications. This paper compares the principal modelling components developed in a detailed study of Dutch day-ahead electricity price formation over 2023-2025. Three methodological families are examined: a zero-parameter economic-dispatch ladder, a parsimonious five-parameter correction, and a 44-parameter hybrid merit-order stack. The comparison isolates the effects of short-run marginal-cost construction, generator bid tranching, combined heat-and-power representation, simplified unit commitment, procurement and scarcity adders, weather and behind-the-meter solar proxies, and four treatments of cross-border trade. Models are evaluated under a frozen-parameter protocol using hourly point errors, distributional tests, statistical benchmarks, plant-level dispatch validation, cross-border flow diagnostics, and battery-arbitrage performance. The central result is methodological: the representation of market topology and neighbour-price coupling has a larger effect on reconstructed Dutch prices than incremental domestic physical detail or extensive calibration. Endogenous trade against observed neighbouring prices under transfer limits reduces RMSE to approximately 23-24 EUR/MWh without fitted parameters and remains stable across the held-out years. Conversely, prescribing realised border flows as exogenous demand adjustments worsens performance because flows are outcomes of price arbitrage. The calibrated model captures domestic bidding structure and price distributions more flexibly, but its coefficients drift out of sample. A five-parameter correction becomes competitive when its solar term is indexed to observed photovoltaic-capacity growth. Storage validation further shows that RMSE, distributional accuracy, and economic value preservation need not rank models identically. The findings support a sequenced modelling strategy: represent market boundaries first, non-electric obligations second, domestic supply refinements third, and calibration last.

[1] Energy Transition Campus Amsterdam (ETCA), Grasweg 31, 1031 HW Amsterdam, The Netherlands, arnoud.higler@shell.com

EFE2026 ENERGY FUELS ENVIRONMENT
INTERNATIONAL CONFERENCE
17-20 NOVEMBER 2026, KRAKÓW, POLAND

Exergy Analysis of Hydrogen Supply Chains: Methods, Applications and a Framework for Consistent Assessment

Arnoud P. Higler [1,2]*

Keywords: hydrogen supply chain, exergy, hydrogen Carrier, energy density, thermodynamic screening

ABSTRACT

Hydrogen supply chains are often compared using hydrogen mass fraction, gravimetric energy density and volumetric energy density. These metrics are useful for sizing transported inventory, but they do not describe the work required to create a carrier state, the quality of heat required to recover hydrogen, or the location at which those thermodynamic duties occur. This paper develops a technology-agnostic, first-principles framework based on exergy and applies it to compressed gaseous hydrogen, liquid hydrogen, ammonia, a toluene/methylcyclohexane liquid organic hydrogen carrier (LOHC), magnesium hydride and aqueous bicarbonate/formate. The framework is deliberately simple: it requires reaction stoichiometry, thermodynamic state properties, pressure, temperature and a reference environment. A common functional boundary is used, from gaseous hydrogen at 20 bar at the source to gaseous hydrogen at 500 bar at the receiving location, while primary conversion steps are separated between source and destination. Enthalpy identifies heat-management duties; exergy identifies the maximum useful-work content and places mechanical work, refrigeration, chemical conversion and heat at different temperatures on a common basis. The contrast is particularly important for hydrogen liquefaction, ammonia cracking and LOHC dehydrogenation. Low-temperature LOHC research demonstrates that reducing dehydrogenation temperature improves heat integration, but also that vacuum generation and purification can introduce mechanical or electrical duties that cannot be met by waste heat. The bicarbonate/formate pair illustrates the complementary limitation of exergy: its intrinsic aqueous reaction is close to Gibbs-energy neutrality, yet practical hydrogen density falls rapidly with dilution and real systems can be dominated by recycle, separation and catalyst behaviour. Exergy is therefore not proposed as a replacement for density, process modelling, economics, safety or technology readiness. Rather, it is an inexpensive and reproducible thermodynamic screening layer that provides substantially more insight than density-based comparison alone and establishes a transparent lower bound before detailed supply-chain modelling.

[1] Shell Global Solutions International BV, Arnoud.Higler@shell.com
[2] AGH University of Krakow, ESMLab, Krakow, Poland

EFE2026 ENERGY FUELS ENVIRONMENT
INTERNATIONAL CONFERENCE
17-20 NOVEMBER 2026, KRAKÓW, POLAND

Techno-Economic and Environmental Assessment of a Hybrid Cogeneration and Heat Pump System for District Heating Modernization

Karol Sztekler[1], Mateusz Płatek[2], Witold Płatek[2], Łukasz Mika[1]

Keywords**:** district heating, high-efficiency cogeneration, absorption heat pump, transcritical CO_2 heat pump, decarbonization

ABSTRACT

The decarbonization of district heating systems requires solutions that reduce fossil fuel consumption while ensuring a reliable heat supply and economically feasible operation. European energy-efficiency and renewable-energy policies provide a framework for the modernization of heating networks [1, 2]. One promising approach is the integration of combined heat and power (CHP) generation with thermally driven and electrically driven heat pumps. This study evaluates the technical, environmental, and economic performance of a hybrid heat generation system proposed as an alternative to a conventional natural-gas-fired heating plant.

The investigated configuration combines a gas-fired cogeneration unit, an absorption heat pump, and four electrically driven compression heat pumps using carbon dioxide (R744) as the refrigerant. The integration of CO_2 heat pumps with CHP systems has been investigated as a route to improving operational flexibility and useful heat recovery [3], while the development of two-stage CO_2 compressors has demonstrated technological progress in heat-pump water heating [4]. The CHP unit simultaneously produces heat and electricity, while the absorption heat pump recovers and upgrades available thermal energy. After accounting for the auxiliary electricity requirements, the remaining generated electricity is sufficient to supply the four CO_2 heat pumps during the heating season. Related field experience with large heat-pump systems has also been documented [5].

A comparative assessment was performed for the reference gas heating plant and the proposed hybrid system under an equivalent annual useful heat output. The analysis included an energy balance, annual natural gas demand, the contribution of renewable heat, direct CO_2 emissions, a wider emissions balance accounting for electricity produced by high-efficiency cogeneration, and a simplified economic evaluation. The emission savings attributed to cogenerated electricity were calculated using the NFOŚiGW methodology adopted in the underlying study. The economic analysis considered changes in natural gas consumption, CO_2 emission costs, and the assumed support for high-efficiency cogeneration, in the context of the relevant Polish support framework [6].

The proposed hybrid CHP–heat pump system therefore offers a technically feasible pathway for district heating modernization, with substantial reductions in gas consumption and direct emissions and potentially attractive economic performance.

[1] European Parliament and Council of the European Union, Directive (EU) 2023/1791 of 13 September 2023 on energy efficiency and amending Regulation (EU) 2023/955 (recast), Off. J. Eur. Union L 231 (2023) 1–111. http://data.europa.eu/eli/dir/2023/1791/oj.

[2] European Parliament and Council of the European Union, Directive (EU) 2018/2001 of 11 December 2018 on the promotion of the use of energy from renewable sources (recast), Off. J. Eur. Union L 328 (2018) 82–209. http://data.europa.eu/eli/dir/2018/2001/oj.

[1] Department of Thermal and Fluid Flow Machines, Faculty of Energy and Fuels, AGH University of Krakow, A. Mickiewicza Av. 30, 30-059 Krakow, Poland, * sztekler@agh.edu.pl

[2] Centrum Elektroniki Stosowanej CES sp. z o.o. 32-003 Podłęże 676

[3] H. Chen, X. Yao, J. Li, G. Xu, Y. Yang, W. Liu, H. Chen, Thermodynamic analysis of a novel combined heat and power system incorporating a CO_2 heat pump cycle for enhancing flexibility, Appl. Therm. Eng. 161 (2019) 114160. https://doi.org/10.1016/j.applthermaleng.2019.114160.
[4] H. Sato, Y. Kimata, Y. Hotta, T. Goto, H. Mizuno, H. Kobayashi, Development of two-stage compressor for CO_2 heat-pump water heaters, Mitsubishi Heavy Ind. Tech. Rev. 49 (2012) 92–97. https://www.mhi.com/technology/review/sites/g/files/jwhtju2326/files/tr/pdf/e491/e491092.pdf.
[5] T. Walfridson, Case study report for Backadalen, Göteborg, Sweden, IEA Heat Pumping Technologies TCP, Annex 52, 2022. https://doi.org/10.23697/r7zd-s388.
[6] Republic of Poland, Act of 14 December 2018 on the promotion of electricity from high-efficiency cogeneration, consolidated text, Journal of Laws of the Republic of Poland (2025) item 602. https://dziennikustaw.gov.pl/DU/2025/602.

EFE2026 ENERGY FUELS ENVIRONMENT
INTERNATIONAL CONFERENCE
17-20 NOVEMBER 2026, KRAKÓW, POLAND

Synthesis and Characterisation of Carbon Nanodots for CO_2 Capture Applications

Małgorzata Hasal[1,2], Izabela Rzeźnicka[2], Jakub Szczurowski[1,*]

Keywords: absorption, carbon nanodots, CO_2 capture, amine-based CCUS

ABSTRACT

Carbon nanodots (CNDs) are a recently discovered class of nanomaterials characterised by unique properties such as photoluminescence, chemical stability, and low toxicity. These features have attracted significant attention for environmental applications, particularly due to their scalable and cost-effective synthesis using abundant precursor materials [1]. Structurally, CNDs consist of a carbon core surrounded by surface functional groups, whose modification allows precise tuning of their physicochemical properties [2]. This study investigates the use of CNDs as dopants in amine-based absorption solvents for post combustion CO_2 capture. Nitrogen doping was used to introduce functional amine groups, as a strategy to enhance the affinity of nanomaterials for CO_2. Incorporation of CNDs into amine systems is expected to improve both the absorption capacity of CO_2 and the absorption kinetics [3]. The aim of this work is to expand the current understanding of CND by investigating how synthesis conditions and precursor selection influence CND properties and their potential application in CO_2 capture, contributing to a more structured understanding of their functionality in this emerging field.

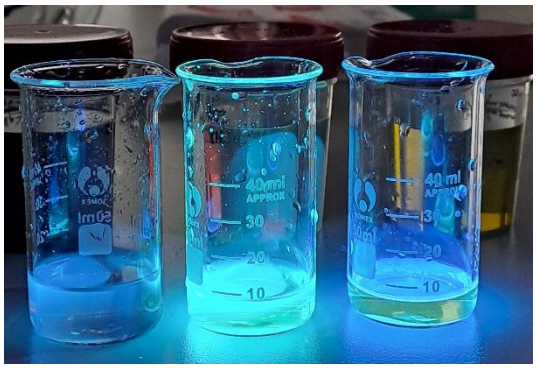


Figure 1. CNDs synthesised solvothermally and excited with UV light

The synthesis of CNDs was conducted via solvothermal, microwave-assisted, and space confined vacuum heating methods. Citric acid or L-ascorbic acid was used as the carbon source, while urea was used as the nitrogen precursor in a 1:2 mass ratio. Deionised water, ethanoloamine, or diethanoloamine was used as solvents. Solvothermal synthesis was conducted at 180°C for 8 h, while microwave synthesis was carried out at 900 W for 1-3 minutes. The space-confined vacuum heating samples were first dried at 120°C for 1 hour. The heating temperature increased to 200°C in 20°C increments, keeping the system at each temperature for 1 hour.

[1] Graduate School of Engineering and Science, Shibaura Institute of Technology,Tokyo, Japan
[2] Faculty of Energy and Fuels, AGH University of Krakow, Krakow, Poland; *szczurow@agh.edu.pl

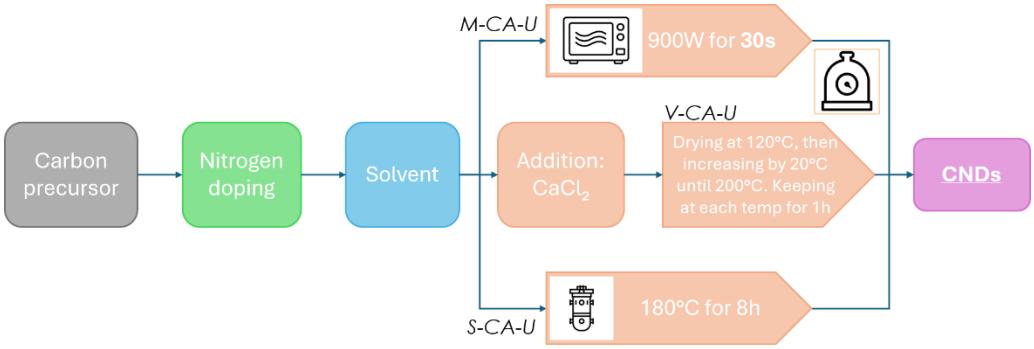


Figure 2. Flowchart of CND synthesis methodologies

The resulting materials were characterised using ultraviolet-visible (UV-Vis) spectroscopy and ATR spectroscopy. Morphology of CNDs was analysed by scanning electron microscope. Preliminary CO_2 absorption experiments indicated improved absorption performance after the incorporation of CNDs into the investigated amine systems. Spectroscopic characterisation provided insight into the optical properties and surface functional groups of the synthesised materials.

This study explores the potential of CND-modified amine solvents as an approach to improve post-combustion CO_2 capture. By investigating the synthesis and physicochemical properties of CNDs alongside their performance in amine-based systems, this work contributes to the development of nanomaterial-assisted carbon capture technologies.

[1] S.N. Baker, G.A. Baker, Luminescent carbon nanodots: Emergent nanolights, Angew. Chem. Int. Ed. 49 (2010) 6726–6744. https://doi.org/10.1002/anie.200906623.

[2] Y. Xiao, Z. Wang, J. Fu, J. Zhang, Q. He, H. Lu, Q. Zhou, H. Wang, Recent advances in the synthesis, characterization, and application of carbon dots in the field of wastewater treatment: A comprehensive review, Water 17 (2025) 210. https://doi.org/10.3390/w17020210.

[3] P.C. Sahoo, R. Singh, P. Sivagurunathan, D. Singh, M. Kumar, R.P. Gupta, U. Srivastava, Carbon dot-blended mixed amine for efficient CO2 capture under highly oxidative flue gas conditions, Int. J. Greenh. Gas Control 142 (2025) 104340. https://doi.org/10.1016/j.ijggc.2025.104340.

Acknowledgments:
This work was carried out under an IDUB subsidiary – Action 21, Application 18209 and Polish National Agency for Academic Exchange (NAWA), within the Strategic Partnerships Programme with Shibaura Institute of Technology, Japan, Project No. BPI/PST/2024/1/00046.

Influence of Accident-Tolerant Fuel Cladding Concepts on Hydrogen Accumulation and Mitigation in PWR Containments: A Reduced-Order Screening Assessmentment

Tomasz Bury[1*], Kacper Bury[2], Sławomir Zdziebło[1]

Keywords: accident-tolerant fuel, hydrogen generation, containment, passive autocatalytic recombiners, reduced-order modelling

ABSTRACT

During severe accidents in pressurized water reactors, high-temperature cladding oxidation can generate hydrogen that may accumulate in the containment atmosphere. Accident-tolerant fuel (ATF) cladding concepts can reduce this source, but lower production need not imply a proportional reduction in containment concentration or demand on passive autocatalytic recombiners (PARs). This study examines that relationship using material-dependent oxidation histories and a reduced-order containment hydrogen balance.

Four cladding cases are considered: conventional zirconium alloy (Zr), 9-μm Cr-coated Zr with sustained protection, Cr-coated Zr with assumed early substrate oxidation, and nuclear-grade FeCrAl C26M2. Hydrogen source histories originate from a previously developed zero-dimensional oxidation model. Kinetic correlations are evaluated under an identical prescribed thermal history (1275–1473 K, 2000 s), isolating material-oxidation behaviour from differences in fuel-rod thermal response. The Cr protection-loss transition is an illustrative thermal-exposure proxy, not a mechanistic coating-failure prediction. FeCrAl calculations remain within the protective-oxide kinetic regime [1, 2].

Hydrogen-production histories per unit reacting area are transformed into containment-release surrogates using a mass-conserving first-order transfer relation, distinguishing in-core production from release. A well-mixed, one-zone EPR-type reference volume of 80,235 m³ is considered, with 47 PARs, a prescribed gas temperature of 333.15 K and a 2% hydrogen activation threshold. Cases without PARs are compared with an extended PAR model retaining the published hydrogen-dependent recombination characteristic [3] and applying corrections for temperature, oxygen availability and catalyst activity. Two hypothetical reacting areas (5105 and 9000 m²) test source-scale sensitivity. The reference release time constant is 600 s.

For the 9000 m² case, cumulative hydrogen production amounts to 307.91 kg for Zr, 41.69 kg for protected Cr-coated Zr, 201.23 kg for the assumed early protection-loss case and 0.672 kg for FeCrAl. The corresponding peak mean containment hydrogen fractions are shown in Table 1. The PAR model reduces the Zr peak from 4.947% to 3.554% and the early Cr protection-loss peak from 3.289% to 2.520%. The protected Cr-coated Zr and FeCrAl cases remain below the adopted 2% PAR activation threshold. This threshold describes device activation, not mixture flammability.

Varying the transfer time constant from 300 to 1200 s changes the PAR-model peak hydrogen fraction from 3.756% to 3.151% for Zr and from 2.688% to 2.258% for the early Cr protection-loss case. For the smaller hypothetical reacting area (5105 m²), the corresponding peaks at 600 s are 2.236% and 1.893%, respectively; source scale also

[1]Silesian University of Technology, Faculty of Energy and Environmental Engineering, Gliwice, Poland, * tomasz.bury@polsl.pl
[2]Cracow University of Technology, Faculty of Chemical Engineering and Technology, Kraków, Poland

determines whether the activation threshold is exceeded. The relationship between the ATF hydrogen-source benefit and the PAR response is therefore nonlinear.

Table 1. Peak mean containment H_2, % mol., for a hypothetical reacting area of 9000 m² and release t = 600 s

Cladding concept	**No PAR, %**	**PAR M3, %**
Zr	4.947	3.554
Cr-coated Zr, protected	0.700	0.700
Cr-coated Zr, early protection loss	3.289	2.520
FeCrAl C26M2	0.011	0.011

These results demonstrate the usefulness of a transparent material-to-containment modelling chain for ranking source-term assumptions and identifying conditions warranting more detailed assessment. They do not represent a plant-specific severe-accident prediction: thermal histories and reacting areas are imposed, the release surrogate is uncalibrated, and perfect mixing with prescribed gas temperature excludes local stratification and thermal-hydraulic feedback. A subsequent multi-zone HEPCAL assessment will be needed to investigate spatial hydrogen accumulation, transport pathways and the robustness of mitigation conclusions.

[1] E.B. Kashkarov, D.V. Sidelev, M.S. Syrtanov, C. Tang, M. Steinbrück, Oxidation kinetics of Cr-coated zirconium alloy: Effect of coating thickness and microstructure, Corros. Sci. 175 (2020) 108883. https://doi.org/10.1016/j.corsci.2020.108883.
[2] C. Kim, C. Tang, M. Große, Y. Maeng, C. Jang, M. Steinbrück, Oxidation mechanism and kinetics of nuclear-grade FeCrAl alloys in the temperature range of 500–1500 °C in steam, J. Nucl. Mater. 564 (2022) 153696. https://doi.org/10.1016/j.jnucmat.2022.153696.
[3] T. Bury, Evaluation of passive autocatalytic recombiners operation efficiency by means of the lumped parameter approach, Nukleonika 60 (2015) 339–345. https://doi.org/10.1515/nuka-2015-0042.

Circular Economy in Cementitious Systems: Valorization of Phosphogypsum and Slag in Low-Carbon Alkali-Activated Binders for Winter Decarbonized Construction

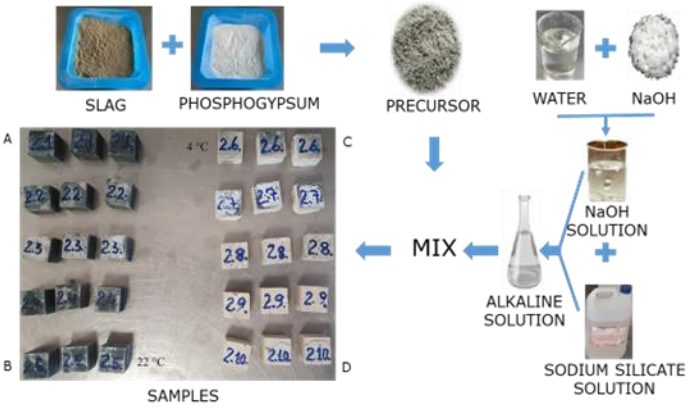
Povilas Telešius[1,*], Danutė Vaičiukynienė[1], Gabija Vinikaitė-Bačinskienė[1], Rėda Bistrickaitė[1]

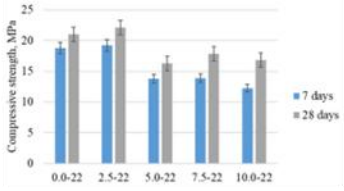
Keywords: alkali-activated slag, phosphogypsum, low-temperature curing, compressive strength, efflorescence

ABSTRACT

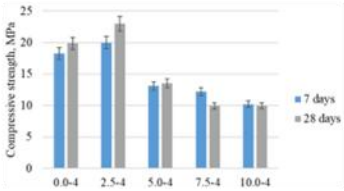
The production of alkali-activated binders from industrial by-products is a promising approach for reducing the environmental impact of the construction industry. Slag (ground granulated blast furnace slag, GGBFS) is widely used as a precursor for alkali-activated materials, while phosphogypsum (PG), a by-product of phosphoric acid production, can modify the reaction process and microstructure of the resulting binders [1]. However, the influence of phosphogypsum on alkali-activated slag systems cured at low temperatures remains insufficiently understood [3]. This study investigates the effect of phosphogypsum addition and curing temperature on the mechanical performance and microstructural development of alkali-activated slag binders. Slag was partially replaced with PG at levels of 0, 2.5, 5.0, 7.5, and 10 wt. % to get precursor. Sodium hydroxide and sodium silicate solutions were used as alkaline activators. The specimens were then mixed and cured at 22 °C and 4 °C and tested after 7 and 28 days. The results showed that both curing temperature and phosphogypsum dosage significantly influenced compressive strength. The highest 28-day compressive strengths were obtained for mixtures containing 2.5 wt. % PG, reaching 22.1 MPa at 22 °C and 23.0 MPa at 4 °C. Moderate PG addition promoted slag activation and the formation of reaction products, whereas higher PG contents reduced strength due to the formation of sulphate-rich crystalline phases.

[1] Faculty Civil Enginiering and Architecture, Kaunas University of Technology, Lithuania,
* povilas.telesius@ktu.edu

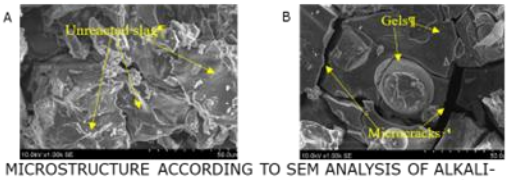




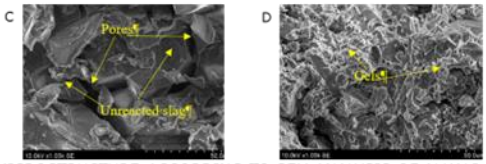
SAMPLES CURED AT ROOM TEMPERATURE 22°C, FOR 7 AND 28 DAYS



SAMPLES CURED AT LOW TEMPERATURE 4°C, FOR 7 AND 28 DAYS



MICROSTRUCTURE ACCORDING TO SEM ANALYSIS OF ALKALI-ACTIVATED SLAG WITH PJOSPHOGYPSUM A)0.0-22 AND B)10.00-22 SAMPLES CURED AT ROOM TEMPERATURE (22 °C) AFTER 28 DAYS



MICROSTRUCTURE ACCORDING TO SEM ANALYSIS OF ALKALI-ACTIVATED SLAG WITH PJOSPHOGYPSUM A)0.0-22 AND B)10.00-22 SAMPLES CURED AT LOW TEMPERATURE (4 °C) AFTER 28 DAYS

Figure 1 illustrates the experimental workflow of slag–phosphogypsum alkali-activated binders, such as precursor and activator preparation, sample preparation, compressive strength evaluation, and SEM microstructural analysis.

XRD analysis confirmed the formation of C-(A)-S-H and hybrid aluminosilicate gels as the main reaction products. The broad amorphous hump observed in the diffraction patterns was associated with reaction gel formation and partially with residual unreacted slag. Thenardite (Na_2SO_4) was detected only in samples containing 10 wt. % PG. FT-IR analysis indicated a greater degree of reaction for mixtures with 2.5 wt.% PG, particularly under low-temperature curing conditions. Furthermore, increased PG content reduced visible efflorescence by promoting incorporation of alkalis into the reaction products. The results demonstrate that phosphogypsum can be successfully utilized in alkali-activated slag binders [2], particularly at low dosages. The incorporation of 2.5 wt. % PG improved performance under both ambient and low-temperature curing conditions, providing a sustainable route for the valorization of industrial by-products and the development of low-carbon construction materials.

[1] Gijbels K., Iacobescu R.I., Pontikes Y., Schreurs S., Schroeyers W. Alkali-activated binders based on ground granulated blast furnace slag and phosphogypsum. Construction and Building Materials, 215 (2019) 371-380.
[2] Feng Y., Xue Z., Zhang B., Xie J., Chen C., Tan J., Zhao C. Effects of phosphogypsum substitution on the performance of ground granulated blast furnace slag/fly ash-based alkali-activated binders. Journal of Building Engineering, 70 (2023) 106387.
[3] Zhang G., Yang H., Ju C., Yang Y. Novel selection of environment-friendly cementitious materials for winter construction: Alkali-activated slag/Portland cement. Journal of Cleaner Production, 258 (2020) 120592.

EFE2026 ENERGY FUELS ENVIRONMENT
INTERNATIONAL CONFERENCE
17-20 NOVEMBER 2026, KRAKÓW, POLAND

Impact of NaCl Contamination on the Durability and Performance of Reversible PEM Fuel Cells

Monika Piech[1,*], Bartosz Adamczyk[2], Magdalena Dudek[2], Adam Szurlej[3]

Keywords: hydrogen, salt, rewersible polymer exchange membrane fuel cells,

ABSTRACT

Reversible polymer membrane exchange fuel cells (R-PEMFCs) – capable of operating either as hydrogen generators (fuel producers) or as units for the direct generation of electricity and heat – are attracting significant global interest. A key advantage of such devices is the simplification of their design, not only in terms of size and weight (combining two modules into one) but also in relation to the technical and economic aspects of balancing hydrogen and electricity production profiles. A second strategic challenge involves the management of saline process waters from industrial operations and seawater. Current literature indicates that the presence of NaCl in the water reduces hydrogen production efficiency due to the accumulation of impurities on the surface of electrode materials or within their internal structures.

A deterioration in the performance of PEMFC fuel cells also occurs when NaCl and hydrogen fuel permeate the system. However, the mechanisms governing the degradation of MEA assemblies in fuel cells, electrolysers and reversible PEMFCs are not yet fully understood. These difficulties stem from the diverse operating conditions the devices face under varying electrical loads. This paper presents preliminary results regarding the impact of experimental factors – including the presence of NaCl contamination (in either solid or dissolved form) – on the operating parameters of single PEMFC fuel cells. Specific electrochemical techniques, including cyclic voltammetry (CV), chronoamperometry (CA) and electrochemical impedance spectroscopy (EIS), were employed to assess changes in the performance of a fuel cell fed with humidified hydrogen containing trace amounts of NaCl. Experimental measurements were conducted across a range of PEMFC operating temperatures (approximately 0°C to 40°C) and varying humidity levels. Based on these findings, the conditions under which the effects of NaCl contamination in the hydrogen feed can be reversibly eliminated – allowing the fuel cell to return to its baseline operating state – were determined. This paper also discusses the results of studies surrounding the effect of NaCl on the operation of the hydrogen electrolyser.

This research work was funded as part of the "Implementation Doctorate" programme V/2021

[1] ORLEN S.A.; AGH University of Krakow, Faculty of Energy and Fuels, * piech@agh.edu.pl
[2] AGH University of Krakow, Faculty of Energy and Fuels
[3] AGH University of Krakow, Faculty of Drilling, Oil and Gas

EFE2026 ENERGY FUELS ENVIRONMENT
INTERNATIONAL CONFERENCE
17-20 NOVEMBER 2026, KRAKÓW, POLAND

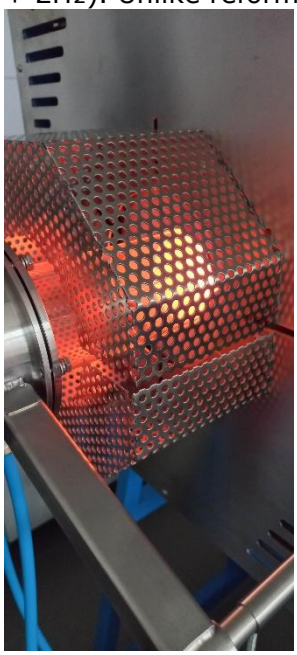
Methane Pyrolysis as an Alternative Source of Hydrogen

Michał Wojtasik[1,*], Grażyna Żak[1], Wojciech Krasodomski[1]

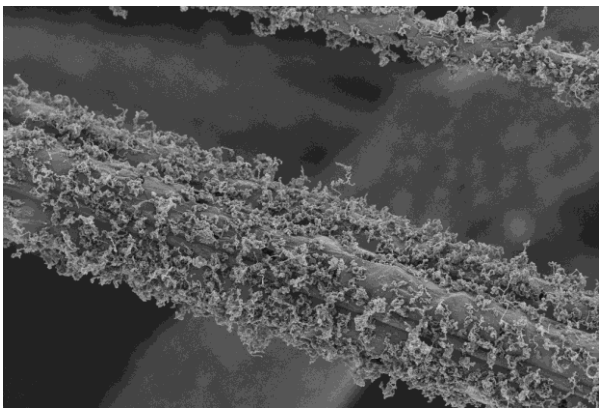
Keywords: methane pyrolysis, turquise hydrogen, fibrous catalyst, low emission hydrogen

ABSTRACT

Methane pyrolysis is an emerging route for hydrogen production that may complement conventional steam methane reforming and water electrolysis. The process involves the thermal or catalytic decomposition of methane into hydrogen and solid carbon ($CH_4 \rightarrow C + 2H_2$). Unlike reforming, the primary reaction does not generate carbon dioxide, offering a potential pathway to low-carbon "turquoise" hydrogen, provided that process heat is supplied with a low carbon footprint and methane leakage is minimised. The solid carbon can potentially be used as an industrial material, creating an additional value stream. However, the technology faces significant challenges, including the high temperatures required for non-catalytic decomposition, energy demand, carbon deposition on reactor surfaces, catalyst deactivation, and the continuous separation and handling of solid products.



This contribution presents laboratory-scale investigations of methane pyrolysis conducted at the Oil and Gas Institute – National Research Institute (INiG-PIB), focusing on the feasibility of hydrogen generation, process performance, and options for further technological development. Experiments were performed in a high-temperature laboratory reactor with a heated reaction zone approximately 1,200 mm long and an internal diameter of 85 mm. The studies provide a basis for evaluating the effects of reaction conditions on methane decomposition and for identifying limitations associated with heat transfer, carbon accumulation and stable long-term operation.



An additional research direction addresses methane-containing gases originating from hard coal mining. Within the Meth2Gen project, methane pyrolysis is considered as an alternative approach to the management and decarbonisation of mine gases. Rather than releasing methane into the atmosphere or simply oxidising it to carbon dioxide, the proposed route aims to convert recovered methane into hydrogen while retaining its carbon content in solid form. This concept is particularly relevant because methane is a potent greenhouse gas and its emissions from mining operations represent a significant environmental challenge. At the same time, variable methane concentrations, the presence of other gas components and fluctuating gas supply create additional requirements for feed-gas conditioning, process control and reactor design.

[1] Oil and Gas Institute – National Research Institute, Kraków, Poland

The current research also explores innovative catalytic systems based on fibrous supports, including modified mineral-derived materials. Their open structure and the possibility of depositing catalytically active metals offer a promising basis for improving gas–solid contact and tailoring the distribution of active sites. Laboratory studies examine support modification, catalyst preparation and the potential use of transition-metal-based active phases for methane decomposition.

Overall, the results highlight both the potential and the limitations of methane pyrolysis as an alternative hydrogen production technology. Its integration with methane recovery from coal mines, combined with further development of structured fibrous catalysts, may contribute to reducing greenhouse gas emissions and to the more efficient utilisation of methane-containing streams. Further work is required to evaluate long-term stability, energy efficiency, carbon-product management and the environmental performance of the complete process.

[1] T.I. Korányi, M. Németh, A. Beck, A. Horváth, Recent Advances in Methane Pyrolysis: Turquoise Hydrogen with Solid Carbon Production, Energies, 15 (2022) 6342. https://doi.org/10.3390/en15176342
[2] J. Prabowo, L. Lai, B. Chivers, D. Burke, A.H. Dinh, L. Ye, Y. Wang, Y. Wang, L. Wei, Y. Chen, Solid carbon co-products from hydrogen production by methane pyrolysis: Current understandings and recent progress, Carbon, 216 (2024) 118507. https://doi.org/10.1016/j.carbon.2023.118507
[3] J. Song, S. Park, Review of methane pyrolysis for clean turquoise hydrogen production, Journal of Analytical and Applied Pyrolysis, 183 (2024) 106727. https://doi.org/10.1016/j.jaap.2024.106727
[4] M. Wojtasik, W. Krasodomski, G. Żak, K. Wojtasik, W. Pakieła, Morphological and Structural Analysis of Pyrolytic Carbon from Simple Thermal Methane Pyrolysis, Applied Sciences, 15 (2025) 10742. https://doi.org/10.3390/app151910742
[5] K. Wojtasik, K. Suchanek, M. Wojtasik, P. Dulian, K. Matus, M. Mitura-Nowak, Ultrasonic Dispersion of Pyrolytic Carbon: Synthesis, Characterization, and Photoluminescence Properties of Stable Colloidal Solutions, Applied Sciences, 15 (2025) 12655. https://doi.org/10.3390/app152312655
[6] M. Wojtasik, Z. Burnus, J. Markowski, G. Żak, J. Lubowicz, Piroliza metanu – wpływ wybranych parametrów na przebieg procesu, Nafta-Gaz, 79 (2023) 484–489. https://doi.org/10.18668/NG.2023.07.06
[7] J. Markowski, M. Wojtasik, Piroliza metanu na tle wybranych metod otrzymywania wodoru, Nafta-Gaz, 79 (2023) 428–435. https://doi.org/10.18668/NG.2023.06.07
[8] M. Wojtasik, G. Żak, J. Markowski, Z. Burnus, W. Krasodomski, W. Pakieła, Dekarbonizacja metanu z udziałem katalizatorów na bazie żelaza, Przemysł Chemiczny, 102 (2023) 259–263. https://doi.org/10.15199/62.2023.3.4
[9] W. Krasodomski, M. Wojtasik, J. Markowski, G. Żak, Dekarbonizacja metanu – kierunki zagospodarowania węgla popirolitycznego, Nafta-Gaz, 78 (2022) 56–63. https://doi.org/10.18668/NG.2022.01.06
[10] M. Wojtasik, J. Markowski, G. Żak, Katalityczna dekompozycja metanu jako źródło cennego wodoru, Przemysł Chemiczny, 101 (2022). https://doi.org/10.15199/62.2022.3.1

Funded by:
- Methane to Hydrogen Conversion for Emission Reduction and Energy Generation – METH2GEN, RFCS BIG TICKET PROJECT Agreement No. 6180/FBWiS/2025/2
- National Science Centre, Poland, Grant number: 2025/09/X/ST5/00196

EFE2026 ENERGY FUELS ENVIRONMENT
INTERNATIONAL CONFERENCE
17-20 NOVEMBER 2026, KRAKÓW, POLAND

How Human Activity on Long Weekends Affect Air Pollution with Fine Particulate Matter (PM1 and PM2.5) in the Coastal Zone of the Baltic Sea (Gdynia Case Study)?

Eliza Wolak[1*], Justyna Pyssa[1], Agnieszka Orzechowska-Zięba[1], Łukasz Nuckowski[2], Katarzyna Styszko[1], Anita Urszula Lewandowska[2]

Keywords: suspended particulate matter, anthropogenic pressure, meteorology influence, coastal urban area

ABSTRACT

Air pollution by particulate matter constitutes a significant environmental issue, particularly in urbanized coastal areas, where it can be influenced by both, natural and anthropogenic emission sources as well as changing synoptic situation [1]. Fine and ultrafine particulate fractions - including PM2.5 and PM1 - are of particular importance due to their ability to penetrate deep into the respiratory system and their potential impact on human health [2]. Characterization of the concentrations of these fractions enables a better assessment of air pollution variability and the identification of the factors responsible for its occurrence.

This paper presents the results of PM2.5 and PM1 particulate matter monitoring conducted in the coastal zone of the Baltic Sea during the spring and summer of 2026. The measurements covered periods associated with long weekends in May and June, as well as the transition between June and July, enabling an assessment of PM2.5 and PM1 concentration variability during specific times of heightened human activity and intensified traffic.

The study was conducted in the central part of Gdynia (54°31'N, 18°48'E) at a monitoring station located on the roof of the Faculty of Oceanography and Geography building (University of Gdańsk). Gdynia is a highly urbanized city situated approximately 1 km from the Baltic Sea coast. The immediate vicinity of the monitoring site is dominated by residential, commercial, and industrial areas. The station is located about 300 m from one of the city's main thoroughfares, characterized by heavy traffic and dense urban development. Additionally, the Tricity Bypass—a major transport route for both local and transit traffic—runs approximately 2 km to the southwest. Air quality in the study area is also influenced by nearby industrial zones, including ports infrastructure, shipyards, and food and chemical processing plants. The location of the monitoring site allows for the assessment of the impact of both natural and anthropogenic emissions on atmospheric aerosol composition.

Sampling of PM2.5 and PM1 aerosols was conducted in 24-hour cycles using low-volume (2.3 $m^3 \cdot h^{-1}$) HYDRA Dual Sampler (FAI Instruments, Italy) equipped with PM2.5 and PM1 inlets. To minimize the impact of atmospheric conditions on the sampling process, the temperature and humidity inside the sampler were regulated using an integrated heating and ventilation system. Atmospheric aerosols were collected on Whatman Q-MA quartz filters (47 mm in diameter). Prior to exposure, the filters were preheated at 850°C for a minimum of 6 hours to remove organic contaminants and minimize blank values. After sampling, the mass concentration of suspended particulate matter was determined by calculating the difference in filter weight before and after exposure and relating the

[1] Department of Fuel Technology, Faculty of Energy and Fuels, AGH University of Krakow, Al. Mickiewicza 30, 30-059 Krakow, Poland, * eklimows@agh.edu.pl
[2] Oceanography Institute, University of Gdańsk, Al. Marszałka J. Piłsudskiego 46, 81-378 Gdynia, Poland

resulting value to the volume of filtered air. Filter weighing was performed with a precision of 10^{-5} g using an XA analytical balance (RADWAG). All mass measurements were conducted under controlled laboratory conditions: a temperature of 23 ± 2°C and a relative humidity of 40 ± 5%. The measurements were supplemented by meteorological parameters (wind speed and direction, relative humidity and air temperature, amount of precipitation, atmospheric pressure) obtained for station Gdynia from ARMAAG [3]. In order to determine the movement of air masses, the HYSPLIT model developed by NOAA was used [4].

In Gdynia, during the period from 30 April to 13 May 2026, daily PM1 concentration ranged from 0.4 to 9.2 μg·m^{-3}, with a mean value of 3.9 ± 2.0 μg·m^{-3}. Daily PM2.5 concentration ranged from 2.7 to 14.5 μg·m^{-3}, averaging 8.4 ± 2.5 μg·m^{-3}. For both particulate matter fractions, the highest concentration was recorded on 3 May, corresponding to the last day of the May holiday weekend. During the period from 2 to 15 June 2026, daily PM1 concentration was even lower than during May long weekend, with an average value of 1.9 ± 1.8 μg·m^{-3}. The highest PM1 concentration (7.1 μg·m^{-3}) was recorded on 8 June, one day after the Corpus Christi holiday weekend. PM2.5 concentration ranged from 0.7 to 12.1 μg·m^{-3}, with an average of 4.4 ± 3.2 μg·m^{-3} and was also lower than during measurements conducted in May. The highest PM2.5 concentration (12.1 μg·m^{-3}) was recorded on 7 June, on the Sunday of the Corpus Christi weekend. The third measurement period covered the interval from 26 June to 2 July 2026. Daily PM1 concentration ranged from 2.2 to 8.3 μg·m^{-3}, with a mean value of 5.2 ± 2.2 μg·m^{-3}, while PM2.5 concentration ranged from 4.2 to 40.6 μg·m^{-3}, averaging 13.0 ± 11.6 μg·m^{-3}. The highest daily PM1 concentration (8.3 μg·m^{-3}) was recorded on 27 June, one day after the end of the school year. In the case of PM2.5, the highest concentration observed during all measurement periods was 40.6 μg·m^{-3}. This value was recorded on 29 June, one day after a Sunday with unrestricted retail trading. Furthermore, between 26 and 28 June, PM2.5 concentrations remained within the range of 9.8 to 12.3 μg·m^{-3}, representing relatively elevated levels compared with two previous measurement periods.

During the measurement campaigns conducted in Gdynia between 2 and 15 June 2026 and 26 June and 2 July 2026, considerable variability in air mass transport directions was observed. During the first period, winds alternated predominantly between the southern to southeastern (S-SE) and western to northwestern (W-NW) sectors. In contrast, during late June and early July, the initial inflow of air masses from the south was gradually replaced by transport from the northwestern to northern (NW-N-W) sectors. The prevailing air mass transport patterns indicate the potential influence of both anthropogenic emission sources, associated with urban areas, road traffic, and port-related activities, as well as marine aerosols characteristic of the coastal environment.

The planned chemical analyzes of suspended particulate matter (ionic composition, PAHs, OC and EC) supplemented by an analysis of meteorological conditions and air mass inflow directions will enable the determination of air quality indicators and allow for the identification of potential pollution sources within the study area.

[1] A.U. Lewandowska, L.M. Falkowska, High concentration episodes of PM10 in the air over the urbanized coastal zone of the Baltic Sea (Gdynia—Poland), Atmos. Res. 120–121 (2013) 55–67. https://doi.org/10.1016/j.atmosres.2012.08.002.
[2] D. Uchmanowicz, K. Styszko, X. Chen, G. Terribile, R. Jakhar, G. Sancini, J. Pyssa, Microplastics in airborne particulate matter: A comprehensive review of separation techniques, in vitro toxicity and health impacts, Int. J. Mol. Sci. 26 (2025) 10332. https://doi.org/10.3390/ijms262110332.
[3] Fundacja ARMAG, Air Quality Monitoring in the Gdańsk Metropolitan Area. https://armaag.gda.pl/ (accessed 28 September 2026).
[4] National Oceanic and Atmospheric Administration (NOAA), Air Resources Laboratory, HYSPLIT – Hybrid Single-Particle Lagrangian Integrated Trajectory Model. https://ready.arl.noaa.gov/HYSPLIT.php (accessed 28 September 2026).

Acknowledgments: The authors acknowledge the financial support of AGH University of Krakow, grant number 501.00-210000-10000. Research supported by AGH University of Krakow within the framework of the "Excellence Initiative-Research University" program.

Variability of Hydroxylated Polycyclic Aromatic Hydrocarbons (OH-PAHs) in Raw and Treated Municipal Wastewater

Justyna Pyssa[1,*], Laura Węgrzyn[1], Zuzanna Prus-Frączek[2], Karolina Cwynar[1], Dominika Uchmanowicz[1], Katarzyna Styszko[1]

Keywords: wastewater treatment; hydroxylated PAHs; biomarkers

ABSTRACT

As a result of increasing industrial activity, intensive agricultural development, population growth, and consumer lifestyle, the environment is becoming increasingly exposed to various pollutants. One of the largest groups of these compounds, often referred to as micropollutants, includes polycyclic aromatic hydrocarbons (PAHs). PAHs enter the natural environment through two primary pathways. The first is driven by natural factors. The second is anthropogenic emission [1]. As reported by [2], these compounds are routinely detected in water reservoirs - including rivers, lakes, and occasionally drinking water. However, due to their high hydrophobicity, their concentrations in water are typically much lower than in sediments and soils.

Aromatic hydrocarbons are metabolized in living organisms. As a result of these transformations, they are transformed into hydroxy derivatives of PAHs, which are then excreted in urine and sent to sewage treatment plants [3]. OH-PAHs are therefore biomarkers of human exposure to PAHs [4].

The aim of this study was to investigate the occurrence of selected hydroxylated polycyclic aromatic hydrocarbons (OH-PAHs) in raw wastewater and after the biological treatment process. Particular attention was paid to seasonal variability.

The material for the research came from the Kraków-Płaszów Wastewater Treatment Plant. Krakow is one of the largest cities in Poland. The Kraków-Płaszów Wastewater Treatment Plant has an average capacity of 165,000 m^3/day. It serves more than 780,000 residents. 70% of the wastewater generated in Krakow is treated there. It is the largest wastewater treatment plant in the city and the third largest in the country.

Samples for testing were collected in a cycle of 24 hours of collection during the period from the 5th to the 16th of February 2024 and 18th to the 30th August 2024. The research procedure employing LC-MS/MS is described in publication [3].

The target compounds were subsequently determined by liquid chromatography coupled with tandem mass spectrometry (LC-MS/MS). The investigated target compounds included 1-hydroxynaphthalene (1-OH-NAP), 2-hydroxynaphthalene (2-OH-NAP), 2-hydroxyfluorene (2-OH-FLU), the sum of 2-and 3-hydroxyphenanthrene (2-, 3- OH-PHEN), 1-hydroxypyrene (1-OH-PYR), and 3-hydroxybenzo[a]pyrene (3-OH-BaP).

Neither 3-OH-BaP nor 1-OH-PYR was detected in any of the analyzed samples. Prior to the treatment process, the highest concentrations were recorded for fluorenols (reaching up to 1100 ng/L in winter) and 1-OH-NAP (up to 614 ng/L in summer). The wastewater treatment process exhibited highly variable efficiency in winter, concentrations of 2-OH-NAP in the treated effluent reached nearly 2000 ng/L.

The results indicate significant variability in the occurrence and phase distribution of hydroxylated PAHs (OH-PAHs) in municipal wastewater treatment systems. Seasonal

[1] Department of Fuel Technology, Faculty of Energy and Fuels, AGH University of Krakow, Al. Mickiewicza 30, 30-059 Krakow, Poland, * jpyssa@agh.edu.pl

[2] Department of Heat Engineering and Environment Protection, Faculty of Metals Engineering and Industrial Computer Science, AGH University of Krakow, Al. Mickiewicza 30, 30-059 Krakow, Poland

variability linked to weather conditions, such as temperature fluctuations and precipitation is evident, as these factors influence the quality of the treated wastewater. The dataset provides new information for wastewater monitoring and for understanding the fate and phase distribution of these compounds.

[1] L. Frydel, Z. Prus, K. Cwynar, J. Pamuła, J. Pyssa, R. Rego, K. Styszko, Determination of hydroxy derivatives of PAHs in sewage sludge by GC-MS/MS, Desalin. Water Treat. 321 (2025) 101015. https://doi.org/10.1016/j.dwt.2025.101015.
[2] A. Celma, A.-K. Dahlberg, K. Wiberg, Analysis of polycyclic aromatic hydrocarbons (PAHs) and their derivatives in biochar treated stormwater, MethodsX 10 (2023) 102232. https://doi.org/10.1016/j.mex.2023.102232.
[3] K. Styszko, W. Bolesta, J. Worek, Z. Prus, K. Cwynar, J. Pyssa, D. Uchmanowicz, L. Frydel, A.P. Daso, B. Kasprzyk-Hordern, Tracking nonregulated micropollutants in sewage sludge: Antimicrobials, OH-PAHs, and microplastics—Environmental risks, fertilizer implications and energy considerations, Energy Rep. 13 (2025) 4756–4768. https://doi.org/10.1016/j.egyr.2025.04.013.
[4] Z. Yang, C. Guo, Q. Li, Y. Zhong, S. Ma, J. Zhou, X. Li, R. Huang, Y. Yu, Human health risks estimations from polycyclic aromatic hydrocarbons in serum and their hydroxylated metabolites in paired urine samples, Environ. Pollut. 290 (2021) 117975. https://doi.org/10.1016/j.envpol.2021.117975.
Acknowledgments: The project was funded by the Polish National Science Centre (grant no. 2022/45/B/ST10/02108).

EFE2026 ENERGY FUELS ENVIRONMENT
INTERNATIONAL CONFERENCE
17-20 NOVEMBER 2026, KRAKÓW, POLAND

Effect of Cerium and Lanthanum Addition on Vermiculite-Supported Nickel Catalysts for CO_2 Methanation

Michał Szymaszek[1,*], Agnieszka Szymaszek-Wawryca[1], Monika Motak[1]

Keywords: CO_2 methanation; vermiculite; nickel catalysts; cerium; lanthanum; melt infiltration

ABSTRACT

The catalytic hydrogenation of carbon dioxide (CO_2) to methane is an attractive route for CO_2 utilization and its efficiency strongly depends on the properties of the applied catalyst [1]. Nickel-based catalysts are widely investigated for this reaction, and their performance can be modified through support selection and changes in catalyst composition [1,2]. The addition of rare-earth elements, including ceria (CeO_2) and lanthanum oxide (La_2O_s), can influence surface basicity and nickel particle size, thereby, affecting catalytic behavior [3]. Additionally, layered aluminosilicates, such as vermiculite, can act as alternative, eco- friendly support the novel, sustainable methanation catalysts [4,5]. The presented study focused on evaluating the effect of cerium and lanthanum addition on the physicochemical properties and CO_2 methanation performance of nickel catalysts supported on chemically- modified vermiculite. The support was prepared by acid leaching of the clay using 0.5M HNO_3 at 100 °C for 24 h, followed by calcination at 600 °C for 4 h. Nickel and the promoters (CeO_2 or La_2O_3) were subsequently introduced onto the modified support by mechanical grinding followed by slow melt infiltration of the metal precursor salts into the inner porous structure of the acid-modified clay. Three catalysts with a nominal nickel content of 15 wt.% were prepared: 15N, containing nickel without a rare-earth additive; 15N15C, additionally containing 15 wt.% cerium; and 15N15L, additionally containing 15 wt.% lanthanum (the contents of Ni, Ce, and La were calculated on the metal basis). The resulting samples were calcined at 550 °C for 4 h. The materials were characterized by N_2 sorption at 77 K, X-ray diffraction (XRD), hydrogen temperature-programmed reduction (H_2-TPR), carbon dioxide temperature-programmed desorption (CO_2-TPD), and X-ray fluorescence (XRF). These techniques were used to assess the textural properties, phase composition, reducibility, surface basicity, and elemental composition of the catalysts, respectively. Their catalytic performance in CO_2 methanation was evaluated in a laboratory-scale set-up in terms of CO_2 conversion, methane selectivity, and methane yield. In general, the obtained results showed that vermiculite activated with nitric acid can be used as a promising support of CO_2 methanation catalyst. Additionally, the reducibility of the CeO_2-promoted sample was notably improved compared with the non- promoted 15N catalyst, which contributed to enhanced CO_2 hydrogenation at low temperature.

[1] M. Sánchez-González, A. Villardon, R. Campana, L. Sánchez-Silva, F. Dorado, A. Romero, Ni-catalysts supported on N,B-doped graphene aerogels for CO_2 methanation, ACS Appl. Nano Mater. 8 (2025) 21813–21827. https://doi.org/10.1021/acsanm.5c03770.
[2] P. Summa, M. Gajewska, L. Li, C. Hu, B. Samojeden, M. Motak, P. Da Costa, Solution combustion synthesis as an alternative synthesis route for novel Ni-Mg-Al mixed-oxide catalyst for CO_2 methanation, J. CO_2 Util. 60 (2022) 101983. https://doi.org/10.1016/j.jcou.2022.101983.
[3] J.B. Branco, P.E. Brito, A.C. Ferreira, Methanation of CO_2 over nickel-lanthanide bimetallic oxides supported on silica, Chem. Eng. J. 380 (2020) 122465. https://doi.org/10.1016/j.cej.2019.122465.
[4] P. Li, B. Wen, F. Yu, M. Zhu, X. Guo, Y. Han, L. Kang, X. Huang, J. Dan, F. Ouyang, B. Dai, High efficient nickel/vermiculite catalyst prepared via microwave irradiation-assisted synthesis for carbon monoxide methanation, Fuel 171 (2016) 263–269. https://doi.org/10.1016/j.fuel.2015.12.076.
[5] D. Cortés-Murillo, C. Blanco-Jiménez, C.E. Daza, Clay exfoliation method as a route to obtain mesoporous

1 AGH University of Krakow, michal.szymaszek@agh.edu.pl

catalysts for CO_2 methanation, MethodsX 10 (2023) 101955. https://doi.org/10.1016/j.mex.2022.101955.

Acknowledgments: This research was funded by the Polish Ministry of Science and Higher Education through research subsidy No. 501.00-210000-10000.

Influence of Oxidative Modification of Activated Carbon on the Removal of Organic Micropollutants from Water

Agnieszka Orzechowska-Zięba[1*], Laura Węgrzyn[1], Eliza Wolak[1], Elżbieta Vogt[1], Dominika Uchmanowicz[1], Justyna Pyssa[1], Gabriela Kulka[1], Katarzyna Styszko[1]

Keywords**:** activated carbon, oxidative modification, adsorption, pharmaceuticals, OH-PAHs

ABSTRACT

Organic micropollutants, including pharmaceuticals, endocrine-disrupting compounds, and polycyclic aromatic hydrocarbon (PAH) derivatives, are frequently detected in surface waters, groundwater, and treated wastewater. Their occurrence in aquatic environments results from increasing pharmaceutical consumption, incomplete removal during conventional wastewater treatment processes, and the persistence of many organic compounds [1]. Due to their biological activity and potential adverse effects on aquatic organisms, these contaminants have become an important challenge for modern water treatment technologies [1,2].

Adsorption onto activated carbon is considered one of the most effective methods for the removal of trace organic contaminants from water. The efficiency of the process depends not only on the porous structure of the adsorbent but also on the physicochemical properties of its surface. Chemical modification of activated carbon using oxidizing agents may alter surface characteristics and consequently influence the adsorption of compounds exhibiting different physicochemical properties [3].

The aim of this study was to evaluate the effectiveness of unmodified and chemically modified activated carbon in the removal of selected organic micropollutants from aqueous solutions. The investigated compounds included pharmaceuticals representing different therapeutic classes, endocrine disrupting compounds, a biomarker of tobacco smoke exposure, and hydroxylated PAH derivatives recognized as important indicators of anthropogenic pressure and environmental quality.

Materials and Methods

A commercial activated carbon (AC) and three chemically modified carbon materials were used in the study. Oxidative modification was performed using:

- 65% nitric acid (AC-HNO_3),
- a 1:1 (v/v) mixture of 65% nitric acid and deionized water (AC-HNO_3/H_2O),
- 30% hydrogen peroxide (AC-H_2O_2).

Modification with nitric acid and diluted nitric acid was carried out under reflux conditions at the boiling temperature of the reaction mixture for 2 h. Oxidation with hydrogen peroxide was conducted for 24 h at room temperature. After modification, the adsorbents were washed with deionized water until neutral pH was achieved and subsequently dried to constant weight.

Adsorption experiments were performed under batch conditions. Activated carbon samples (0.05 g) were added to model solutions containing a mixture of micropollutants at an initial concentration of 100 ng cm^{-3}. The maximum contact time was 4 h. Samples were collected after 30 min and 4 h of adsorption.

A total of 38 compounds belonging to different groups of emerging contaminants were investigated, including pharmaceuticals, antibiotics, non-steroidal anti-inflammatory drugs (NSAIDs), endocrine-active compounds, biomarkers, and hydroxylated PAHs (OH-PAHs).

[1] Department of Fuel Technology, Faculty of Energy and Fuels, AGH University of Krakow, Al. Mickiewicza 30, 30-059 Krakow, Poland, *azieba@agh.edu.pl

Concentrations of the target compounds were determined using liquid chromatography coupled with tandem mass spectrometry (LC-MS/MS).

Results and Discussion

The applied modification procedures enabled the assessment of the influence of different oxidizing agents on the adsorption of organic micropollutants exhibiting diverse physicochemical properties. The investigated compounds included both relatively polar pharmaceuticals and metabolites, as well as more hydrophobic hydroxylated PAHs, allowing a comparison of adsorption behaviour among different contaminant classes.

The obtained results demonstrated differences in adsorption performance depending on both the type of adsorbent and contact time. The most pronounced decrease in micropollutant concentrations was observed during the initial stages of the process, indicating the importance of rapid adsorption mechanisms in the removal of trace organic contaminants.

The comparison between unmodified and oxidized activated carbons showed that chemical modifications improve the sorption properties of adsorbents and increase the removal efficiency of micropollutants from water in comparison with unmodified activated carbon. observed differences were associated with the physicochemical characteristics of the adsorbates as well as the properties of the adsorbents resulting from the applied modification procedure.

Conclusions

Chemical modification of commercial activated carbon using nitric acid and hydrogen peroxide affected the removal efficiency of the investigated organic micropollutants.

Adsorption performance depended on both the type of adsorbent and the physicochemical properties of the target compounds.

The obtained results confirm the potential applicability of modified activated carbons as adsorbents for the removal of trace organic contaminants from water.

[1] K. Styszko, K. Proctor, E. Castrignanò, B. Kasprzyk-Hordern, Occurrence of pharmaceutical residues, personal care products, lifestyle chemicals, illicit drugs and metabolites in wastewater and receiving surface waters of Krakow agglomeration in South Poland, Sci. Total Environ. 768 (2021) 144360. https://doi.org/10.1016/j.scitotenv.2020.144360.

[2] E. Kmiecik, K. Styszko, K. Wątor, M. Dwornik, B. Tomaszewska, BPA – an endocrine disrupting compound in water used for drinking purposes, a snapshot from South Poland, Geol. Geophys. Environ. 46 (2020) 5–16. https://doi.org/10.7494/geol.2020.46.1.5.

[3] R.M.C. Viegas, A.S. Mestre, E. Mesquita, M. Machuqueiro, M.A. Andrade, A.P. Carvalho, M.J. Rosa, Key factors for activated carbon adsorption of pharmaceutical compounds from wastewaters: A multivariate modelling approach, Water 14 (2022) 166. https://doi.org/10.3390/w14020166.

Acknowledgments: The project was funded by the Polish National Science Centre (grant no. 2022/45/B/ST10/02108). Research supported by AGH University of Krakow within the framework of the "Excellence Initiative-Research University" program.

EFE2026 ENERGY FUELS ENVIRONMENT
INTERNATIONAL CONFERENCE
17-20 NOVEMBER 2026, KRAKÓW, POLAND

Experimental Investigation of Fuel-Cell Waste Heat Recovery for Thermal Management of a Metal-Hydride Hydrogen Storage Cylinder

Jakub Cebo[1,*], Ignacy Czajkowski[1], Jakub Ekes[1], Norbert Jamrozik[1], Kacper Wądołkowski[1], Stanisław Pilarski[1]

Keywords: Hydrogen fuel cell, Waste heat recovery, Metal hydride storage, Thermal management

ABSTRACT

Hydrogen fuel cells generate electrical power while releasing heat that is commonly removed by a cooling system. Recovering this thermal energy may improve the overall utilization of energy in hybrid power modules. This study presents the design, construction and preliminary experimental assessment of a laboratory test bench intended to investigate the use of waste heat from a hydrogen fuel cell to control the temperature of a metal-hydride hydrogen storage cylinder. The system is based on a Horizon H-500W fuel cell and directs its cooling air through a dedicated duct towards a copper heat exchanger mounted on the cylinder.

Preliminary measurements were performed to characterize the available heat stream and the thermal properties of the storage cylinder. At a fuel-cell current of 40 A, the thermal power carried by the cooling air was estimated from the experimental graph at approximately 580 W. This value refers specifically to the cooling-air stream and should not be interpreted as the total waste heat generated by the fuel cell. The thermal properties of the metal-hydride storage cylinder were determined in a preliminary calorimetric experiment, with the cylinder placed inside a calorimeter. The determined heat capacity of the cylinder was 2889 J/K, while its average specific heat capacity was 893 J/(kg·K). These values were used as input data for the subsequent design of the test bench.

The initial manually monitored arrangement offered no means of adjusting the airflow directed towards the cylinder, creating a risk of excessive heating. To address this limitation, a test bench with adjustable airflow gates and digital data acquisition was developed. The selected exchanger consists of a copper cylindrical sleeve with soldered copper fins perpendicular to the cylinder axis. The exchanger was fitted tightly onto the cylinder using a hydraulic press. Selected structural and control components were designed for additive manufacturing.

An original Python application running on a Raspberry Pi 4B controls two servomechanisms that position the airflow gates. The interface allows calibration and adjustment of gate opening from 0 to 100%, displays selected sensor signals in real time, and records measurements to CSV files at approximately one-second intervals. The system supports up to eight temperature sensors and two combined temperature, pressure and humidity sensors. Following assembly, control measurements were carried out to evaluate operation of the integrated test bench.

During the main experimental run, 2610 readings were collected over 43.5 minutes at four temperature measurement locations. The temperature measured at the cylinder (T2) increased from 21.9 to 39.6 °C, corresponding to a rise of 17.7 °C. This observation demonstrates heat transfer from the fuel-cell cooling-air stream to the cylinder equipped with the copper exchanger. It does not, however, establish that closed-loop temperature stabilization has already been achieved.

The completed test bench provides a platform for systematic investigation of fuel-cell

[1] AGH University of Krakow, Faculty of Energy and Fuels, FENEC Reserch Student Club

waste-heat recovery and metal-hydride storage thermal management. Future work will extend the instrumentation to hydrogen pressure, airflow and gate-position measurements and implement automatic cylinder temperature regulation. The present results confirm the functionality of the experimental platform and support further evaluation of controlled heat recovery in hybrid hydrogen power systems.

EFE2026 ENERGY FUELS ENVIRONMENT
INTERNATIONAL CONFERENCE
17-20 NOVEMBER 2026, KRAKÓW, POLAND

Modular Reactor for Direct and Indirect Electrolysis Manufactured Using 3D Printing: From Dimensional Prototyping with Cost-Effective PETG to a Leak-Tight ABS Process Reactor

Aleksandra Chwała[1], Alekander Pizoń[1], Aleksander Piasecki[1], Wiktor Piekarski[1], Jacek Kowalczyk[1], Maciej Siekierski[1]

Keywords: rapid prototyping, 3D printing, electrochemical reactor, brackish water, ABS

ABSTRACT

Electrochemical water splitting offers a route to hydrogen production using electricity from renewable energy sources. The use of brackish water can reduce the demand for purified feedwater, but also introduces technological challenges associated with chloride ions, other dissolved species, electrode corrosion and competing reactions [1]. The proposed

laboratory reactor is designed as a membraneless flow-through electrolyzer, intended for water electrolysis, including brackish-water feeds, and for investigating a potential

configuration combining water electrolysis with electrochemical CO2 reduction. Its modular construction allows individual components to be rearranged, replaced or attached, enabling different process configurations, including the potential integration of a membrane. Two process routes are considered: direct electrolysis of brackish water without preliminary desalination and indirect electrolysis using pretreated water. The latter may reduce contamination-related problems, whereas the former can limit the extent of feedwater pretreatment. The formation and possible recovery of chlorine-containing products [2], as well as any water-treatment benefits, remain research questions rather than established

Comparing these process routes using separately constructed laboratory reactors would require substantial time and repeated fabrication of components [3,4]. Rapid prototyping based on 3D printing opens new possibilities for designing multifunctional electrochemical reactors [3,4]. The main challenges, however, remain the microporosity of printed parts, susceptibility to leakage, and the chemical resistance of the material in the electrolyte and electrochemical reaction products [3,5].

The aim of this work was to design a multifunctional electrolyzer capable of accommodating both direct and indirect water electrolysis, with the planned experimental investigation focused primarily on direct electrolysis of brackish water, and to develop an optimal material and manufacturing route ensuring system leak-tightness.

Methodology and Research Path. The design is modular: components can be rearranged and additional elements attached, initially allowing the reactor to be modified into three separate functions/process configurations. After being designed using Autodesk Inventor CAD tools, the components can be manufactured within a few days (the main limitations are printer dimensions and printing capacity). Assembly of the selected configuration takes from 15 minutes to one hour.

Preliminary Stage (Verification of Design Assumptions). The first prototypes were made of glycol-modified polyethylene terephthalate (PETG). They were used to verify the fit of system components (including electrodes), tightness between individual parts, and the geometry of flow channels. Slight deformations of the PETG channels were observed, but they did not significantly affect system operation; the channels are designed to connect to silicone tubing.

[1] Politechnika Warszawska, Warszawa, Polska, 01212275@pw.edu.pl

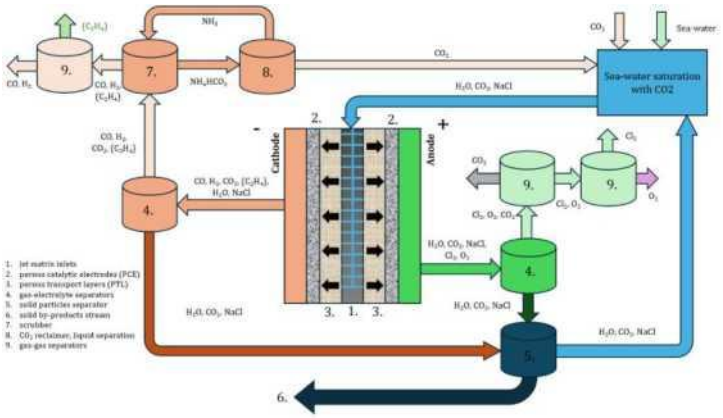


Figure1.Conceptual process scheme supplied with the draft

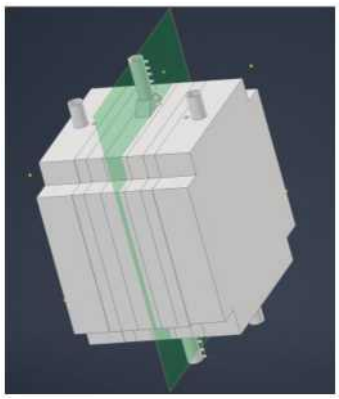


Figure 2. Preliminary CAD model of the modular reactor (authors' own design).

Target Stage (ABS and Sealing). Acrylonitrile–butadiene–styrene (ABS) was selected as the target construction material owing to its high chemical resistance; its electrochemical durability remains to be verified after commissioning. To reduce interlayer porosity associated with 3D printing, the ABS components ready for assembly will undergo chemical sealing and smoothing, either in solvent vapour or by direct application of dichloromethane (methylene chloride, CH_2Cl_2) to finished parts using a brush or immersion. This method and solvent were selected on the basis of reports of its effectiveness in smoothing ABS.

Results and Conclusions. Dimensional verification using the PETG model confirmed the correctness of the CAD design assumptions and the repeatability of manufacturing while maintaining the 3D printing parameters. Planned tests include a comparative assessment of pressure drop (system leak-tightness) before and after chemical smoothing of ABS, analysis of possible geometric deformations caused by chemical treatment, and examination of the system's electrochemical performance in different configurations. These tests will help identify the most suitable method of electrochemical water splitting and assess the possibility of operating the reactor, and its service life, using brackish or contaminated water.

[1] J. Guo, Y. Zheng, Z. Hu, C. Zheng, J. Mao, K. Du, M. Jaroniec, S.-Z. Qiao, T. Ling, Direct seawater electrolysis by adjusting the local reaction environment of a catalyst, Nat. Energy 8 (2023) 264–272. https://doi.org/10.1038/s41560-023-01195-x.
[2] S. Zhao, H. Li, J. Dai, Y. Jiang, G. Zhan, M. Liao, H. Sun, Y. Shi, C. Ling, Y. Yao, L. Zhang, Selective electrosynthesis of chlorine disinfectants from seawater, Nat. Sustain. 7 (2024) 148–157. https://doi.org/10.1038/s41893-023-01265-8.
[3] R. Granados-Fernández, A. Cárdenas-Arenas, M.A. Montiel, Revolutionizing lab-scale electrochemical reactors: Innovative breakthroughs with 3D printing fabrication, ChemElectroChem 11 (2024) e202400205. https://doi.org/10.1002/celc.202400205.
[4] A. Ambrosi, M. Pumera, 3D-printing technologies for electrochemical applications, Chem. Soc. Rev. 45 (2016) 2740–2755. https://doi.org/10.1039/C5CS00714C.
[5] C. Neff, M. Trapuzzano, N.B. Crane, Impact of vapor polishing on surface quality and mechanical properties of extruded ABS, Rapid Prototyp. J. 24 (2018) 501–508. https://doi.org/10.1108/RPJ-03-2017-0039.

EFE2026 ENERGY FUELS ENVIRONMENT
INTERNATIONAL CONFERENCE
17-20 NOVEMBER 2026, KRAKÓW, POLAND

Heavy Industry Waste as an Alternative Means of Supporting Fire and Rescue Actions

Radosław Wójcik[1]*, Anna Magiera[1], Aneta Magdziarz[1]

Keywords**:** glass dust, blast furnace slag, industrial waste valorisation, fire and rescue operations, circular economy in fire safety

ABSTRACT

All kinds of industries cause air, soil, and water pollution and generate hazardous solid waste. Using heavy industry waste is feasible only if environmental and economic sustainability are successfully met. Much of heavy industry waste is used as an addition to either cement or concrete because they have major beneficial effects on the performance of reinforced structures – e.g. blast furnace slags [1,2]. Reusing other industrial waste, e.g. glass sand dust, has a lower environmental footprint [3].

In Poland, the State Fire Service and business entities successfully use several materials to remove various oil spills and to eliminate environmental hazards (e.g. during fire and rescue actions and in case of leaks at gas stations). The most universal sorbent is diatomite, but the final product requires thermal and mechanical processing, which determines its mineralogical composition, specific surface area, and particle morphology [4]. Each processing step adds cost, and the accelerating depletion of natural resources (especially raw materials from diatomite mines) becomes a limitation. These challenges have put the industry sector under considerable pressure to reduce waste-related environmental impact and use it as an alternative solution.

This work provides the theoretical background for effectively applying iron/steel slag and glass dust in fire prevention as fire-extinguishing powder and absorbent material. Considering their properties (e.g., thermal decomposition and powder constituents), "glass dust" or "slag" fire extinguishers can be a common fire safety equipment, as they can extinguish different kinds of fires, such as paper, wood, gasoline, electrical wires, and electronic devices. Currently, experimental results are limited, but researchers have discussed the possible fire-extinguishing mechanisms of new materials many times [5], especially for battery [6,7] and photovoltaic fires [8].

[1] J. Bijen, Benefits of slag and fly ash, Constr. Build. Mater. 10 (1996) 309–314. https://doi.org/10.1016/0950-0618(95)00014-3.
[2] S. Nasier, Utilization of recycled form of concrete, E-wastes, glass, quarry rock dust and waste marble powder as reliable construction materials, Mater. Today Proc. 45 (2021) 3231–3234. https://doi.org/10.1016/j.matpr.2020.12.381.
[3] S.C. Bostanci, Use of waste marble dust and recycled glass for sustainable concrete production, J. Clean. Prod. 251 (2020) 119785. https://doi.org/10.1016/j.jclepro.2019.119785.
[4] M. Łach, K. Pławecka, J. Marczyk, C. Ziejewska, M. Hebdowska-Krupa, M. Nykiel, M. Hebda, K. Miernik, D. Mierzwiński, K. Korniejenko, J. Mikuła, K. Smoroń, Use of diatomite from Polish fields in sustainable development as a sorbent for petroleum substances, J. Clean. Prod. 389 (2023) 136100. https://doi.org/10.1016/j.jclepro.2023.136100.
[5] X. Ni, K. Kuang, D. Yang, X. Jin, G. Liao, A new type of fire suppressant powder of NaHCO3/zeolite nanocomposites with core–shell structure, Fire Saf. J. 44 (2009) 968–975. https://doi.org/10.1016/j.firesaf.2009.06.004.
[6] O. Mammacıoğlu, G. Coskun, A new experimental approach to lithium-ion battery fires in electric vehicles: Investigation of fire behavior and effectiveness of extinguishing agents, Case Stud. Therm. Eng. 73 (2025) 106554. https://doi.org/10.1016/j.csite.2025.106554.

[1] AGH University of Krakow, Faculty of Metals Engineering and Industrial Computer Science, Department of Heat Engineering and Environment Protection, *rwojcik@agh.edu.pl

[7] Z. Bai, X. Li, J. Deng, C.-M. Shu, Y. Zhang, Overview of anti-fire technology for suppressing thermal runaway of lithium battery: Material, performance, and applications, J. Power Sources 640 (2025) 236767. https://doi.org/10.1016/j.jpowsour.2025.236767.
[8] M.M.B.A. Mohamed, Y.X. Ang, R.J.H. Tan, L.S. Tung, X. Xiao, M. Das, L.W.T. Ng, Investigating the fire dynamics of mounted PV weathering effects and material changes, iScience 28 (2025) 113410. https://doi.org/10.1016/j.isci.2025.113410.

Acknowledgements: This research was funded by the Ministry of Science and Higher Education, Poland [AGH grant no. 16.16.110.663/501.00-110000-10000].

EFE2026 ENERGY FUELS ENVIRONMENT
INTERNATIONAL CONFERENCE
17-20 NOVEMBER 2026, KRAKÓW, POLAND

PROZA: A Sectoral Econometric Model for Long-Term Energy Demand Forecasting in Poland

Wojciech Suwała[1], Janusz Zyśk[1,*], Artur Wyrwa[1], Marcin Pluta[1], Maciej Raczyński[1]

Keywords: energy demand forecasting, econometric modelling, PROZA model, sectoral energy consumption, energy scenarios

ABSTRACT

Long-term forecasting of energy demand is an essential component of national energy planning, particularly in the context of economic transformation, improvements in energy efficiency and ambitious decarbonisation targets. Reliable projections require modelling approaches that capture the relationships between economic activity, demographic developments, technological progress and energy consumption across different sectors of the economy. This paper presents PROZA, a sectoral energy demand forecasting model developed to analyse long-term changes in fuel and energy consumption in Poland up to 2050.

The methodological framework combines econometric analysis of historical energy consumption with scenario-based projections of macroeconomic, demographic and sector-specific variables. The model adopts a demand-oriented approach in which future energy requirements are determined by changes in economic activity and other explanatory factors rather than by optimisation of energy supply technologies. Historical data from Eurostat and Statistics Poland covering the period 2001–2024 provide the basis for identifying and estimating relationships between energy consumption and its principal determinants.

The model distinguishes major energy-consuming sectors, including industry, transport, households, services and agriculture, allowing their specific demand characteristics to be represented. Sectoral equations incorporate selected explanatory variables such as gross value added, industrial production, population-related indicators, residential floor area and heating and cooling degree days. Where appropriate, lagged energy consumption and dummy variables are introduced to account for consumption persistence and exceptional historical conditions. The estimated econometric relationships provide a quantitative basis for assessing how changes in the explanatory variables influence future sectoral energy requirements.

The modelling approach allows alternative assumptions concerning economic growth, industrial development, demographic trends and improvements in energy efficiency to be translated into long-term energy demand trajectories. Particular attention is given to energy-intensive industrial activities, where physical production indicators, including steel and fertiliser output, can complement conventional macroeconomic variables. The model can therefore support analyses of structural changes in the Polish economy and their implications for future energy consumption.

An important feature of PROZA is its potential application within integrated energy–economy modelling frameworks. By translating projected economic activity and demand for products and services into physical energy demand drivers, the model can provide consistent scenario inputs for complementary energy system analyses. This functionality is particularly relevant for assessing the consequences of industrial transformation, electrification and the development of low-carbon fuels.

The presented framework demonstrates how sector-specific econometric relationships

[1] AGH University of Krakow, Faculty of Energy and Fuels, Krakow, Poland, * jazysk@agh.edu.pl

can support transparent and flexible long-term energy demand forecasting. PROZA provides a basis for evaluating alternative development pathways and their implications for national energy planning, while also offering opportunities for further integration with broader energy and macroeconomic modelling tools.

EFE2026 ENERGY FUELS ENVIRONMENT
INTERNATIONAL CONFERENCE
17-20 NOVEMBER 2026, KRAKÓW, POLAND

Modeling of Electrochemical Processes Occurring in Porous Materials by Means of a TLM-Based Impedance Model

Wiktor Piekarski[1], Jacek Kowalczyk[1], Maciej Siekierski[1]

Keywords: Electrochemical Impedance Spectroscopy (EIS), porous electrodes, Transmission Line Model (TLM), Gerischer element, Anomalous diffusion element

ABSTRACT

Electrochemical impedance spectroscopy (EIS) probes the frequency-dependent response of an electrochemical system to a small alternating perturbation. It provides information on interfacial polarization, reaction kinetics, adsorption and mass transport, making it useful for investigating porous electrode materials used in electrochemical energy storage.

The response of a porous electrode depends on processes occurring both at its outer surface and within electrolyte-filled pores. The depth of the region contributing to the measured response depends on frequency and on the transport and interfacial properties of the material. This spatially distributed behavior can be represented by a transmission line model (TLM), in which successive sections describe transport along the electrode and local polarization at the electrode–electrolyte interface.

This contribution outlines the use of TLM-based impedance models to describe electrochemical processes in porous materials. Attention is given to the presence or absence of charge-transfer reactions and to the boundary conditions of finite and semi-infinite models. The relationship between the model structure and the resulting impedance response is discussed at a qualitative level. Modified elements can account for departures from ideal behavior, while a double-rail representation allows transport in both the solid and electrolyte phases to be considered.

Fig 1 The general scheme od the correspondence between the electrochemical qualities of the porous structure of the electrode and the corresponding TLM based equivalent circuit of the non-lump element representing its immitance response.

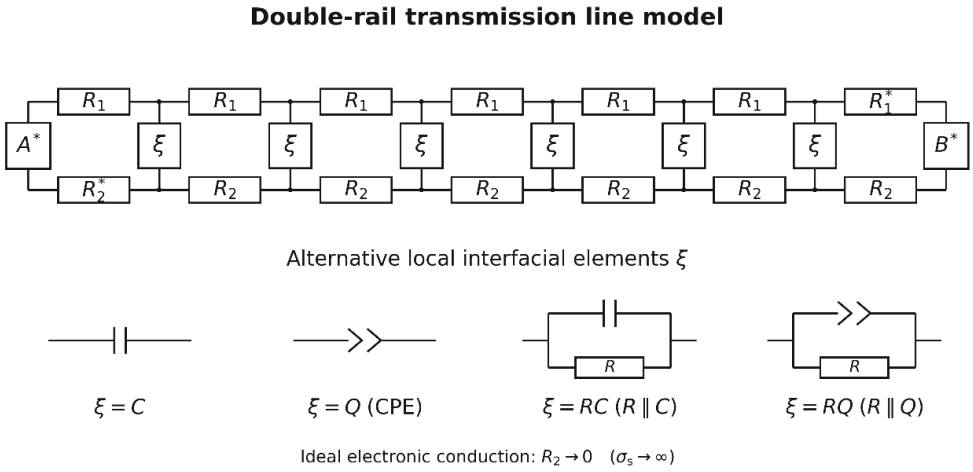


Figure 1. Double-*rail transmission line model of a porous electrode with alternative interfacial elements ξ.*

[1] Warsaw University of Technology, wiktor.piekarski2.stud@pw.edu.pl

Therefore, it is worth stressing that the same in terms of topology trnasmission line model can represent both the situation in which the charge accumulation process in th eleectroactive material is realted to the 'real' faradaic preocess occurring (X=RC or RQ depending on the importnace of the fractal/disperssive nature of the structure) what results in the Gerischer type repsonse or to intercalation/double layer charging process (X=C or Q) what characterized its Bisquert based counterpart. In addition to that one should note that both this cases idealize the conductivity of the electrode material up to infinity neglecting the need of the second series element located in the lower branch of the scheme.

Two battery examples illustrate the application of these concepts to equivalent-circuit fitting. The first concerns lead-acid batteries described using a Gerischer-type diffusion element (Fig. 2); the second concerns lithium-ion batteries described using an M-type diffusion element (Fig. 3). The impedance spectra and their corresponding fits provide a basis for discussing the choice of model elements and their physical interpretation. The emphasis is on relating the equivalent circuit to the porous nature of the electrode and to the processes represented by the model.

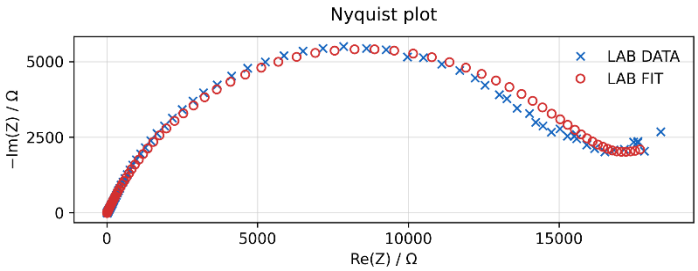


Figure 2. Fitting of an equivalent circuit using a Gerischer-type diffusion element in lead-acid batteries.

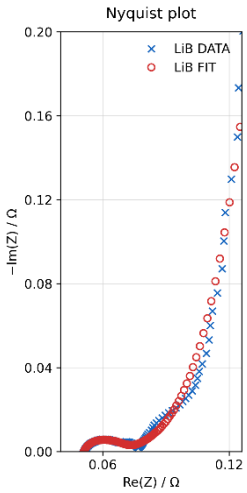


Figure 3. Fitting of an equivalent circuit using an M-type diffusion element in lithium-ion batteries.

Acknowledgements: This work was supported by the National Centre for Research and Development (NCBR) under Grant WPC3/2022/29/IMPRESSION/2025 and has been additionally supported by the Faculty of Chemistry, Warsaw University of Technology.

EFE2026 ENERGY FUELS ENVIRONMENT
INTERNATIONAL CONFERENCE
17-20 NOVEMBER 2026, KRAKÓW, POLAND

Weather-Related Price Patterns in the Polish Electricity Market

Patryk Garnek[1], Mikołaj Rzepka[2]*, Szymon Podlasek[3]

Keywords: electricity prices, wind speed, solar irradiance, price analysis

ABSTRACT

The rapid growth of weather-dependent sources of energy like photovoltaics or wind generators in Poland is changing the way electricity prices are formed. High solar generation can contribute to low or negative prices during the day, while prices may rise sharply in the evening. Understanding these changes is important for developing better energy storage and energy management solutions.

This study presents a Python-based framework for collecting and analysing Polish electricity market data and weather data. The analysed price is the market price of electricity (RCE) published by the Polish Power Grid Operator (PSE) at 15-minute resolution. Those prices were aggregated into hourly values and combined with weather data from Open-Meteo for 18 locations covering all 16 voivodeships and a national average. Both data sets were aligned to local time (CET/CEST). The analysed period spans July 2024 to June 2026, so each calendar month is represented twice. Data from July to September 2026 were set aside as an independent validation set for future forecasting work.

Pearson and Spearman correlation coefficients between prices, solar irradiance and wind speed were calculated for all hours, for daylight hours only (irradiance above 0 W/m²) and for hours with irradiance of at least 50 W/m², which excludes twilight and heavily overcast conditions. Negative prices occurred in approximately 4% of all hours, 7% of daylight hours and 9% of hours with irradiance of at least 50 W/m². Of all negative-price hours, more than 92% fell within daylight hours and 86% between 10:00 and 17:00. During hours with negative prices the mean solar irradiance was approximately 575 W/m², compared with approximately 250 W/m² for all daylight hours. The average electricity price was approximately 270 PLN/MWh for the hour starting at 13:00 and rose to almost 710 PLN/MWh for the hour starting at 20:00. Across the full period, prices showed a moderate negative correlation with solar irradiance (Pearson $r = -0.52$; Spearman $\rho = -0.33$) and wind speed (Pearson $r = -0.37$; Spearman $\rho = -0.35$). Restricting the analysis to daylight hours strengthened the relationship with irradiance considerably ($r = -0.67$; $\rho = -0.71$), while the relationship with wind speed remained similar ($r = -0.37$; $\rho = -0.34$).

The analysis will be extended to seasonal differences in weather–price correlations. The presented results identify the weather conditions linked to extreme price events in the Polish market and provide a dataset that can be used as input for short-term price forecasting methods combining weather forecasts and market data. In the longer term, such methods may support energy management strategies for hybrid renewable energy systems with energy storage. The results describe statistical associations rather than causal relationships, as prices are also affected by demand, cross-border exchange, fuel prices and network constraints.

[1] Faculty of Energy and Fuels, AGH University of Krakow, Kraków, Poland
[2]Faculty of Mechanical Engineering and Robotics, AGH University of Krakow, Kraków, Poland
* mikrze@student.agh.edu.pl
[3] Faculty of Mechanical Engineering and Robotics, AGH University of Krakow, Kraków, Poland

Development of a Modular Dual-Atmosphere High-Temperature Electrochemical Furnace Insert

Aleksander Pizoń[1,*], Maciej Siekierski[1]

Keywords: High-temperature electrochemistry, ceramic electrolyte, dual atmosphere, reactor design

ABSTRACT

High-temperature electrochemical reactors enable the investigation of gas-phase reactions involving solid ceramic electrolytes and catalytic electrodes. Their experimental application requires controlled gas supply, electrical contact with the electrodes, reliable separation of reactive atmospheres and mechanical stability under thermal cycling. This work presents the design of a modular electrochemical furnace insert intended for two principal applications: electrochemical conversion of light alkanes in solid oxide electrolysis cells (SOECs) and electrochemical ammonia synthesis in protonic ceramic electrolysis cells (PCECs).

The device was designed for operation in a tubular furnace and consists of two axially aligned reaction chambers connected through a central membrane holder. The ceramic electrolyte separates the gas compartments, while independently assembled electrode units provide electrical contact and gas distribution near its surfaces. The metallic housing incorporates threaded joints, compression seals, ceramic insulation and dedicated gas and electrical feedthroughs. The longitudinal cross-section of the proposed construction is presented in Figure 1.

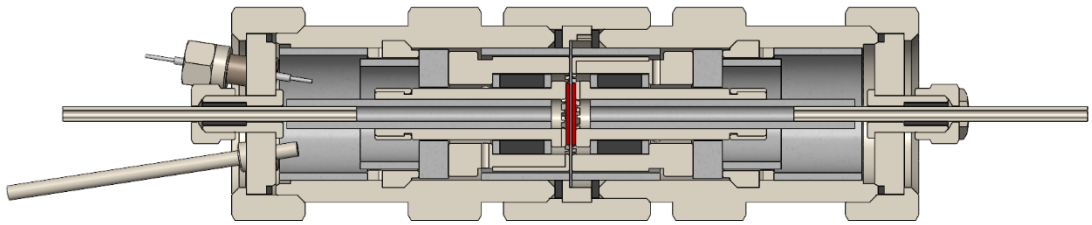


Figure 5. Longitudinal cross-sectional view of the modular high-temperature electrochemical furnace insert, showing the membrane holder, reaction chambers, electrode assemblies and gas and electrical feedthroughs.

The first intended application is the electrochemical dehydrogenation of light alkanes in an oxygen-ion-conducting SOEC configuration. For propane conversion, steam reduction generates oxide ions that migrate through the ceramic electrolyte and participate in the anodic dehydrogenation reaction:

Cathode: $H_2O + 2e^- \rightarrow H_2 + O^{2-}$

Anode: $C_3H_8 + O^{2-} \rightarrow C_3H_6 + H_2O + 2e^-$

The resulting overall reaction is:

$C_3H_8 \rightarrow C_3H_6 + H_2$

[1] Faculty of Chemistry, Warsaw University of Technology, Warsaw, Poland
*corresponding author: Aleksander.pizon.stud@pw.edu.pl

The second application involves electrochemical ammonia synthesis in a PCEC configuration, employing a proton-conducting ceramic electrolyte. In a representative hydrogen-fed arrangement, hydrogen is oxidized at one electrode, while the transported protons participate in nitrogen reduction at the opposite electrode:

Cathode: $N_2 + 6H^+ + 6e^- \rightarrow 2NH_3$

Anode: $3H_2 \rightarrow 6H^+ + 6e^-$

The corresponding overall reaction is:

$N_2 + 3H_2 \rightarrow 2NH_3$

These processes require different electrolyte and electrode materials, but share fundamental mechanical requirements concerning gas separation, electrical insulation and access to the active electrode regions. The modular design is intended to accommodate these differences through the selection of suitable membrane-electrode assemblies and experimental gas configurations.

Particular attention was given to the mechanical integration of metallic and ceramic components. The membrane is positioned in a central holder, while internal electrode assemblies incorporate ceramic insulating elements and compression layers to limit mechanical loading of the electrolyte. Gas is introduced through axial channels and distributed near the active electrode surfaces before leaving the chambers through separate outlet passages. Replaceable sealing elements and threaded connections allow the assembly to be dismantled for component replacement and inspection after thermal exposure.

The proposed construction provides a configurable experimental platform for investigating distinct high-temperature electrochemical processes within a common mechanical architecture. Its validation will include gas-tightness measurements, electrical insulation tests, verification of gas-flow paths and inspection following thermal cycling. The developed furnace insert establishes a basis for laboratory studies of electrochemical alkane conversion and ammonia synthesis using oxide-ion- and proton-conducting ceramic electrolytes, respectively.

This work was supported by the National Centre for Research and Development (NCBR) under Grant WPC3/2022/29/IMPRESSION/2025.
This work has been additionally supported by the Faculty of Chemistry, Warsaw University of Technology.

EFE2026 ENERGY FUELS ENVIRONMENT
INTERNATIONAL CONFERENCE
17-20 NOVEMBER 2026, KRAKÓW, POLAND

1D Transient Heat Transfer Model for Inverse Thermal Conductivity Retrieval for Porous Materials

Mikołaj Woźny[1], Jakub Dworczyk[1*], Mieszko Tokarski[1]

Keywords: inverse problem, thermal conductivity, porous materials, finite difference method,

ABSTRACT

The effective thermal conductivity of porous materials, such as beds of spherical grains, is difficult to measure directly because it depends on the grain material, the porosity and the gas filling the pores [1]. A common alternative is a transient experiment combined with an inverse approach: temperature histories are recorded at several points of the sample and the unknown conductivity is retrieved by fitting a heat transfer model to the measurements [2]. Because the fitting requires the model to be solved many times, the forward model must be both fast and accurate, and the choice of its numerical scheme is a key part of the problem.

The aim of this work is to develop a heat transfer model for the inverse retrieval of the thermal conductivity of porous materials. For this purpose, a series of experiments is carried out in a test rig consisting of a porous bed heated from below. Temperatures are recorded by nine thermocouples spaced along the vertical axis of the bed.

The model is based on a Finite Difference Method with central space and time discretization [3,4], implemented in MS Excel as a VBA macro. It solves the transient one-dimensional heat transfer equation in a porous bed. The bed is treated as a uniform continuum with effective density, effective specific heat, and effective thermal conductivity, which include the air in the inter-particle spaces. The bed is contained in a closed cylindrical vessel, which is heated from one side by a heater. The heater is represented by a Dirichlet boundary condition, while the rest of the vessel's walls are insulated. In the inverse problem the unknown k_s (apparent) grain conductivity and the unknown displacement of the thermocouples are found by minimising the sum of squared errors between the simulated and measured temperature profiles of all thermocouples. This procedure is carried out with the use of the MS Excel add-in "Solver" [5].

[1] P. Zehner, E.U. Schlünder, Wärmeleitfähigkeit von Schüttungen bei mäßigen Temperaturen, Chem. Ing. Tech. 42 (1970) 933–941. https://doi.org/10.1002/cite.330421408.
[2] K.A. Woodbury, H. Najafi, F. de Monte, J.V. Beck, Inverse Heat Conduction: Ill-Posed Problems, 2nd ed., John Wiley & Sons, Hoboken, NJ, 2023. https://doi.org/10.1002/9781119840220.
[3] J.C. Strikwerda, Finite Difference Schemes and Partial Differential Equations, 2nd ed., Society for Industrial and Applied Mathematics (SIAM), Philadelphia, 2004. https://doi.org/10.1137/1.9780898717938.
[4] J. Crank, P. Nicolson, A practical method for numerical evaluation of solutions of partial differential equations of the heat-conduction type, Math. Proc. Cambridge Philos. Soc. 43 (1947) 50–67. https://doi.org/10.1017/S0305004100023197.
[5] D. Fylstra, L. Lasdon, J. Watson, A. Waren, Design and use of the Microsoft Excel Solver, Interfaces 28 (1998) 29–55. https://doi.org/10.1287/inte.28.5.29.

[1] AGH University of Krakow, SKN Fluid Flow * Jdworczyk@student.agh.edu.pl

EFE2026 ENERGY FUELS ENVIRONMENT
INTERNATIONAL CONFERENCE
17-20 NOVEMBER 2026, KRAKÓW, POLAND

Beyond Typical Weather: Assessing Residential HVAC Capacity Adequacy During Historical and Future Heatwaves Across Climate Zones

Majid Rafi[1,*], Muhammad Asif[1]

Keywords: heatwaves, HVAC capacity adequacy, building energy simulation, climate change, residential buildings

ABSTRACT

Residential air-conditioning systems are commonly assessed using typical meteorological years, while equipment is sized with historical percentile-based design conditions. These inputs support conventional energy calculations but do not preserve the intensity, duration and sequence of multi-day heatwaves. During extreme heat, the cooling load increases while the available capacity and efficiency of air-cooled equipment may decline as condenser inlet temperature rises. A system that performs satisfactorily during a typical year may therefore be unable to maintain indoor setpoints during an extreme event. Existing building studies more frequently report annual energy use or indoor overheating than the time-resolved relationship between required cooling load and temperature-corrected HVAC capacity. This study addresses that gap by assessing the adequacy of conventionally sized residential cooling systems during historical and projected heatwaves in contrasting climate zones.

A controlled comparative framework is developed using one standardized residential archetype simulated in EnergyPlus. Abu Dhabi, Singapore and Montreal represent extremely hot-dry, extremely hot-humid and cold-humid ASHRAE climate zones, respectively. For each city, the analysis considers a historical typical meteorological year, a historical heatwave year and a mid-century projected heatwave year. Geometry, envelope properties, internal gains, occupancy, ventilation and thermostat schedules are held constant to isolate the climatic influence. Full-year simulations preserve antecedent conditions before event-level analysis.

HVAC capacity is first determined for each city using historical climatic design conditions and is then fixed for all typical and heatwave simulations. Two complementary EnergyPlus representations are used. An unlimited ideal-load system quantifies the hourly cooling required to maintain the prescribed setpoint, while a fixed-capacity air-cooled direct-expansion system quantifies the cooling actually available. Temperature-dependent capacity and energy-input-ratio curves represent high-ambient equipment derating as functions of indoor entering wet-bulb and outdoor condenser dry-bulb temperatures. The comparison separates heatwave-driven load growth from the simultaneous deterioration of equipment performance. Base sizing and moderate design-margin cases are examined to determine whether conventional sizing allowances remain sufficient under projected extremes.

At each timestep, capacity adequacy is expressed as the ratio of required cooling load to temperature-adjusted available capacity. A ratio above unity identifies a capacity shortfall, from which the magnitude, duration and cumulative unmet cooling requirement are calculated. Equipment is not re-autosized for the future scenarios because doing so would conceal the vulnerability of systems designed under historical conditions. Model verification checks EnergyPlus warnings, energy balances and equipment-curve validity

[1] Department of Architectural Engineering and Construction Management, College of Design and Built Environment, King Fahd University of Petroleum and Minerals, Dhahran 31261, Saudi Arabia
* g202417100@kfupm.edu.sa

across the simulated temperature range.

Performance is evaluated using peak cooling load, load-to-capacity ratio, maximum capacity deficit, capacity-deficit hours, cumulative unmet cooling energy, setpoint-not-met hours, occupied operative-temperature degree-hours, cooling electricity use and effective coefficient of performance. Loads and deficits are normalized by floor area and rated capacity to enable cross-climate comparison. Within-city comparisons quantify changes from typical weather to historical and mid-century heatwaves, while sensitivity analysis examines sizing margin, cooling setpoint and heatwave-event selection. The resulting framework identifies when, for how long and by how much residential cooling capacity becomes inadequate, rather than treating annual energy performance as evidence of heatwave readiness. The study supports climate-resilient HVAC sizing, selection of appropriate extreme-weather files and development of high-efficiency cooling systems capable of maintaining acceptable indoor conditions under a warming climate.

Comparison of Model-Less and Model-Based Approaches to Multi-Phenomena Immittance Data

Jacek Kowalczyk[1,*], Paweł Kulesza, Wiktor Piekarski, Aleksander Pizoń, Aleksander Piasecki, Aleksandra Chwała, Maciej Siekierski

Keywords: Distribution of Relaxation Times (DRT), Electrochemical Impedance Spectroscopy (EIS), Equivalent Circuit Model (ECM), galvanic cells, electrochemical modelling

ABSTRACT

Electrochemical Impedance Spectroscopy (EIS) has emerged as a quintessential, non-destructive diagnostic tool for characterizing complex electrochemical devices, most notably lithium-ion batteries, supercapacitors, and fuel cells. The primary challenge in EIS data analysis lies in extracting meaningful, physically sound kinetic and transport parameters, as for systems such as galvanic cells impedance spectra consist of multiple physicochemical processes, often overlapping and occurring across various frequencies.

Traditionally, the analysis of EIS data relies heavily on Equivalent Circuit Models (ECMs). ECMs employ a combination of electrical elements - such as resistors, capacitors, inductors with more abstract entities, like Constant Phase Elements (CPEs) or various Diffusion Elements - assembled in specific topologies to mimic the electrochemical behavior of the system. While ECMs are computationally efficient and widely adopted in industrial applications for online state-of-health (SoH) and state-of-charge (SoC) estimation, they suffer from inherent limitations. The selection of an appropriate circuit topology often relies on *a priori* knowledge and subjective user bias and may lead to over- or under-parameterization and physically unfounded interpretations.

In contrast, the Distribution of Relaxation Times (DRT) has gained significant traction as a powerful, model-free (or semi-non-parametric) alternative. DRT transforms the complex impedance spectrum into a continuous distribution function of relaxation times without requiring a predefined circuit structure.

Despite the apparent superiority of DRT in resolving complex relaxation dynamics, it also demands prior knowledge/scientific intuition. Thus, a comprehensive, systematic comparative framework evaluating the practical advantages, limitations, computational overhead, and error sensitivity of both approaches across diverse operating conditions remains crucial for both researchers and practitioners. The study presented aims to bridge this gap by providing a rigorous comparative evaluation of ECM and DRT methodologies using both synthetic and experimental impedance data.

In ECM approach the parameter identification is performed using non-linear least squares (NLLS) optimization constrained by Kramers-Kronig validation criteria to ensure data causality and linearity.

The DRT approach avoids structural assumptions by expressing the impedance:

$$Z(f) = R_\infty + i\omega L_0 + \int_{-\infty}^{+\infty} \frac{\gamma(\log\tau)}{1+i2\pi f\tau} d\log\tau \qquad (1)$$

where R_∞ is the high-frequency ohmic resistance, iwL_0 is the inductance, $2\pi f$ is the angular frequency, τ is the relaxation time, and $\gamma(\log\tau)$ is the distribution function of relaxation

[1] Faculty of Chemistry, Warsaw University of Technology, Warsaw, Poland, [1] Faculty of Chemistry, Warsaw University of Technology, Warsaw, Poland, *jacek.kowalczyk2.dokt@pw.edu.pl
[2] Faculty of Chemistry, University of Warsaw, Warsaw, Poland

times. The ill-posed inversion problem is solved by implementing high-resolution regularization algorithms incorporating derivative penalty matrices and optimal regularization parameter selection.

Figure 1. presents the simulated spectrum, alongside DRT curve and ECM, Table 1. presents the values of fitting the R/Q subcircuits using both approaches and the simulated spectrum parameters.

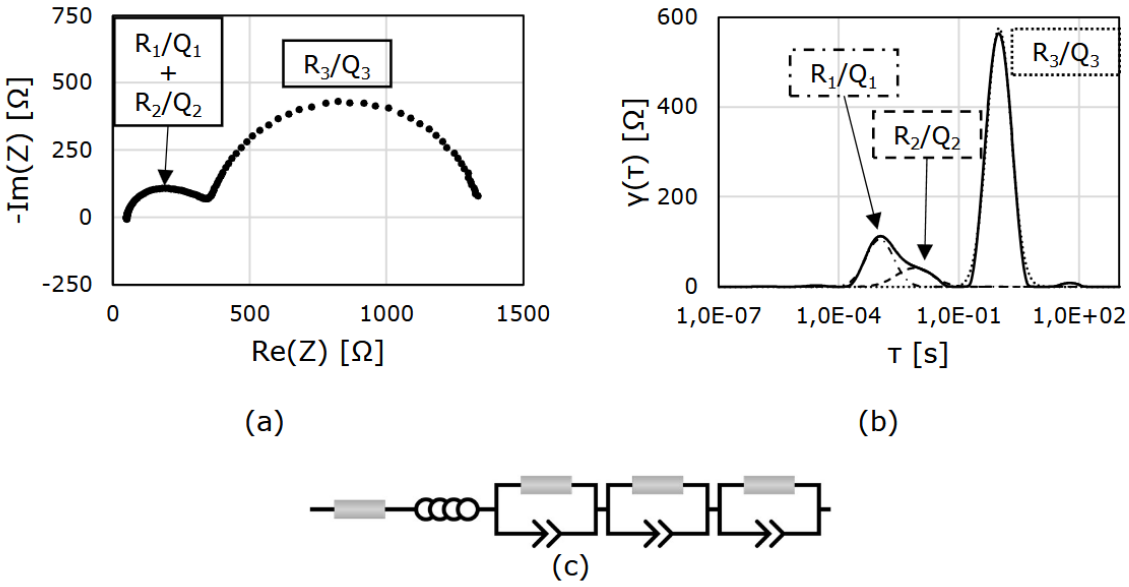


Figure 1. (a) Simulated EIS spectrum, (b) DRT curve (solid) alongside with three peaks fitted (dash-dot – R1/Q1, dash – R2/ Q 2 and dot – R3/Q3), (c) equivalent circuit.

Table 1. Simulated data and its fit parameters.

	Simulation (0.3% magnitude and phase angle noise)	**DRT**	**ECM**
R1/Q1	R=200 Ω, τ=0.00100 s	R=211 Ω, τ=0.00105 s	R=204 Ω, τ=0.00102 s
R2/Q2	R=100 Ω, τ=0.00599 s	R=109 Ω, τ=0.00762 s	R=97 Ω, τ=0.00626 s
R3/Q3	R=1000 Ω, τ=1.00 s	R=1010 Ω, τ=1.00 s	R=999 Ω, τ=1.00 s

Both methodologies can find the resistance and time-constant of multiple R/Q subcircuits, even with close resonance frequencies. Their (dis)advantages and potential uses are evaluated based on:

i) the ability to decouple closely spaced time constants;
ii) processing time, algorithmic stability, and scalability for embedded or real-time diagnostic systems;
iii) sensitivity to experimental noise and artifacts typically encountered at ultra-low or high-frequency boundaries;
iv) direct correlation between extracted spectral features and underlying thermodynamic or kinetic mechanisms.

This work provides a comprehensive benchmark comparing model-free DRT and circuit-based ECM approaches for electrochemical impedance spectroscopy analysis. Ultimately, this study advocates for a synergistic framework: employing DRT for exploratory analysis, mechanistic validation, and optimal ECM topology design, followed by deploying optimized ECMs for real-time diagnostics. This integrated approach maximizes both scientific rigor and practical engineering utility in advanced energy storage research.

This work was supported by the National Centre for Research and Development (NCBR) under Grant WPC3/2022/29/IMPRESSION/2025 and has been additionally supported by the Faculty of Chemistry, Warsaw University of Technology.

EFE2026 ENERGY FUELS ENVIRONMENT
INTERNATIONAL CONFERENCE
17-20 NOVEMBER 2026, KRAKÓW, POLAND

Photo-Oxidative Aging of Plastics in Indoor Environments: Chemical Emissions and Markers of Polymer Degradation in Airborne Particulette Matter

Anna Nowak[1], Katarzyna Styszko[1]*

Keywords: plastic degradation, chemical markers, particulate matter, photochemical aging

ABSTRACT

The use of plastics has increased continuously since their introduction due to their durability, moldability and resistance to moisture and corrosion. Nowadays, plastics are widely used across multiple sectors and can be used also in indoor environments, where they are present in building materials, furniture, electronic devices, and synthetic textiles [1]. The widespread presence of plastic materials in indoor environments raises concerns about their potential contribution to airborne chemical pollution. Although microplastics and nanoplastics in particulate matter (PM) have received increasing scientists' attention, the chemical transformations of polymers under indoor environmental conditions and their contribution to PM composition remain insufficiently understood.

The photo-oxidative aging of plastics can be promoted by exposure to ultraviolet (UV) radiation, temperature fluctuations and varying humidity, altering their polymeric structure and potentially facilitating the release of degradation products and additives into indoor air. These processes may involve free-radical chain reactions in which polymer radicals react with molecular oxygen, forming reactive intermediates that undergo further transformations. These reactions can cause chain scission, itroduce oxygen-containing functional groups and low-molecular-weight degradation products, including ketones, aldehydes, and carboxylic acids. Photo-oxidative aging may also facilitate the release of embedded chemical additives, such as plasticizers, antioxidants, stabilizers, and dyes, as well as polymer-derived oligomers. Depending on their physicochemical properties, these compounds may be emitted into the gas phase or become associated with airborne particles, including PM10 and PM2.5. The nature and extent of these processes depend on polymer composition and exposure conditions [2].

A further focus is placed on the potential application of chemical markers to identify plastic degradation products and investigate its contribution to indoor airborne particulate matter. Analytical techniques such as gas chromatography coupled with tandem mass spectrometry (GC-MS/MS) and liquid chromatography coupled with tandem mass spectrometry (LC-MS/MS) offer complementary approaches for characterizing volatile, semi-volatile, and less volatile compounds associated with polymer aging. The identification of polymer-specific degradation products may provide additional information about the sources and transformation pathways of plastic-derived pollutants, complementing conventional approaches based primarily on particle abundance and physical characteristics [3].

By synthesizing current knowledge on polymer aging, chemical emissions, and analytical approaches, this review seeks to identify key knowledge gaps and challenges in the characterization of plastic-derived compounds in indoor air. Particular attention is given to the limited understanding of emission kinetics, the relationship between environmental conditions and chemical release, and the reliability of potential degradation markers. Improved chemical characterization of these processes could support the development of analytical strategies for tracing plastic degradation and assessing its contribution to indoor air pollution.

[1] AGH University of Krakow, Poland, * styszko@agh.edu.pl

EFE2026 ENERGY FUELS ENVIRONMENT
INTERNATIONAL CONFERENCE
17-20 NOVEMBER 2026, KRAKÓW, POLAND

Beyond Decarbonization: Reframing the Energy Transition Through Systems Modelling, Material Constraints and Economic Futures

Cesar Yalderrama[1,*], Sergi Yinardell[1], Sacha Dawid[1], Luke Quinn[1], Julia Otero[1], Francesca Stefanini[1]

Keywords: Energy transition; Systems modelling; ; Decoupling; Critical raw materials; Post-growth

ABSTRACT

The energy transition is commonly framed as a technological challenge cantered on replacing fossil fuels with renewable energy, electrification, and efficiency improvements while sustaining economic growth. Yet this framing may overlook fundamental interactions between decarbonisation, material demand, supply-chain resilience, and the economic structures that ultimately drive energy and resource consumption. This contribution examines these interactions through three complementary modelling perspectives, progressively expanding the system boundaries of energy-transition analysis.

First, the feasibility of decoupling economic growth from greenhouse gas emissions is examined using historical trends, scenario modelling, and life-cycle assessment. While absolute decoupling is theoretically possible, climate-compatible pathways require reductions in technology intensity and emissions substantially beyond historical trends. Moreover, incorporating upstream supply-chain processes increases the estimated greenhouse gas emissions of electricity and heat generation by approximately 20%, further increasing the required pace of transformation [1].

This raises a second question: even if rapid decarbonisation can be achieved, what are the material consequences of the technologies required to deliver it? A prospective life-cycle assessment of the European energy transition through 2050 shows that environmental pressures increasingly shift toward material-intensive technologies and their supply chains. Battery technologies dominate the projected mineral-resource burden, particularly through nickel and copper demand, whereas solar PV and wind make comparatively minor contributions. Geographic diversification consistent with European critical-material strategies substantially redistributes supply-chain dependence but produces only modest reductions in aggregate environmental burdens, revealing an important distinction between resilience and environmental sustainability [2].

These material constraints, in turn, open a broader economic question: can deep decarbonisation and reductions in resource throughput be reconciled with economies structurally dependent on continued growth? Comparative macroeconomic modelling across growth-oriented, post-growth and degrowth-compatible frameworks shows that the representation of energy demand, welfare, labour, redistribution and biophysical constraints fundamentally affects projected transition pathways. Scenarios combining technological change with sufficiency, demand reduction and redistributive policies achieve substantial emission reductions without necessarily worsening social outcomes [3].

Taken together, the three modelling perspectives reveal a common progression: from carbon constraints, to material constraints, to the economic structures driving both. The results suggest that the energy transition cannot be understood solely as a technological substitution problem. It is a systemic transformation in which technology deployment, resource use, economic organization and societal well-being are deeply interconnected.

[1] Chemical Engineering Department, Escola d'Enginyeria de Barcelona Est (EEBE), Universitat Politecnica de Catalunya (UPC)-BarcelonaTECH and Barcelona Research Center for Multiscale Science and Engineering, Campus Diagonal-Besos, Barcelona 08930, Spain,
* cesar.alberto.valderrama@upc.edu

Consequently, future energy-system models and policies need to move beyond optimizing decarbonisation alone and consider whether transition pathways are simultaneously climate-compatible, materially feasible, economically resilient and socially desirable.

[1] S. Dawid, S. Vinardell, C. Valderrama, Can green economic growth and carbon emission reduction coexist? A decoupling study in the energy sector, J. Clean. Prod. 549 (2026) 147867. https://doi.org/10.1016/j.jclepro.2026.147867.

[2] L. Quinn, J. Otero, S. Vinardell, C. Valderrama, Toward a sustainable and resilient EU energy transition: Prospective life cycle assessment of material stocks and supply-chain alternatives, J. Clean. Prod. 580 (2026) 149682. https://doi.org/10.1016/j.jclepro.2026.149682.

[3] F. Stefanini, S. Vinardell, C. Valderrama, Beyond renewable expansion: Evaluating macroeconomic models for degrowth pathways on the energy transition, Sustain. Futures 11 (2026) 101802. https://doi.org/10.1016/j.sftr.2026.101802.

EFE2026 ENERGY FUELS ENVIRONMENT
INTERNATIONAL CONFERENCE
17-20 NOVEMBER 2026, KRAKÓW, POLAND

Integrating Environmental Emissions and Pollution Control into Ghana's Mining Sector: Pathways to a Circular Economy and Sustainable Energy Transition

Kamal Razak[1]

Keywords: Energy transition, circular economy, emissions control, mining pollution, mine-waste management, environmental rehabilitation, Minerals Development Fund, Ghana

ABSTRACT

The global transition to clean energy and a circular economy presents both significant opportunities and environmental challenges for mineral-producing countries such as Ghana. Rising demand for critical minerals, together with the expansion of mining activities, underscores the need for effective strategies to control emissions, minimise pollution, and promote sustainable resource utilisation. Although the mining sector makes a substantial contribution to Ghana's economic development, its operations may generate air pollution, water contamination, land degradation, and considerable volumes of mine waste and tailings.

This paper examines practical approaches to strengthening emissions and pollution control in Ghana's mining sector within the broader context of the energy transition and the circular economy. It identifies opportunities to adopt cleaner production technologies, integrate renewable energy into mining operations, improve mine-waste management, recover minerals from tailings, recycle water, and reuse mining by-products. It also examines the roles of institutional financing, environmental governance, and stakeholder collaboration in supporting the rehabilitation of degraded mining areas and improving environmental outcomes in mining communities.

Particular attention is given to the potential role of the Minerals Development Fund in supporting sustainable community development, environmental restoration, and initiatives aimed at reducing the long-term environmental and social costs of mining. The paper argues that integrating circular-economy principles into mineral-resource development can reduce pollution, enhance resource efficiency, create green employment opportunities, and strengthen the resilience of mining communities.

The paper concludes that a successful energy transition must extend beyond the extraction of minerals required for clean-energy technologies to encompass responsible production, effective pollution control, and the sustainable management of mining-related environmental impacts. A coordinated approach involving government institutions, mining companies, research organisations, and local communities is essential to achieving environmentally responsible and economically inclusive mineral development in Ghana.

[1] Minerals Development Fund (MDF), Ghana, razak.kamal@yahoo.com

Electrochemical Performance and Intercalation Mechanism of Prussian Blue Analogues for Na-Ion Cells

Kamil Michalski[1,2]*, Marta Wolczko[2], Janina Molenda[2]

Keywords: Na-ion, intercalation, energy storage, spectroscopy, Prussian Blue analogues

ABSTRACT

Prussian Blue (PB), Prussian White (PW), and their analogues (PBA – Prussian Blue analogues, PWA – Prussian White analogues) are among the most promising cathode materials for sodium-ion batteries. Their main advantages include the wide availability and abundance of their constituent elements, environmental stability, high operating potential vs. Na/Na^+, high theoretical capacity, and an open framework with three-dimensional diffusion channels for sodium ions [1].

This work focuses on iron-based PBAs, which can be generally described by the formula $Na_xFe[Fe(CN)_6]_{1-y}\cdot nH_2O$ ($0 < x < 2$). One of the main challenges in developing these materials is defect engineering, as defects are considered among the key factors influencing their electrochemical performance. Defect engineering involves controlling cyanide vacancies, $[Fe(CN)_6]^{4-}$ vacancies, cationic doping, and residual water content. Controlling these defects can significantly improve ionic diffusion, reaction kinetics, electrochemical capacity, and stability [2].

A key step in developing cathode materials for Na-ion cells is a thorough understanding of the intercalation/deintercalation reaction mechanisms and their kinetics. Materials belonging to the PBA group exhibit complex (de)intercalation mechanisms, as iron in their structures exists in both low-spin (Fe^{2+}–LS) and high-spin states (Fe^{2+}–HS and Fe^{3+}–HS for PBAs, or Fe^{2+}–HS for PW). Most of the available literature indicates the electrochemical activity of high-spin iron and the limited activity of low-spin iron. The electrochemical activity of low-spin iron is mainly influenced by its coordination environment, including $[Fe(CN)_6]^{4-}$ groups and water molecules, which can shield active sites and reduce sodium-ion mobility [2,3].

This work presents a synthesis method for obtaining PWAs. The resulting materials were characterised using advanced electrochemical techniques, revealing high reversible specific capacities exceeding 150 mAh/g and diffusion coefficients ranging from 10^{-9} to 10^{-6} cm^2/s. The materials were also investigated using operando and in situ Raman spectroscopy to determine the mechanisms of iron redox reactions during cell operation. Additionally, X-ray absorption spectroscopy (XAS) was employed to directly investigate the evolution of iron oxidation states and spin configurations.

[1] Y. Xiao, J. Xiao, H. Zhao, J. Li, G. Zhang, D. Zhang, X. Guo, H. Gao, Y. Wang, J. Chen, G. Wang, H. Liu, Prussian Blue analogues for sodium-ion battery cathodes: A review of mechanistic insights, current challenges, and future pathways, Small 20 (2024) 2401957. https://doi.org/10.1002/smll.202401957.

[2] X. Liu, Y. Cao, J. Sun, Defect engineering in Prussian Blue analogs for high-performance sodium-ion batteries, Adv. Energy Mater. 12 (2022) 2202532. https://doi.org/10.1002/aenm.202202532.

[3] J. Song, L. Wang, Y. Lu, J. Liu, B. Guo, P. Xiao, J.-J. Lee, X.-Q. Yang, G. Henkelman, J.B. Goodenough, Removal of interstitial H_2O in hexacyanometallates for a superior cathode of a sodium-ion battery, J. Am. Chem. Soc. 137 (2015) 2658–2664. https://doi.org/10.1021/ja512383b.

Acknowledgement: This work was funded by the National Science Centre, Poland (NCN), under the OPUS 26 programme, decision No. 2023/51/B/ST11/00768. The XAS spectra were obtained at the SOLARIS National Synchrotron Radiation Centre, at the PIRX beamline, under proposal No. 251081.

[1] Faculty of Materials Science and Ceramics, AGH University of Krakow, al. A. Mickiewicza 30, 30-059 Krakow, Poland, michalskik@student.agh.edu.pl

[2] Department of Hydrogen Energy, Faculty of Energy and Fuels, AGH University of Krakow, al. A. Mickiewicza 30, 30-059 Krakow, Poland

Non-Euclidean Metrics of Similarity Applicable to Semi-Automated Analysis of Multicomponent Immittance Spectra of Electroactive Materials and Processes

Maciej Siekierski[1,*], Jacek Kowalczyk[1], Aleksandra Ossowska-Górzyńska[1], Wiktoria Zieńkowska[1], Władysław Wieczorek[1], Paweł Kulesza[2], Janusz Lewiński[1]

Keywords: EIS, DRT, Wasserstein Metrics, spectral divergence, numerical classificaiton

ABSTRACT

Modern energy conversion and storage infrastructures – ranging from utility-scale battery energy storage systems (BESS) based on multi-cell galvanic strings, to megawatt-scale polymer electrolyte membrane (PEM) and solid oxide electrolyzer arrays, or high-power fuel cell (FC) stacks –can generate unprecedented volumes of dielectric and electrochemical immittance spectroscopic data. On the other hand, various types of electrochemical laboratory experiments conducted for numerous materials compositions, reagent streams and operational conditions, due to the increasing availability of multi-channel electrochemical setups, deliver a similarly bulky datasets, and therefore, suffer from the same throttle of time- and qualifications-consuming processing and interpretation. Conventionally, the quantitative interpretation of immittance spectra relies on Complex Non-Linear Least Squares (CNLS) fitting of Equivalent Electrical Circuits (EECs). As it was stated previously CNLS fitting requires subjective, manual selection of circuit topologies, is notoriously sensitive to initial parameter guesses, suffers from local minima convergence, and exhibits severe parameter cross-compensation (particularly between constant phase element exponents and charge-transfer resistances).

To eliminate circuit-topology bias, model-agnostic deconvolution into the Distribution of Relaxation Times (DRT) has emerged as an authoritative diagnostic framework, converting complex immittance $Z(\omega)$ into continuous relaxation spectra $\gamma(\ln\tau)$. However, comparing, classifying, and tracking the temporal evolution of these high-dimensional distributions across broad operational envelopes introduces a fundamental mathematical challenge – the failure of conventional Euclidean metrics. In typical situation the Euclidean metric penalizes a minor kinetic acceleration emerging as a peak shifting along $\ln\tau$ axis identically to the emergence of an entirely new degradation mechanism, while failing to reflect the physical magnitude of the time displacement. Therefore alternative approaches were herein validated against sets of laboratory-originating immittance data. These include:

i) **Wasserstein-1 Metric (W_1)** treating normalized relaxation distributions as probability measures, the tool evaluates the minimal "transport work" required to morph one spectral state into another:

$$W_1(\tilde{\gamma}_1, \tilde{\gamma}_2) = \int_{-\infty}^{\infty} |\, F_1(\ln\tau) - F_2(\ln\tau)\,|\, d\ln\tau$$

This metric natively couples vertical resistance variations with horizontal kinetic shifts providing an absolute, operator-free criterion for electrochemical stationarity and drift velocity, as well as isolates the net kinetic restructuring under polarization.

ii) **Total Variation (TV) and Isorelaxational Topologies:** The L_1-based total variation of normalized difference profiles ($\Delta\tilde{\gamma} = \tilde{\gamma} - \tilde{\gamma}_0$) directly quantifies the exact

[1] Faculty of Chemistry, Warsaw University of Technology, Warsaw, Poland, *maciej.siekierski@pw.edu.pl
[2] Faculty of Chemistry, University of Warsaw, Warsaw, Poland

percentage of total polarization resistance reallocated across time domains. Furthermore, tracking stationary zero-crossing nodes ($\Delta\tilde{\gamma} = 0$) provides automated detection of isorelaxational behavior, proving conservative two-state transitions without intermediate states.

iii) **Peak Shift Tracking** is here evaluated as a tool allowing to isolate localized kinetic phenomena by means of monitoring the trajectories of modal relaxation time coordinates ($\Delta \ln \tau_{\text{peak}}$) with parallel decoupling of the timescale of the elementary processes' overall amplitude changes of the representation analysed.

iv) **Angular Morphology** identified by the **Cosine Similarity (S_C)** probe relies on normalizing the functional inner product which decouples pure spectral shape alterations from global ohmic scaling.

v) **Spectral KL divergence (d_{KL})**

$$d_{\text{KL}}(\ln \tau) = \tilde{\gamma}(\ln \tau) \ln\left(\frac{\tilde{\gamma}(\ln \tau)}{\tilde{\gamma}_0(\ln \tau)}\right)$$

applicable as a hypersensitive early-warning effectively capturing subtle onset of phenomena such as interfacial film breakdown.

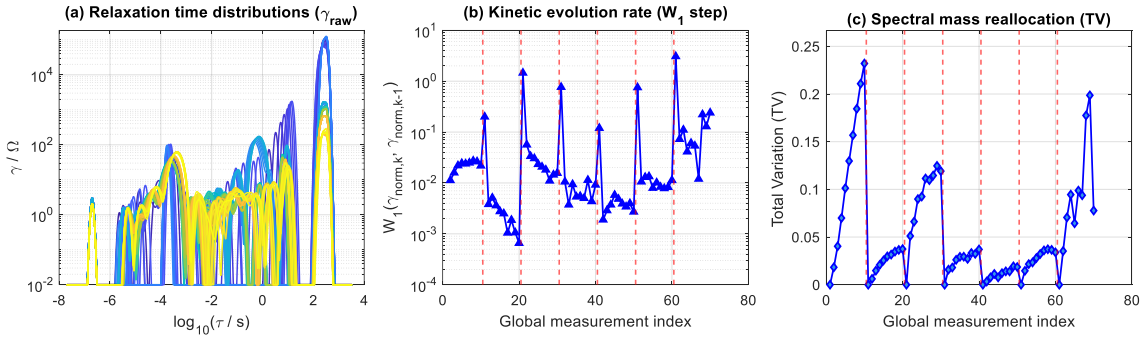


Figure 1 a) a set of DRT curves representing seven series of ten measurements each performed for a perovskite based composite electrode material; b) respective Wasserstein metrics proving both the relaxation within the series and the occurrence of the Faradaic shift of the material properties between them; c) correlated set of spectral mass reallocation curves.

On the basis of data originating from various electrochemical systems (exemplary data shown in Figure 1) of interest it will be proven that integration of these complementary estimators yields in an efficient, hierarchical diagnostic stack. By progressing from rapid macroscopic screening (via Wasserstein transport work and trajectory tortuosity) to localized mechanistic pinpointing (via KL divergence density, directional peak shifts, and cosine similarity), this non-Euclidean framework eliminates the convergence failures and operator dependency of equivalent circuits, unlocking autonomous, real-time health monitoring for utility-scale battery strings, fuel cell stacks, and advanced insertion materials.

EFE2026 ENERGY FUELS ENVIRONMENT
INTERNATIONAL CONFERENCE
17-20 NOVEMBER 2026, KRAKÓW, POLAND

Benchmarking Local Energy Market Mechanisms in a Virtual Power Plant

Oskar Antonik[1,2]*, Pablo Benalcazar[2]

Keywords: Virtual Power Plant; Local Energy Market; Rule-Based Pricing; Auction-Based Trading; Prosumers

ABSTRACT

Virtual Power Plants (VPPs) aggregate distributed energy resources and coordinate them as a single energy system. In addition to managing interactions with the external electricity grid, a VPP can establish a Local Energy Market (LEM), enabling participating prosumers and consumers to trade energy. The design of this internal market can affect transaction prices, the allocation of locally generated electricity, participant benefits, and the overall use of distributed renewable energy resources.

In this context, this study aims to determine how the choice of LEM mechanism affects a VPP's technical and economic performance under comparable operating conditions. Moreover, this study benchmarks four LEM mechanisms implemented within a prosumer-based VPP: three use predefined pricing or settlement rules, while an auction-based mechanism sets transaction terms through bids and offers submitted by market participants.

To ensure a consistent comparison of alternative internal market designs, all mechanisms are evaluated using identical electricity demand and photovoltaic generation profiles. The assessment examines both economic and operational performance, including participant electricity costs, revenues from surplus generation, internal energy trading volumes, imports from and exports to the external grid, local utilization of photovoltaic generation, and variability in internal transaction prices. Differences in computational requirements and implementation complexity are also considered. The results highlight the differences between simple rule-based settlement schemes and market-based price mechanisms, offering insights into designing effective internal energy markets for prosumer-oriented VPPs.

Acknowledgments: The research was conducted as part of the CoEnerBuild project, funded by the Polish National Center for Research and Development and the European Union under the CETPartnership program (project code Cetp-FP2023-00014)

[1] AGH University of Krakow, Kraków, Poland, * oantonik@student.agh.edu.pl
[2] Mineral and Energy Economy Research Institute of the Polish Academy of Sciences, Division of Energy Economics, Kraków, Poland

Electrospinning: Advanced Nanofiber Production

Marcin Moszczak[1]

Keywords: electrospinning, nanofibers, Linari NanoTech, energy materials

ABSTRACT

Electrospinning is a versatile electrohydrodynamic technique for producing micro- and nanofibers with tunable structural and functional properties [1, 2]. Its origins date back to 1600, when William Gilbert described electrostatic effects on liquid droplets. Technology evolved through early fiber-spinning patents in the late nineteenth and early twentieth centuries, followed by the development of theoretical models and modern electrospinning systems that established it as an important tool in advanced materials research [1, 2].

The process involves applying a high-voltage electric field to a polymer solution or melt delivered through a spinneret. Once electrostatic forces overcome surface tension, a charged liquid jet is formed, stretched and progressively thinned as it travels towards a grounded or oppositely charged collector. Solvent evaporation or cooling solidifies the jet into fibers, typically ranging from tens of nanometers to several micrometers in diameter. The resulting material is usually a porous, nonwoven nanofibrous mat, although aligned fibers, tubular structures and core-shell architectures can also be produced. Depending on the desired properties, the process can use synthetic or natural polymers, polymer blends, solvents and functional additives. Fiber morphology and material performance can be tailored by adjusting voltage, flow rate, collector distance, solution composition and collection geometry [1, 2].

Electrospun nanofibers combine high specific surface area, interconnected porosity, tunable pore structure and adaptable surface chemistry. These properties make them valuable in a broad range of scientific and industrial applications. In biomedicine, nanofibrous scaffolds can mimic aspects of the extracellular matrix and support research into tissue engineering, wound dressings and artificial skin. In pharmaceutical research, fibers can encapsulate active compounds and enable controlled drug release. Filtration is another major application area: nanofiber membranes can capture fine airborne particles and support the development of respiratory masks, air filtration systems and water treatment technologies [1, 2].

Beyond these established fields, electrospinning offers significant opportunities in energy materials research. Nanofibrous structures are being investigated for battery separators, electrode components, catalyst supports, supercapacitors, fuel cells and water electrolysis. Their high surface area and tunable architecture can facilitate ion transport, improve access to active sites and support catalyst distribution, depending on the material composition and device design. Research on electrospun cellulose-nanocrystal-reinforced separators for lithium-ion batteries illustrates the potential of this approach in electrochemical energy storage [4].

[1] J. Xue, T. Wu, Y. Dai, Y. Xia, Electrospinning and Electrospun Nanofibers: Methods, Materials, and Applications, *Chemical Reviews*, 119 (2019) 5298–5415. https://doi.org/10.1021/acs.chemrev.8b00593.
[2] A. Greiner, J.H. Wendorff, Electrospinning: A Fascinating Method for the Preparation of Ultrathin Fibers, *Angewandte Chemie International Edition*, 46 (2007) 5670–5703. https://doi.org/10.1002/anie.200604646.
[3] Linari NanoTech, Our Electrospinning Technology (accessed on: 19 October 2026). https://www.linarinanotech.com/pages/our-technology (on-line).
[4] A. Laezza et al., Cellulose Nanocrystals as Additives in Electrospun Biocompatible Separators for Aprotic Lithium-Ion Batteries, ACS Applied Polymer Materials (2023). https://doi.org/10.1021/acsapm.2c01956

[1] Technolutions Sp. z o.o., ul. Wiejska 7, 99-400 Łowicz, Poland, marcin.moszczak@technolutions.pl

EFE2026 ENERGY FUELS ENVIRONMENT
INTERNATIONAL CONFERENCE
17-20 NOVEMBER 2026, KRAKÓW, POLAND

Research Tools for Energy Materials and Fuel Emissions

Mateusz Ścigaj[1]

Keywords: surface engineering, electrode materials, micromechanics, Raman spectroscopy, emissions

ABSTRACT

Research on energy materials and fuel emissions requires tools that connect preparation conditions with evidence of function, degradation and environmental impact. This application-oriented presentation examines published experiments using equipment from manufacturers represented by Technolutions. The examples cover interface engineering, electrode fabrication, mechanical failure, three-dimensional imaging and chemical analysis. Instrument configurations are discussed through the research questions they enable, with attention to sample geometry, measurement conditions and the interpretation of complementary data.

Atomic layer deposition is illustrated by protective barriers for perovskite solar cells. Davis et al. used a Beneq TFS-200 to grow alumina on completed devices. Initial growth with water followed by ozone reduced deposition damage while providing a barrier against moisture and oxygen [1]. Device ageing was assessed at 45°C and 85% relative humidity. The case links oxidant selection and growth temperature with barrier performance and device compatibility.

Physical vapour deposition also provides model systems for investigating degradation. Pitillas et al. deposited LNMO cathode films by radio-frequency sputtering in a Kurt J. Lesker Company system connected to a glovebox. Their experiments showed that the response to water exposure depended on the lithiation state, with partially delithiated films becoming electrochemically inactive [2]. The example demonstrates how thin-film electrodes can simplify the analysis of material-electrolyte interactions.

Ultrasonic spraying addresses electrode preparation over larger areas. Ma et al. used a Cheersonic UAM4000L to deposit catalyst inks on carbon paper for large-area gas-diffusion electrodes in an acidic-alkaline tandem CO_2 electrolysis study [3]. The discussion focuses on ink delivery, coating coverage and catalyst loading as process variables relevant to electrode fabrication.

Local mechanical testing provides a different view of electrode reliability. Wheatcroft et al. used an Alemnis microindenter inside a scanning electron microscope to compress individual single-crystal NMC811 particles and observe deformation and fracture [4]. The influence of crystallographic loading direction is considered alongside the requirements for particle positioning, indenter geometry and simultaneous imaging.

X-ray tomography complements these local tests with internal structural information. Valisammagari et al. used an RX Solutions EasyTom Nano for laboratory imaging of SiO_x/C electrodes before and after cycling [5]. These measurements are distinguished from the synchrotron in-situ tomography and digital volume correlation reported in the same work. Sample size, image contrast and spatial sampling are discussed as criteria for selecting a useful laboratory imaging configuration.

Raman spectroscopy is illustrated by an in-situ electrocatalysis study. Zheng et al. used a Renishaw inVia Qontor to examine structural changes in RuO_2-based catalysts under applied potential during acidic oxygen evolution [6]. Spectra were collected with 532 nm excitation in 0.5 M aqueous H_2SO_4 under controlled potential. The contribution of Raman spectra to assessing catalyst stability is considered together with the complementary

[1] Technolutions Sp. z o.o., ul. Wiejska 7, 99-400 Łowicz, Poland, mateusz.scigaj@technolutions.pl

spectroscopic evidence. Excitation wavelength, optical access and electrochemical control are discussed as requirements for measurements under working conditions.

Finally, Wang et al. used a Vocus PTR-TOF mass spectrometer from TOFWERK, recording data at 1 s resolution, to characterise organic vapours from wood, straw, cow dung and coal combustion [7]. The example links changing combustion phases with time-dependent organic emissions. Ionisation chemistry, mass resolving power, calibration and sampling are discussed in relation to the analytical question. Across the case studies, the emphasis is on selecting equipment and experimental configurations that provide interpretable evidence for the next research decision.

[1] M.A. Davis, K. Schutt, D.N. Minh, X. Zhang, C. Xie, R.A. Kerner, T. Liu, M.O. Reese, L.T. Schelhas, M.D. Kempe, A.F. Palmstrom, J.M. Luther, Enabling long term, shelf-stable perovskite solar cells: Alumina barriers to protect perovskite devices from moisture and oxygen, Adv. Energy Mater. 16 (2026) e70834. https://doi.org/10.1002/aenm.70834.
[2] A.I. Pitillas, L.L. De Taeye, P.M. Vereecken, Deactivation of partially (dis)charged LNMO in contact with water by electrochemical protonation of Li(1−x)Ni0.5Mn1.5O4, Adv. Mater. Interfaces 11 (2024) 2400003. https://doi.org/10.1002/admi.202400003.
[3] X. Ma, J. Zhang, D. He, W. Jiang, Y. Sun, J. Cui, C. Chen, Y. Lin, T. Yao, H. Zhou, Y. Li, Y. Wu, Acidic-alkaline tandem system for durable CO_2–CO–C_2+ conversion, Sci. Adv. 12 (2026) eaea2538. https://doi.org/10.1126/sciadv.aea2538.
[4] L. Wheatcroft, A. Bird, N. Gollapally, S.G. Booth, S.A. Cussen, B.J. Inkson, In situ fracture behavior of single crystal LiNi0.8Mn0.1Co0.1O2 (NMC811), Batteries Supercaps 7 (2024) e202400077. https://doi.org/10.1002/batt.202400077.
[5] A. Valisammagari, J. Lachambre, J. Adrien, L. Broche, M. Petit, V. Esnault, E. Maire, Study of microstructural evolution and strain analysis in SiOx/C negative electrodes using in-situ X-ray tomography and digital volume correlation, Batteries Supercaps 8 (2025) e202400416. https://doi.org/10.1002/batt.202400416.
[6] W. Zheng, Y. Zhao, K. Jiang, F. Xie, L. Meng, S. Gao, J. Li, J. Lan, M. Luo, L. Liu, Y. Tan, Heteroatom dopants overcome the activity-stability trade-off in RuO_2 for acidic oxygen evolution, Nat. Commun. 16 (2025) 6716. https://doi.org/10.1038/s41467-025-62036-x.
[7] T. Wang, J. Zhang, H. Lamkaddam, K. Li, K.Y. Cheung, L. Kattner, E. Gammelsæter, M. Bauer, Z.C.J. Decker, D. Bhattu, R. Huang, R.L. Modini, J.G. Slowik, I. El Haddad, A.S.H. Prévôt, D.M. Bell, Chemical characterization of organic vapors from wood, straw, cow dung, and coal burning, Atmos. Chem. Phys. 25 (2025) 2707–2724. https://doi.org/10.5194/acp-25-2707-2025.

Methodology of Determination of Hydroxyl Derivatives of PAHs by LC-MS/MS

Laura Węgrzyn[1,*], Karolina Cwynar[1], Zuzanna Prus-Frączek[2], Justyna Pyssa[1], Katarzyna Styszko[1]

Keywords: PAHs, OH-PAHs, LC-MS/MS

ABSTRACT

Polycyclic aromatic hydrocarbons (PAHs) are well-known organic pollutants composed of two or more aromatic rings [1,2]. Their presence in various environmental compartments has been repeatedly confirmed. These compounds can occur in the air as constituents of suspended particulate matter, as well as in aquatic environments, wastewater, and sewage sludge. Sources of PAHs in the environment can be either natural or anthropogenic. Major sources include the incomplete combustion of fossil fuels, coke, natural gas, wood, and organic waste (Figure 1) [3]. These compounds have been shown to exhibit carcinogenic, mutagenic, and teratogenic effects [1,2]. Hydroxyl derivatives (OH-PAHs) are among the most common biomarkers for PAHs. Upon entering the body, PAHs are metabolized into OH-PAHs and subsequently excreted, including via urine [4,5]. Analyzing the presence of specific hydroxyl derivatives of PAHs in environment is crucial, as it allows for inferences regarding the exposure of PAHs in the environment.

The aim of this study was to develop a method for the determination of OH-PAHs using LC-MS/MS. Separating the chromatographic peaks corresponding to some of the compounds was difficult due to their overly similar structures, therefore some of the compounds were analyzed as a sum of concentrations. The compounds investigated were: 1-naphthol, 2-naphthol, the sum of 2-, 3-, and 9-hydroxyfluorene, the sum of 1- and 9-hydroxyphenanthrene, the sum of 2- and 3-hydroxyphenanthrene, 4-hydroxyphenanthrene, 1-hydroxypyrene, and 3-hydroxybenzo(a)pyrene. A biphenyl column (ACCUCORE BIPHENYL, 100 x 2.1 mm x 2.6 µm) was used for the analyses and water (phase A) and methanol (phase B) were used as the mobile phases. Validation parameters for the measurement method were determined based on the obtained calibration curves. The results confirmed that the method exhibits high accuracy and selectivity and can be successfully applied to the detection and quantification of OH-PAHs in various environmental samples. Studies on OH-PAH content in the environment provide valuable information regarding the potential accumulation of these compounds in various environmental compartments, and monitoring their concentrations contributes to the risk assessment of the impact of organic pollutants on human health and life.

[1] Department of Fuel Technology, Faculty of Energy and Fuels, AGH University of Krakow, Al. Mickiewicza 30, 30-059 Krakow, Poland, *frydel@agh.edu.pl

[2] Department of Heat Engineering and Environment Protection, Faculty of Metals Engineering and Industrial Computer Science, AGH University of Krakow, Al. Mickiewicza 30, 30-059 Krakow, Poland

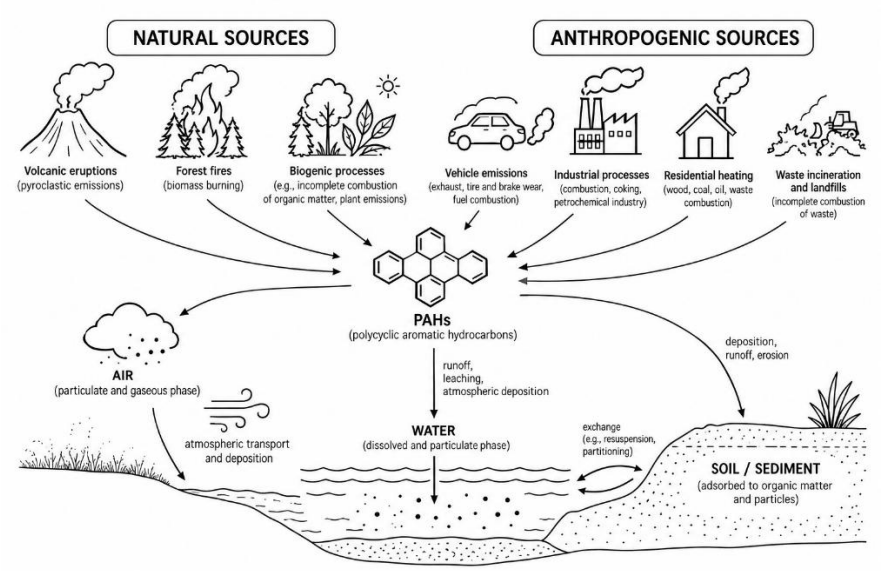


Figure 1. Sources of PAHs [3]

[1] K.-H. Kim, S.A. Jahan, E. Kabir, R.J.C. Brown, A review of airborne polycyclic aromatic hydrocarbons (PAHs) and their human health effects, Environ. Int. 60 (2013) 71–80. https://doi.org/10.1016/j.envint.2013.07.019.
[2] I. Abbas, G. Badran, A. Verdin, F. Ledoux, M. Roumié, D. Courcot, G. Garçon, Polycyclic aromatic hydrocarbon derivatives in airborne particulate matter: Sources, analysis and toxicity, Environ. Chem. Lett. 16 (2018) 439–475. https://doi.org/10.1007/s10311-017-0697-0.
[3] M. Moazzen, R. Ahmadkhaniha, M.E. Gorji, M. Yunesian, N. Rastkari, Magnetic solid-phase extraction based on magnetic multi-walled carbon nanotubes for the determination of polycyclic aromatic hydrocarbons in grilled meat samples, Talanta 115 (2013) 957–965. https://doi.org/10.1016/j.talanta.2013.07.005.
[4] J. Jacob, A. Seidel, Biomonitoring of polycyclic aromatic hydrocarbons in human urine, J. Chromatogr. B 778 (2002) 31–47. https://doi.org/10.1016/S0378-4347(01)00467-4.
[5] L.C. Romanoff, Z. Li, K.J. Young, N.C. Blakely, D.G. Patterson, C.D. Sandau, Automated solid-phase extraction method for measuring urinary polycyclic aromatic hydrocarbon metabolites in human biomonitoring using isotope-dilution gas chromatography high-resolution mass spectrometry, J. Chromatogr. B 835 (2006) 47–54. https://doi.org/10.1016/j.jchromb.2006.03.004.

Acknowledgments: The project was funded by the Polish National Science Centre (grant no. 2022/45/B/ST10/02108).

EFE2026 ENERGY FUELS ENVIRONMENT
INTERNATIONAL CONFERENCE
17-20 NOVEMBER 2026, KRAKÓW, POLAND

Forecasting Prices for Balancing Services in the Balancing Market in Poland

Michał Rybiński[1,*], Piotr Dzierwa[1]

Keywords: balancing market, forecasting, balancing services, energy market

ABSTRACT

On June 14, 2024, new Balancing Terms and Conditions [1] came into effect in Poland, introducing a number of changes to the operation of the Polish National Power System and the Balancing Market. In addition to the existing market-based pricing mechanism for balancing energy, a market-based pricing mechanism was also introduced for balancing services related to frequency reserves (upward and downward) during specific activation periods, with prices varying by the hour [2]. The Balancing Market reform removed price caps on balancing energy, which may result in significant revenues for flexible generation sources, as well as substantial losses in the event of incorrect generation forecasts and improper (non-compliant with the contract) balancing of the source, which is of particular importance for weather-dependent sources—wind farms and photovoltaic plants.

The changes introduced by the new Balancing Terms and Conditions have also created new revenue opportunities for renewable energy sources, which—in addition to entering into contracts on the Day-Ahead Market, long-term contracts, or support mechanisms—can also submit bids for balancing power, which is purchased by the Transmission System Operator for each hour of the day separately for upward and downward frequency bands: frequency containment reserve (FCR), automatic frequency restoration reserve (aFRR) and manual frequency restoration reserve (mFRR), and replacement reserve (RR)[2].

This change has created additional revenue opportunities for many power plants, including wind and solar power plants as well as energy storage facilities, which may become an additional source of revenue for these sources [3]. The price of these products is determined based on the "merit order" mechanism using the marginal price, i.e., the most expensive bid among all those that have been contracted [2], [4]. They exhibit significant volatility over the course of individual hours of the day—Figure 1 shows an example of the price trends for various balancing capacities over the course of a single day.

In order to submit a competitive bid that will be selected by the TSO, the owner of an energy source or storage facility should estimate or forecast the price of each balancing capacity during specific hours of the day. In [5], [6], [7] list a number of methods for forecasting energy and balancing power prices, including, among others:

a) Multi-agent models
b) Fundamental models
c) Reduced-form models
d) Statistical models (time series, machine learning, deep learning)
e) Hybrid models

[1] Cracow University of Technology, Faculty of Environmental and Energy Engineering
* michal.rybinski@doktorant.pk.edu.pl

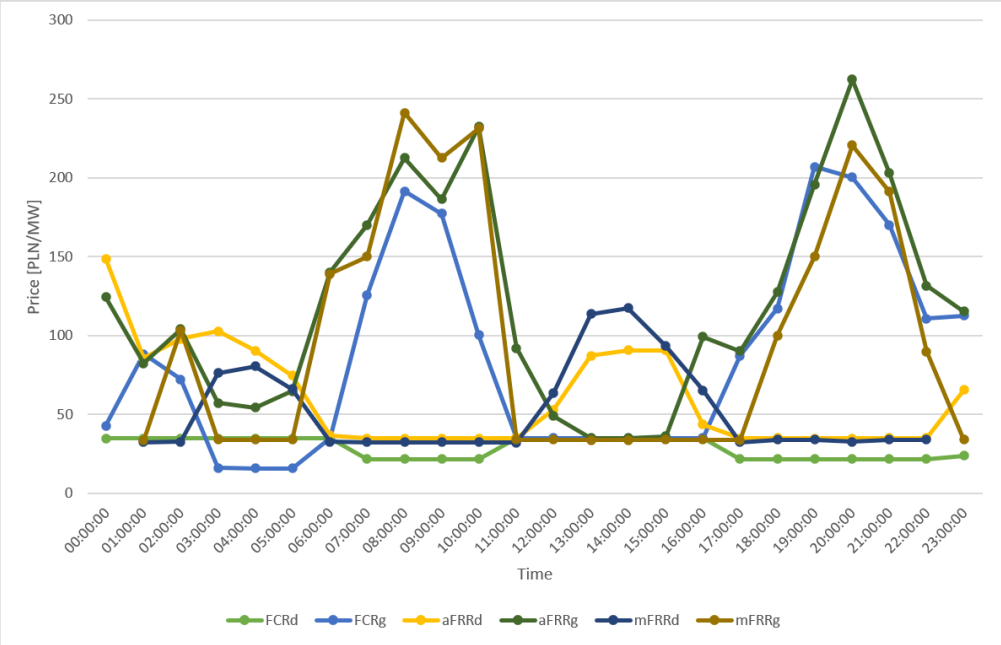


Figure 1. Chart showing hourly prices for balancing capacity purchased in the base market on the Balancing Market in Poland on March 31, 2025. Source: Author's own work based on hourly balancing capacity price data from the Balancing Market [8].

The conducted research focused on the use of machine learning methods that belong to the group of statistical models. Based on a review of the literature and observations of the energy market, a number of factors related to the operation of the National Power System, commodity prices, and public holidays in the national economy were selected.

The results regarding errors and the coefficient of determination obtained by the best models developed for individual power types vary significantly. The models for RRg capacity yield the best results, while those for mFRRg yield the worst. In many cases, despite achieving a high coefficient of determination R^2 (at the level of 0.8–0.9), the RMSE and MAE error values reach levels amounting to several dozen percent of the annual average price. In practical applications, these models can accurately forecast the general trend in price changes, but accurately predicting extremely high prices may be problematic.

[1] Urząd Regulacji Energetyki (URE), Dziś wchodzi w życie drugi etap reformy Rynku Bilansującego, 14 June 2024. https://www.ure.gov.pl/pl/urzad/informacje-ogolne/aktualnosci/12002,Dzis-wchodzi-w-zycie-drugi-etap-reformy-Rynku-Bilansujacego.html (accessed 17 January 2026).
[2] Polskie Sieci Elektroenergetyczne S.A. (PSE), Warunki dotyczące bilansowania, 14 September 2023. https://www.pse.pl/documents/20182/4493072298/Warunki_Dotyczace_Bilansowania_z_20230914.pdf/2bd652e7-db8b-47ee-847e-6ab5dd5c74d8.
[3] Urząd Regulacji Energetyki (URE), Ocena wpływu reformy rynku bilansującego na stosowanie ograniczeń alokacji w krajowym systemie elektroenergetycznym w okresie 14.06.2024–30.06.2025 oraz rekomendacje dalszych działań, URE, Warszawa, 2025. https://www.ure.gov.pl/pl/urzad/informacje-ogolne/edukacja-i-komunikacja/publikacje/ocena-wplywu-reformy-rynku-bil/12984,Ocena-wplywu-reformy-rynku-bilansujacego-na-stosowanie-ograniczen-alokacji-w-kra.html.
[4] Polski Komitet Energii Elektrycznej (PKEE), Wyznaczanie ceny energii na Towarowej Giełdzie Energii, czyli jak działa mechanizm ceny krańcowej, 28 September 2022. https://pkee.pl/aktualnosci/informacje-prasowe/wyznaczanie-ceny-energii-na-towarowej-gieldzie-energii-czyli-jak-dziala-mechanizm-ceny-krancowej (accessed 12 April 2026).
[5] A. Sobotka, P. Sobotka, K. Badyda, Koncepcja budowy modelu prognostycznego dla cen energii elektrycznej na rynku polskim, Rynek Energii 1 (2019). https://www.cire.pl/pliki/2/2019/04___sobotka_badyda___zet19.pdf.
[6] R. Weron, Electricity price forecasting: A review of the state-of-the-art with a look into the future, Int. J. Forecast. 30 (2014) 1030–1081. https://doi.org/10.1016/j.ijforecast.2014.08.008.
[7] A. Lucas, K. Pegios, E. Kotsakis, D. Clarke, Price forecasting for the balancing energy market using machine-learning regression, Energies 13 (2020) 5420. https://doi.org/10.3390/en13205420.
[8] Polskie Sieci Elektroenergetyczne S.A. (PSE), Raporty OSP / Market Data, PSE. https://raporty.pse.pl/ (accessed 30 March 2026).

EFE2026 ENERGY FUELS ENVIRONMENT
INTERNATIONAL CONFERENCE
17-20 NOVEMBER 2026, KRAKÓW, POLAND

Improving the Energy Efficiency of Natural Gas-Fired Cogeneration Systems: Energy and Economic Assessment

Piotr Dzierwa[1,*], Marcin Trojan[1], Karol Kaczmarski[2], Jan Taler[1], Dawid Taler[1], Patryk Peret[1]

Keywords: natural gas-fired cogeneration, combined heat and power, energy efficiency, thermodynamic analysis, economic assessment

ABSTRACT

Improving energy efficiency in natural gas-fired combined heat and power (CHP) systems is a key challenge in the modern energy sector, particularly amid rising fuel prices, environmental requirements, and the need to enhance the economic performance of energy generation. Gas engine cogeneration units are widely used in combined heat and power plants for their high overall efficiency and ability to supply electricity and heat simultaneously [1]. However, a significant amount of thermal energy remains available in the exhaust gases after conventional heat recovery processes [2]. The effective utilisation of this energy can increase useful heat production, reduce energy losses, and improve the overall performance of cogeneration systems [3]. This study presents a comprehensive energy and economic assessment of three technical solutions to improve the efficiency of natural gas-fired cogeneration units.

The analysis was conducted for a representative gas engine cogeneration system with a nominal electrical output of 4.4 MW and a thermal output of 4.2 MW. The reference unit achieves a total net efficiency of 87.3%, with the exhaust gases cooled to approximately 120°C in the conventional heat recovery system. The proposed modifications were evaluated by considering the year-round temperature variations of the return water from the district heating network. Three configurations were investigated: an additional economiser for direct preheating of district heating water, an economiser integrated with a compressor heat pump, and an economiser integrated with a gas-fired absorption heat pump (Fig.1). The energy balances were established to determine the available thermal energy, additional heat production, auxiliary energy consumption, and resulting changes in the overall efficiency of the CHP system.

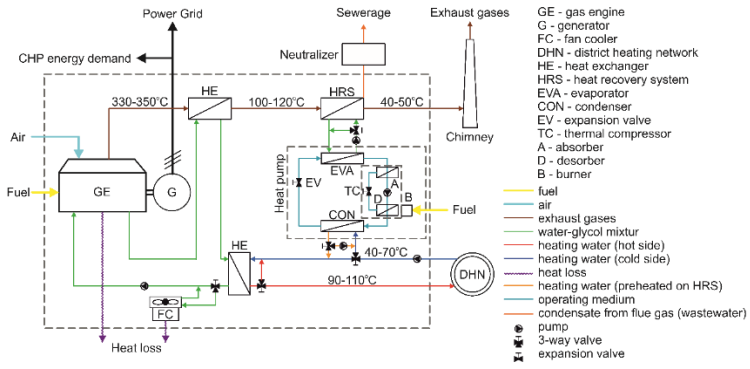


Figure 1. Simplified process diagram of a gas-fired cogeneration unit with absorption heat pump

The results demonstrate that all three configurations can improve the utilization of energy supplied to the cogeneration unit, although the magnitude of the benefits depends on the applied technology. The additional economizer provides a relatively simple solution,

[1] Cracow University of Technology, Faculty of Environmental and Energy Engineering,
* piotr.dzierwa@pk.edu.pl

increasing annual heat production by approximately 3,035 MWh and raising the total net efficiency to 91.8%. The corresponding increase in heat production is approximately 9.0% relative to the reference configuration. The integration of a compressor heat pump enables a substantially greater increase in useful heat production, reaching approximately 8,337 MWh per year, corresponding to a 24.6% increase. In this configuration, the total net efficiency reaches 96.3%. The gas-fired absorption heat pump achieves the highest additional heat production, at approximately 17,091 MWh annually, representing a 50.4% increase over the reference system. Its total net efficiency also reaches 96.3%. These results indicate that heat pump integration can substantially improve the utilization of low-temperature thermal energy, although the associated electricity or additional fuel consumption must be considered when evaluating the overall performance of each solution.

The economic assessment included capital expenditures, operating costs, and revenues associated with additional heat production. Investment profitability was evaluated using net present value (NPV), internal rate of return (IRR), and simple payback time (SPBT). The results reveal significant differences in the economic performance of the investigated configurations. The additional economizer requires a capital investment of approximately EUR 130,000 and achieves an NPV of approximately EUR 2.80 million, an IRR of 150.5%, and a simple payback time of approximately 0.7 years. The economizer combined with a compressor heat pump requires a substantially higher investment of approximately EUR 2.16 million. Its NPV is approximately EUR 0.92 million, its IRR is 4.8%, and its simple payback period is approximately 10.5 years. In contrast, the configuration incorporating a gas-fired absorption heat pump requires an investment of approximately EUR 840,000 and achieves an NPV of approximately EUR 2.55 million, an IRR of 26.1%, and a simple payback time of approximately 3.7 years.

Table 1. Increase in heat production and total generation net efficiency

Parameter	Economizer	Economizer + compressor heat pump	Economizer + absorption heat pump	Unit
NPV	2,803,806.91	922,131.31	2,549,380.48	€
IRR	150.5%	4.8%	26.1%	-
SPBT	0.7	10.5	3.7	years

The comparison demonstrates that the solution delivering the greatest additional heat production does not necessarily provide the most favorable economic indicators. The additional economizer is the most attractive option in terms of investment cost and payback time, whereas the absorption heat pump offers the highest additional heat production among the investigated alternatives. The economic performance of the absorption heat pump is nevertheless sensitive to natural gas prices and the associated operating costs. The compressor heat pump, despite its substantial contribution to additional heat production, is characterised by a longer payback period and a lower internal rate of return under the economic assumptions analysed.

In conclusion, the investigated modifications offer considerable potential for improving the energy efficiency and economic performance of natural gas-fired cogeneration systems. The selection of the most appropriate solution should account for the required heat output, investment expenditure, auxiliary energy demand, operating costs, and prevailing energy market conditions. The results provide a basis for comparing alternative efficiency improvement strategies and supporting investment decisions in combined heat and power plants.

[1] G. Xu, S. Huang, Y. Yang, Y. Wu, K. Zhang, C. Xu, Techno-economic analysis and optimization of the heat recovery of utility boiler flue gas, Appl. Energy 112 (2013) 907–917. https://doi.org/10.1016/j.apenergy.2013.04.048.
[2] H. Chen, Y. Zhou, S. Cao, X. Li, X. Su, L. An, D. Gao, Heat exchange and water recovery experiments of flue gas with using nanoporous ceramic membranes, Appl. Therm. Eng. 110 (2017) 686–694.

https://doi.org/10.1016/j.applthermaleng.2016.08.191.
[3] R. Nandhini, B. Sivaprakash, N. Rajamohan, Waste heat recovery at low temperature from heat pumps, power cycles and integrated systems – Review on system performance and environmental perspectives, Sustain. Energy Technol. Assess. 52 (2022) 102214. https://doi.org/10.1016/j.seta.2022.102214.

EFE2026 ENERGY FUELS ENVIRONMENT
INTERNATIONAL CONFERENCE
17-20 NOVEMBER 2026, KRAKÓW, POLAND

Emission Intensity of Hydrogen Production by Methane Pyrolysis and Steam Methane Reforming

Tomasz Chmielniak[1,*], Marek Ściążko[2], Wojciech Nowak[2], Leszek Stępień[3]

Keywords: hydrogen production, methane pyrolysis, steam methane reforming, catalyst regeneration, greenhouse gas emissions

ABSTRACT

Assessing opportunities to reduce greenhouse gas emissions from hydrogen production requires a comparison of complete process configurations, including feedstock conversion, hydrogen purification, heat supply and the management of carbon-containing products [1,2]. This study presents a comparative process analysis of hydrogen production by methane pyrolysis and steam methane reforming, with particular emphasis on the influence of catalyst regeneration on the emission intensity of the pyrolysis pathway.

The analysis was performed using process models developed in the CHEMCAD simulator. The models represent the main process units of the hydrogen production systems, with defined calculation algorithms and specified operating parameters. These units are interconnected by process streams comprising gases, steam at different pressure levels, process water, cooling water, boiler water and solids. The models provide mass and energy balances, process gas compositions, energy requirements and CO_2 emissions for the configurations considered.

The steam methane reforming configuration allows CO_2 removal from both the process gas and the flue gas generated by fuel combustion to supply heat to the reformer. For methane pyrolysis, catalyst regeneration was investigated through hydrogasification and combustion of carbonaceous deposits strongly attached to the catalyst. Oxidative regeneration can supply heat to the integrated process, but converts the deposited carbon into gaseous carbon oxides [3]. Hydrogasification consumes hydrogen and converts deposited carbon into methane, which can be recycled to the pyrolysis section [4]. Accordingly, the regeneration route affects the carbon balance, internal hydrogen consumption and heat supply. Accounting for these interactions is essential when comparing the emission intensity of the pyrolysis configurations and their net hydrogen production.

The emissions assessment included direct process emissions and indirect emissions associated with electricity consumption and the upstream carbon footprint of natural gas. Greenhouse gas emission intensity was expressed in kilograms of CO_2 equivalent per kilogram of net hydrogen produced. The analysis provides a preliminary identification of the process conditions under which methane pyrolysis can achieve lower emission intensity than steam methane reforming and establishes the influence of catalyst regeneration on this comparison.

The process simulations indicate that all the technological configurations considered have the potential to enable efficient low-carbon hydrogen production under the specified operating conditions. The calculated emission intensities meet the EU threshold of approximately 3.38 kg CO_2eq/kg H_2, derived from the definition of low-carbon hydrogen from non-renewable sources set out in Article 2(11) of Directive (EU) 2024/1788. The

[1] Department of Thermal and Fluid Flow Machines, Faculty of Energy and Fuels, AGH University of Krakow, al. Mickiewicza 30, 30-059 Krakow, Poland, *chmielniak@agh.edu.pl
[2] Center of Energy, AGH University of Krakow, al. Mickiewicza 30, 30-059 Krakow, Poland;
[3] Department of Fuel Technology, Faculty of Energy and Fuels, AGH University of Krakow, al. Mickiewicza 30, 30-059 Krakow, Poland

results highlight the importance of integrating CO_2 capture into hydrogen production processes, selecting an appropriate catalyst regeneration strategy and optimising electricity consumption to minimise the emission intensity of hydrogen production.

[1] A.O. Oni, K. Anaya, T. Giwa, G. Di Lullo, A. Kumar, Comparative assessment of blue hydrogen from steam methane reforming, autothermal reforming, and natural gas decomposition technologies for natural gas-producing regions, Energy Conversion and Management, 254 (2022) 115245. DOI: 10.1016/j.enconman.2022.115245.
[2] M. Shokrollahi, N. Teymouri, O. Ashrafi, P. Navarri, Y. Khojasteh-Salkuyeh, Methane pyrolysis as a potential game changer for hydrogen economy: Techno-economic assessment and GHG emissions, International Journal of Hydrogen Energy, 66 (2024) 337–353. DOI: 10.1016/j.ijhydene.2024.04.056.
[3] G. Ruoppolo, P. Ammendola, Hydrogen production by catalytic methane decomposition and catalyst regeneration by oxygen mixtures in fluidised and fixed bed reactors, International Journal of Nuclear Hydrogen Production and Applications, 2 (2009) 4–20. DOI: 10.1504/IJNHPA.2009.023823.
[4] L. Alves, V. Pereira, S. Delgado, N. Atashi, P. Dias, T. Lagarteira, G. Prieto, A. Mendes, Regeneration of methane splitting catalysts by interfacial hydrogenation, Chemical Engineering Journal, 500 (2024) 157046. DOI: 10.1016/j.cej.2024.157046.

Acknowledgement
This work and the authors' participation in the conference were supported by the Excellence Initiative – Research University (IDUB) programme of AGH University of Krakow under Action 21, Task No. 18257.

Ni-Al-Co Hydrotalcites as Precursors of CO_2 Methanation Catalysts: Effect of Cobalt Substitution for Nickel

Bogdan Samojeden[1,*], Katarzyna Bania[1], Monika Motak[1]

Keywords: CO_2 methanation, hydrotalcites, nickel catalysts, cobalt, Power-to-Gas

ABSTRACT

Carbon dioxide methanation is a promising route for CO_2 utilisation and a key element of Power-to-Gas technology, enabling the conversion of renewable energy into synthetic methane. The aim of this work was to synthesise and characterise Ni-Al-Co hydrotalcite-based materials and to evaluate their activity in the Sabatier reaction.

Five hydrotalcite precursors with a constant Al content (x = 0.25) and progressive substitution of Ni by Co (Ni/Co = 0.75/0, 0.50/0.25, 0.25/0.50, 0/0.75) were prepared by co-precipitation and calcined. Two Ni-Al samples of identical composition were synthesised using different solvent volumes to assess the influence of preparation conditions. The materials were characterised by N_2 adsorption (BET), XRD and FTIR spectroscopy. Catalytic tests were performed in a flow reactor at 250-450 °C using a stoichiometric mixture ($CO_2/H_2/Ar$ = 15/60/25 vol.%) at 100 mL/min.

All materials were mesoporous (90-139 m^2/g) and exhibited surface hydroxyl and carbonate groups favouring CO_2 adsorption. XRD revealed NiO, Co_3O_4, CoO and Al_2O_3 phases after calcination, together with $NiAl_2O_4$ and $CoAl_2O_4$ spinels in the cobalt-containing samples. All catalysts showed CH_4 selectivity close to 100%. The highest activity was obtained for Ni/Al = 0.75/0.25, reaching approximately 85% CO_2 conversion at 250-300 °C. The two Ni-Al samples differed markedly in activity at 250 °C (65% vs. 85%), indicating that the catalyst structure is defined at the synthesis stage. Substituting Ni by Co promoted less reducible spinel phases, lowered low-temperature activity and shifted the optimum to 350-400 °C.

Ni-Al hydrotalcites are therefore promising precursors of low-temperature CO_2 methanation catalysts, whose properties can be tailored by controlling composition and synthesis parameters.

This work was supported by the AGH University of Krakow under the IDUB programme (Action 21, Application No. 18209).

[1] AGH University, al. Mickiewicza 30, 30-059 Kraków, Poland, * bsamo1@agh.edu.pl

EFE2026 ENERGY FUELS ENVIRONMENT
INTERNATIONAL CONFERENCE
17-20 NOVEMBER 2026, KRAKÓW, POLAND

Assessment of Selected Valuable and Critical Elements in Metallurgical Wastes

Alicja Barczyk[1,*], Marta Seman[1], Katarzyna Król[1], Michał Szwamel[1], Natalia Skowrońska[1], Karolina Kolarz[1], Piotr Soprych[1], Dorota Makowska[1]

Keywords: critical elements, steelworks waste, circular economy

ABSTRACT

The growing demand for strategically important metals has intensified interest in industrial residues as potential secondary raw materials. Iron and steel production generates chemically diverse waste streams, including dusts, slags, iron-bearing sludges, and mill scale. Although these materials are commonly managed as process residues, they may contain elements of economic or technological interest [1,2]. A reliable assessment of their resource potential requires both characterization of the bulk matrix and measurement of target elements, including consideration of analytical detection limits.

This study aimed to characterize selected metallurgical residues and assess their potential as secondary sources of valuable and critical elements. A total of 22 samples, including steelmaking and blast furnace dusts and slags, iron-bearing sludges, and mill scale, were examined. The basic chemical composition was determined by X-ray fluorescence spectrometry (XRF), while selected elements were quantified using flame atomic absorption spectrometry (FAAS). Due to the relatively high detection limits of FAAS, several elements could not be quantified in some samples.

The measured element concentrations varied markedly between waste types and individual samples. Copper ranged from approximately 1–3 mg/kg in blast furnace slags to more than 200 mg/kg in mill scale and steelmaking dusts. Nickel concentrations extended from approximately 6 mg/kg to 154 mg/kg, with the highest reported value found in mill scale. Silver was present at approximately 1 mg/kg in selected slag and mill scale samples and reached approximately 15 mg/kg in iron-bearing sludges. Cobalt reached about 10 mg/kg in mill scale. Manganese concentrations ranged from 0.05 wt.% in blast furnace dust to about 1 wt.% in steelmaking dust.

The results highlight the heterogeneity of metallurgical residues and their potential as secondary metal sources. However, metal concentrations alone do not confirm recovery feasibility, while FAAS detection limits constrain the assessment. Further evaluation requires investigating element distribution among operationally defined fractions using the BCR sequential extraction procedure [3].

[1] Simoni, M., et al. (2024). Towards the Circularity of the EU Steel Industry: Modern Technologies for the Recycling of the Dusts and Recovery of Resources. Metals, 14(2), 233, doi.org/10.3390/met14020233.
[2] Rudnik, E. (2025). Hydrometallurgical Treatment of EAF By-Products for Metal Recovery: Opportunities and Challenges. Metals, 15(8), 914, doi.org/10.3390/met15080914.
[3] Davidson, C. M., et al. (1998). A Critical Evaluation of the Three-Stage BCR Sequential Extraction Procedure to Assess the Potential Mobility and Toxicity of Heavy Metals in Industrially-Contaminated Land. Analytica Chimica Acta, doi:10.1016/S0003-2670(98)00057-9.

Acknowledgments:
The research was financed from the Research the Resarch Found of „Rozkręć koło z Arcelor-Mittal 2026” for AGH University of Krakow no 3/AMP/2026 for Student Scientific Group FENIKS AGH.

[1] Facutly of Energy and Fuel, AGH University of Krakow, al. A. Mickiewicza 30, 30-059 Krakow, Poland, * abarczyk@student.agh.edu.pl

EFE2026 ENERGY FUELS ENVIRONMENT
INTERNATIONAL CONFERENCE
17-20 NOVEMBER 2026, KRAKÓW, POLAND

Robust Regional Energy Planning under Data Uncertainty: A TIMES-Based Analysis of Sardinia to 2050

Roberto Ricciu[1],*, Pier Luca Maria Buonomo[1]

Keywords: Regional energy planning, TIMES model, Energy data uncertainty, Energy transition scenarios, Sardinia

ABSTRACT

Regional energy planning relies on data collected from different sources, often developed for statistical, regulatory or administrative purposes rather than for energy-system modelling. Differences in definitions, temporal resolution and sectoral boundaries may therefore significantly affect long-term scenarios.

This presentation examines Sardinia as a case study for regional energy planning using the TIMES framework. Starting from the reconstruction of the regional energy system, it discusses the main inconsistencies affecting electricity, heat and fuel data and their implications for pathways to 2030, 2040 and 2050. Particular attention is given to the propagation of uncertainty in selected input parameters and to its effects on technology choices, investments, system costs and CO_2 emissions. A possible increase in electricity demand associated with data centres is also considered as a stress test for the regional system.

The aim is to distinguish decisions that remain robust under different assumptions from those that depend strongly on the quality of the initial data.

[1] Department of Environmental and Energy Engineering, University of Cagliari, Italy, *ricciu@unica.it

Hollow-SiO_2@CuZnMgAl-LDH-derived Catalyst for Direct CO_2 Hydrogenation to Methanol

Tomasz Kondratowicz[1,2]*, Dermot O'Hare[1], Monika Motak[2]

Keywords: CO_2 hydrogenation; methanol synthesis; layered double hydroxides; Cu–Zn–Mg–Al catalysts; memory effect

ABSTRACT

The catalytic hydrogenation of carbon dioxide (CO_2) to methanol has attracted considerable attention as a promising strategy for carbon capture and utilization (CCU), providing an opportunity to convert CO_2 into a valuable chemical feedstock and alternative energy carrier. Methanol is an important platform chemical widely used in the production of formaldehyde, acetic acid, dimethyl ether, and other industrial products. It can also serve as a fuel, fuel additive, or hydrogen carrier, making it an important component of the emerging methanol economy [1,2]. When combined with hydrogen produced from renewable energy sources, CO_2 hydrogenation offers a potential pathway toward more sustainable chemical production and reduced dependence on fossil-based feedstocks. However, efficient CO_2 hydrogenation to methanol remains challenging due to the high thermodynamic stability of CO_2, competition from the reverse water–gas shift (RWGS) reaction, which reduces methanol selectivity, and catalyst deactivation under reaction conditions. Consequently, the development of highly active, selective, and stable heterogeneous catalysts is essential for improving methanol productivity and process efficiency.

Cu-based catalysts, particularly $Cu/ZnO/Al_2O_3$ systems, are widely employed in industrial methanol synthesis due to their high catalytic activity, relatively low cost, and proven industrial performance. Their performance is strongly influenced by copper particle size and dispersion, the accessibility of active sites, synergistic interactions between Cu and ZnO, and catalyst structural stability. In this context, layered double hydroxides (LDHs) represent promising precursors for the synthesis of multicomponent catalysts with tailored chemical compositions and physicochemical properties. Their unique layered structure enables different metal cations to be incorporated and homogeneously distributed within positively charged hydroxide layers. Upon calcination, LDHs are transformed into mixed metal oxides, commonly referred to as layered double oxides (LDOs), which can exhibit favourable textural properties and intimate interactions between constituent metal species. Furthermore, the ability of certain LDH-derived oxides to reconstruct their layered structure under suitable conditions, known as the *memory effect*, offers additional opportunities for controlled metal incorporation and catalyst design.

In this work, a synthetic strategy for the preparation of well-organized, mesoporous CuZnMgAl-LDH catalyst precursors with a hollow spherical architecture is presented (Figure 1). Hollow-SiO_2@$Cu_xZn_yMg_z$Al-LDH materials were synthesized by exploiting the memory effect of LDH-derived mixed metal oxides. The synthesis involved the formation of SiO_2@MgAl-LDH core–shell structures, followed by selective etching of the silica core and subsequent calcination to obtain hollow-SiO_2@MgAl-LDO materials. The resulting mixed

[1] University of Oxford, Department of Chemistry, Chemistry Research Laboratory, Mansfield Road 12, OX1 3TA Oxford, UK

[2] AGH University of Krakow, Faculty of Energy and Fuels, Mickiewicza Ave. 30, 30-059 Krakow, Poland, * tkondratowicz@agh.edu.pl

metal oxides were then subjected to reconstruction in aqueous solutions containing Cu^{2+} and Zn^{2+} ions, enabling their incorporation into the LDH structure while preserving the desired hollow spherical morphology. The effects of Cu^{2+} and Zn^{2+} precursor concentrations ranging from 20 to 80 mM, as well as five successive calcination–reconstruction cycles, on the chemical composition, crystallinity, morphology, and textural properties of the resulting materials were investigated.

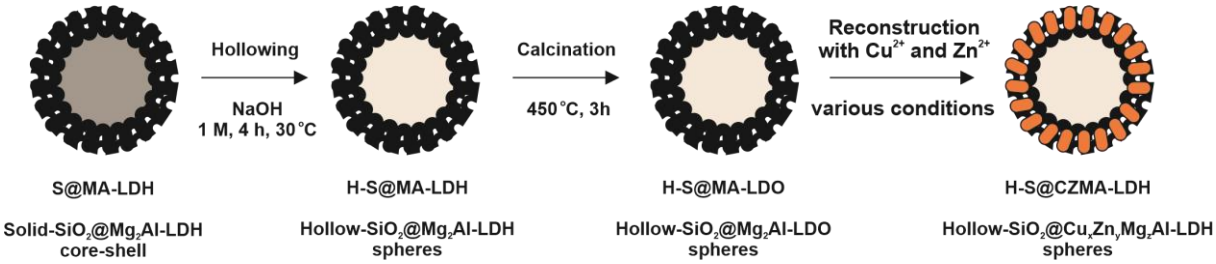


Figure 1. Schematic representation of the synthesis of hollow-SiO_2@$Cu_xZn_yMg_z$Al-LDH catalyst precursors.

The results demonstrate that reconstruction conditions play a crucial role in determining the composition, crystalline structure, morphology, and textural properties of the LDH materials, thereby affecting the properties of the resulting catalysts. A precursor concentration of 20 mM enabled the formation of a well-defined LDH phase while preserving the hollow morphology and favourable porosity. In contrast, higher precursor concentrations promoted the formation of additional crystalline phases, including $Cu_2(OH)_3NO_3$, accompanied by reduced porosity and deterioration of the hollow architecture. Repeated calcination–reconstruction cycles provided an alternative route for the gradual incorporation of Cu and Zn species while maintaining the desired structural and textural characteristics. The catalytic performance of the resulting materials was evaluated in CO_2 hydrogenation to methanol. The most active catalyst achieved a methanol space-time yield of 1.68 $g_{MeOH} \cdot g_{Cu}^{-1} \cdot h^{-1}$ at 270°C and 30 bar, representing a 1.7-fold improvement compared with a commercial $Cu/ZnO/Al_2O_3$ catalyst under identical reaction conditions. Importantly, increasing the total metallic copper content did not necessarily lead to improved catalytic performance. Catalysts containing smaller, more uniformly dispersed Cu^0 particles exhibited higher methanol productivity than those with higher copper content but larger Cu^0 particles. These findings highlight the importance of controlling copper particle size and dispersion rather than simply increasing the amount of the active metal.

Overall, this study demonstrates that the LDH memory effect provides a versatile strategy for preparing multicomponent catalyst precursors with tailored composition, morphology, and porosity. The combination of controlled metal incorporation and hollow spherical architecture offers a promising approach to the development of efficient Cu-based catalysts for CO_2 hydrogenation to methanol. The findings provide insights into the relationships between synthesis conditions, physicochemical properties, and catalytic performance, contributing to the design of advanced heterogeneous catalysts for sustainable methanol production and CO_2 valorization.

[1] A. Goeppert, M. Czaun, J.-P. Jones, G.K.S. Prakash, G.A. Olah, Recycling of carbon dioxide to methanol and derived products – closing the loop, Chem. Soc. Rev. 43 (2014) 7995–8048. https://doi.org/10.1039/C4CS00122B.
[2] H. Kolmeijer, A. Nabera, A.J. Martín, G. Guillén-Gosálbez, J. Pérez-Ramírez, A feasible methanol economy for a green future, Green Chem. 28 (2026) 174–185. https://doi.org/10.1039/D5GC04615G.

Acknowledgment: This work was partially supported by Research Subsidy AGH no. 501.00-210000-10000.

EFE2026 ENERGY FUELS ENVIRONMENT
INTERNATIONAL CONFERENCE
17-20 NOVEMBER 2026, KRAKÓW, POLAND

Material Requirements of the Polish Power Sector Transition: Linking Electricity Demand and Energy System Models

Patrycja Rzeszut[1], Artur Wyrwa[1,*], César Valderrama[2], Maciej Raczyński[1]

Keywords: system dynamics, TIMES model, electricity demand, critical raw materials, Poland

ABSTRACT

The material needs associated with the energy transition of the power sector depend on the technologies deployed, the pace of expansion, and the replacement of ageing assets and cannot be revealed only on the basis of electricity demand projections. In this work, Poland was used as a case study. A system-dynamics Vensim model was integrated with the TIMES-PL energy-system model and an assessment of material requirements. The Vensim model is driven by GDP and population in order to determine the electricity demand up to the year 2050. Electrification is captured through the turnover of end-use equipment. The TIMES-PL model is run on the calculated electricity demand under two policy pathways that are adopted in order to compare the demand for electricity, generation capacity, and material flows. The determined cost-optimal mix of generation and storage capacities is converted into the requirements of bulk and critical materials. These requirements are then compared with the domestic production of silver, copper, and steel for Poland in 2025. Electricity demand increases from 146.4 TWh in 2020 to 220.8–246.0 TWh in 2050. The newly installed capacities of wind, solar photovoltaics, and battery storage technologies reach 103–114 GW, implying the need for 8.4–9.2 Mt of steel, 305–326 kt of copper, 2.3–2.6 kt of neodymium, and 1.2–1.6 kt of lithium. The total capacity additions are 10.8% higher under more ambitious pathway assumptions, which results in the increase in battery deployments and lithium demand by 40.6%. The demand for rare-earth materials is highly sensitive to changes in offshore wind generation design, with wind-related neodymium differing by a factor of 5.8 across configurations. By 2050, the copper stock in retiring equipment surpasses the copper needed for new installations. The results indicate that technology selection and the timing of capacity additions and retirements can substantially influence material requirements.

[1] Faculty of Energy and Fuels, AGH University of Krakow, 30-059 Kraków, Poland
[2] Department of Chemical Engineering, Universitat Politècnica de Catalunya (UPC), 08034 Barcelona, Spain
*corresponding author: awyrwa@agh.edu.pl

EFE2026 ENERGY FUELS ENVIRONMENT
INTERNATIONAL CONFERENCE
17-20 NOVEMBER 2026, KRAKÓW, POLAND

From Carbon Dioxide to Alternative Fuels: Catalytic Routes for CO_2 Utilization

Bogdan Samojeden[1], Monika Motak[1*]

Keywords: CO_2 utilization; dry reforming of methane; CO_2 methanation; nickel catalysts; Power-to-Gas

ABSTRACT

The utilization of carbon dioxide as a feedstock for fuel production is attracting increasing scientific and technological interest. Alongside carbon capture and storage (CCS), catalytic CO_2 conversion offers opportunities to recycle carbon into useful products. Relevant pathways include CO_2 hydrogenation to methane and methanol, as well as synthesis gas production through the dry reforming of methane. This contribution discusses selected catalytic routes for CO_2 utilization, with particular emphasis on the activity, selectivity and stability of nickel-based catalysts.

One of the processes investigated by our group is the dry reforming of methane (DRM), in which CO_2 reacts with CH_4 to produce synthesis gas. The stoichiometric H_2:CO molar ratio is 1:1, although the actual composition depends on the reaction conditions and competing reactions. Following appropriate adjustment of its composition, the resulting gas can be used in downstream processes, including Fischer-Tropsch synthesis and the production of methanol or dimethyl ether. DRM can be conducted at atmospheric pressure, but its strongly endothermic nature and the high operating temperatures required pose significant challenges. Nickel-based catalysts are attractive because of their activity and relatively low cost; however, carbon deposition and sintering can lead to deactivation. Improving catalyst stability therefore remains a key research objective.

Another important pathway is CO_2 hydrogenation to methane, commonly known as CO_2 methanation. Although thermodynamically favourable at low temperatures, this reaction requires a suitable catalyst to overcome kinetic limitations and achieve high conversion and methane selectivity. Nickel supported on alumina is a widely studied catalytic system. When coupled with hydrogen produced using renewable electricity, methanation provides a route to synthetic natural gas within the Power-to-Gas concept.

Synthesis gas can also be processed to increase its hydrogen content through the water-gas shift reaction, in which CO reacts with steam to form CO_2 and additional H_2. Iron- and copper-based catalysts are commonly employed in the high- and low-temperature shift stages, respectively. Subsequent purification is required to meet the specifications of the intended application, particularly the stringent limits on CO in hydrogen supplied to low-temperature proton-exchange membrane fuel cells.

The development of durable and selective catalysts is essential for advancing CO_2 conversion technologies. The contribution of these technologies to reducing greenhouse gas emissions must be assessed across the full process life cycle, taking into account the sources of hydrogen and energy. These considerations are central to the development of alternative fuels based on captured CO_2.

This work was supported by the AGH University of Krakow under the IDUB programme (Action 21, Application No. 18209).

[1] AGH University, al. Mickiewicza 30, 30-059 Kraków, Poland, * motakm@agh.edu.pl

EFE2026 ENERGY FUELS ENVIRONMENT
INTERNATIONAL CONFERENCE
17-20 NOVEMBER 2026, KRAKÓW, POLAND

Identification of the Parameters of a Two-Zone Energy Balance Model of a Solar Domestic Hot Water Storage Tank Subject to Physical Constraints, Based on Field Operation Data

Wiktor Filipek[1], Barbara Tora[1]*, Krzysztof Broda[1], Stanisław Pietrzyk[2]

Keywords: solar thermal system, DHW storage tank, two-zone SDHW model, SolarComp 971SD1 controller, waste heat recovery, overheating, renewable energy sources (RES)

ABSTRACT

In a domestic solar thermal system, the domestic hot water (DHW) storage tank is the node that determines how much of the heat collected by the solar collectors is stored, how much is delivered to the consumers, and how much is lost or rejected as surplus heat. Parameters of storage tank models are usually determined on laboratory test rigs (e.g. according to EN 12977-3), under controlled flow rates and draw-off profiles. In systems operating under real conditions, however, typically only the data logged by the controller are available, without measurements of flow rates or DHW draw-offs, which makes parameter identification and the assessment of heat flows considerably more difficult.

The aim of this work is to develop a method for identifying the parameters of a two-zone energy balance model of a DHW storage tank supplied by a solar collector system, using exclusively the data logged by the SolarComp 971SD1 controller. The main research problem is to determine to what extent the relationship between collector operation and changes in the energy state of the tank can be reconstructed from a limited set of measurements, in the absence of measurements of the heat transfer fluid flow rate, DHW draw-off and pump operating states. Unlike approaches based on unconstrained fitting of model parameters, the proposed method incorporates constraints arising from the tank volume and the principle of conservation of energy. Without these constraints, a possible scaling error in the power computed by the controller could be compensated by non-physical values of the zone heat capacities.

The analysis is based on operational data from real solar thermal systems coupled with DHW storage tanks with a nominal volume of 400 l. The central heating (CH) circuit can either provide auxiliary heating to the tank or remove excess heat from it. The available time series comprise the solar collector temperature, the temperatures of the lower and upper zones of the tank, the CH boiler circuit temperature, and the instantaneous solar system power computed by the controller. The data are logged during normal operation, without additional measuring equipment; more recent data are available at a sampling interval of approximately 3 min, and older data at 15 min. The buildings are occupied seasonally, so for most of the year there is no DHW draw-off.

For this reason, the solar thermal system has two principal seasonal operating modes. Outside the heating season it is used for DHW preparation, whereas during the heating season, when the CH boiler is not in operation, it protects the building against excessive cooling by transferring solar energy to the CH system. During this period, the tank temperature may remain for long periods below the level required for hygienic reasons (risk of Legionella growth); DHW is therefore prepared using another energy source.

In the first stage, the dependence of the controller-computed power on the collector temperature, its rate of change, and the temperature difference between the collector and the lower zone of the tank will be investigated. Models with an increasing number of explanatory variables will be compared, taking into account time lags and the

[1] AGH University of Krakow, Poland, * tora@agh.edu.pl

discontinuities associated with switching on the solar loop. The analysis is intended to show whether the observed temperature profiles allow the power reported by the controller to be reproduced with sufficient accuracy. This will not be equated with an independent measurement of the actual heat transfer rate.

Subsequently, characteristic operating states of the system will be analysed for which simple physical energy balance models can be applied. Particular attention will be paid to periods with neither DHW draw-off nor auxiliary heat sources, in which changes in tank temperatures result primarily from the energy supplied by the collector. For these periods, the tank will be represented as a system of two zones with effective heat capacities, and the aim of the analysis will be to identify the model parameters and to assess the feasibility of determining changes in stored energy and the net heat balance. Constraints arising from the actual tank volume, parameter positivity and the principle of conservation of energy will be taken into account.

The expected outcome is to determine the range within which the thermal dynamics of the tank can be reliably reproduced without flow measurements, and to identify the limitations of such a method. The proposed approach may serve as a basis for further analysis of energy flows in solar thermal systems, for detecting periods of unused surplus heat, and for indirectly estimating DHW draw-off as the residual of the energy balance under conditions in which the remaining heat flows can be excluded or estimated.

[1] W. Filipek, K. Broda, B. Tora, Ciepło odpadowe z instalacji grzewczej w domu jednorodzinnym – odzysk i zagospodarowanie, in: XXXIX Konferencja Zagadnienia Surowców Energetycznych i Energii w Gospodarce Krajowej, Zakopane-Kościelisko, 18–21 October 2026. https://se.min-pan.krakow.pl/program-konferencji/ (accessed 30 October 2026).
[2] J.A. Duffie, W.A. Beckman, Solar Engineering of Thermal Processes, 4th ed., John Wiley & Sons, Hoboken, NJ, 2013. https://doi.org/10.1002/9781118671603.
[3] J. Mirek, K. Słomczyńska, P. Mirek, Model efektywnego systemu ciepłowniczego na bazie energii solarnej, Instal 11 (2022) 19–27. https://doi.org/10.36119/15.2022.11.1.
[4] B. Zaporowski, Modelowanie matematyczne procesów wymiany ciepła w elementach systemów energetycznych, Wydawnictwo Politechniki Poznańskiej, Poznań, 2015.

This research was funded by the Excellence Initiative – Research University (IDUB) programme and a scientific research subsidy of AGH University of Krakow.

EFE2026 ENERGY FUELS ENVIRONMENT
INTERNATIONAL CONFERENCE
17-20 NOVEMBER 2026, KRAKÓW, POLAND

Synthesis of GIS and LTA Zeolites from Fly Ash and Their Application as Adsorbents of Phosphate Ions from Aqueous Solution

Jakub Mokrzycki[1,*]

Keywords: fly ash, zeolite, phosphate ions, adsorption

ABSTRACT

The increasing demand for effective technologies for phosphate ions removal from wastewater has stimulated research into alternative adsorbent materials, particularly those derived from industrial waste streams. Among the available secondary raw materials, coal fly ash represents a promising precursor for the synthesis of zeolitic materials due to its considerable content of silica and alumina. The conversion of fly ash into zeolites offers a dual environmental benefit by enabling the valorisation of industrial by-products while providing functional materials for water treatment applications. The aim of this study was to develop a synthesis procedure for obtaining zeolitic materials from coal fly ash and investigate their potential for phosphate ions removal from aqueous solutions. Particular emphasis was placed on determining the influence of hydrothermal synthesis conditions on the resulting zeolite framework structure and evaluating the effects of ion-exchange modification on adsorption performance.

The synthesis procedure involved two consecutive stages. Initially, fly ash was subjected to alkaline fusion with NaOH at 550°C for 2 h to enhance the reactivity and availability of silica-containing species. Subsequently, hydrothermal treatment was performed at 80°C using two different reaction times (6 and 24 h). X-ray diffraction (XRD) analysis confirmed that the duration of hydrothermal treatment had a significant influence on the crystalline phases formed. After 6 h, a material containing GIS-type zeolite, identified as Na-P1, was obtained, whereas extending the synthesis time to 24 h favoured the formation of an LTA-type zeolite, identified as Na-A. Nevertheless, neither product exhibited a purely zeolitic composition. The GIS-containing material also comprised residual silica and mullite originating from the fly ash, while the LTA-containing material contained minor amounts of an additional FAU-type zeolite phase and residual silica. These observations indicate that the mineralogical complexity of the starting material and the incomplete conversion of its components affect the phase composition of the final products. Despite these limitations, the applied synthesis approach enabled the successful conversion of fly ash into materials containing two distinct zeolite framework structures (Figure 1a).

To investigate the role of charge-compensating cations in phosphate ions adsorption, the synthesized Na-P1 and Na-A materials were subjected to ion exchange using 1 M aqueous solutions of potassium, calcium and ammonium nitrates. The exchange process was carried out in three consecutive cycles at 80°C, each lasting 1.5 h. Additionally, ammonium-exchanged materials were calcined at 500°C for 4 h to obtain their protonic forms. The adsorption performance of the resulting materials was initially evaluated using a single-point experimental approach. Potassium dihydrogen phosphate (KH_2PO_4) was used as the phosphate ions source, with an initial $PO43-$ concentration of 100 mg/L, an adsorbent dose of 1 g/L and a contact time of 24 h. The results are demonstrated in Figure 1b.

[1]AGH University of Krakow, Faculty of Energy and Fuels, al. A. Mickiewicza 30, 30-059 Kraków, Poland, mail: jmokrzycki@agh.edu.pl

The experimental results revealed a pronounced dependence of phosphate ions removal efficiency on both the zeolite framework structure and the type of exchanged cation. In their original sodium forms, GIS-type zeolite (Na-P1) exhibited an almost 20-fold higher removal capacity than LTA-type zeolite (Na-A). This substantial difference may be associated with variations in framework topology, pore architecture and the accessibility of adsorption sites. Ion exchange resulted in a further improvement in phosphate ions removal, particularly following the introduction of Ca^{2+} ions. In the case of GIS-type zeolite, conversion into the calcium form resulted in an approximately 2.8-fold increase in phosphate ions removal compared with the corresponding sodium form. An even more pronounced enhancement was observed for the LTA-type material, for which Ca-A exhibited approximately 26 times higher phosphate ions removal than Na-A. These findings suggest that the presence of calcium ions plays an important role in promoting phosphate retention, potentially through additional interactions involving calcium and phosphate species, including the formation of sparingly soluble calcium phosphate phases. This effect appears particularly relevant for LTA-type zeolite, which exhibited relatively poor adsorption properties in its original sodium form [1-2].

Further investigations included preliminary adsorption kinetic measurements and equilibrium isotherm analysis. The kinetic experiments indicated that adsorption equilibrium was reached after approximately 12 h.

Overall, the findings demonstrate that coal fly ash can be effectively converted into zeolitic materials with different framework structures and that their adsorption performance can be substantially improved through appropriate ion-exchange modification. Particularly noteworthy is the significant enhancement observed for calcium-exchanged LTA-type zeolite, demonstrating that ion-exchange modification can compensate for the relatively low phosphate removal efficiency of the original sodium form. The study highlights the importance of combining waste valorisation with the functional modification of porous materials and identifies fly ash-derived, calcium-exchanged zeolites as promising candidates for further development of adsorbents intended for phosphate ions removal from aqueous environments.

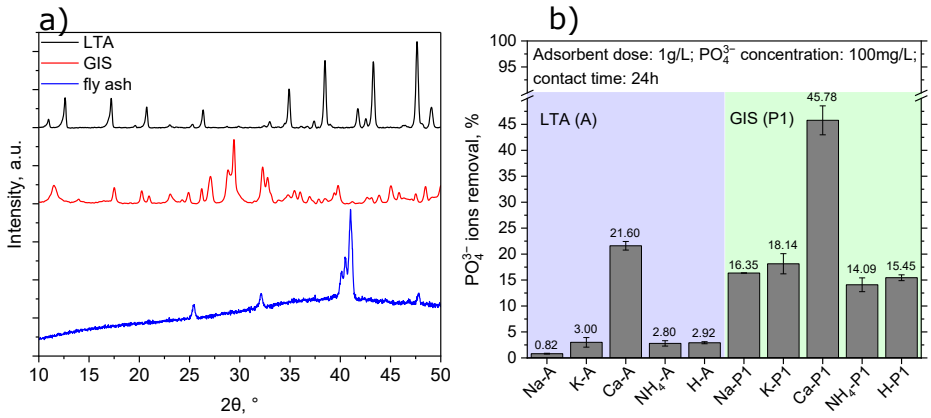


Figure 1. XRD profile of fly ash and derived fly ashes (a); and single-point adsorption of phosphate ions using ion-exchanged zeolites (b).

[1] J. Mokrzycki, M. Fedyna, M. Marzec, J. Szerement, R. Panek, A. Klimek, T. Bajda, M. Mierzwa-Hersztek, Copper ion-exchanged zeolite X from fly ash as an efficient adsorbent of phosphate ions from aqueous solutions, J. Environ. Chem. Eng. 10 (2022) 108567. https://doi.org/10.1016/j.jece.2022.108567.
[2] J. Mokrzycki, M. Fedyna, M. Marzec, R. Panek, J. Szerement, L. Marcińska-Mazur, R. Jarosz, T. Bajda, W. Franus, M. Mierzwa-Hersztek, The influence of zeolite X ion-exchangeable forms and impregnation with copper nitrate on the adsorption of phosphate ions from aqueous solutions, J. Water Process Eng. 50 (2022) 103299. https://doi.org/10.1016/j.jwpe.2022.103299.

Jakub Mokrzycki would like acknowledge the Polish National Science Centre for financial support (grant NCN MINIATURA 9 No. 2025/09/X/ST8/00807, project title: "Adsorpcja jonów fosforanowych z wykorzystaniem zeolitów wytworzonych z popiołu lotnego". The research was financed by AGH University of Krakow grant no. 501.00_210000_10000. Also, the research was supported by IDUB grant (Action 21, Application No. 18209).

EFE2026 ENERGY FUELS ENVIRONMENT
INTERNATIONAL CONFERENCE
17-20 NOVEMBER 2026, KRAKÓW, POLAND

Modernization of the Drivetrain for the "Zephyr AGH" Hybrid Vehicle

Maciej Kulawik[1,]*, Przemysław Guziak[1,], Mikołaj Miodoński[1,], Jakub Ekes[1], Kamil Iwańczyk[1,], Jakub Kurek[1,], Tomasz Maciejowski[1], Joanna Michalik[1], Jafar Alijev[1,], Piotr Miroń[1], Olaf Sulima[1], Joanna Domańska[1], Tadeusz Olkuski[1,]

Keywords: Hybrid vehicle, Pneumatic motor, Electric motor, Zephyr AGH vehicle.

ABSTRACT

This paper presents the modernization process of the drivetrain for the single-seater hybrid vehicle "Zephyr AGH," designed and developed by the "Nova Energia" Student Scientific Club. The initial design of the vehicle relied solely on a pneumatic drive, which suffered from key limitations such as low maximum speed and insufficient motor power relative to the heavy structural mass. To address these issues, a decision was made to implement a hybrid drivetrain combining a Gast pneumatic motor (4 kW power, maximum speed of 2,500 rpm, and 23 Nm torque at 7 bar pressure) with a BLDC electric motor (18 kW power, 86 V supply voltage, and 42 Nm torque).

The scope of the engineering work described in this paper included the design, fabrication, and optimization of a new pneumatic supply system using lightweight, composite cylinders (Tuxing 6.8 L, 300 bar), as well as the development of a dedicated gearbox. This transmission allows for efficient torque combining from both power units (yielding a total torque of 59.7 Nm at 2,000 rpm) and transfers it effectively to the driveshaft while maintaining an optimal total vehicle weight (including the driver) of approximately 400 kg. Additionally, empirical research was conducted to evaluate the interaction between the pneumatic and electric drives. The simulation and test results demonstrated the higher efficiency of the hybrid setup, directly resulting in significant improvements in dynamics, acceleration time, and overall performance of the "Zephyr AGH" vehicle. The vehicle represents a response to the search for lower-emission transportation solutions.



Figure 1. "Zephir AGH" Hybryd vehicle construction. Photograph by Maciej Kulawik

This research was funded by the Excellence Initiative – Research University (IDUB) programme and a scientific research subsidy of AGH University of Krakow; WEiP AGH, nr IDUB UB-696000-00001-Z01 and 501.00-210000-10000

[1] Faculty of Energy and Fuels, AGH University of Krakow, Al. Mickiewicza 30, 30-059 Krakow, Poland; Student Research Group „Nova Energia" * mkulawik@student.agh.edu.pl

EFE2026 ENERGY FUELS ENVIRONMENT
INTERNATIONAL CONFERENCE
17-20 NOVEMBER 2026, KRAKÓW, POLAND

In-Mold Embedding of Photovoltaic Cells in the Wings of an Unmanned Solar-Powered Aircraft

Izabella Rosikoń[1,2]*, Ignacy Kępa[1,3], Filip Gajda[1,3], Marta Łopusiewicz[1,4], Michał Pietrzykowski[1,5], Kacper Krempa[1,6], Filip Materowski[1,5], Jakub Konior[1,4], Krzysztof Sornek[3]

Keywords: Solar-powered UAV, photovoltaic cell integration, in-mold lamination, composite solar wing manufacturing

ABSTRACT

As unmanned aircraft technology develops rapidly, simple drone designs are no longer considered innovative. Broader applications and increasing industry expectations have shifted attention towards areas such as cooperative drone swarms and long-range UAVs. In the latter field, alongside the growing interest in hydrogen-powered drones, solar-powered UAVs are also being developed, although they remain a niche technology. Such aircraft typically feature high-aspect-ratio wings with photovoltaic (PV) cells covering their upper surfaces and, in some cases, the tail surfaces. The cells power the electric propulsion system and charge onboard batteries, allowing flight to continue under varying weather conditions. The electrical system is supported by maximum power point tracking (MPPT) and battery management system (BMS) boards, which convert, distribute, and monitor electrical power throughout the aircraft. Increasingly, AI-based algorithms are also being explored to dynamically optimize energy harvesting.

This study focuses on embedding PV cells into the wing structure, which is one of the key aspects of solar-powered aircraft development. Since the wing serves as both a lifting surface and a power source, the method of integrating PV cells into its structure directly affects both the aerodynamic performance and the energy yield of the aircraft.

Various methods of integrating solar cells into wings have been investigated. Previous work by the AGH Solar Plane team [1] compared two methods of laminating PV cells onto wings with extruded polystyrene (XPS) foam cores. Aimasso et al. [2] compared bonding prefabricated cell arrays to the wing, laminating cells directly with the carbon fiber skin, and bonding cells pre-encapsulated in polymer films. Direct lamination was rejected due to excessive efficiency losses caused by the opacity of the protective layers, while the polymer-film method was selected instead.

This presentation discusses the challenges of in-mold embedding of PV cells in the wings of an unmanned solar-powered aircraft, in which the cells are laminated simultaneously with the composite layers forming the wing structure in negative molds. The main advantage of this approach is the elimination of surface irregularities at core-segment joints. Such irregularities often occur in XPS-core wings, where the cores must be cut into segments due to the limited working area of cutting machines. Since PV cells cannot be placed over these joints, fewer cells can be accommodated on the wing, reducing

[1] AGH University of Krakow, Faculty of Energy and Fuels, AGH Solar Plane Student Research Group, Kraków, Poland, *izabella.rosikon@solarplane.agh.edu.pl
[2] AGH University of Krakow, Faculty of Computer Science, Kraków, Poland
[3] AGH University of Krakow, Faculty of Energy and Fuels, Kraków, Poland
[4] AGH University of Krakow, Faculty of Computer Science, Electronics and Communication, Kraków, Poland
[5] AGH University of Krakow, Faculty of Mechanical Engineering and Robotics, Kraków, Poland
[6] AGH University of Krakow, Faculty of Space Technologies, Kraków, Poland

its energy yield.

At the current stage, several solar wing samples with embedded PV cells have been manufactured (Fig. 1). The first sample consisted of one layer of 24 g/m² and two layers of 160 g/m² glass fabric impregnated with resin, together with a Herex foam layer insulating the cell from the 80 g/m² carbon fiber. No protective layer was applied to the cell surface before lamination, resulting in partial coverage of the cell with resin. Although the cell was effectively insulated from the carbon fiber, the large amount of glass fabric significantly increased the weight of the wing. The second sample was manufactured using two layers of 24 g/m² and one layer of 80 g/m² glass fabric placed beneath the carbon fiber laminate. The cell surface was waxed before placement in the mold to prevent resin adhesion.



Figure 1. Comparative tests of solar wing samples with in-mold embedded PV cells.

Compared with cells encapsulated only in thermal lamination film using the process described in [1], efficiency losses of approximately 2.5 and 6 percentage points were observed for the first and second samples, respectively. The loss in the first sample was most likely caused by microcracks formed before lamination and by resin covering the cell surface. The considerably larger loss in the second sample was presumably caused by shunt paths formed by carbon fibers penetrating the thin glass fabric layer and contacting the cell. To verify this hypothesis, further samples are being tested with fewer glass fabric layers and with carbon fiber placed directly on the cell.

[1] R. Łopusiewicz, N. Książek, Challenges of integrating photovoltaic cells onto the wings of an unmanned solar-powered aircraft, in: Proceedings of the 34th Congress of the International Council of the Aeronautical Sciences (ICAS 2024), Florence, Italy, 2024, pp. 1–10. https://www.icas.org/icas_archive/icas2024/data/papers/icas2024_1132_paper.pdf.

[2] A. Aimasso, M.D.L. Dalla Vedova, C.M. Bruggi, A. Borgia, A. Facci, G. Ferrero, V. Ingrosso, B. Ravenna, S. Regondi, The integration of solar panels onto a carbon fiber structure for a solar-powered UAS, Eng. Proc. 90 (2025) 57. https://doi.org/10.3390/engproc2025090057.[1] AGH University of Krakow, Faculty of Energy and Fuels, AGH Solar Plane Student Research Group, Kraków, Poland

This work was carried out as part of the research conducted by the AGH Solar Plane Student Research Group and was funded from the state budget through a grant awarded by the Minister of Science and Higher Education under the programme "Student Scientific Circles Create Innovations" (project No. SKN/SP/658367/2026).

EFE2026 ENERGY FUELS ENVIRONMENT
INTERNATIONAL CONFERENCE
17-20 NOVEMBER 2026, KRAKÓW, POLAND

Contribution of Combustion to Ambient Particles in Different Parts of the World

Andre Prevot[1]

Keywords: particulate matter, emissions, combustion

ABSTRACT

In the last decade we have seen changes in particulate matter concentrations in many places around the world. Especially in China the reduction in pollution levels were very strong by reducing emissions from cars but especially by reducing uncontrolled residential coal combustion. In India, especially in northern India, concentrations are often the highest in the world and comparably little reduction has been observed so far. In Europe, concentrations have been decreasing a lot, However the concentrations in Eastern and Southeastern Europe are still rather polluted. Especially in the Balkans, concentrations are exceptionally high. The reasons will be discussed in detail. An important observation is that the contribution of secondary particulate matter, so not directly emitted particles but formed in the atmosphere are becoming relatively more important with the reduction of emissions. Ill-controlled solid fuel combustion is one the major sources world-wide, also in Africa where cities and population will grow substantially.

[1] Center for Energy and Environmental Sciences, Paul Scherrer Institute, Switzerland, andre.prevot@psi.ch

EFE2026 ENERGY FUELS ENVIRONMENT
INTERNATIONAL CONFERENCE
17-20 NOVEMBER 2026, KRAKÓW, POLAND

Experimental and Numerical Investigation of Micro-Wind Turbine Performance under Urban Airflow Conditions

Krzysztof Sornek[1,*], Flaviu Mihai Frigura-Iliasa[2], Maksymilian Homa[1], Zuzanna Topolska[1]

Keywords: renewable energy; urban wind energy; micro-wind turbine; building-integrated wind turbines

ABSTRACT

The increasing integration of renewable energy sources into buildings and urban energy systems creates growing interest in micro- and small-scale wind generation as a complementary technology to photovoltaics. However, applying wind turbines in cities remains challenging because airflow around buildings is highly non-uniform and strongly affected by roof edges, façades, neighboring structures, and other obstacles. These interactions may cause local flow acceleration, separation, recirculation, wake formation, and increased turbulence. Consequently, wind conditions at a turbine installed on or near a building can vary significantly across the rotor-swept area and strongly influence its operational performance.

This study aimed to investigate the influence of selected urban airflow phenomena on the performance of a micro-scale wind turbine and to identify conditions that may reduce or enhance its energy-generation potential. The analysis combined experimental measurements under controlled disturbed-flow conditions with numerical simulations conducted in SimScale.

The experimental results demonstrated that micro-wind turbine performance is highly sensitive not only to the overall wind velocity but also to the spatial distribution of airflow across the rotor plane. Relatively small disturbances near the rotor's lateral edges resulted in limited power losses, generally below approximately 7%. In contrast, disturbances affecting the lower-central and central regions of the rotor had a much stronger influence on turbine performance. Depending on the extent and location of the disturbed region, rotational speed and generated power dropped substantially, with power losses exceeding 80% under the most unfavorable conditions.

Numerical simulations were used to investigate airflow phenomena at the building scale. The analysis considered both airflow around a single building and wind acceleration between two parallel buildings. In the first case, a strongly disturbed flow region was identified immediately above the roof, with wind velocity increasing with height above the roof surface, confirming the importance of turbine installation height near roof edges. In the second case, pronounced airflow acceleration was observed within the passage between buildings, with the maximum-to-inlet velocity ratio increasing from approximately 1.57 for a 20 m gap to 1.86 for a 10 m gap. These results indicate that urban geometry can either deteriorate local wind conditions or create zones of enhanced wind-energy potential.

The combined experimental and numerical results show that urban structures should not be considered solely as obstacles that reduce the available wind resource. Depending

[1] AGH University of Krakow, Faculty of Energy and Fuels, Department of Sustainable Energy Development, * ksornek@agh.edu.pl
[2] Politehnica University of Timisoara, Faculty of Electrical and Power Engineering, Power Systems Department, Timisoara, Romania

on their geometry and on turbine location, buildings may either deteriorate turbine performance through turbulence and asymmetric inflow or create local regions of accelerated airflow that can enhance energy-generation potential. Therefore, assessments based only on average urban wind velocity are insufficient for selecting suitable micro-wind turbine locations. Local airflow distribution, turbine height above roof level, position relative to building edges, and interactions between neighboring buildings should also be considered. The presented approach provides a basis for developing practical guidelines for placing and integrating micro-wind turbines in urban environments.

Acknowledgment: This work was carried out under Subvention no. 501.00-210000-10000 from the Faculty of Energy, AGH University of Krakow. The research project was supported by the „Excellence initiative – research university" program for the AGH University of Krakow (grant no. 18125).

Co-creation between Local Authorities and Grassroots Initiatives in Sustainable Transitions: Evidence from Three Polish Case Studies

Aleksandra Komorowska[1,*], Wojciech Kowalik[1], Wit Hubert[1], Monika Pepłowska[1], Dominik Kryzia[1], Lidia Gawlik[1]

Keywords: co-creation, sustainable transition, political participation, grassroots initiatives, local governance

ABSTRACT

1. INTRODUCTION

Citizen participation is increasingly recognised as a factor that determines both the pace and the direction of sustainable transitions. Depending on its form, it may accelerate the deployment of low-carbon solutions and secure long-term public support for green policies, or it may become a source of resistance to change. Transition research has traditionally focused on top-down governance, whereas collaborative practices linking civic actors and public authorities remain less explored. Political participation can take latent forms (involvement, civic engagement) and manifest forms (formal political participation, activism) [1], each of which may interact differently with local policy-making.

The main aim of this study was to identify the conditions under which co-creation between local authorities and collective grassroots initiatives supports the sustainable transition in Poland. The analysis covers three cases: the Krakow Smog Alert (KSA), a citizen-led movement against air pollution; the Clean Transport Zone (CTZ) in Krakow; and the Przylesie Housing Cooperative (PHC), a housing community engaged in the local energy transition. The study contributes to the literature by showing how institutional, geographical and socio-political factors shape the effectiveness and scope of collaborative practices.

2. MATERIALS AND METHODS

The study was carried out within the Horizon Europe project CO-SUSTAIN [2], which examines 18 historic examples of political participation in six European countries, classified according to the four forms of participation distinguished in [1]. The Polish cases were analysed using a combination of qualitative and systemic methods. The empirical material was collected through in-depth interviews (IDIs) and textual analysis. The data were then structured with Social Network Analysis, system mapping and the Multi-Level Perspective [3], which made it possible to trace how local initiatives interact with wider governance structures. Finally, the three cases were compared in terms of their origin and drivers, governance and actors, outcomes, tensions and key lessons.

3. RESULTS AND DISCUSSION

The three cases represent different forms of political participation and different modes of co-creation. KSA emerged as a grassroots response to severe smog and public health concerns [4]. By mobilising residents, scientists and the media, and by drawing on scientific evidence in the context of EU air quality requirements, the movement exerted pressure on local and regional authorities and contributed to the ban on solid fuel combustion in Krakow, adopted by the Małopolska Regional Assembly in 2016 and in force since September 2019 [4, 5]. Its long-term impact, however, depends on continuous engagement and carries a risk of activism fatigue.

The CTZ was initiated by the municipality within the framework of the 2018 Act on

[1] Mineral and Energy Economy Research Institute of the Polish Academy of Sciences, ul. Wybickiego 7A, 31-261 Kraków, Poland, * komorowska@min-pan.krakow.pl

Electromobility and Alternative Fuels [6, 7]. Krakow was the first Polish city to launch a pilot zone (Kazimierz district, December 2018); as the original legal framework admitted only a limited range of vehicles, the scheme was perceived as socially unfair and withdrawn after protests [7]. Subsequent revisions broadened the criteria to Euro emission standards and introduced phased implementation; the city-wide zone has been in force since January 2026 [7]. This shows that institutional design can either limit or expand the legitimacy of a policy.

PHC was driven by neglected infrastructure, high heating costs and strong leadership within the cooperative. With support from the Voivodeship Fund for Environmental Protection, it carried out deep thermal modernisation, replaced coal-fired heating with gas and installed photovoltaic panels [8], becoming recognised as a model of housing transformation. At the same time, divisions between older and newer residents, debt concerns and a heavy reliance on the leadership have led to recent stagnation.

Across the cases, institutional factors (legal frameworks, access to funding) determined whether citizen-driven initiatives could be translated into policy; geographical factors, such as Krakow's location in a valley prone to pollution accumulation, shaped the urgency of the problems; and socio-political dynamics influenced legitimacy, trust and inclusiveness.

4. CONCLUSION

Co-creation between civic actors and public authorities in Poland takes diverse forms, ranging from bottom-up activism to municipality-led regulation and community co-ownership. The effectiveness and scope of these practices depend not only on their internal organisation, but also on the interplay of institutional, geographical and socio-political conditions. Trust-building, long-term engagement, phased implementation and inclusive governance emerge as key enablers for sustaining collaborative transitions, offering lessons for other European cities and communities pursuing a just and sustainable transition.

[1] J. Ekman, E. Amnå, Political participation and civic engagement: Towards a new typology, Hum. Aff. 22 (2012) 283–300. https://doi.org/10.2478/s13374-012-0024-1.
[2] European Commission, CO-SUSTAIN – Pathways for CO-creation between local authorities and collective actions for a SUSTAINable transition, Horizon Europe, Grant Agreement No. 101132467, 2024–2026. https://doi.org/10.3030/101132467.
[3] F.W. Geels, Technological transitions as evolutionary reconfiguration processes: A multi-level perspective and a case-study, Res. Policy 31 (2002) 1257–1274. https://doi.org/10.1016/S0048-7333(02)00062-8.
[4] M. Pepłowska, L. Gawlik, W. Kowalik, From solid fuel combustion to clean urban air: Civil activism and low-carbon energy transition in Kraków, Poland, Sustainability 18 (2026) 9673. https://doi.org/10.3390/su18189673.
[5] Regional Assembly of the Małopolska Voivodeship, Resolution No. XVIII/243/16 of 15 January 2016 on the introduction of restrictions on the operation of fuel combustion installations in the Municipality of Kraków, Official Journal of the Małopolska Voivodeship (2016) item 812 (in Polish). https://edziennik.malopolska.uw.gov.pl/WDU_K/2016/812/akt.pdf.
[6] Republic of Poland, Act of 11 January 2018 on Electromobility and Alternative Fuels, Journal of Laws of the Republic of Poland (2018) item 317 (in Polish). https://eli.gov.pl/eli/DU/2018/317/ogl.
[7] W. Hubert, D. Kryzia, L. Gawlik, Formal political participation and urban climate governance: The case of the Clean Transport Zone in Kraków, Sustainability 18 (2026) 10750. https://doi.org/10.3390/su182110750.
[8] M. Pepłowska, Energy transition in multi-family residential buildings: A multi-level perspective on photovoltaic integration and deep energy retrofit, in: Proceedings of the 2026 6th International Conference on Electrical, Computer and Energy Technologies (ICECET), Rome, Italy, 2026, pp. 1–6. https://doi.org/10.1109/ICECET65726.2026.11632680.

This research was carried out within the project CO-SUSTAIN – Pathways for CO-creation between local authorities and collective actions for a SUSTAINable transition, funded by the European Union under the Horizon Europe programme (grant agreement No. 101132467).

EFE2026 ENERGY FUELS ENVIRONMENT
INTERNATIONAL CONFERENCE
17-20 NOVEMBER 2026, KRAKÓW, POLAND

Numerical and Experimental Studies on the Limitations of Cold Starting an Anion-Exchange Membrane Electrolyser and the Optimization of Green Hydrogen Production in an Off-Grid System

Andrzej Raźniak[1,*], Łukasz Mazur[1], Magdalena Dudek [1]

Keywords: green hydrogen; AEM electrolyser; energy storage; dynamic operation

ABSTRACT

This paper presents numerical and experimental studies on optimising green hydrogen production in a modular, off-grid system comprising a photovoltaic (PV) installation, an electrical energy storage unit, and an anion exchange membrane (AEM) electrolyser. Variability in the power and energy profiles from both the PV installation and the energy storage system frequently leads to interruptions in hydrogen production, resulting in a high and undesirable number of electrolyser start–stop cycles. Frequent start–stop operations, and the associated increase in the number of so-called "cold starts", have a highly detrimental effect on the durability and operational lifespan of the electrolyser.

The objective of this paper was to develop a mathematical model, conduct numerical simulations, and perform experimental studies to establish conditions enabling "continuous" operation of the device. A second aim was to determine the operational limitations of a commercial AEM electrolyser and to evaluate the potential for improving the efficiency of a PV–electrolyser system through rational management of start-up procedures and the integration of energy storage. Based on the experimental data collected, the study analysed the electrolyser's start-up and shutdown cycles, the rationale for preheating the electrolyte, and the internal energy consumption profile associated with the start-up phase. The simulation data were incorporated into an annual system performance model, based on a minute-by-minute production profile from a PV installation. A comparison was made between an operating scenario without energy storage and one utilising an electrochemical battery as an energy buffer. Furthermore, the impact of AEM electrolyser stack degradation on hydrogen production variability was assessed, and a simplified techno-economic and emissions analysis was conducted, including hydrogen drying, compression, and storage.

The research shows that limiting the number of cold starts is crucial for the energy efficiency of an off-grid system. Cold starts lasted an average of approximately 63.5 minutes, whereas warm starts took 26 minutes. Using the "preheat" function required only 0.347 kWh of energy and reduced the start-up time to approximately 49 minutes. The energy storage system increased annual hydrogen production from 10.87 kg to 22.79 kg – an increase of approximately 109.6%—primarily by bridging short-term drops in PV power output. Accounting for stack degradation reduced cumulative hydrogen production by approximately 3.8%. The calculated Levelised Cost of Hydrogen (LCOH) was 238.0 PLN/kg H_2 for 300-bar storage and 161.9 PLN/kg H_2 for 35-bar storage. The results indicate that in small-scale PV–AEM systems it is particularly important to minimize cold starts, buffer short interruptions in electricity generation from the PV installation, and tailor the hydrogen compression level to the end user's actual requirements.

Funding: This research was funded by the IDUB project at AGH University of Krakow, No. 501.00-210000-10000.

[1]AGH University of Krakow, Faculty of Energy and Fuels, Al. A. Mickiewicza 30, 30-059 Kraków, Poland * razniak@agh.edu.pl

EFE2026 ENERGY FUELS ENVIRONMENT
INTERNATIONAL CONFERENCE
17-20 NOVEMBER 2026, KRAKÓW, POLAND

Entropy- and Thermal-Driven Control of Local Structure in Disordered Rock Salt Cathodes

Yanxin Wang[1,*], Konrad Świerczek[1,2]

Keywords: lithium-ion battery, cathode materials, transition metals, disordered rock salts, partial order

ABSTRACT

Among the most promising novel cathode materials for Li-ion cells are lithium-excess cation-disordered oxides with a rock salt structure (DRXs). It has been documented that properly selected compositions, such as Mn- and Ti-based $Li_{1.2}Mn_{0.4}Ti_{0.4}O_2$ (LMTO), can deliver reversible capacities approaching 300 mAh g^{-1} and operate at relatively high voltage, yet their actual performance in the cells is often limited by sluggish Li^+ transport, low electrical conductivity, and other intrinsic issues [1]. A high degree of cation disorder in the crystal structure is essential to establish a percolating Li^+ network; however, the availability of the so-called 0-TM migration pathways remains statistically constrained, impeding Li migration between octahedral and tetrahedral sites [2]. Owing to their compositional flexibility, DRX materials offer opportunities to tailor local structural and electronic environments, for example, via multi-element, high-entropy doping strategies.

In this work, we investigate the role of post-annealing cooling procedures in suppressing disorder-to-order conversion during the synthesis of pristine and doped LMTO. Operando X-ray diffraction was employed to monitor structural evolution and identify relevant temperature regimes suitable for the preparation route. The measurements revealed the emergence of spinel-like diffraction features at specific temperatures, which, considering the intrinsic cation disorder of DRX materials, suggest the presence of spinel-like domains in LMTO, embedded within the rock salt framework. This is consistent with the short-range or partial cation ordering in the material. Additional room-temperature structural characterization has been performed by scanning and transmission microscopy. To further explore the discussed behavior, a multicomponent $Li_{1.2}Mn_{0.4}Ti_{0.25}Al_{0.05}Fe_{0.05}Mo_{0.05}O_2$ composition was designed to increase configurational entropy and modulate local cation arrangements.

It was found that the disorder rearrangement is eased due to the multi-metal doping modification, allowing to obtain the desired crystal structure with a flat cooling rate, which demonstrates that controlled thermal history combined with high-entropy doping provides an effective route for preparing high-performance DRX cathodes.

[1] H.-M. Hau, T. Holstun, E. Lee, B.L.D. Rinkel, T.P. Mishra, M.M. DiPrince, R.S. Mohanakrishnan, E.C. Self, K.A. Persson, B.D. McCloskey, G. Ceder, Disordered rocksalts as high-energy and earth-abundant Li-ion cathodes, Adv. Mater. 37 (2025) 2502766. https://doi.org/10.1002/adma.202502766

[2] R.J. Clément, Z. Lun, G. Ceder, Cation-disordered rocksalt transition metal oxides and oxyfluorides for high energy lithium-ion cathodes, Energy Environ. Sci. 13 (2020) 345–373. https://doi.org/10.1039/C9EE02803J

Acknowledgements: We gratefully acknowledge IDUB AGH, as this work was supported by the program "Excellence Initiative-Research University" for the AGH University of Krakow (IDUB AGH, Action 4, ID: 17195 and Action 21, ID: 17978).

[1] AGH University of Krakow, Faculty of Energy and Fuels, al. Mickiewicza 30, 30-059 Krakow, Poland,
* yxwang@agh.edu.pl
[2] AGH University of Krakow, AGH Centre of Energy, Czarnowiejska 36, 30-054 Krakow, Poland

Nb-modified $Li_{1.02}Ni_{0.905}Co_{0.043}Al_{0.052}O_2$ Cathode for High-Energy-Density Li-ion Cells: Development, Optimization, and Degradation Studies with Transformer Based Model

Boya Fu[1,*], Boyang Fu[1], Marcin Kurdziel[2], Konrad Świerczek[1,3]

Keywords: Li-ion cells, Nb-modified, Ni-rich cathodes, Transformer model

ABSTRACT

The growing demand for high-energy-density Li-ion batteries, driven by the rapid expansion of the electric vehicle market, has intensified research on Ni-rich layered oxide cathodes, particularly 9-series materials with Ni content ≥0.9. Although higher Ni content improves specific capacity, their practical application is limited by rapid capacity fading and structural instability during cycling. A major degradation mechanism is the H2–H3 phase transition at high voltages, which causes anisotropic lattice contraction, particle cracking, surface reconstruction, and accelerated side reactions. Elemental doping and surface coating are effective strategies to mitigate these issues. Among them, niobium modification has attracted attention due to its ability to stabilize the layered structure, suppress unfavourable phase transitions, and enhance interfacial stability through the formation of robust surface layers [1,2].

In this work, $Li_{1.02}Ni_{0.905}Co_{0.043}Al_{0.052}O_2$ cathode material is modified through Nb doping (0.1–1 mol%) and surface treatment using ammonium niobium oxalate (ANO). Structural, morphological, surface, and electrochemical analyses reveal that 0.5 mol% Nb provides optimal stabilization, significantly suppressing the H2–H3 transition. Meanwhile, ANO treatment removes residual lithium and forms an in situ $LiNbO_3$ surface layer. As a result, the modified cathode delivers a capacity of 178.1 mAh^{-1} with 96.4% retention after 100 cycles at 1C.

To further interpret degradation behaviour, a Transformer based model is applied to analyse the temporal evolution of discharge curves. The model accurately captures key degradation features, including plateau shifts and attenuation of H2–H3 transition signatures, consistent with experimental observations.

Overall, this work combines Nb-based material modification with Transformer[3] based data-driven analysis to better understand degradation suppression in Ni-rich cathodes and demonstrates the potential of data-driven approaches for battery performance prediction and materials optimization.

[1] G.-T. Park, B. Namkoong, S.-B. Kim, J. Liu, C.S. Yoon, Y.-K. Sun, Introducing high-valence elements into cobalt-free layered cathodes for practical lithium-ion batteries, Nat. Energy 7 (2022) 946–954. https://doi.org/10.1038/s41560-022-01106-6

[2] W. Zhang, L. Xiao, J. Zheng, Y. Zhong, B. Shi, H. Chen, H. Fu, Effect of Nb2O5 nanocoating on the thermal stability and electrochemical performance of LiNi0.6Co0.2Mn0.2O2 cathode materials for lithium ion batteries, J. Alloys Compd. 880 (2021) 160415. https://doi.org/10.1016/j.jallcom.2021.160415

[3] A. Vaswani, N. Shazeer, N. Parmar, J. Uszkoreit, L. Jones, A.N. Gomez, L. Kaiser, I. Polosukhin, Attention is all you need, Adv. Neural Inf. Process. Syst. 30 (2017) 5998–6008.

[1] AGH University of Krakow, Faculty of Energy and Fuels, al. Mickiewicza 30, 30-059 Krakow, Poland,
* boyafu@agh.edu.pl

[2] AGH University of Krakow, Faculty of Computer Science, al. Mickiewicza 30, 30-059 Krakow, Poland

[3] AGH University of Krakow, AGH Centre of Energy, Czarnowiejska 36, 30-054 Krakow, Poland

Acknowledgements: We gratefully acknowledge IDUB AGH, as this work was supported by the program "Excellence Initiative-Research University" for the AGH University of Krakow (IDUB AGH, Action 4, ID: 17202 and Action 21, ID: 17978).

Rare-Earth Engineering of Oxygen-Electrode Materials for Solid Oxide Cells

Jacek Winiarski[1*], Piotr Winiarz[1], Konrad Świerczek[2]

Keywords: Solid oxide cells, Fuel cell, Rere-earth elements, Perovskites

ABSTRACT

Solid oxide cells (SOCs) are considered one of the most promising technologies for efficient energy conversion and storage. Depending on the operating mode, they can function as Solid Oxide Fuel Cells, converting hydrogen and other fuels into electricity and heat, or as Solid Oxide Electrolysis Cells, using surplus renewable electricity to produce hydrogen and other valuable energy carriers. Their high efficiency, fuel flexibility, and potential for reversible operation make SOCs particularly attractive for integration with renewable energy systems [1]. Nevertheless, their wider implementation is still limited by several technological challenges, including insufficient long-term stability, high operating temperatures, and relatively slow oxygen reduction and oxygen evolution reactions [2]. The performance and durability of SOCs strongly depend on the properties of the materials used in their electrodes. In particular, oxygen-electrode materials must provide high catalytic activity, efficient charge and oxygen transport, suitable thermal compatibility, and stable operation under both oxidizing and reducing conditions [3]. For this reason, current research increasingly focuses on the rational design of electrode compositions and on understanding how individual chemical components influence their functional properties. The family of double perovskites with the general formula $AA'B_2O_{5+\delta}$ (A: rare-earth metals; A': alkaline earth metals, typically Ba; B: 3d metal elements, usually, with high amount of Co) represents attractive properties for oxygen electrodes in SOCs [4].

In this work, $REBa_{1-x}Sr_xCo_{2-y}Cu_yO_{5+\delta}$ (RE: Pr, Nd, Sm, Gd) perovskite oxides were investigated as potential oxygen-electrode materials, with particular emphasis on the role of rare-earth elements. The choice of the rare-earth cation can influence the crystal structure, oxygen non-stoichiometry, defect chemistry, electrical conductivity, oxygen-ion transport, and electrochemical activity of the material. Consequently, even relatively small compositional changes may significantly affect the overall performance of the electrode and its suitability for operation in reversible solid oxide cells. A combined computational and experimental approach was applied to evaluate these composition–property relationships and to support the selection of promising materials. Density Functional Theory (DFT) was used to identify general trends associated with the modification of the rare-earth sublattice; unit cell parameters, total energies, oxygen vacancy formation energies, electron localization functions and density of states. Selected materials were subsequently synthesized and characterized using structural (XRD), electrical, and electrochemical methods (EIS+DRT). The experimental results were then compared with the theoretical predictions to assess the usefulness of the proposed screening strategy.

The obtained results demonstrate that control of material composition, particularly the selection and combination of rare-earth elements, provides an effective way to tailor the functional properties of oxygen electrodes. The study highlights the importance of materials engineering in overcoming current limitations of solid oxide cell technology and shows that the integration of computational prediction with laboratory verification can

[1] AGH University of Krakow, Faculty of Energy and Fuels, al. Mickiewicza 30, 30-059 Krakow, Poland, * jwiniarski@agh.edu.pl
[2] AGH University of Krakow, AGH Centre of Energy, Czarnowiejska 36, 30-054 Krakow, Poland

support the development of more efficient, durable, and versatile SOC systems.

[1] S. Khojaste Effatpanah, H.R. Rahbari, M.H. Ahmadi, A. Farzaneh, Green hydrogen production and utilization in a novel SOFC/GT-based zero-carbon cogeneration system: A thermodynamic evaluation, Renew. Energy 219 (2023) 119493. https://doi.org/10.1016/j.renene.2023.119493
[2] M. Naeini, J.S. Cotton, T.A. Adams II, Economically optimal sizing and operation strategy for solid oxide fuel cells to effectively manage long-term degradation, Ind. Eng. Chem. Res. 60 (2021) 17128–17142. https://doi.org/10.1021/acs.iecr.1c03146
[3] S. Akkurt, C. Sindiraç, T. Özmen Egesoy, E. Erğen, A review on new cobalt-free cathode materials for reversible solid oxide fuel cells, J. Met. Mater. Miner. 33 (2023) 1654. https://doi.org/10.55713/jmmm.v33i3.1654
[4] V. Dhongde, M. Velpandian, S. Basu, Exploring the impact of structural modification of double perovskite composite cathode material on oxygen reduction reaction in intermediate temperature solid oxide fuel cell, Ionics 30 (2024) 8175–8190. https://doi.org/10.1007/s11581-024-05847-0

Acknowledgements: We gratefully acknowledge IDUB AGH, as this work was supported by the program "Excellence Initiative-Research University" for the AGH University of Krakow (IDUB AGH, Action 4, ID: 16906 and Action 21, ID: 17978).

EFE2026 ENERGY FUELS ENVIRONMENT
INTERNATIONAL CONFERENCE
17-20 NOVEMBER 2026, KRAKÓW, POLAND

Temporal Spectral Analysis in Electrochemistry

Aleksander Piasecki[1,*], Jacek Kowalczyk[1], Maciej Siekierski[1]

Keywords: Electrochemistry, time-frequency analysis, Fourier transform, wavelet analysis, non-stationary signals

ABSTRACT

Electrochemical experiments are commonly presented as current–time, potential–time or current–potential curves. These views show the overall response but may conceal periodic components, characteristic timescales and fluctuations superimposed on slower trends. Frequency-domain analysis provides another perspective by describing how signal variability is distributed across frequencies. This is useful when electrode surfaces, transport conditions or reaction environments change during a measurement. Such information may be present without being apparent from a conventional plot.

The Fourier transform is a fundamental tool for examining frequency content. For a stable periodic oscillation, its spectrum can reveal a well-defined frequency even against a drifting baseline. Applied to electrochemical recordings, Fourier analysis can help characterize oscillatory current or potential responses and investigate fluctuations associated, for example, with corrosion, electrodeposition or gas evolution. Although applicable to non-stationary data, a conventional Fourier spectrum combines information from the entire analysed interval. Oscillations occurring at different times can appear alongside each other as if simultaneous, while brief events or changing frequencies may produce broadened, ambiguous features. Moreover, frequency peaks alone do not identify their physicochemical origin. Spectral analysis of a spontaneous current or potential trace should also be distinguished from electrochemical impedance spectroscopy, which requires an appropriately defined excitation and response.

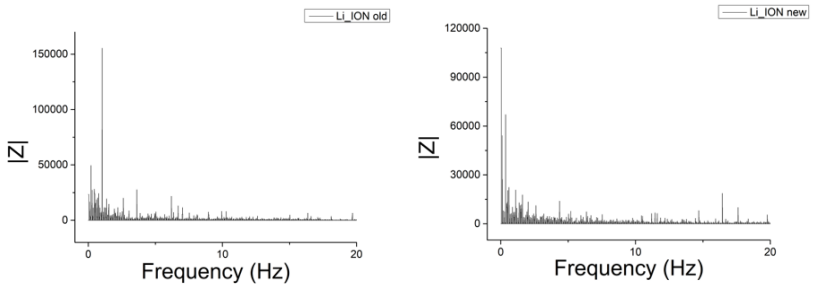


Fig. 1. Demonstration of the difference in frequency domain response to the same stimulus delivered to two 18650 NMC cells of various ageing levels.

A natural extension is the short-time Fourier transform (STFT), which applies Fourier analysis to successive, partially overlapping segments of a signal. The resulting spectrogram displays frequency content as a function of time, making it possible to locate oscillatory episodes, follow shifts in dominant frequency and distinguish transient events from persistent behaviour. In electrochemistry, they may help examine evolving current oscillations, potential fluctuations during galvanostatic operation or intermittent gas-evolution events. Their interpretation remains tied to the timescale of the measurement and to whether the signal can be treated as approximately stationary within each window.

STFT does not, however, eliminate the limitations of spectral analysis. A short analysis window improves temporal localization but reduces frequency resolution, whereas a longer window has the opposite effect. One window length may be unsuitable for signals containing both rapid transients and slow oscillations. Window shape, spectral leakage,

[1] Faculty of Chemistry, Warsaw University of Technology, Noakowskiego 3 st, Warsaw

sampling rate, noise and baseline treatment can further affect the appearance of a spectrogram. Complementary methods address different difficulties. Wavelet-based representations provide scale-dependent time localization, time-varying autoregressive models can estimate evolving spectral features under explicit modelling assumptions, and change-point detection can identify transitions without forcing every variation into a frequency description. Each method introduces its own choices and limitations rather than providing a universally reliable answer.

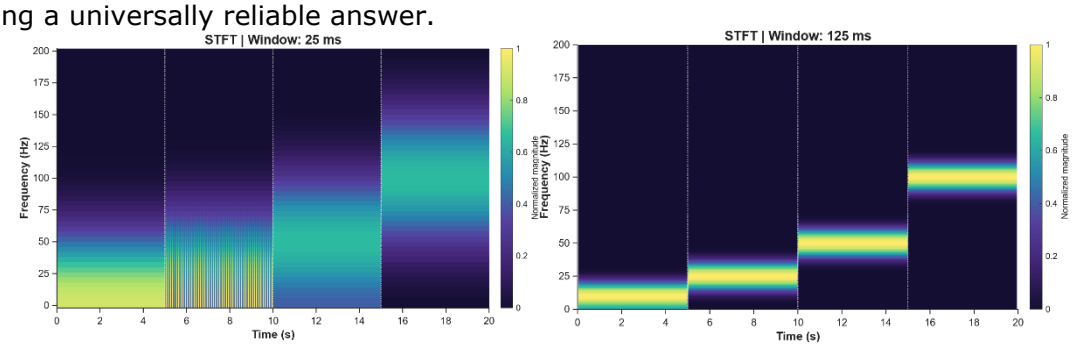


Fig 2. Demonstration of the effect of window length on frequency resolution in an artificial "stair" signal in STFT.

The poster will compare the same signals as time traces, Fourier spectra and time-frequency representations. Examples will show which features each approach reveals or obscures. Electrochemically relevant scenarios will be used to connect these examples with the interpretation of measured current and potential signals. Particular attention will be given to the differences between detecting a frequency, determining when it occurs and assigning physical meaning to it, as well as the practical consequences of choosing analysis methods.

The central message is that electrochemical recordings often contain more information than is immediately visible in their familiar graphical representations. Extracting requires more than applying increasingly sophisticated algorithms: the method must match the physical character of the signal, the experimental conditions and the question being asked. A convincing spectral feature is not automatically evidence of a particular mechanism, just as an uninformative spectrum does not imply that the underlying data lack structure. The poster encourages critical selection of complementary tools for interpreting time-dependent electrochemical behaviour.

Acknowledgements:
This work was supported by the National Centre for Research and Development (NCBR) under Grant WPC3/2022/29/IMPRESSION/2025. This work has been additionally supported by the Faculty of Chemistry, Warsaw University of Technology.

Author Index

Alphabetical index of contributors. Select a page number to open the corresponding abstract.

A

Abushaikha, Ahmad 185
Acar, Canan 185
Adamczyk, Bartosz 203
Adamski, Andrzej 101, 103, 110, 113
Alijev, Jafar 263
AlShafi, Manal 185
Amir, Laiba 53, 106
Andruszkiewicz, Artur 85
Andrzejczyk, Rafał 187
Antoniadou, Despoina 112
Antonik, Oskar 239
Asif, Muhammad 228
Ayalew, Belayneh 187

B

Bajan, Bartłomiej 35
Bała, Anna 128
Bałys, Aleksandra 43
Bania, Katarzyna 252
Barczyk, Alicja 253
Benalcazar, Pablo 112, 239
Berliński, Marek 125
Bernauer, Milan 76
Biały, Michał 157
Bicer, Yusuf 185
Bistrickaitė, Rėda 201
Bobowska, Aleksandra 74, 75
Bordulenko, Mariia 68, 80
Bornes, Carlos 83
Borowski, Marek 123
Broda, Krzysztof 259
Buczkowska-Fertała, Agnieszka 157
Buczyński, Rafał 33
Budziak, Andrzej 104
Bueno-Ferrer, Juan 64
Bueno-Lopez, Agustin 64
Bukowiec, Patrycja 132
Buonomo, Bernardo 164
Buonomo, Pier Luca Maria 254
Burmistrz, Piotr 136
Bury, Kacper 199
Bury, Marcelina 126
Bury, Tomasz 199

C

Cebo, Jakub 214
Chen, Ming 119, 152
Chen, Yan 82
Chen, Zihao 55
Cheng, Liang 88
Chmielniak, Tomasz 250
Cholewa-Kowalska, Katarzyna 110
Chwała, Aleksandra 216, 230
Cierpińska, Małgorzata 108

Cieślar, Paweł 33
Cwynar, Karolina 143, 148, 208, 243
Czajkowski, Ignacy 214
Czaplicka, Marianna 171
Czekańska, Julia 180
Czerski, Grzegorz 79, 160
Czosnek, Cezary 136

D

Datka, Jerzy 182
Davo-Quinonero, Arantxa 64
Dawid, Sacha 233
de Zea Bermudez, Verónica 66, 86
Diapouli, Evangelia 154
Dobrzyńska-Inger, Agnieszka 170
Domańska, Joanna 263
Du, Zhihong 41
Dudek, Magdalena 130, 203, 271
Dulęba, Natalia 49
Dworczyk, Jakub 227
Dziadek, Michał 110
Dzierwa, Piotr 245, 247
Dzwonkowski, Ariel 85

E

Ekes, Jakub 214, 263

F

Faraji, Mehrdad 119
Fernine, Yasmine 86
Filipek, Wiktor 259
Freindl, Kinga 80
Frigura-Iliasa, Flaviu Mihai 176, 267
Frigura-Iliasa, Mihaela 176

G

Fu, Boya 273
Fu, Boyang 273
Gajda, Filip 264
Gałaś, Natalia 180
Garnek, Patryk 224
Gawlik, Lidia 269
Gawnikowki, Sylwester 101
Gilson, Jean-Pierre 57
Gogacz, Michał 47, 155
Golijanek-Jędrzejczyk, Anna 85
Góra-Marek, Kinga 57, 76, 83, 92, 94
Górecki, Jerzy 118, 136
Grajciar, Lukáš 83
Grela, Jakub 178, 187
Grudziński, Leszek 172
Gryboś, Joanna 80, 101
Grzęda, Karolina 170
Grzelczyk, Przemysław 91
Grzesik, Katarzyna 150
Grzybek, Gabriela 68, 72, 80, 110
Grzywacz, Przemysław 124
Guillen-Bas, Esteban 64
Guo, Youmin 62, 97
Guziak, Przemysław 263

H

Hansen, Emil Riis 119
Haruna, Uzeru 78
Hasal, Małgorzata 197
Hasiak, Mariusz 157
Higler, Arnoud P. 193, 194
Homa, Maksymilian 164, 267
Hu, Haibo 90, 177
Hubert, Wit 269
Hudek-Pietras, Aleksandra 168

I

Inger, Marek 170
Iwańczyk, Kamil 263

J

Jafarov, Erkin 123
Jakhar, Rakshit 145, 154
Jamrozik, Norbert 214
Jarosz, Anna 184
Jaszczur, Marek 85, 98, 123, 134, 137
Jeżewska, Julia 174
Jodłowski, Grzegorz S. 27
Júnior, Tomé 86

K

Kaczmarski, Karol 247
Kalka, Maciej 112
Kapelewska, Justyna 162
Kapusta, Katarzyna 39, 124
Karweta, Julia 104
Kasprzyk-Hordern, Barbara 192
Kaucký, Dalibor 76, 83
Kaufmann, Damian 47
Kępa, Ignacy 264
Khan, Atif 51
Khosravi, Soheil 119
Klimkowicz, Alicja 49
Kocot, Michał 171
Kogut, Krzysztof 39
Kokuryo, Shinya 94
Kolarz, Karolina 124, 136, 253
Komorowska, Aleksandra 43, 269
Kondratowicz, Tomasz 255
Konior, Jakub 264
Kordek, Agata 57, 92, 94
Korecki, Józef 80
Kornas, Agnieszka 76, 83
Korzeniewska, Anna 116, 118
Korzeniowski, Łukasz 70
Kotarba, Andrzej 68, 72, 80
Kotowska, Urszula 162
Kowal, Bartłomiej 168
Kowalczyk, Jacek 216, 222, 230, 237, 277
Kowalik, Wojciech 269
Krasodomski, Wojciech 204
Krempa, Kacper 264
Król, Katarzyna 253
Kryzia, Dominik 269
Ksepko, Ewelina 74, 75, 78

Książek, Dominika 37
Kulawik, Maciej 263
Kulesza, Paweł 230, 237
Kulka, Gabriela 212
Kumar, Kanak 29
Kurdziel, Marcin 273
Kurek, Jakub 263
Kusz, Zuzanna 141

L, Ł

Lach, Jakub 47
Lakiss, Louwanda 57
Wang, Yanxin 272
Winiarski, Jacek 275
Łamacz, Agata 103
Łaszcz, Amadeusz 157
Latoń, Dominik 178
Legutko, Piotr 110
Lenar, Szymon 180
Lewandowska, Anita Urszula 206
Lewandowski, Marek 168
Lewiński, Janusz 237
Lhotka, Miloslav 76
Ling, Yihan 45, 47
Liu, Wenzhong 168
López, Iván Martínez 64, 72, 80
Łopusiewicz, Marta 264
Lozano-Castello, Dolores 64
Lubańska, Alicja 174
Luo, Linghong 88

M

Ma, Zilin 82
Machaj, Krystian 174
Maciejowski, Tomasz 263
Magdziarz, Aneta 70, 168, 218
Magiera, Anna 218
Makowska, Dorota 124, 136, 253
Mankowski, Kacper 35
Marçal, Bernardo Miguel Grilo 59
Marcinkowski, Mateusz 132
Marczak, Patryk 85, 137
Marko, Michal 113
Martin-Garcia, Iris 64
Marzec, Mateusz 110
Materowski, Filip 264
Mazur, Łukasz 271
Mertas, Bartosz 172
Michałek, Aneta 172
Michalik, Joanna 263
Michalski, Kamil 236
Mika, Łukasz 195
Miodoński, Mikołaj 263
Miroń, Piotr 263
Misiurek, Kamil 190
Mlekodaj, Kinga 76, 83
Mochnaczewski, Michał 113
Mokrzycki, Jakub 37, 121, 261
Molenda, Janina 236
Moskalewicz, Katarzyna 39

Moszczak, Marcin 240
Motak, Monika 32, 103, 121, 147, 210, 252, 255, 258
Moździerz, Marcin 49
Mrówczyńska-Kamińska, Aldona 35, 91
Mrowiec, Andrzej 85
Mroziński, Adam 187
Muzyka, Roksana 124, 141

N

Nakashima, Rafael Nogueira 119
Nardini, Sergio 164
Nawrocki, Jan 101
Niemczyk-Sobieszek, Anna 174
Niesler, Marian 171
Nishiyama, Norikazu 94
Niu, Helin 96
Nowak, Anna 139, 232
Nowak, Wojciech 250
Nuckowski, Łukasz 206

O

O'Hare, Dermot 255
Oettingen, Mikołaj 128, 131
Olapade, Olushola 98, 134
Olkuski, Tadeusz 190, 263
Oluwalana, Oluwapelumi John 150
Orzechowska-Zięba, Agnieszka 30, 139, 206, 212
Ossowska-Górzyńska, Aleksandra 237
Ostapko, Jakub 101
Oszajca, Marcin 80
Otero, Julia 233

P

Pac, Agnieszka 148
Panicker, Akhil 119
Papagiannis, Stefanos 154
Pepłowska, Monika 269
Peret, Patryk 247
Perez-Dieste, Virginia 64
Perzyński, Konrad 168
Piasecki, Aleksander 216, 230, 277
Piech, Monika 203
Piechota, Piotr 85
Piechówka, Tomasz 32, 147
Piekarski, Wiktor 216, 222, 230
Pietrzyk, Stanisław 259
Pietrzykowski, Michał 264
Pilarski, Stanisław 214
Pinheiro, Maria Margarida Faustino 59
Piofczyk, Maciej 180
Piskorz, Witold 68
Pizoń, Alekander 216
Pizoń, Aleksander 225, 230
Plata, Piotr 160
Płatek, Mateusz 195
Płatek, Witold 195
Pluta, Marcin 166, 220
Podlasek, Szymon 224
Podobiński, Jerzy 182
Polczyk, Tomasz 101, 103

Ponikowski, Michał 33
Prevot, Andre 266
Proszowska, Allison 103
Prus-Frączek, Zuzanna 143, 148, 208, 243
Przedwojska, Patrycja 110
Ptak, Stefan 115
Pyssa, Justyna 143, 148, 206, 208, 212, 243

Q

Quddusi, Abul Hassan 70
Queijo, Ana 86
Quinn, Luke 233

R

Rączka, Katarzyna 121
Raczyński, Maciej 166, 220, 257
Radu, Cristian 47
Rafi, Majid 228
Razak, Kamal 235
Raźniak, Andrzej 130, 271
Reddy, B. Rajasekhar 29
Rego, Rosa 86
Rejdak, Michał 172
Ricciu, Roberto 254
Rodź, Anna 172
Rogala, Oliwia 57, 83, 94
Rokosz, Adam 47
Rosikoń, Izabella 264
Rybiński, Michał 245
Rybowicz, Paweł 103, 113
Ryfa, Arkadiusz 171
Ryś, Anna 154
Rzepka, Mikołaj 224
Rzepka, Przemysław 76, 83
Rzeszut, Patrycja 166, 257
Rzeźnicka, Izabela 197

S, Ś, Š

Sacha, Kacper 180
Sajdak, Marcin 141
Salhab, Hala 164
Samek, Lucyna 145, 154
Samojeden, Bogdan 26, 103, 170, 252, 258
Santarelli, Massimo 127
Ściążko, Marek 250
Ścigaj, Mateusz 240
Seman, Marta 253
Shao, Mengen 62, 97
Shu, Yuying 57
Siekierski, Maciej 216, 222, 225, 230, 237, 277
Skowrońska, Natalia 253
Skrzypiec, Maksymilian 104
Slobodkina, Lyudmila 141
Sobalska, Julia 76, 83
Sobek, Szymon 141
Sochacka-Tatara, Elżbieta 148
Song, Wei 96
Soprych, Piotr 79, 253
Sornek, Krzysztof 164, 176, 180, 264, 267
Šoukal, František 113

Sousa, Duarte M. 59
Śpiewak, Katarzyna 79, 160
Spiridis, Nika 80
Stańczyk, Jarema 79
Stefanini, Francesca 233
Stępak, Weronika 118
Stępień, Leszek 250
Styszko, Katarzyna 139, 143, 145, 148, 206, 208, 212, 232, 243
Sulima, Olaf 263
Sultan, Amir 53, 106
Suwała, Wojciech 220
Świerczek, Konrad 41, 147, 152, 272, 273, 275
Szarłowicz, Katarzyna 128
Szczurowski, Jakub 197
Szramowiat-Sala, Katarzyna 116, 118
Sztekler, Karol 195
Sztybel, Katarzyna 136
Szumowski, Stanisław 174
Szurlej, Adam 203
Szwamel, Michał 253
Szymaszek, Michał 32, 210
Szymaszek-Wawryca, Agnieszka 32, 37, 147, 210

T

Tabor, Edyta 76, 83, 94
Taler, Dawid 46, 247
Taler, Jan 46, 132, 247
Tarach, Karolina 83, 92
Tarach, Karolina A. 57, 94
Tauris, Emil Frederik 119
Telešius, Povilas 201
Teymurov, Eyvaz 131
Tokarski, Mieszko 33, 227
Topolska, Zuzanna 267
Tora, Barbara 259
Trojan, Marcin 247
Türkyılmaz, Serhat 172
Tynkevych, Olena 76, 83

U

Uchmanowicz, Dominika 139, 208, 212
Ulitska, Olena 85
Ünal, Erdal 172

V

Vaičiukynienė, Danutė 201
Valderrama, Cesar 233
Valderrama, César 257
van Delden, Juliette A. 193
Vassilatou, Vassiliki 154
Vatau, Doru 176
Vidal, Mathieu 76
Vinardell, Sergi 233
Vinikaitė-Bačinskienė, Gabija 201
Vitushynska, Yana 103
Vogt, Elżbieta 30, 212
Vratolis, Stergios 154

W

Wądołkowski, Kacper 214
Wądrzyk, Mariusz 70, 168

Walczyk, Anna 92
Wang, Hao 88
Wang, Leying 88
Wang, Tong 41
Wardecki, Dariusz 76, 83
Wasiela, Stefania 113
Węgrzyn, Laura 143, 148, 208, 212, 243
Werle, Sebastian 141
Wieczorek, Władysław 237
Wierońska-Wiśniewska, Faustyna 160
Wieteska, Szymon 98, 134
Winiarz, Piotr 152, 275
Wójcik, Marta 27
Wójcik, Radosław 218
Wojtasik, Michał 204
Wojtaszek-Kalaitzidi, Małgorzata 172
Wójtowicz, Andrzej 68, 72, 80
Wolak, Eliza 30, 139, 206, 212
Wolczko, Marta 236
Woźny, Mikołaj 227
Wu, Chunfei 70
Wyrwa, Artur 51, 166, 220, 257

X

Xu, Xu 88

Y

Yi, Ziheng 88

Z, Ż

Zafar, Rameez 53, 106
Żak, Grażyna 204
Zasada, Filip 68
Zawadziński, Kamil 94
Zawiślak, Patrycja 162
Zbroja, Katarzyna 85
Zdziebło, Sławomir 199
Zhang, Rui 78
Zhao, Hailei 41
Zheng, Kun 47, 53, 55, 88, 99, 106, 152, 155
Zhu, Panpan 90
Zieliński, Michał 180
Zieńkowska, Wiktoria 237
Zimowska, Małgorzata 182
Zubień, Patrycja 190
Zych, Dariusz 33
Zych, Marcin 85, 137
Zyśk, Janusz 166, 220

Keyword Index

Alphabetical index of keywords used in the abstracts. Select a page number to open the corresponding contribution.

3

3D printing 216

A

A-site deficiency 53, 155
ABS 216
absorption 197
absorption heat pump 195
Accelerator-Driven System (ADS) 131
accident-tolerant fuel 199
acetic acid 83
activated carbon 212
activated sludge 143
activation 27
adsorption 212, 261
advanced materials 119
advanced oxidation processes 162
AEM electrolyser 271
agribusiness 35
air pollutant emissions 116
alginate biopolymer 86
alkali-activated slag 201
Alkali promotion 80
amine-based CCUS 197
ammonia 113
anaerobic digestion 39
Anomalous diffusion element 222
anomaly detection 190
anthropogenic pressure 206
ascorbic acid 139
Aspen Plus 70
atmospheric emissions 118
attemperator 46
Auction-Based Trading 239

B

balancing market 245
balancing services 245
BAT 116, 118
Battery Energy Storage System 178
battery housing 150
battery storage 193
bentonite 32
bio-oil 124
biocarbon 172
biochar 124, 172
biochars 27
biocoke 172
biogas 39
biomarkers 143, 208
biomass 49, 74
biosorbents 27
Black Carbon 154
blast furnace 171
Blast furnace cooling 125

blast furnace slag ... 218
brackish water ... 216
building energy simulation ... 228
building-integrated wind turbines ... 267

C

carbon nanodots ... 197
Carbon-Neutral Fuels ... 41
Carbon Neutrality ... 59
catalyst regeneration ... 250
catalysts ... 37, 121
catalytic cracking ... 57
cathode ... 62, 97
cathode materials ... 152, 272
cenospheres ... 103
ceramic electrolyte ... 225
ceria ... 32
cerium ... 210
CFD ... 85, 132, 137, 164, 171
Chemical looping ... 127
chemical markers ... 232
chemical recycling ... 141
circular economy ... 108, 235, 253
circular economy in fire safety ... 218
Climate Change ... 59, 228
climate neutrality ... 118
co-creation ... 269
co-eletrolysis ... 174
co-pyrolysis ... 160
CO2 ... 74
CO2 and CH4 conversion ... 76
CO2 capture ... 182, 197
CO2 hydrogenation ... 64, 255
CO2 methanation ... 32, 37, 147, 210, 252, 258
CO_2 reduction ... 127
CO_2 utilization ... 258
coal ... 75
coal flue gas ... 136
coastal urban area ... 206
cobalt ... 252
cobalt catalyst ... 68
coke ... 33, 172
coking ... 33
combined heat and power ... 247
combustion ... 75, 110, 266
composite solar wing manufacturing ... 264
compressive strength ... 201
Condition monitoring ... 184
containment ... 199
coolant's finite volume capacity ... 46
Cooling circuit integration ... 125
Cooling stave ... 125
core-shell nanoparticles ... 47
correlation analysis ... 123
covalent organic frameworks ... 101
COx methanation ... 64
cracking ... 94
critical elements ... 253
critical raw materials ... 51, 233, 257
Critical Raw Materials Act ... 51

cross-border coupling 193
crystal structure 74
Cu–Zn–Mg–Al catalysts 255
CuO 103
CUPOLA 168
cycling stability 62

D

data-driven energy management 190
Data triangulation 192
decarbonisation 166
decarbonization 59, 172, 195
Decoupling 233
defect engineering 99
Defossilization 127
degradation 174
density functional theory 88
Deoxygenation and Enrichment 45
Design of Experiments 170
DHW storage tank 259
diffuse irradiance 98
digital twin 187
disordered rock salts 272
dispersion modelling 118
Distributed energy resources 112
Distribution of Relaxation Times (DRT) 230
district heating 43, 195
district heating prices 43
dithiothreitol 139
Double perovskite 53
Drop-in fuel precursors 29
DRT 237
dry reforming of methane 258
dual atmosphere 225
dynamic operation 271

E

Early-warning systems 192
econometric modelling 220
economic assessment 247
economic dispatch 193
efflorescence 201
EIS 237
electric boat 180
Electric motor 263
electricity demand 257
electricity price formation 193
electricity prices 224
electrification 166
electrochemical conversion 119
Electrochemical Impedance Spectroscopy (EIS) 222, 230
electrochemical modelling 230
electrochemical reactor 216
Electrochemistry 277
electrochromic smart windows 86
electrode infiltration 174
electrode materials 82, 240
electrospinning 240
Elemental Carbon 154
emissions 240, 266

emissions control 235
energy data analytics 190
Energy data uncertainty 254
energy demand 166
energy demand forecasting 220
Energy Density 177, 194
energy efficiency 171, 247
energy-efficient devices 86
energy intensity 35
Energy Management System 112, 178
energy market 245
energy materials 240
energy recovery 160, 171
Energy recovery efficiency 29
energy scenarios 220
energy sector 113
energy storage 90, 91, 164, 236, 271
energy system modelling 166
energy transition 43, 59, 91, 145, 233, 235
Energy transition scenarios 254
environmental catalysis 103
environmental hazard 113
environmental rehabilitation 235
environmental transparency 116
equivalent black carbon 145
Equivalent Circuit Model (ECM) 230
ethylene 110
exergy 194
Exsolution 55

F

fast reactor 128
Fe-basd perovskites 106
Fe2O3 72
fermentation 39
ferrierite 83
fibrous catalyst 204
finite difference method 227
fire and rescue operations 218
Fischer-Tropsch synthesis 80
flexible carbon nanofiber film 96
floodability index 30
flow properties 30
flowability index 30
fluid catalytic cracking catalyst 57
fly ash 261
fly ashes 103, 113
forecasting 245
Fourier transform 277
framework dynamics 76
Fuel cell 275
fuel electrode 88

G

galvanic cells 230
Gamma-ray absorption 137
gamma-ray absorption radiometry 85
gasification 49, 78
gasifier 49
Geant4 131

Gerischer element ... 222
Ghana ... 235
glass dust ... 218
grassroots initiatives ... 269
green hydrogen ... 134, 271
greenhouse gas emissions ... 250
greenhouse gases utilization ... 83
grid stability ... 123

H

H2-induced reconstruction ... 55
heat pump ... 187
heat- transfer coefficient ... 132
heated cylinder ... 132
heatwaves ... 228
high-efficiency cogeneration ... 195
High energy density ... 90
high-entropy alloys ... 157
high-entropy perovskite ... 88
High-temperature electrochemistry ... 225
HKUST-1 ... 121
hotspots ... 35
HVAC capacity adequacy ... 228
hybrid Eulerian-Volume of Fluid ... 85
hybrid modelling ... 193
Hybrid vehicle ... 263
hydrocarbon separation ... 70
Hydrogen ... 41, 130, 185, 203
hydrogen Carrier ... 194
Hydrogen fuel cell ... 214
hydrogen generation ... 199
hydrogen production ... 250
Hydrogen storage ... 104
hydrogen supply chain ... 194
hydrophobization ... 30
hydrotalcite ... 147
Hydrotalcite-Based Sorbents ... 182
hydrotalcites ... 252
hydroxylated PAHs ... 143, 208

I

idle consumption ... 190
import diversification ... 51
in-mold lamination ... 264
in situ DRIFTS ... 64
in situ exsolution ... 88
in situ FTIR measurments ... 182
industrial energy efficiency ... 190
industrial waste valorisation ... 218
input-output analysis ... 35
Intelligent cooling system ... 125
intercalation ... 236
interface engineering ... 99
intermetallic compounds ... 104
inverse problem ... 227
Iron-based catalysts ... 80
iron complexes ... 162
Iron-mediated catalysis ... 29
iron sites ... 83
IT-SOFCs ... 106

K

kaolin 32
Kraków 145

L

LaCrO3 88
lanthanum 210
Large Language Models 178
layered double hydroxides 255
LC-MS/MS 243
leakage 185
Li-ion cells 273
life-cycle assessment 150
ligand-assisted oxidation 162
Linari NanoTech 240
lithium-ion battery 180, 272
Local Energy Market 239
Local energy markets 112
local governance 269
Low Concentration-Coal Mine Methane 45
low emission hydrogen 204
low-temperature curing 201
low-temperature properties 115
luminescent solar concentrators 66

M

MABI 154
Machine learning 98, 184
macroeconomic resilience 51
marine plastic waste 168
MCR-ALS 92
melt infiltration 210
memory effect 255
mercury removal 136
merit order 193
Metaheuristic Optimization 178
Metal hydride storage 214
meteorology influence 206
methane activation 76, 83
methane pyrolysis 204, 250
methanol synthesis 255
Micro-Redox Capacitors 177
micro-wind turbine 267
micromechanics 240
Microwave-assisted co-pyrolysis 29
mine-waste management 235
Minerals Development Fund 235
mining pollution 235
mixed air-manganate-CO2 78
Mixed plastic waste 29
Mn substitution 53
model 33
model predictive control 187
MOF 121
Monte Carlo 131
MSW 78
MTH reaction 92
multi-fibre composite 150
Multicomponent perovskite 55
Multifluid VOF 137

Multiphase Flows 137
multiple-outcome synthetic control 51
municipal wastewater 148
MXene 177

N

Na-ion 236
nanofiber electrodes 47
nanofibers 155, 240
Nanofibrous electrodes 55
nanomaterials 39
nanoparticles 39
NAP-XPS 64
natural gas-fired cogeneration 247
natural materials 66
Nb-modified 273
negative thermal expansion 152
net-zero energy buildings 66
neutronics 128
NH3-SCR 121
Ni-based catalysts 37
Ni-rich cathodes 273
Ni-YSZ 174
nickel 32, 147
nickel catalysts 210, 252, 258
NiO–CeO2 64
nitrous oxide hydrogenation reaction 82
noise reduction 171
non-stationary signals 277
nuclear materials 157
Nuclear Power 59
numerical 33
numerical classificaiton 237
numerical model 171
Numerical modelling 125

O

OH-PAHs 148, 212, 243
oil jojoba 115
One Health 192
operando 94
operando FTIR 57
operando spectroscopy 92
Operational reliability 125
optical and thermal comfort 66
oven 33
overheating 259
oxidative modification 212
oxidative potential 139
oxide perovskites 74
Oxidized bitumen residue 108
oxygen carriers 74, 75
Oxygen electrode 53, 106
oxygen reduction reaction 62
oxygen transport 99
oxygen vacancies 62, 88
oxygen vacancy 82, 97

P

PAHs 243

part-load operation 134
partial order 272
particulate matter 232, 266
passive autocatalytic recombiners 199
Peer-to-peer energy trading 112
PEM electrolyzer 134
peracetic acid 162
perovskite electrodes 99
Perovskite oxides 47, 127
perovskites 75, 275
pharmaceuticals 212
phosphate ions 261
phosphogypsum 201
photochemical aging 232
photon upconversion 101
photovoltaic cell integration 264
photovoltaic panels 180
Photovoltaic Plants 176
photovoltaic system 134
photovoltaic systems 98, 123
photovoltaics 91
plastic degradation 232
plastic recycling 168
plastic waste 57, 94
PM10 ..... 139, 154
PM2.5 154
Pneumatic motor 263
Poland 257
Polarization resistance 106
political participation 269
polyamide 141
polypropylene 70
Population health surveillance 192
porous electrodes 222
porous materials 227
Post-growth 233
potassium desorption 72
Potassium ferrites 80
potassium promotion 68, 72
potassium silicate glass 110
powder sorbents 30
Power equipment degradation 184
Power Faults 176
Power Output Stability 177
Power-to-Gas 252, 258
Predictive maintenance 184
price analysis 224
process modeling 49
process modelling 70
Prosumer preferences 112
Prosumers 91, 239
Proton ceramic fuel cells 62
Proton-conducting ceramic cells 127
protonic ceramic electrolysis cells 82
PROZA model 220
Prussian Blue analogues 236
PV energy yield 123
Py-GC-MS 70
pyrolysis 27, 108, 124

pyrolytic gas ... 124

Q

quantum-chemical modelling of CO_2 interactions ... 182

R

Radiometric measurement ... 137
railway transport ... 130
Raman spectroscopy ... 240
rapid prototyping ... 216
reactor design ... 225
rebound effect ... 35
Reduced-activation complex concentrated alloys ... 157
reduced-order modelling ... 199
Regional energy planning ... 254
regional transport ... 145
renewable energy ... 43, 123, 267
renewable energy sources (RES) ... 259
Renewable Energy Storage and Conversion ... 41
Rere-earth elements ... 275
RES ... 164
residential buildings ... 228
response surface methodology methanation ... 170
reversible solid oxide cell ... 88
rewersible polymer exchange membrane fuel cells ... 203
Risk assessment ... 185
Rule-Based Pricing ... 239

S

salt ... 203
sand ... 164
Sardinia ... 254
SBA-15 ... 37
seasonal variability ... 145
sectoral energy consumption ... 220
self-supporting electrode ... 96
Service life prediction ... 184
service sector ... 166
sewage sludge ... 124
sewage sludge biochar ... 136
SFM ... 155
SFR ... 128
Smart Grid ... 178
smart windows ... 66
SNG ... 170
sodium-cooled reactor ... 128
solar boat ... 180
solar electric vehicle ... 150
solar energy use ... 101
solar irradiance ... 224
Solar-powered UAV ... 264
solar radiation ... 98
solar thermal system ... 259
Solar thermochemical cycles ... 127
SolarComp 971SD1 controller ... 259
Solid oxide cells ... 53, 55, 97, 99, 119, 155, 275
Solid Oxide Electrochemical cells ... 41
Solid oxide electrolysis ... 127, 174
Solid Oxide Fuel Cell ... 45
solid oxide fuel cells ... 152

solid-water partitioning 143
solvent dewaxing 115
solvolysis 141
soot 110
sorption properties 104
spallation target 131
spandex 141
spatial complementarity 123
spectral divergence 237
spectroscopy 236
Sr-doping 106
steam gasification 79
steam methane reforming 250
steelworks waste 253
storage energy 130
Strouhal number 132
subsidies 91
Supercapacitor 96
surface engineering 240
surface properties 72
surface reconstruction 47, 62
suspended particulate matter 206
sustainable electrolytes 86
sustainable transition 269
symmetrical SOFCs 47
syngas 49
Syngas composition 108
synthesis 74
Synthetic chemicals 127
system dynamics 257
system integration 119
Systems modelling 233

T

thermal alkali desorption 68
TES 164
textile fibres 126
textile waste 79, 126, 141, 160
Thermal alkali desorption 80
thermal conductivity 227
thermal decomposition 126
thermal energy storage 119, 187
thermal expansion coefficient 152
thermal-hydraulics 128
Thermal management 125, 214
thermal shock 46
thermal stress reduction 46
Thermochemical conversion 108, 126
thermochemical recycling ecotoxicity 160
thermochemical utilisation 79
thermodynamic analysis 247
thermodynamic flexibility 187
thermodynamic screening 194
thermogravimetric analysis 126
thin films 101
third-party access 43
time-frequency analysis 277
TIMES model 254, 257
transcritical CO_2 heat pump 195
Transformer model 273

transient temperature 46
transition metals 272
transition-metal doping 110
Transmission Line Model (TLM) 222
triple conductor 97
turquise hydrogen 204
two-phase flow 85
two-zone SDHW model 259

U

UHPLC-MS/MS 148
ultrasonic measurements 85
Underground gas storage 185
urban aerosol 139
urban wind energy 267

V

valorisation 168
valorization 113
vegetable waxes 115
vehicle-integrated photovoltaics 150
vermiculite 210
Virtual Power Plant 239
Voltage Assessment 176
vortex shedding 132

W

Wasserstein Metrics 237
waste characterisation 168
waste-derived sorbents 136
Waste heat recovery 214, 259
waste incineration 116, 118
waste reduction 171
waste-to-energy conversion 78
Wastewater-based epidemiology (WBE) 192
wastewater treatment 143, 208
Water efficiency 125
wavelet analysis 277
WBE 148
wind speed 224
work function 72

Z

zeolite 121, 261
zeolite extrudates 57
zeolites 94
Zephyr AGH vehicle 263
zinc 94
Zinc-halogen batteries 90
Zn-containing zeolites 76
Zn speciation 76
ZnO 103